Exploring the bioenergetics of bacterial spore germination using *Bacillus megaterium*

Pooja Gupta

PhD

University of York

Chemistry

April 2024

Abstract

When confronted with unfavourable growth conditions, *Bacillus* and *Clostridium* species initiate the process of sporulation whereby a bacterial cell undergoes drastic reconfiguration to become a robust, multi-layered, dormant spore. When the availability of nutrients is sensed via germinant receptors, *Bacillus* spores can exit dormancy (germinate) and return to metabolically active life. Spore germination unfolds on a much faster timescale than sporulation, and many aspects of this process are not fully understood – essential events during germination are localised in the spore inner membrane but this is not easily accessible for biochemical experimentation because of the spore's multi-layered architecture. In this work, *Bacillus megaterium* QM B1551 was used as a model to optimise a protocol for producing high-quality membrane preparations from medium-scale spore cultures. A chromatographic method was developed to enable extraction of large membrane protein complexes (e.g. germinant receptors) directly from their atypical spore environment for biochemical/structural characterisation. NADH:O_2 reaction assays, native gel electrophoresis and proteomic analyses on isolated spore membranes revealed the composition of an active, branched membrane-bound electron transport chain present in dormant spores. Two uncharacterised, spore-specific paralogues were found: a type II NADH dehydrogenase (YumB not Ndh) and cyt *bd* oxidase (YthAB not CydAB). To understand when germinating spores resumed glucose-powered oxidative metabolism using this ETC, traditional spore germination assays, enzymatic detection of glucose consumption and H_2O_2 production, O_2 consumption measurements and novel haem remission spectroscopy experiments were carried out. Based on these, a revised timeline of events in germination was proposed, where glucose serves as both a signalling molecule and an exogenous energy source, oxidative metabolism and germination are initiated concurrently, and electron transport precedes detectable germination – YthAB is critical for resumption of bioenergetics in germinating spores. Lastly, a serendipitous cryo-EM map of the enzyme succinate dehydrogenase was refined from crudely enriched membranes of *B. subtilis* cells.

Author’s Declaration

I declare that this thesis is a presentation of original work and I am the sole author. This work has not previously been presented for a degree or other qualification at this University or elsewhere. All sources are acknowledged as references.

Pooja Gupta

2 April 2024

Acknowledgements

"*Pray remember that I leave you all my theory complete,*

Lacking only certain data for your adding as is meet;

And remember men will scorn it; 'tis original and true,

And the obloquy of newness may fall bitterly on you."

—Sarah Williams in the poem 'The Old Astronomer' (1868)

This PhD was started in Jan 2020 by a youthful woman who had not yet lived through a once-in-a-lifetime pandemic. Four years later, I may be greyer, but the forty thousand words in this thesis (that may have contributed to some of the greying) describe a scientific journey that I could not have anticipated at the beginning and one I am incredibly grateful for.

I start by thanking my PhD supervisor Dr. Jamie Blaza, for all that he has taught me over the years in this official capacity, and everything else he has done for me as a kind friend. There were times when neither of us really knew what the data meant, or whether the next experiment would leave the spore bioenergetics project dead in the water, but I am glad I had Jamie's intellectual fierceness to guide me. We attempted something difficult and new – it has its flaws but it is work I am proud of.

I also thank my co-supervisor, our Supreme Leader Prof. Tony Wilkinson for all his support and diverting conversations over coffee/wine about life and cricket. Prof. Gavin Thomas for being my best IPM and my best internal examiner – he is great. Dr. Graham Christie for all the expertise and spore materials, the spectacular conference last April, the indulgent Peterhouse lunches where I amusingly ended up being the only woman and POC, and for his feedback on chapter 1. Dr. Sebastian Pintscher for being an excellent collaborator/friend, and his feedback on chapter 6 as well as the cryoEM methods. Dr. Roger Springett for all his help with the bioenergetic chamber, spectral decomposition, his vast knowledge of bioenergetics, and exhilarating chats about the imminent AI apocalypse.

I want to thank all the past and current members of the JNB lab group, with a few special mentions: Rowan Walters for being a superlative labmate, her help with the bioenergetic chamber and the anaerobic glovebox, pandemic luncheon calls with Sandra Grieve and Katie Jameson that kept us sane during the first lockdown, and many a dinner party. Dr. Morwan Osman for stimulating scientific and sociopolitical discussions (death to trickle-down

economics), and for skilful management of our lab space. Past members who I co-supervised in the labs, Beth Hardman and Elodie Wells, for making important contributions to the spore membrane protein biochemistry/bioenergetics projects. Dr. Matt Rose for measuring the protein concentration of *B. subtilis* membranes used in chapter 6.

The YSBL coffee club is an institution unto itself and the coffee-fuelled absurdity has brought me much joy. I thank Rowan and Dr. Johan Turkenburg for organising it, and the larger YSBL community that coalesces around this daily ritual. Here I want to thank Prof. Fred Anston, Dr. Chris Hill and both their groups for sharing equipment and expertise, as well as the camaraderie. Maria Chechik is a force of nature and the JNB group remains indebted to her for finding the Invitrogen tank on the free table that we have since used reliably for our BN-PAGE experiments.

My gratitude to the wonderful YSBL wet lab technicians Simon Grist, Juliet Borgia, former team member Louise Haigh, and Roksana Osinska; to fellow boardgamer Tim Kirk (and by extension to all our boardgaming friends); and to the brilliant cryo-EM facility staff Sam Hart and Dr. Johan Turkenburg. I thank Dr. Adam Dowle and Dr. Chris Taylor (TF - Metabolomics and Proteomics Lab, Department of Biology) for the expert MALDI-TOF and LC/MS analyses, and Dr. Andrew Leech (TF - Molecular Interactions Lab, Department of Biology) for his assistance with the fluorescence plate reader.

My sincere thanks go to the University of York for the YGRS Overseas Research Scholarship and the COVID-19 PhD Scholarship Fund, and the Department of Chemistry for a studentship that fully funded the 4 years and 3 months of my PhD.

On a more personal note, I want to thank my housemate of 3 years, Ethan Redmond for his friendship and the delicious meals that sustained me as I was frantically finishing this thesis. We were in a COVID bubble together with Dorothy Hawkins and Jake Smith, and our weekly dinner parties could rival the ones in 10 Downing Street. I thank Dorothy for being my dearest friend/confidante over the past few years; Jake Smith for asking me “are you done yet” ever so often and insisting that he be mentioned here. Ellen Harrison for all the Netflix parties that on many days ensured I came home at a reasonable time, shared love of Radio 4 programming and the Guardian to the point that it is slightly ridiculous.

I cannot sufficiently express my gratitude to the most formative influences in my life: my parents and my elder sisters, especially Gauri didi who has always supported my foolhardiness exemplified by my decision to pursue science instead of becoming a medical doctor. I suppose I never will be a real doctor…Heartfelt thanks also to my more recently acquired parents, Liz and Dave, who have supplied everything from Pringles and spare headphones to shoe laces and fingerless gloves that I have needed to make it to the bitter

end. Finally, I want to thank my partner Jake for digitising the haem *d* reference spectra from Borisov et al., 2011 and for loving me the way he has through it all.

Table of contents

Chapter 1: Introduction

"*The problem as to whether an organism can be revived after the complete cessation of all life processes, that is, whether life under certain conditions may be a discontinuous process, has, apart from its great scientific interest, a fascination of its own. In fact it is one of the oldest problems which preoccupied man when he began to think about life, death and immortality. It is reflected in almost all religions, in some legends and even in fairy stories.*"

> —David Keilin in 'The problem of anabiosis or latent life: History and current concept' (1958)

1.1. Cryptobiosis as a survival strategy

Establishment of 'cryptobiosis' in the face of environmental adversity is a recurring theme across the domains of life. David Keilin, most famous for discovering cytochromes and his work on cellular respiration, coined this term in 1958 and defined it as "*latent life, …the state of an organism when it shows no visible signs of life and when its metabolic activity becomes hardly measurable, or comes reversibly to a standstill*." In his 1958 Leeuwenhoek lecture on the subject, Keilin described how loss of water (anhydrobiosis), lowering of temperature (cryobiosis), absence of oxygen (anoxybiosis) and high salt concentration (osmobiosis), or combinations thereof could cause cryptobiosis in living organisms. He also suggested there was a "gradation" between dormancy (*hypo*metabolism) and cryptobiosis (*a*metabolism) – in other words, states of "more or less deep dormancy" could be achieved (Keilin, 1959).

Produced by some bacteria, protozoa, fungi, algae, and plants for the purposes of survival and propagation, spores perhaps epitomise this recurring theme of cryptobiosis. Many bacteria of the phylum Actinomycetota (*Actinomyces*, *Streptomyces*, *Micromonospora* species) form reproductive exospores in their fungi-like hyphae (Sexton and Tocheva, 2020). Other bacteria of the phylum Firmicutes (Gram-positive, aerobic *Bacillus* and anerobic *Clostridium* species, and Gram-negative bacteria of class Negativicutes) form endospores (Beskrovnaya et al., 2021). Filamentous cyanobacteria of the order Nostocales can form spore-like resting cells called akinetes (Garg and Maldener, 2021).

Amongst eukaryotes, pathogenic spore-forming protozoa (*Cryptosporidium*, *Isospora*, and *Cyclospora* species) produce spores called oocysts for faecal-oral transmission (Goodgame, 1996); various fungi form reproductive spores like zygospores, ascospores, basidiospores

etc., and resting spores like chlamydospores (Naranjo-Ortiz and Gabaldón, 2019); red algae/rhodophyta form reproductive spores called carpospores and tetraspores (Vieira et al., 2018); golden algae/chrysophyta form resting spores called statospores (Kristiansen and Škaloud, 2016); and plants such as ferns in the division Pteridophyta reproduce only through spores (Wallace et al., 2011). When optimal conditions are encountered, these spores exit dormancy/cryptobiosis and germinate, giving rise to new individuals.

The focus of this thesis are endospore-forming Bacilli that since their discovery by Ferdinand Cohn and Robert Koch in 1876, continue to be studied intensively nearly 150 years later in both fundamental and applied branches of microbiology (Gould, 2006).

1.2. The sporulation lifecycle in bacteria

When confronted with unfavourable growth conditions, many bacteria initiate sporulation, a tightly regulated and dramatic reconfiguration of vegetative cells into cryptobiotic endospores. Sporulation typically takes 8-10 hours and involves the expression of >600 genes (Eichenberger, 2012) – new sporulation genes continue to be identified and a large fraction of those already identified are not yet functionally characterised (Chan et al., 2022; Galperin et al., 2022). Over the years, studies on sporulation in the model organism *B. subtilis* have contributed immensely to the understanding of fundamental processes like function of transcription factors and regulation of gene expression (Errington and van der Aart, 2020; Barák, 2021).

Sporulation exemplifies cellular differentiation in prokaryotes whereby the chromosome is replicated and asymmetric septation results in the formation of two compartments within the 'sporangium': the larger mother cell and the smaller forespore (Fig 1). These morphological changes are initiated when the master transcription factor Spo0A gets phosphorylated (Spo0A~P) by the kinase KinA. Spo0A~P directly controls 121 genes, positively regulating those involved in the asymmetric cell division and compartment-specific sigma factors σ^E and σ^F that will become active in the mother cell and forespore respectively (Molle et al., 2003). However, as chromosomal segregation is not completed before septation occurs, the forespore chromosome is trapped in the septum and needs to be actively transported into the forespore by the SpoIIIE translocation complex that is assembled at the septal midpoint (Bath et al., 2000).

Subsequently, governed by the σ^E and σ^F regulatory gene networks, the mother cell engulfs the forespore, and complete engulfment creates a double-membraned forespore with the

construction of two additional protective structures: the peptidoglycan cortex between the two membranes, and a complex proteinaceous coat as the outermost layer in this concentric arrangement (Mckenney, Driks and Eichenberger, 2012). In some species, there can be another glycoprotein layer surrounding the coat – either a crust (e.g. *B. subtilis*) or an exosporium (e.g. *C. difficile*) (Shuster et al., 2019; Janganan et al., 2020). The position of the forespore within the mother cell and its relative size can vary across species. Forespores can be terminal (polar location), subterminal, lateral or centrally located, and can develop into bodies larger than the mother cell itself such that the latter bulges around it (de Andrade Cavalcante et al., 2019). After engulfment, transcription factors σ^G and σ^K control gene expression in the forespore and mother cell respectively enabling spore maturation, mother cell lysis and release of the mature spore (Higgins and Dworkin, 2012; Khanna, Lopez-Garrido and Pogliano, 2020). Even though Clostridia and Bacilli share major sporulation-specific transcription and sigma factors, the Clostridial sporulation regime is considerably different, with variations identified even amongst Clostridial species (Al-Hinai, Jones and Papoutsakis, 2015).

Mature bacterial spores are cryptobiotic with a multi-layered architecture and unique biochemical properties which makes them astoundingly robust against a wide range of environmental onslaughts. The chromosome in the spore core is protected by specialised DNA-binding α/β-type small acid-soluble proteins called SASPs that are found in all spore-formers studied to date (Lee et al., 2008). The enzyme SP lyase (spore photoproduct lyase) can repair DNA damage caused by UV-radiation during germination (Slieman, Rebeil and Nicholson, 2000). Crucially, the spore core is relatively dehydrated and contains a calcium-dipicolinic acid (CaDPA) chelate at well above saturation concentration; these properties underpin the characteristic wet heat resistance of dormant spores (Beaman and Gerhardt, 1986). Moreover, the proteinaceous coat composed of >70 proteins and the crust/exosporium function together to confer physical protection from bacterivorous predators (Klobutcher, Ragkousi and Setlow, 2006; Mckenney, Driks and Eichenberger, 2012; Laaberki and Dworkin, 2008).

Thus, spores can survive in highly irradiated environments like outer space (Deshevaya et al., 2024), resist decontamination procedures (Setlow and Christie, 2021, 2023), and can reportedly maintain viability for prolonged periods of time – the most reliable estimates of their longevity range in the hundreds or thousands of years (Kennedy, Reader and Swierczynski, 1994). When favourable growth conditions return, spores germinate to become vegetative cells which can cause fatal diseases (e.g. anthrax, food poisoning, tetanus, botulism, pseudomembranous colitis caused by *Bacillus anthracis*, *B. cereus*, *Clostridium tetani*, *C. botulinum*, *C. difficile* respectively) and fouling in the food and dairy industry (Martin, Quintana-

Pérez and Evanowski, 2023; André, Vallaeys and Planchon, 2017), amongst other serious challenges. However, once spores germinate their susceptibility to decontamination procedures is restored. This forms the basis of the “germinate to eradicate” strategy but requires a species-specific understanding of various germination triggers and pathways (Setlow and Christie, 2021).

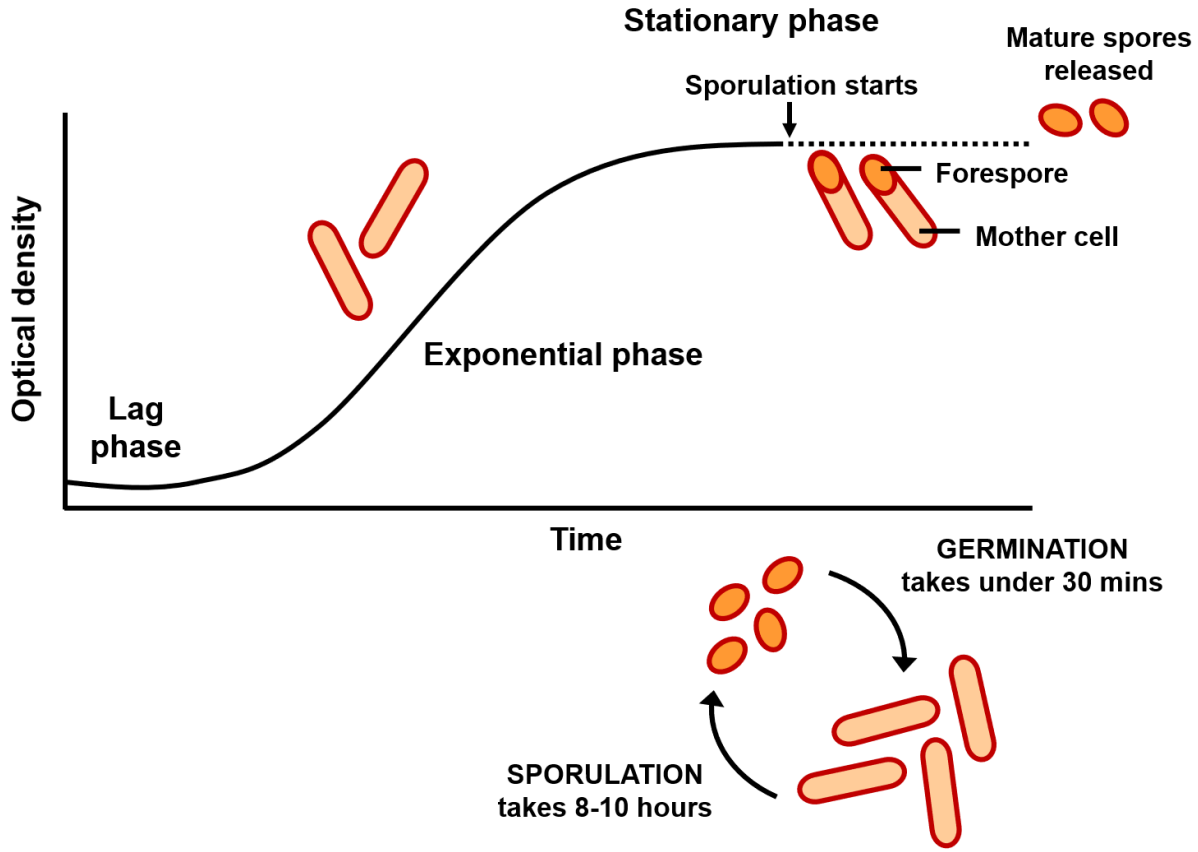

Fig 1. A simplified schematic of the sporulation lifecycle in Bacillus species. When exponential growth becomes limited by nutrient depletion in laboratory cultures, expression of sporulation genes like Spo0A is directed by σ^H, a sigma factor that orchestrates the transition from exponential growth to stationary phase (Britton et al., 2002). With the initiation of the sporulation programme that involves the expression of >600 genes (Eichenberger, 2012), *Bacillus* cells differentiate into the forespore and mother cell, and eventually, one mature spore per cell is released. While sporulation takes 8-10 hours, germination whereby spores exit dormancy proceeds rapidly taking under 30 mins.

1.3. The bioenergetics of cryptobiosis

"*How does the living organism avoid decay? The obvious answer is: By eating, drinking, breathing and (in the case of plants) assimilating. The technical term is metabolism…*"

—Erwin Schrödinger in What is Life? The Physical Aspect of the Living Cell (1944)

"*…the (living active) organism must constantly provide the energy for the upkeep of its complex structure, which has a tendency to collapse…The concept of life as applied to an organism in the state of cryptobiosis becomes synonymous with that of the structure, which supports all the components of its catalytic systems. Only when the structure is damaged…does the organism pass from the state of latent life to that of death.*"

—David Keilin in 'The problem of anabiosis or latent life: History and current concept' (1958)

In his seminal book 'What is Life? The Physical Aspect of the Living Cell' (based on a series of lectures delivered in 1943), the physicist Erwin Schrödinger articulated a simple fact about living organisms in terms of the Second law of Thermodynamics: an active living organism that continually increases its entropy (disorder), must feed on orderliness (e.g. organic compounds in food or energy from light) from its environment to avoid thermodynamical equilibrium i.e. death (Schrödinger, 1944; Phillips, 2021). As Keilin argued in 1958, active organisms are therefore stable in a dynamic way, whereas the stability of cryptobiotic organisms is static – so long as they retain their structure and catalytic machinery, they could return to active life, but even they cannot do so indefinitely. Regarding the subject of cryptobiosis, Keilin mentioned in his 1958 lectures that it had "*direct bearing on some aspects of our (his group's) work on intracellular respiratory catalysts of organisms*." He suggested that during cryptobiosis "…*changes may cause the reversible loss of accessibility between the components of the respiratory chain, with the result that all the metabolic processes come to a standstill*" (Keilin, 1959).

Before further deliberation on the state of the respiratory chain during cryptobiosis, we will briefly describe how organisms use respiratory chains to conserve energy (in the form of adenosine triphosphate or ATP) that is required to drive biochemical reactions in cells. The study of these processes is called bioenergetics. Electrons derived from the oxidation of reduced chemical compounds (chemotrophy) or light excitation of a photosynthetic pigment (phototrophy) are transferred in a stepwise manner from a low redox potential donor (e.g.

cofactor nicotinamide adenine dinucleotide, NADH) to a high potential acceptor (e.g. O_2) through the electron transport chain (ETC) composed of respiratory cytochromes. Electrons move through a series of redox cofactors like flavins (flavin mono/dinucleotide, FMN/FAD), FeS clusters and haem groups present in these cytochromes. As depicted in Fig 2, the free energy released from electron transfers is used to generate a proton electrochemical gradient (also called proton-motive force, PMF) across an energy transducing membrane (e.g. inner mitochondrial, thylakoid, bacterial plasma membranes).

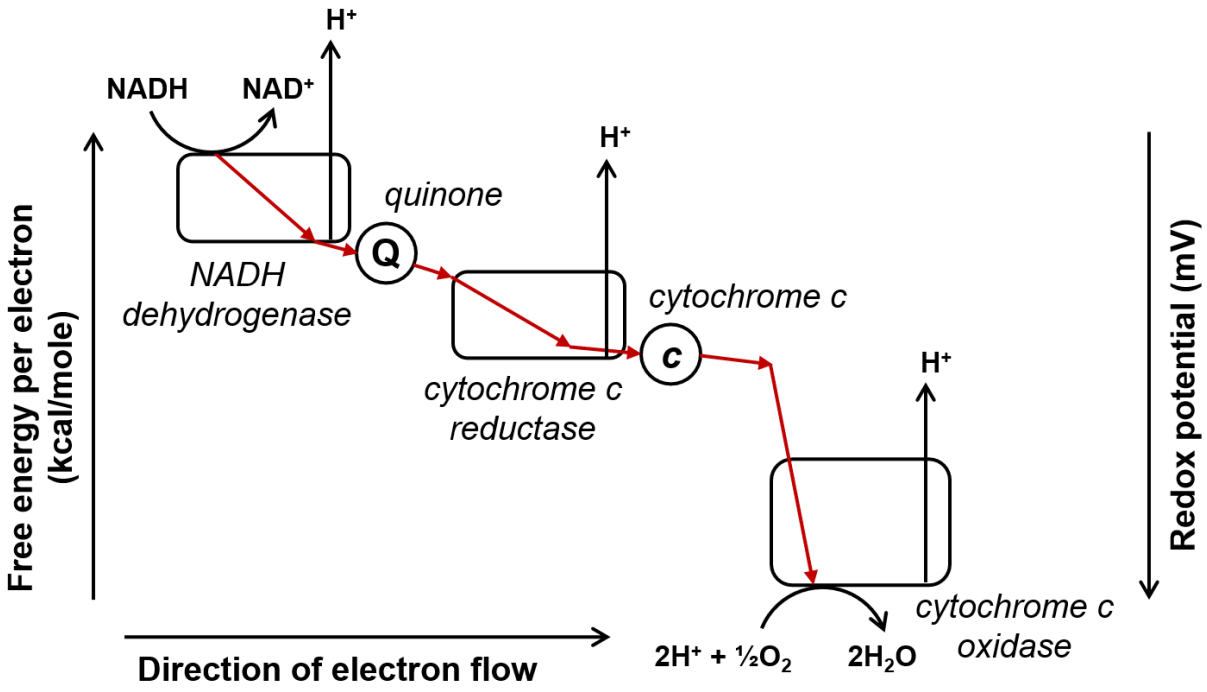

Fig 2. A simplified schematic of electron transport in energy-transducing membranes. In this example, NADH is the electron donor and O_2 is the terminal electron acceptor. Respiratory enzymes in the ETC are arranged such that the redox potential of the electron carriers increases in the direction of electron flow. This difference in redox potential between two electron carriers determines the amount of free energy released during electron transfer between them. Part of this free energy is harnessed by these enzymes to translocate protons across the membrane (indicated by the upward arrows), and a proton electrochemical gradient is thus generated. Adapted from the 4th edition of Molecular Biology of the Cell (Alberts et al., 2002).

The PMF has two components, a proton gradient (ΔpH) and membrane potential (ΔΨ) that arise from differences in the proton concentration and charge respectively between the two phases separated by the membrane. Dissipation of the ΔpH component powers the rotatory mechanism of ATP synthase and the synthesis of ATP from adenosine diphosphate (ADP) and inorganic phosphate (P_i) (Walker, 2013; Kühlbrandt, 2019). This is how energy is transduced, i.e., free energy from electron transfers is stored as electrochemical potential

(PMF) which is then harnessed as chemical energy (ATP). In the cell, the exergonic ATP hydrolysis reaction is coupled to other endergonic reactions to drive them in the desired direction. The coupling of electron transport and ATP synthesis, also called oxidative phosphorylation, was first proposed as the chemiosmotic hypothesis in 1961 by Peter Mitchell (Mitchell, 1961; Slater, 2003).

How an organism balances its energetic demands and supply as it enters then exits cryptobiosis, and the regulation of ETC function in both cases is a compelling problem. One can imagine these to be inverse processes. As an organism enters cryptobiosis, perhaps energetic demands are reduced first, and then the reduction of supply follows in a feedback loop until the system is energetically depleted and dormant. But when an organism returns to life, conceivably the energetic demands are more pressing as many essential processes are restarted simultaneously and supply must rise swiftly to meet demands. Where this has been studied, such as in germinating plant seeds (Rosental, Nonogaki and Fait, 2014), *Saccharomyces* recovering from anhydrobiosis (Kuliešienė et al., 2021), and germinating *Bacillus* spores (Frentz & Dworkin, 2020; Korza et al., 2023; Wilkinson et al., 1977), the ability to restart bioenergetic pathways and generate ATP early is positively correlated with successful return to active life; but what is less well understood is which pathways become operational and how during this transition.

1.4. The state of cryptobiosis in bacterial spores

Bacterial spores are fascinating for how they establish metabolic dormancy and sustain it over long periods of time. Upon sensing nutritional availability, their ability to exit this dormancy within minutes is even more remarkable. Bacterial spores, unlike eukaryotic systems, can suspend metabolism without replacing most of the cell water with glass-forming osmolytes such as sucrose. Instead, in the largely dehydrated spore core which is gel-like with little but mobile water (Sunde et al., 2009; Kaieda et al., 2013), >800 mM of the characteristic calcium dipicolinic acid chelate (CaDPA) is present in a solid state, imported into the forespore during sporulation (Kong, Setlow and Li, 2012; Gao et al., 2022). The inner membrane (IM) presents a permeability barrier, and possibly due to its compression, the constituent lipids are mostly immobilised (Cowan et al., 2004). Despite this, the IM is known to harbour the germinant receptors (GRs) and some of the SpoVA channel proteins which are directly involved in the initiation of germination (Paidhungat and Setlow, 2001; Vepachedu and Setlow, 2005), along with respiratory enzymes of the ETC (Chen et al., 2019; Escamilla & Benito, 1984; Racine & Vary, 1980; Wilkinson & Ellar, 1975). Moreover, dormant spores are energetically depleted as

they have no detectable levels of ATP/other nucleoside triphosphates or reduced pyridine nucleotides (NAD(P)H) (Setlow and Kornberg, 1970; Setlow and Setlow, 1977). Menaquinone (MK), an electron carrier in the ETC required for ATP synthesis, has been reported to get depleted during sporulation (Escamilla et al., 1986). However, spores do have a large pool of ribonucleoside monophosphates like AMP and oxidised pyridine nucleotides like $NAD(P)^+$, and lesser amounts of ADP and inorganic phosphate (Ghosh et al., 2015) ready to be deployed when they exit dormancy.

1.5. Bacterial bioenergetics

The sheer diversity displayed by archaea and bacteria in terms of the electron donors and acceptors used and their vast functional repertoire of respiratory enzymes to catalyse energy transduction is astonishing (Schäfer, 2004; Borisov and Forte, 2022; Allen et al., 2023). It has allowed bacteria to colonise ecological niches no other organisms can and has made them arguably the most dominant lifeforms on Earth.

Unlike mammalian mitochondrial respiratory chains that have a rigid, linear organisation, bacterial ETCs are recognised to often be branched, modular and plastic. This allows electron entry and transfer via different routes from a variety of reductants (e.g. NADH, succinate, H_2) to equally varied terminal acceptors (e.g. O_2, fumarate, nitrate). Many bacterial respiratory enzymes are functionally redundant, such that one enzyme can be replaced by another better suited to function under the prevailing growth conditions. Depending on O_2 tension, some bacteria can also replace high-potential quinones like ubiquinone with low-potential ones like menaquinone. The free energy released from electron transfers is conserved in many bacteria as both proton- and sodium-motive force, which is used to power ATP synthase and drive active transport against concentration gradients. The mitochondrial respiratory complexes and some of their divergent bacterial counterparts are listed (Kaila and Wikström, 2021):

Mitochondrial enzyme	Bacterial enzymes (in addition to homologues of the mitochondrial ones)	Key differences in bacteria
NADH:ubiquinone oxidoreductase (complex I)	Type II NADH:quinone oxidoreductase, Na^+-pumping NADH:quinone oxidoreductase (Na^+-NQR)	Type II NADH dehydrogenases are not H^+-pumping, Na^+-NQR pumps Na^+ instead of H^+

Succinate dehydrogenase (complex II)	Fumarate reductase (QFR)	QFR catalyses the reverse reaction in anaerobic respiration
Ubiquinol-cyt *c* oxidoreductase (complex III)	Alternative complex III	No structural similarity
Cyt *c* oxidase (complex IV)	Quinol oxidases (cyt aa_3-600) cyt *bd* oxidases, cyanide-insensitive oxidases (cyt *bb*)	Directly oxidise quinols, can either be H^+-pumping or not, lack haem *a* and Cu centres

The maintenance of PMF is a priority for bacteria as membrane potential (ΔΨ) is crucial for key physiological processes in addition to oxidative phosphorylation, including flagellar motility, cell division, pH regulation, membrane transport and sensing mechanisms (Benarroch and Asally, 2020). In *E. coli*, it was shown that PMF can change within tens of milliseconds and is instantaneously homogenised across the membrane; this implies that a local change in PMF is experienced simultaneously by all PMF sources/sinks in the bacterial membrane and can allow modulation of global PMF generation/consumption (Biquet-Bisquert et al., 2023). It is known that many bacterial ATP synthases can hydrolyse ATP instead to generate PMF (Feniouk, Suzuki and Yoshida, 2007; Meyrat and von Ballmoos, 2019). Under energy-limited fermentative conditions, for example, ATP hydrolysis is supplemented with electrogenic symport of protons and weak organic acids to generate a sufficient PMF (Trchounian and Trchounian, 2019). Therefore, it is expected that germinating bacterial spores would also reestablish a ΔΨ as quickly as possible to restart essential processes as they return to life – when and how they do it is not yet understood.

1.6. The germination cascade and its energetics in *Bacillus* spores

1.6.1. Key proteins in germinant sensing and CaDPA release

Dormant *Bacillus* spores sense the availability of nutrients using germinant (ger) receptors or GRs, which respond to specific ‘germinants’, typically sugars, amino acids, and ions. When germinants are recognised by their cognate receptors, the germination cascade is initiated to exit dormancy. The signal is somehow transduced from the GRs to the SpoVA channels, which

then start extruding the CaDPA chelate allowing rehydration to begin. Concomitantly, the cortex, composed of modified peptidoglycan (N-acetylmuramic acid as well as muramic acid-δ-lactam) undergoes degradation by cortex-lytic enzymes (CLEs) CwlJ and SleB, permitting bulk expulsion of CaDPA and inward movement of water. Complete cortex lysis leads to the expansion of the fully hydrated core and IM, and only at this level of hydration (comparable to a vegetative cell) it is thought that general metabolism is resumed in preparation for outgrowth (Christie and Setlow, 2020).

Most of what is known about GRs and SpoVA proteins has been inferred from mutagenesis, western blot, and fluorescence microscopy experiments as they have not yet been purified and studied *in vitro*. GRs are membrane protein complexes composed of three subunits designated -A, -B and -C. While -A and -B are integral membrane proteins (-A also has a large globular domain), C is a lipoprotein anchored to the outer leaflet of the IM. Different *Bacillus* species have between 2 to 7 GRs that recognise a variety of germinants, and it has been shown that GRs are clustered together in a “germinosome” for which another protein called GerD may serve as a scaffold; a spore can have 1-2 such germinosomes and the physical proximity may allow the receptors to bind to their cognate germinants in a cooperative manner (Griffiths et al., 2011; Yi et al., 2011; Breedijk et al., 2020; Wang et al., 2021). It has been estimated in *B. subtilis* that there are ~2500 GRs/spore (Stewart and Setlow, 2013). *B. subtilis* has 3 GRs (GerA, GerB, and GerK) that respond to L-alanine and L-valine, L-asparagine and L-alanine, and glucose and fructose respectively (Ross and Abel-Santos, 2009). *B. megaterium* has 6 GRs (GerA, $GerA_2$, GerK, $GerK_2$, $GerK_3$ and GerU) which respond to single germinants like glucose, L-proline, L-leucine and certain inorganic salts like potassium bromide (KBr), or respond to a mixture of glucose and either L-alanine, L-asparagine, or L-glutamic acid with functional redundancy (Gupta et al., 2013; Foerster and Foster, 1966; Rode and Foster, 1962).

The SpoVA channel proteins, at least three of which are encoded by the *spoVA* operon in all *Bacillus* and *Clostridium* species, are called SpoVAA, SpoVAB, SpoVAC, SpoVAD, SpoVAEa, SpoVAEb and SpoVAF (the three conserved proteins are -C, -D, and -Eb). SpoVAA, -B, -C, -Eb and -F are predicted to be integral membrane proteins, whereas -D and -Ea are soluble proteins. The functions of -A, -B, -D are undetermined, -C was shown to form a mechanosensitive channel (Velásquez et al., 2014), -Ea is a mobile, soluble protein of unknown function associated with the outer leaflet of the IM (Wang et al., 2022); -F has a high sequence identity with GR A subunit proteins but both -Ea and -F are not strictly required for sporulation or germination (Perez-Valdespino et al., 2014). Unlike the GRs, the SpoVA channel proteins are abundant and some are distributed across the IM (Stewart and Setlow, 2013; Griffiths et al., 2011; Gao et al., 2022).

The available X-ray structures of *B. subtilis* GerBC (PDB entry: 3N54), *Geobacillus stearothermophilus* GerD (PDB entry: 4O8W), the N-terminal domain of *B. megaterium* $GerK_3A$ (PDB entry: 6O59), and SpoVAD (PDB entry: 3LM6) have provided few insights into the structure and function of the germinant receptors or SpoVA channels (Li et al., 2010, 2019, 2014). It has become apparent over the years that structural characterisation of GRs and SpoVA proteins does not lend itself to X-ray crystallography.

More recently, Deep learning-based tools like AlphaFold (Jumper et al., 2021) have enabled accurate prediction of protein structures to an unprecedented degree, with >200 million structural models currently available in the AlphaFold database. For the spore field, this meant that high-quality models of membrane proteins like GRs and SpoVA channels could now be generated and studied, to some extent eliminating the arduous task of disrupting spores and isolating these proteins from spore membrane preparations. For example, mutational analyses guided by the AlphaFold-predicted structure of the *B. subtilis* GerA receptor B subunit strengthened the case for B subunits containing the germinant-binding pocket (Artzi et al., 2021). Using a similar approach for SpoVA channel proteins, it was proposed that a minimal channel formed by SpoVAC and SpoVEb with SpoVAD as a cytoplasmic plug was required for CaDPA import during sporulation and export during germination (Gao et al., 2022). Then, using the multimer modelling capabilities of AlphaFold (Evans et al., 2022), it was proposed that GRs are penta-/hexameric ligand-gated ion channels that, upon binding to the cognate nutrient germinants, release ions like K^+. This coordinates the opening of the SpoVA channels that release bulk CaDPA which allows progressive hydration of the spore core (Gao et al., 2023; Kilian and Bischofs, 2023).

1.6.2. Energetics of germination explored in the model system *B. megaterium*

Discovered in 1884 by Anton de Bary (Bary, 1884), *B. megaterium* is a Gram-positive, aerobic, endospore-forming bacterium renowned for its large size and a cell volume, reportedly 100 times that of the Gram-negative model organism *Escherichia coli* (Vary et al., 2007) – hence its name, which means ‘big beast’. It is considered soil-dwelling but is found ubiquitously. Owing to the large size of its vegetative cells and distinctive spores, *B. megaterium* has traditionally been used for morphological studies of cell division, cell wall biosynthesis, sporulation, germination, protein localisation, membrane lipid composition etc. (Vary, 1994). Its extensive metabolic capabilities (it can utilise >62 different carbon sources) likely enables it to thrive in diverse habitats, and has contributed to its emergence as an important organism

for biotechnological/industrial applications (Vary et al., 2007; Biedendieck et al., 2021). Reclassification of *B. megaterium* to a new genus *Priestia* was proposed a few years ago (Gupta et al., 2020), but the organism will be referred to by its basonym in this work for historical consistency.

In *B. megaterium* QM B1551 spores, glucose alone can lead to rapid germination, and the receptor GerU is involved in glucose recognition (Gupta et al., 2013; Christie and Lowe, 2007). A substantial release of monovalent cations (H^+, Na^+ and K^+) and CaDPA leakage starts immediately after glucose addition as the internal spore pH increases from 6.4-6.5 to 7.5 in the first 10 mins (Swerdlow, Setlow and Setlow, 1981). This could conceivably generate a PMF across the germinating spore membrane, but this has not been trivial to measure directly. Dormant *B. subtilis* spores display high autofluorescence because of their proteinaceous coat that can also adsorb the widely used (Strahl and Hamoen, 2010) potentiometric carbocyanine dyes like $DiOC_6(3)$ and $DiSC_3(5)$; the coat thus prevents potentiometric dyes from permeating the spore core (Magge et al., 2009). Another study employed a charge-neutral thioflavin-T (ThT) dye to demonstrate that dormant spores store a K^+ electrochemical gradient (Kikuchi et al., 2022), but this finding was disputed by a later study showing that like other dyes, ThT was simply adsorbed by the coat and could not reflect the membrane potential of dormant or germinating spores (Li et al., 2023).

Recently, early cation release was linked with the activation of the alanine germinant receptor GerA in *B. subtilis* with the suggestion that the germinant signal could be transduced to the SpoVA channel by this ion release. Bulk CaDPA release by SpoVA channel and hydration that starts soon after leads to the loss of initial absorbance/refractility, marking the initiation of detectable germination (Gao et al., 2023). However, it is curious that despite the renewed interest in electrochemical gradients and transmembrane charge movement during initiation of germination, the energetics of these processes are rarely considered (Moir, 2023). It is generally believed that the cations, CaDPA and water move along their respective concentration gradients, so their transport does not need to be powered – besides, spores are energetically depleted and have no measurable energy metabolism before loss of absorbance starts.

However, as will be discussed extensively in chapter 5, in *B. megaterium* which was used for these early influential metabolic/biochemical studies, NAD(P)H and ATP generation have been measured to start concurrently with absorbance loss (Setlow and Kornberg, 1970; Setlow and Setlow, 1977). Glucose uptake and O_2 consumption start not long after (Dills and Vary, 1978; Sano et al., 1988; Racine, Dills and Vary, 1979; Maruyama et al., 1980), along with the restoration of membrane fluidity and MK levels (Cowan et al., 2004; Laue et al., 2018;

Escamilla et al., 1988) as hydration progresses. At present, bioenergetic processes are not believed to be essential for the initiation of germination for three main reasons: a) none of the events mentioned above have been measured to precede loss of absorbance/rehydration, so the former cannot cause the latter, b) spores can initiate germination in the presence of various metabolic inhibitors and anoxia so oxidative energy metabolism is not required for rehydration to begin and, c) it is thought that a germinating spore cannot support any metabolic processes until complete cortex degradation and core rehydration is achieved (Korza et al., 2023b).

This conventional wisdom has seemingly discouraged new studies on how germinating spores restart bioenergetic processes that, based on everything we have discussed so far, would be at the heart of any organism's dormancy exit strategy. Reviewing the literature, one gets the impression that energy metabolism not being measurable during the initiation of spore germination has been erroneously conflated with it not being relevant to germination at all.

1.7. Electron microscopy to study bacterial spores

Bacterial spores were first visualised as refractile bodies with light microscopy by Cohn and Koch in 1876, and phase contrast microscopy is still how the transition of dormant phase bright spores to germinating phase dark spores is routinely observed. Nearly a century later, cytological studies by transmission electron microscopy revealed the spore ultrastructure (Rode, 1968; Rode et al., 1962), along with the morphogenesis during sporulation (Chapman, 1956) and germination (Santo and Doi, 1974). The more modern techniques of cryogenic electron microscopy/tomography (cryo-EM/ET) have now been used for studying the intricate organisation of spore coats and exosporia (Kailas et al., 2011; Rodenburg et al., 2014; Bauda et al., 2024), endospore appendages that may facilitate adhesion (Sleutel et al., 2023; Pradhan et al., 2021), septation and engulfment during sporulation (Khanna et al., 2019) and identification of the intracellular membrane reservoirs in dormant spores that allow inner membrane expansion during germination (Laue et al., 2018).

Cryo-ET studies of sporulation have also inspired the theory that spore-forming gram-negative bacteria (like the extant Negativicutes group), that possess the Gram-positive spore-forming ability as well as Gram-negative outer membranes could be a missing evolutionary link, evidence that a monoderm progenitor in a sporulation-like event gave rise to the diderm cell configuration. It is further hypothesised that the earliest cellular life may have been spore-forming – Earth as a young planet was cataclysmic and perhaps only sporulating lifeforms were able to survive and evolve further (Tocheva, Ortega and Jensen, 2016).

In addition to whole cell/spore morphogenetic studies, cryo-EM is being applied to characterising the large protein machines involved in sporulation, e.g. a 600 kDa 30-mer complex of the SpoIIIAG extracellular domain, that is part of a “feeding tube” between the forespore and the mother cell (Zeytuni et al., 2017). Structural/biochemical approaches are required to understand functional proteins involved in germination as well. AlphaFold protein structure predictions for Ger receptors and SpoVA channel proteins combined with persuasive genetic evidence has recently reinvigorated the field with new models of how the germinant signal is received and transduced to end dormancy. Going forward, these models must be augmented with biochemical and biophysical evidence. Cryo-EM structures to pursue include receptor-germinant complexes because there is still no direct experimental evidence for germinants binding to their cognate receptors; and the SpoVA channel complexes to probe the exact mechanism of CaDPA transport – is CaDPA transported as a chelate, is the transport active or passive?

1.8. Aims of the thesis

Bioenergetic processes play an understudied and underappreciated role in *Bacillus* spore germination. The Ger receptors, SpoVA channel proteins, and respiratory complexes are membrane complexes that lend themselves more readily to structure determination by cryo-EM. For these structures to be the most physiologically relevant and informative, proteins should ideally be isolated from dormant spore membranes. However, the inner membranes are difficult to access and purify because of the multi-layered spore architecture.

In this thesis, we aimed to address the paucity of methods for spore membrane protein biochemistry using *B. megaterium* QM B1551 as our model organism. Detailed in chapter 3, this involved optimisation of protocols for spore disruption, membrane isolation, and purification of large membrane complexes in a structurally intact and functional state for further BN-PAGE and proteomic analyses. Chapter 6 describes a serendipitous cryo-EM structure of the complex II enzyme succinate dehydrogenase obtained from crudely enriched native membranes of wild-type *B. subtilis* cells. Work in chapter 6 may be viewed as a pilot test for what could be attempted with high-quality spore membrane preparations in future.

Regarding the bioenergetics of spore germination, the aim was to bring old and new observations together, reappraise these data through the lens of modern bioenergetics, and propose a model for how germinating spores restart energy metabolism. Presented in chapters 4 and 5, this work involved traditional spore germination assays, enzymatic detection

of glucose consumption and H_2O_2 production, O_2 consumption measurements and a novel haem remission spectroscopy technique to understand the nature of energy metabolism in germinating spores of *B. megaterium* QM B1551. Based on this we propose a revised timeline of events in germination, where glucose serves as both a signalling molecule and an exogenous energy source, oxidative phosphorylation and spore rehydration start concurrently, and electron transport precedes detectable rehydration.

Chapter 2: Materials and methods

2.1. Bacterial strains

Wild-type and mutant *Bacillus* spores were provided by Dr. Graham Christie (Department of Chemical Engineering and Biotechnology, University of Cambridge, UK). From these, spore stocks were raised that were stored at -20 ℃ and 1-2 µL of this was used as inoculum for a 5 mL starter culture in all subsequent experiments. Strains used in this work are:

Strain	**Genotype/phenotype**
B. subtilis 168	Wild-type
B. megaterium QM B1551	Wild-type, contains 7 plasmids (Eppinger et al., 2011)
B. megaterium PV361	Plasmid-less derivative of strain QM B1551
B. megaterium PV361 Ger-null pHT-GerU*	PV361 Δ*gerKK*$_2$*AA*$_2$ + pHT-*gerU** (*gerUA*+*gerVB*+*gerUC*) (Gupta et al., 2013)

2.2. Composition of culture media used

1. LB broth/agar (Melford Laboratories Ltd), per litre of dH_2O (dH_2O):

Yeast extract	5 g
Casein digest peptone	10 g
NaCl	10 g
Agar	12 g

   Pre-buffered with 10 mM Tris/Tris-HCl (pH 7.2 at 20 °C). Media were autoclaved before use.

2. 2x Schaeffler's medium (2xSG) for *B. subtilis* sporulation (Leighton and Doi, 1971), per litre of dH_2O:

BD Difco™ Nutrient Broth	16 g
KCl	2 g
$MgSO_4.7H_2O$	0.5 g
Agar	17 g

The pH was adjusted to 7 with 1 M NaOH and autoclaved. After the medium was cooled down to 55 °C, the following were added (membrane-sterilised solutions):

1 M $Ca(NO_3)_2$	0.5 mL
0.1 M $MnCl_2.4H_2O$	0.5 mL
1 mM $FeSO_4.7H_2O$	0.5 mL
50% (w/v) glucose	1 mL

3. Supplemented Nutrient Broth (SNB) for *B. megaterium* sporulation (Shay and Vary, 1978; English and Vary, 1986), per litre of dH_2O:

BD Difco™ Nutrient Broth	8 g
Glucose	1 g
KCl	1 g
$MgSO_4.7H_2O$	0.25 g
$CaCl_2.2H_2O$	0.15 g
$MnCl_2.\ 4H_2O$	4 mg
$FeSO_4.7H_2O$	0.3 mg

The pH was adjusted to 7.2 before the medium was autoclaved.

2.3. Culture conditions, spore harvesting and washing

For *B. subtilis*, 1 mL of the starter culture (grown in LB broth at 37 ºC until mid-late exponential phase) was plated on ~230 mL 2XSG agar in a square bioassay dish and incubated at 37 ºC for 48 hours. The spores were scraped off the plate and suspended in ice cold dH_2O. This was followed by centrifugation at 18K RCF for 10 mins. The pellet was resuspended in fresh cold dH_2O and centrifuged again. This was done at least 6 times until the appearance of the pellet was satisfactory (uniform white colour). The final clean pellet was resuspended in 5-10 mL of autoclaved ultrapure water and stored on ice in the cold room at 4 ºC.

For *B. megaterium*, 1 mL of the starter culture (grown to late exponential phase in LB broth at 30 ºC) was used to inoculate 500 mL of SNB medium in a 2 L baffled flask. The flask was incubated at 30 ºC with shaking at 225 rpm. The spores were harvested after 2.5 days by centrifugation at 4K RCF for 20 mins at 4 ºC. The pellet was resuspended in cold dH_2O and centrifuged again. The spores were washed this way 5-6 times until the pellet had a uniform

pale orange/pink colour. The pellet was resuspended in 5 mL autoclaved ultrapure water and stored on ice in the cold room at 4 ºC.

2.4. Spore disruption and membrane isolation

B. subtilis spores were disrupted in the following manner:

1. Chemical decoating
   Spore suspension in water, 0.1 M of NaCl, NaOH and DTT each, 1% SDS in a 20 mL volume. Incubation in a water bath set at 80 °C for 1 hour, followed by extensive washing with cold dH_2O (18K RCF, 10 mins, 4 ºC)

2. Lysozyme treatment
   Decoated spores in 30 mL reaction mixture: 50 mM Tris-HCl pH 8, 100 mM NaCl, 5 mM EDTA, 2 $mg.mL^{-1}$ lysozyme (Roche Diagnostics). Incubated in a water bath set at 37 °C for 30 mins

3. Mechanical disruption
   30 mL lysozyme reaction mixture passed 4 times through the cell disruptor (Constant systems Ltd) at a pressure of 40 kilopound per square inch (KPSI)

4. Debris Spin
   Lysate from the cell disruptor centrifuged for 5-10 minutes at 18K RCF, a turbid supernatant obtained.

5. Membrane Spin
   Supernatant from the debris spin centrifuged for 2 hours at 50K RCF. The membrane pellets were resuspended in buffer (50 mM Tris-HCl pH 7.5, 50 mM NaCl) and stored at 4 ºC overnight.

B. megaterium spores were disrupted in the following manner:

1. Chemical decoating
   Spore suspension in water, 0.1 M of NaCl, NaOH and DTT each, 0.5% SDS in a 20 mL volume. Incubation in a water bath set at 37 °C for 1.5-2 hours, followed by extensive washing (5-6 times) with cold dH_2O (4K RCF, 10 mins, 4 °C).

2. Enzymatic treatment

   Decoated spores in a 15 mL reaction mixture containing 50 mM Tris-SO_4 pH 7.5, 50 mM NaCl, 1 cOmplete™, Mini protease inhibitor cocktail tablet (Roche Diagnostics), 0.01 $mg.mL^{-1}$ DNase I (Sigma-Aldrich), 5 mM $MgCl_2$, 1 $mg.mL^{-1}$ lysozyme. Incubated at 37 °C for 15-20 minutes. In other experiments, incubation was carried out at 4 °C for 45 minutes.

3. Mechanical disruption

   Lysozyme reaction mixture passed 4-5 times through the cell disruptor at 30 KPSI.

4. Debris spin

   Lysate from the cell disruptor centrifuged for 15 minutes at 4K RCF, a turbid supernatant with red colouration obtained. In other experiments, centrifugation was carried out at 50K RCF but the duration was varied between 15 and 30 mins.

5. Membrane spin and separation of the soluble fraction

   Supernatant from the debris spin centrifuged for 2 hours at 50K RCF, 4 °C. In other experiments, the supernatant from the debris spin was centrifuged for 1.5-2 hours at 100K RCF, 4 °C, or at 150K RCF, 4 °C for 15-16 hours. The red-coloured membrane pellet was resuspended in 3-4 mL 50 mM Tris-SO_4 pH 7.5, 50 mM NaCl buffer, homogenised using a 7 mL KIMBLE dounce homogeniser (Sigma-Aldrich).

   The supernatant from the 16-hour ultracentrifugation run was syringe filtered (Filtropur S 0.22 µm, Sarstedt), concentrated using a Vivaspin 20 30 kDa molecular weight cut off (MWCO) polyethersulphone (PES) centrifugal concentrator (Sartorius) to a ~5 mL volume, aliquoted and stored at -70 ºC.

6. Membrane washes

   Washed with 50 mM Tris-HCl/Tris-SO_4 pH 7.5, 50 mM NaCl buffer by high-speed centrifugation (50K RCF, 4 ºC, 1 hour) or ultracentrifugation (150K RCF, 4 ºC, 1 hour) twice. The washed membrane pellet was resuspended in 2-3 mL of lysis buffer using a dounce homogeniser, aliquoted and stored at -70 ºC. This step was introduced based on work with Ms. Hardman (chapter 3).

2.5. DDM solubilisation and clarification

1. *B. subtilis* membranes

   The overnight membrane pellet suspension was centrifuged the following day at 16K RCF, and the pellet was resuspended in 300 µL of fresh buffer. 60 µL of 10% n-dodecyl β-D-maltoside (DDM, GLYCON Biochemicals GmbH) was added (final concentration ~2%) and the mixture was left to incubate in the cold room with gentle agitation for 2 hours or less. The mixture was centrifuged at 16K RCF for 10 mins, the supernatant was transferred into a fresh tube and centrifuged again. The supernatant from this spin was passed through a 0.22 µm PES membrane filter just before it was loaded onto a pre-equilibrated column.

2. *B. megaterium* membranes

   Similarly, the membrane pellet suspension was centrifuged at 16K RCF, and the pellet was resuspended in 400 µL of fresh buffer. 80 µL of 10% DDM was added (final DDM concentration ~2%) and the mixture was left to incubate in the cold room with gentle agitation for 2 hours or less. The mixture was centrifuged at 16K RCF for 10 mins, the supernatant was transferred into a fresh tube and centrifuged again. The supernatant from this spin was passed through a 0.42 µm cellulose acetate membrane filter just before it was loaded onto a pre-equilibrated column.

   In later experiments, solubilisation was carried out for 1 hour with 1% DDM in a 10 mL volume such that the total protein concentration was 10 $mg.mL^{-1}$. The DDM extract was clarified with centrifugation, syringe filtered, and applied to a pre-equilibrated column.

2.6. Size-exclusion chromatography and ion-exchange chromatography

Size-exclusion chromatography (SEC) was performed using the following columns with a ~24 mL column volume (CV): Superdex 200 Increase 10/300 GL, Superose 6 Increase 10/300 GL (Cytiva) using method runs (500 µL sample loaded, isocratic elution over 1.5 CVs, 0.5/0.25 mL fractions) implemented on an Akta Pure Chromatography system (Cytiva) at room temperature. On an Akta Micro system (Akta Pure except with small-volume tubing), a 50 µL sample was loaded onto a Superose 6 3.2/300 column (~2.4 mL CV, Cytiva). Isocratic elution

was performed over 1.5 CVs and 50 µL fractions were obtained either at room temperature or at 4 ºC.

Anion exchange chromatography (AEX) was performed using 1 mL HiTrap Q FF columns (Cytiva) at room temperature using an Akta Pure system. 1 M NaCl-containing buffers were used for gradient elution. 0-100% or 0-50% gradients were implemented using a method run over elution volumes of 120 mL and 100 mL respectively, and 0.5/0.25 mL fractions were collected.

The buffers used are described for each experiment along with the results in chapter 3.

2.7. Denaturing sodium dodecyl sulphate polyacrylamide gel electrophoresis (SDS-PAGE)

Polyacrylamide gels of desired percentages (7.5, 12 and 15%) were prepared using a Mini-PROTEAN Tetra Handcast System (Bio-Rad Laboratories). The recipes given here were used to prepare the resolving gels, the stacking gels, and the sample loading buffers. The glass plates and the spacer were assembled and checked for leakage, then the resolving gel was poured first. Depending on the percentage required, the mixture contained:

Components	**7.5% gel**	**12% gel**	**15% gel**
1.5 M Tris pH 8.8, 0.4% SDS (resolving buffer)	2.5 mL	2.5 mL	2.5 mL
30% Acrylamide:0.8% Bis-Acrylamide stock	2.5 mL	4.2 mL	5 mL
dH_2O	4.9 mL	3.2 mL	2.4 mL
10% Ammonium persulphate (APS)	50 µL	50 µL	50 µL
Tetramethylethylenediamine (TEMED)	8 µL	8 µL	8 µL

After the resolving gels were set, the stacking gel was poured, and combs were inserted to create 10/12/15 wells as required for the experiment. The stacking gel mixture contained:

Components	**3% gel**
0.5 M Tris pH 6.8, 0.4% SDS (stacking buffer)	1.3 mL
30% Acrylamide:0.8% Bis-Acrylamide stock	0.5 mL
dH_2O	3.2 mL
1% Bromophenol blue	10 µL
10% APS + TEMED	25 µL + 8 µL

Before the experiment, the comb was removed, the homemade gel or a 4-20% pre-cast gradient gel (Bio-Rad Laboratories) was fastened in the electrode assembly and placed in a Mini-PROTEAN Tetra cell tank (Bio-Rad Laboratories). The gel was immersed in ~700 mL running buffer containing Tris base and glycine, either with SDS added or without where specified. Typically, 5-10 µL of the sample was mixed with an equal volume of the sample loading buffer, prepared using the following recipe:

Component	**With β-mercaptoethanol**	**Without β-mercaptoethanol**
0.5 M Tris-HCl pH 6.8	1.2 mL	1.2 mL
Glycerol	1 mL	1 mL
10% SDS	2 mL	2 mL
1% Bromophenol blue	0.5 mL	0.5 mL
β-mercaptoethanol	0.5 mL	0 mL
Ultrapure water	4.8 mL	5.3 mL
Total volume	10 mL	10 mL

As these samples contained detergent-solubilised membrane proteins, they were not boiled. 5-10 µL of the Precision Plus Protein Standard (dual colour, Bio-Rad Laboratories) was used as the molecular weight marker. After suitable volumes of the samples and the marker were loaded (depending on the number of wells), electrophoresis was performed at 200 V for 30 mins at room temperature. Afterwards, the gel was rescued from the glass plates, rinsed with dH_2O, and fixed for 10 mins in a mixture of 50% ethanol and 10% acetic acid on a gel rocker. The fixing solution was removed with dH_2O, and the gel was destained by submerging the gel in dH_2O, heating it in the microwave, and gently agitating it on the gel rocker for 10 mins. After 2-3 washes, the gel was submerged in the staining solution (Coomassie brilliant blue G-250 dye and HCl), heated, and left to stain overnight on the gel rocker – this was needed to stain the low abundance membrane proteins for maximum contrast. The following morning, the gel was destained again. Once sufficiently destained, the gel was imaged.

2.8. Blue native polyacrylamide gel electrophoresis (BN-PAGE)

BN-PAGE analyses were performed using the well-established NativePAGE Novex Bis-Tris Gel System (Invitrogen, ThermoFisher Scientific). Instead of the denaturing anionic detergent SDS, Coomassie G-250 dye is utilised to impart a net negative charge to proteins that then retain their structure and function during and after electrophoretic separation. The 3-12% pre-

cast gradient gels were used that can resolve proteins in the molecular weight range of 30 kDa to 10 MDa. Routinely, two buffers were prepared: 250 mL cathode buffer and 500 mL running buffer, using 20X stocks of the running buffer and the cathode buffer additive (Invitrogen). These were stored in a cold room (4 °C) for a low temperature run.

The spore membranes were solubilised at specified protein:detergent ratios with gentle agitation for 1 hr at 4 ºC in a 50 µL volume. Membranes at a protein concentration of 2,4, and 8 $mg.mL^{-1}$ were solubilised with 0.5, 1 and 2% DDM. In another experiment, membranes at a protein concentration of 4 $mg.mL^{-1}$ were either solubilised with 0.5/1% DDM or 0.5/1% glycol-diosgenin (GDN, Anatrace). In all cases, the extracted proteins were clarified at 16K RCF, 4 ºC for 15 mins. The supernatants were transferred to fresh tubes and centrifuged again to remove any insoluble membrane material. All samples for BN-PAGE were prepared on ice in the following manner and kept cold regardless of the subsequent temperature of the BN-PAGE run:

Component	Volume
4x sample loading buffer (recipe from the NativePAGE manual used)	2.5-5 µL
Membrane protein sample	5-15 µL
1% G-250 additive	~1/4th the detergent concentration 0.5 µL for the elution fractions of SEC/AEX chromatography 3/6 µL for 0.5/1% detergent
Total volume	~25 µL

The insertion of the gel into the XCell SureLock Mini-Cell apparatus created two chambers. The cathode buffer (blue) was poured into the upper chamber and was in direct contact with the gel. The comb was carefully removed and the wells were rinsed out using a pipette with the cathode buffer. Samples were loaded into individual wells, along with 2-5 µL of either 2 $mg.mL^{-1}$ bovine serum albumin (BSA, 66 kDa monomer and 132 kDa dimer) or the NativeMark Unstained Protein Standard. Finally, the running buffer was poured into the lower chamber. Room temperature BN-PAGE runs were performed at constant voltage of 150 V for 90 mins. Low temperature runs were performed in a 4 °C cold room in two phases: for the first 60 mins, voltage was set to 150 V, and for the remaining 30-45 mins it was increased to 250 V. After the run was completed, a BN-PAGE gel was fixed and destained in the same manner as previously described for SDS-PAGE gels.

2.9. Cryo-EM grid preparation and screening

For experiments in chapter 3, UltrAuFoil R 1.2/1.3 300 mesh grids were glow discharged (PELCO easiGlow, Ted Pella Inc.) for 90 secs on both sides. Grids were prepared at 4 °C, relative humidity 100% in a Vitrobot system (Thermo Scientific). 2.5 µL sample was applied to the grid, and it was blotted for 4 secs with a force of -5. The grid was then plunge-frozen in liquid ethane, transferred to an autogrid box and stored in a liquid N_2 dewar. The grids were clipped by Dr. Blaza/Cryo-EM facility staff and loaded into the Glacios cryo-electron microscope (Thermo Fischer) using an autoloader. Thereafter, the EPU software was used to atlas the grids. Grids were screened one at a time at a nominal magnification of 290Kx, 240Kx or 150Kx depending on the samples.

For experiments in chapter 6, Quantifoil R 1.2/1.3 Cu 200 mesh grids (glow discharged for 60 secs on both sides) were used instead and prepared at 4 or 12 °C with a relative humidity of 80 or 100%. After sample application, grids were blotted for 2 secs with a force of either -5 or -1 and plunge-frozen as described.

2.10. Bicinchoninic acid assay for protein quantification

The protein concentration was measured using the Bicinchoninic acid (BCA) protein assay kit (Sigma-Aldrich) following the recommended protocol. BSA (2 $mg.mL^{-1}$) was used to make standards and a dilution series was prepared for the membrane preparations (1/10, 1/20, 1/40, 1/80, 1/160, 1/320, 1/640 and 1/1280). 25 µL standards/sample dilutions were pipetted in triplicate into a 96-well plate followed by 200 µL BCA reagent added to each well using a multichannel pipette. The plate was then incubated at 37 °C for 30 mins. Absorbance was measured at 562 nm in the SpectraMax ABS Plus microplate reader (Molecular Devices) and the data analysed using a predefined protocol in Softmax Pro 7.1.

During the chromatographic enrichment and separation of GDH and NOX activities from the whole spore soluble fraction, the protein concentration of SEC/AEX fractions was also measured with single-point readings. Dilution factors of 2.5 (after SEC I), 25 (after AEX) and 12.5 (after SEC II) were used – 25 µL of the diluted samples was used for assay as described, and the value obtained was multiplied by the dilution factor to get the protein concentrations of the SEC/AEX fractions.

2.11. NADH oxidation assays

The reaction buffer used was 50 mM Tris-SO4 pH 7.5, 50 mM NaCl in a reaction volume of 200 µL containing 200 µM NADH and 0.05 or 0.1 mg.mL^{-1} membrane protein. The volume of the buffer was adjusted accordingly where 1 mM KCN (solution prepared in the same buffer) was added. Data were recorded at 340-380 nm every 7 secs for 20 mins in the SpectraMax ABS Plus microplate reader maintained at 30 °C. Slopes (mAU.min^{-1}) for the linear region of the oxidation curves were calculated in the software Softmax Pro 7.1. Values of the slopes were used for further calculations:

Rate (µmol.L^{-1}.min^{-1}) = $\frac{\text{mAU.min}^{-1} \times 10^3}{\varepsilon \times \text{PL}}$,

where ε = 4810 M^{-1}cm^{-1}, extinction coefficient of NADH at wavelengths 340-380 nm (Blaza et al., 2014), and PL is pathlength (cm)

Rate (µmol.min^{-1}.mg^{-1}) = $\frac{\text{Rate } (\mu\text{mol.L}^{-1}\text{.min}^{-1})}{\text{Protein conc. } (\text{mg.L}^{-1})}$

2.12. Glucose dehydrogenase and NADH oxidase assays for activity enrichment

The whole spore soluble fraction was first subjected to SEC (Superdex 200 Increase 10/300 GL, 8 °C), then AEX (HiTrap Q FF, 21 °C) and lastly to SEC (Superdex 200 Increase 3.2/300 GL, 4 °C). Following each of these chromatographic steps, the resulting fractions were screened for two enzymatic activities using spectrophotometric assays at 30 °C in a 96-well plate format. To measure flavin-dependent NADH oxidase (NOX) activity, 50/5 µL of each fraction was added in a 200 µL reaction also containing 100 µM NADH and 0.5 µM FAD, and absorbance at 340-380 nm was measured every 15 secs or 6-7 secs for 30 mins. Similarly, to measure glucose dehydrogenase (GDH) activity, 50/5 µL of each SEC fraction was added in a 200 µL reaction also containing 100 µM NAD^+ and 1 mM glucose. These reactions were performed in a 50 mM Tris-SO_4 pH 7.5, 50 mM NaCl buffer. Using the Softmax Pro 7.1, slopes were obtained for the linear regions of the activity curves which gave a rate of absorbance loss or gain (NOX and GDH respectively) in mAU.min^{-1}. Additionally, BCA assays were carried out for each fraction as described previously. The slopes (mAU.min^{-1}), pathlengths and protein concentration measured for each reaction were used to calculate the specific NOX/GDH activity in µmol.min^{-1}.mg^{-1} for each fraction as follows:

Rate (μmol.L^{-1}.min^{-1}) = $\frac{\text{mAU.min}^{-1} \times 10^3}{\varepsilon \times \text{PL}}$, where ε (340-380 nm) of NADH = 4810 M^{-1}cm^{-1} and PL is pathlength (cm)

Protein concentration of the SEC or AEX fraction in the 200 μL reaction volume was calculated as:

Protein conc. (mg.L^{-1}) = $\frac{\text{Volume of fraction (μL)}}{200\ \mu\text{L}} \times \text{prt. conc. of fraction (mg. mL}^{-1}) \times 10^3$

Rate (μmol.min^{-1}.mg^{-1}) = $\frac{\text{Rate (μmol.L}^{-1}\text{.min}^{-1}}{\text{Protein conc. (mg.L}^{-1})}$

These rates were then plotted against the corresponding fraction number to visualise regions of enriched and separated NOX/GDH activities.

2.13. Histodenz density gradient purification

Washed spores were subjected to further purification using a Histodenz density gradient for subsequent experiments. 250 μL of the washed spore suspension was centrifuged and the pellet resuspended in 200 μL 20% Histodenz, which was layered on top of 1.2 mL 60% Histodenz in a 2 mL microcentrifuge tube. This was centrifuged at 16K RCF for 15 mins at 4 ºC, after which the supernatant containing vegetative debris was carefully removed. The purified spore pellet was resuspended, transferred to a fresh tube, and washed 3-4 times with ultrapure water at 4K RCF, 4 ºC to remove residual Histodenz after which the purified spores were resuspended in 250 μL ultrapure water. The optical density (OD at 600 nm) of such Histodenz-purified spore suspensions varied between 200-400. Purified spores were always stored on ice and all experiments were performed within 10 days of spore harvest.

2.14. Heat activation of spores

Depending on its OD, 40-100 μL of the Histodenz-purified spore suspension was added to 1 mL autoclaved ultrapure water in a 1.5 mL microcentrifuge tube and heat activated at 70 ºC for 20 mins in a heating block. The heat-activated spores were centrifuged at 4K RCF, 4 ºC for 10 mins and the pelleted spores were resuspended in 5 mL 50 mM potassium phosphate buffer pH 7.5. The assays were performed within 30 mins after this.

2.15. Oxic and anoxic germination assays

In a 96-well plate with the germinants/nutrient broth/inhibitors/ethanol and combinations thereof already present in triplicates, the spore suspension was added to start the assay using a multichannel pipette such that the initial absorbance was 0.6-0.8 in a 200 µL volume. Absorbance measurements at 600 nm were then started immediately in a SpectraMax ABS Plus microplate reader (Molecular Devices) set at 30 ºC with a read interval of 10 secs. Germination assays under anaerobiosis were carried out in an anaerobic/dry glove box system (Belle Technology UK Ltd) maintained at 2.5 ppm (0.00025%) O_2 with the same microplate reader inside. 100 mL of the phosphate buffer was first deoxygenated by bubbling N_2 through it with continuous stirring for 2 hours. Also, 0.18 g of glucose was weighed out in a 1.5 mL microcentrifuge tube and covered with parafilm (lid left open). Both were placed in the main port of the glove box along with a P200 multichannel pipette and a reagent reservoir and purged with N_2 for 30 mins. The buffer was stirred continuously, and all items were left in the main port overnight.

The following day they were moved into the glove box. The buffer was left stirring with the lid open for 2-3 hours and the parafilm was removed from the tube containing glucose to allow further exchange with the N_2 atmosphere. 1 mL of the deoxygenated buffer was used to prepare a 1 M glucose solution and all other dilutions. Spores were heat activated and centrifuged, the supernatant was discarded and the microcentrifuge tube with the spore pellet was taken into the glove box via the rapid port after 10 mins of purging with N_2 (lid left open). The pellet was resuspended in 5 mL of deoxygenated buffer and transferred into a deoxygenated 7 mL bijou tube, with repeated pipetting to flush the suspension with more N_2. Concentrated stocks of KBr (2 M) and nutrient broth (10x) were similarly taken into the glove box via the rapid port and diluted to suitable working stocks using deoxygenated buffer and plasticware. Thereafter the assay was performed in the way described previously.

The data were imported from the microplate reader software SoftMax Pro 7.1 into Microsoft Excel and the absorbance values across replicates was averaged. Absorbance measured at t=0 min (t_0) was taken as the initial absorbance, and the percentage loss of initial absorbance was calculated for all subsequent time points (t_p) as:

$$\% \text{ loss } (t_p) = \frac{t_0 - t_p}{t_0} \times 100$$

The % loss (t_p) values were plotted against time to give rehydration and outgrowth curves. The rate of rehydration was given by the first derivative of % loss (t_p) values. This was calculated using a window of 11 data points and the function SLOPE (known_ys, known_xs) which

returned the slope of the line at the centre of the window as the window moved to the next data point. The first derivative (% loss of initial absorbance/min) was then plotted against time.

2.16. Glucose uptake assays

10 microcentrifuge tubes containing 20 µL of Histodenz-purified spore suspension (O.D. 200-300) in 1 mL autoclaved ultrapure water each were heat-activated and centrifuged as described. Each pellet was resuspended in 285 µL 50 mM potassium phosphate pH 7.5 buffer and transferred to a 2 mL microcentrifuge tube. All 10 tubes were moved to a heating block set at 30 ºC, 300 rpm shaking, with their lids open. Germination was initiated with the addition of 15 µL 20 mM glucose (final concentration 1 mM in 300 µL volume) and tubes were incubated for the stipulated period (0, 2, 4, 6, 8, 10, 12, 14, 16, 20 mins) after which they were quickly relocated to a heating block set at 100 ºC for 10 mins to stop germination, then put in ice until all samples were ready. The tubes were then centrifuged at 16K RCF, 4 ºC for 15 mins. The supernatants were transferred to fresh tubes and centrifuged again to remove all the spore debris. These supernatants along with the 1 mM glucose control (without any spores) were then subjected to enzymatic glucose quantification using the D-Mannose/D-Fructose/D-Glucose assay kit (Megazyme Ltd) with minor modifications to the recommended kit protocol. Stoichiometric amounts of NADPH were formed in a 126 µL reaction volume containing 50 µL of each sample. This was performed in triplicates for each time point and the control. Thus, the amount of glucose in each replicate was given by:

$$\text{Glucose (M)} = \frac{126\ \mu\text{L}}{50\ \mu\text{L}} \times [\text{NADH}]$$

$$[\text{NADH}] = \frac{\text{A}_{\text{replicate}(340-380)} - \text{A}_{\text{blank}(340-380)}}{\text{PL} \times \varepsilon \times 2}$$

where $\varepsilon_{(340–380)}$ = 4810 $M^{-1}.cm^{-1}$ and absorbance of the reaction mixture was measured after 1:1 dilution in water (the water was first used for the blank measurement).

This gave the amount of glucose that remained in the medium after t mins of germination initiation. The triplicate values from the glucose assay were averaged for each time point ‘t’ and the control, and the amount of glucose consumed (mM) by t mins was calculated as:

$$\text{Glucose consumed (t)} = 1\ \text{mM} - [\text{glucose}]_{\text{t}}$$

In total this was done 3 times for PV361 spores, and 6 times for QM B1551 spores.

2.17. Hydrogen Peroxide assays

Hydrogen peroxide released by spores germinated with 1 mM/4 mM glucose was measured using an Amplex Red assay kit (Invitrogen, ThermoFisher Scientific). 200 µL reactions were set up in duplicate with 1x (0.5-0.6 O.D.) or 2x (~1 O.D.) heat-activated spores, 0.25 or 0.5 $U.mL^{-1}$ HRP and 50 µM Amplex Red reagent (10-acetyl-3,7-dihydroxyphenoxazine) in a 96-well flat-bottom black microplate (Nunc, ThermoFisher Scientific). The negative control reaction, also used for background subtraction during data analysis, contained 1x or 2x spores, HRP and Amplex Red but instead of glucose, 10 µL buffer was added. The reagent injectors present in the CLARIOstar microplate reader (BMG Labtech) were used to dispense 10 µL of the 20 mM/80 mM glucose stocks to initiate germination in all the other wells, which was immediately following by double orbital shaking at 300 rpm for 30 s, then raw fluorescence measurements every 15 secs for 30 mins at 30 ºC. The excitation/emission wavelengths used were (545-20)/(600-40) which are preset for the reaction product resorufin in the control software, number of flashes/well = 20, gain = 744 and focal height = 8.2 mm. The following H_2O_2 standards were prepared by serial dilution: 0 (blank), 0.16, 0.31, 0.66, 1.25, 2.5, 5, 10 µM. 200 µL reactions were set up in triplicate, containing 50 µM Amplex Red, 0.2 $U.mL^{-1}$ HRP, and the H_2O_2 standard dilution. A single-point measurement using the same optic settings was recorded in the microplate reader, and the blank-subtracted fluorescence values were used to plot a standard curve.

The blank-subtracted fluorescence values obtained for spores germinating with 1/4 mM glucose were plotted against time to compare the effect of spore and HRP concentrations. The rate of fluorescence increase was given by the first derivative of the blank-subtracted fluorescence values, calculated using a window of 5 data points. This first derivative (fluorescence/min) was then plotted against time.

2.18. Bioenergetic chamber experiments

100 µL of Histodenz-purified spore suspension (O.D. ~250) was heat activated and the spores pelleted as described in section 2.14. When resuspended in 5 mL 50 mM potassium phosphate buffer, an O.D. of ~3 was achieved for these experiments. In the bioenergetic chamber, a powerful white LED light source [Luxeon CZ 4000K-90 (Lumileds) used at a current of 300 mA] illuminated the spore suspension in a quartz crucible. The back-scattered light was collected in remission geometry (pathlength of ~39 mm where the light source and

output are 10 mm apart), passed through a spectrograph (Horiba) and complete spectra in the desired wavelength range were collected on a sensitive CCD camera (Andor Technology). The device also incorporates an O_2 optode which relies on the phosphorescence half-life of a platinum-porphyrin compound to measure O_2 concentration (Lee and Okura, 1997). In some experiments, a blend of N_2/O_2 was delivered through silicone tubing (Braintree Scientific. Inc.) submerged in the spore suspension to maintain a constant O_2 concentration throughout (Hollis et al., 2003; Kim, Ripple and Springett, 2011). O_2 consumption rate was calculated from the difference between the O_2 delivery to the spore suspension (where tubing was used) and the rate at which the O_2 concentration in the spore suspension changed during the experiment (Ripple, Kim and Springett, 2013; Rocha and Springett, 2019).

To prepare the device for an experiment, a wavelength calibration for the CCD was performed using a neon lamp, and the optode was calibrated by measuring O_2 dissolved in the experimental buffer exposed to air at the desired temperature vs. the zero-point achieved by the addition of the strong reducing agent sodium dithionite ($Na_2S_2O_4$). Then, with 5 mL buffer in the crucible, tubing in place, and the chamber sealed, the intensity of the LED light source was calibrated (serving as a blank measurement). Next, the chamber was unsealed and the heat-activated spore pellet (kept cold) was resuspended in the buffer. They spores were allowed to equilibrate for 10-15 mins in the re-sealed chamber. The experiment was initiated by the addition of a germinant at t=0 min and one spectrum was recorded every 20 ms in two phases (each phase is 10 ms long). The device was controlled using the accompanying software Palencia, created by Dr. Roger Springett (CellSpex, UK & University of York, UK).

In phase I, the LED was on, the CCD-spectrograph systems were on for 6 ms and off for 4 ms. Phase II is identical except that the LED is turned off. Phase II was subtracted from phase I primarily to remove the optode's phosphorescent signal. 25 such contiguous spectra were averaged to give a temporal resolution of 500 ms, i.e. 120 spectra/min. The spectrograph parameters used were:

Spectrograph position: 624.99 nm; Grating: 300g/mm@500nm; Wavelength range: 489.70 to 759.49 nm; Slit width: 100 µm; Binning: 1 pixel (px). The spectral resolution thus achieved was 1 nm. In some earlier experiments these settings were slightly modified.

The spectra were analysed by decomposition and manipulated (generation of averaged difference spectra, scaling, Savitzky-Golay smoothing, offsetting etc.) in the dedicated analysis software Gerona, also developed by Dr. Roger Springett. Where the Savitzky-Golay smoothing function (Savitzky and Golay, 1964) was used, the half width was 1 nm and the order was 2.

Decomposition of the haem attenuation spectra was performed using the following equation implemented in Gerona as the 'FIT:NIR' model:

$$C = A(S^T S)^{-1} S^T$$

where C is the unknown column matrix containing the concentration of each component, A is the column matrix containing the observed absorbances at each wavelength, and S is the known matrix containing the absorbance of each haem centre at each wavelength (Shinkarev, Crofts and Wraight, 2006; Kim, Ripple and Springett, 2011; Blaza et al., 2014).

Model spectra for the fitting template were taken from various sources. These are listed in the following table:

	Haem component	**Original source and additional manipulations performed**
1	Cyt *c*-550	Beef Heart bc_1 complex, cyt c_1 difference spectrum (reduced by ascorbate), measured by R Springett & Torsten Merbitz-Zahradnik on 6 Dec 2002, x-shifted by -3.1 nm
2	Cyt *c*-555	Beef Heart bc_1 complex, cyt b_H difference spectrum (oxidised by ferricyanide), measured by R Springett & Torsten Merbitz-Zahradnik, on 6 Dec 2002, x-shifted by -6.8 nm
3	Cyt *b*-558	Same as (2), but x-shifted by -3.8 nm instead
4	Cyt *b*-565	Same as (2), but x-shifted by 3.2 nm instead
5	Cyt *b*-571	Same as (2), but x-shifted by 9.5 nm instead
6	Cyt *a*-580	Digitised from Fig 6, the 120 min difference spectrum of fully reduced *B. subtilis* aa_3-600 with O_2 at a high pH (Lauraeus, Morgan and Wikström, 1993)
7	Cyt *a*-600	Haem *a* difference spectrum (Liao and Palmer, 1996), x-shifted by -5 nm
8	Cyt *d*-631	Digitised from Fig 3, the "O" spectrum (Borisov et al., 2011a), x-shifted by 3 and y-shifted by -0.01
9	Cyt *d*-650	Same as (8), but x-shifted by 22 nm instead

2.19. Cryo-EM data collection and processing

Cryo-EM data were collected in the YSBL X-ray and cryo-EM facility, University of York, UK using a 200 kV Glacios electron cryo-microscope (Thermo Scientific) equipped with an

autoloader, Schottky field emission gun (FEG) for a coherent electron beam, and a highly sensitive Falcon-IV direct electron detector to enable high-resolution work. Data were acquired as 40-frame movies in an automated manner using the EPU software at a nominal magnification of 240Kx, a calibrated pixel size of 0.574 Å, with a total exposure rate and total dose of 2.5 e^-/px/s and 50 $e^-/Å^2$ respectively.

As part of our collaboration with Dr. Sebastian Pintscher (Jagiellonian University, Poland), these data were processed using the CryoSPARC software package (Punjani et al., 2017) implemented on the PLGrid Infrastructure supercomputing cluster 'Athena' in Poland (Grant ID: PLG/2023/016614). In total, 2 datasets were processed separately and eventually merged to obtain the 3.1 Å map of *B. subtilis* SDH (succinate dehydrogenase) presented in Chapter 6. The number of micrographs processed and particles used for 3D reconstruction are listed:

Date	**Micrographs processed**	**Micrographs with SDH particles**	**Total SDH particles and resolution**
10 Feb 2023	16403	7129	11416, 3.23 Å
6 Apr 2023	25246	11260	18418, 3.49 Å
Datasets merged			27648, 3.13 Å

Movies were imported into CryoSPARC v4.4.0. Frames were aligned and corrected for both stage drift and beam-induced anisotropic motion using patch-based motion correction. The variable defoci and contrast transfer function (CTF) of different areas in each micrograph were estimated using patch-based CTF estimation. The Blob Tuner feature was used to calculate the best blob picking parameters based on ~200 manually picked particles and a diameter range of 110-130 Å. Particles were extracted (box size 512 px) from a small subset of micrographs (~1000) and images were downsampled to 128 px to make later steps faster. ~120K low-quality particles thus extracted were classified into 150 2D classes with a batchsize per class of 400 (particles to be classified every iteration). The most SDH-like particles obtained after a couple of such 2D classification cycles were used to train the Deep-learning based particle picking algorithm called Topaz (Bepler et al., 2019). Topaz-extracted particles were very heterogeneous and included ATP synthase, fragments of flagella, glutamine synthetase etc. From these classes, SDH-like particles were again picked and classified, and used to re-train Topaz. At this stage, the re-trained Topaz was used to find SDH particles in the entire dataset. After iterative 2D classification (batchsize of 400 per class) and removal of non-SDH particles, the best particles were used for an ab-initio reconstruction of SDH. This was subjected to a heterogeneous refinement that allowed simultaneous map refinement and particle classification. The particles belonging to the best class were re-extracted from their

respective micrographs (full box size 512 px) and lastly, with the imposition of C3 symmetry, subjected to non-uniform refinement which utilises an algorithm designed to improve resolution and map quality of membrane proteins (Punjani, Zhang and Fleet, 2020).

The difference in the datasets that yielded the 3.23 Å and 3.49 Å maps respectively was that peptidisc peptides were added in the former. However, in the map obtained, a DDM detergent belt was still present – perhaps the peptide concentration was not sufficiently high to displace the 0.01% DDM present which was seemingly enough to stabilise proteins even during the subsequent detergent-free SEC run. Therefore, aside from the 0.25 Å difference in resolution, it was found that these data were identical and could be merged. Particles from both datasets were merged and an ab-initio reconstruction was performed, followed by heterogeneous refinement, leading to the loss of 2186 lower-quality particles. The final non-uniform refinement resulted in our highest resolution map (3.1 Å).

Chapter 3: Cultivating and disrupting Bacillus spores for biochemical studies

3.1. Introduction

3.1.1. General principles of laboratory spore cultivation

For spore cultivation, Bacilli are routinely cultured in specialised media that first support maximal growth and then sporulation. But early work on sporogenesis in aerobic Bacilli led to a spore cultivation approach based on the idea of “endotrophic sporulation” which posits that sporulation does not require exogenous nutrients. Thus, vegetative cells removed from their growth media were washed and then could even be transferred to distilled water where they would initiate and complete sporulation (Hardwick & Foster, 1952). Vegetative growth and sporogenesis were thus thought to be mutually exclusive until it was observed that spores can be formed continuously in exponentially growing cultures (Schaeffer, Millet and Aubert, 1965). Further, it was shown that for commitment to and completion of sporulation, phosphate, a carbon source, and divalent cations, especially calcium, must be present in the medium (Greene & Slepecky, 1972; Slepecky & Foster, 1959). We now know that growth and sporulation conditions (medium composition, pH, temperature etc.) exert a great influence on heat resistance properties and refractility of the resulting spores, which are both important measures of their quality (Bressuire-Isoard, Broussolle and Carlin, 2018).

To achieve high spore yields, cultures of the two Bacilli of interest, *B. subtilis* and *B. megaterium* are incubated for 2-3 days in optimal sporulation media. While *B. subtilis* sporulates best on an agar surface, *B. megaterium* requires shaking incubation in a broth culture. Spores of differing densities are obtained which reflects the difference in cell size between the two species; *B. subtilis* has a cell volume ~17 times smaller than *B. megaterium* [(Vary et al., 2007; Weart et al., 2007), Ms. Bethany Hardman’s calculations done as part of her MChem project at York]. To harvest and wash the spores of *B. subtilis*, higher centrifugation speeds are employed as compared to *B. megaterium*. Spores of both species are denser than the vegetative cell remnants present in the spore suspension. Extensive washing with fresh cold distilled water allows removal of major vegetative contamination and the sedimentation of spores as pellets. Further purification of spores using density gradient

centrifugation for reliable microbiological, sensitive biochemical and biophysical assays (Setlow, 2019) will be discussed in the next chapter.

3.1.2. Spore disruption and fractionation – principles and considerations

Dormant spores of *Bacillus* species have a multi-layered architecture as shown in Fig 1A. The coat, outer membrane and the peptidoglycan layers restrict access to the core membrane and the spore core. It is possible to disrupt spores by sheer mechanical force (e.g. sonication in the presence of glass beads) and achieve near-complete breakage (J. C. Vary, 1973; Wilkinson et al., 1977), but is this an uncontrolled approach which will damage the core membrane to varying degrees. In 1980, recognising the need for a gentler disruption method, Racine & Vary published a protocol they developed using *B. megaterium* QM B1551 spores (Racine and Vary, 1980). They combined the chemical removal of the outermost layers (coat and outer membrane) with lysozyme degradation of the peptidoglycan layers, followed by sonication which was interspersed with longer cooling cycles. The liberated membranes were then ultracentrifuged (using a sucrose density gradient) to obtain a clean membrane pellet. The resulting membranes had almost 10 times the specific NADH oxidase activity than previously reported for the KM strain of *B. megaterium* (Wilkinson et al., 1977; Wilkinson & Ellar, 1975), which suggested that the respiratory enzymes were not as damaged in their purer, better quality membrane preparations.

This dramatic improvement in NADH oxidation rates, however, should be caveated – the extent of vesicle inversion in any of these membrane preparations was not determined. As shown in Fig 1B, once spores (or cells) are disrupted, the membrane fragments form vesicles that either retain the same orientation of the respiratory chain as in the intact spore, or they are inverted such that the NADH dehydrogenase active site is exposed to exogenous NADH. Any disruption method will result in both right-side-out and inverted vesicles, but only the latter will allow NADH oxidation. Thus, for NADH oxidation rates to be comparable across membrane preparations, the fraction of vesicle inversion must be too. This can be determined by dividing the maximal NADH oxidation rates achieved in gramicidin-uncoupled vesicles by the rate obtained with pore-forming alamethicin [(Gostimskaya et al., 2003), Fig 1B]. The degree of vesicle inversion depends on the spore/cell disruption method employed so with an optimal protocol a consistent trend can be achieved across biological replicates, as the work with Ms. Bethany Hardman and Ms. Elodie Wells has shown (section 3.2.14).

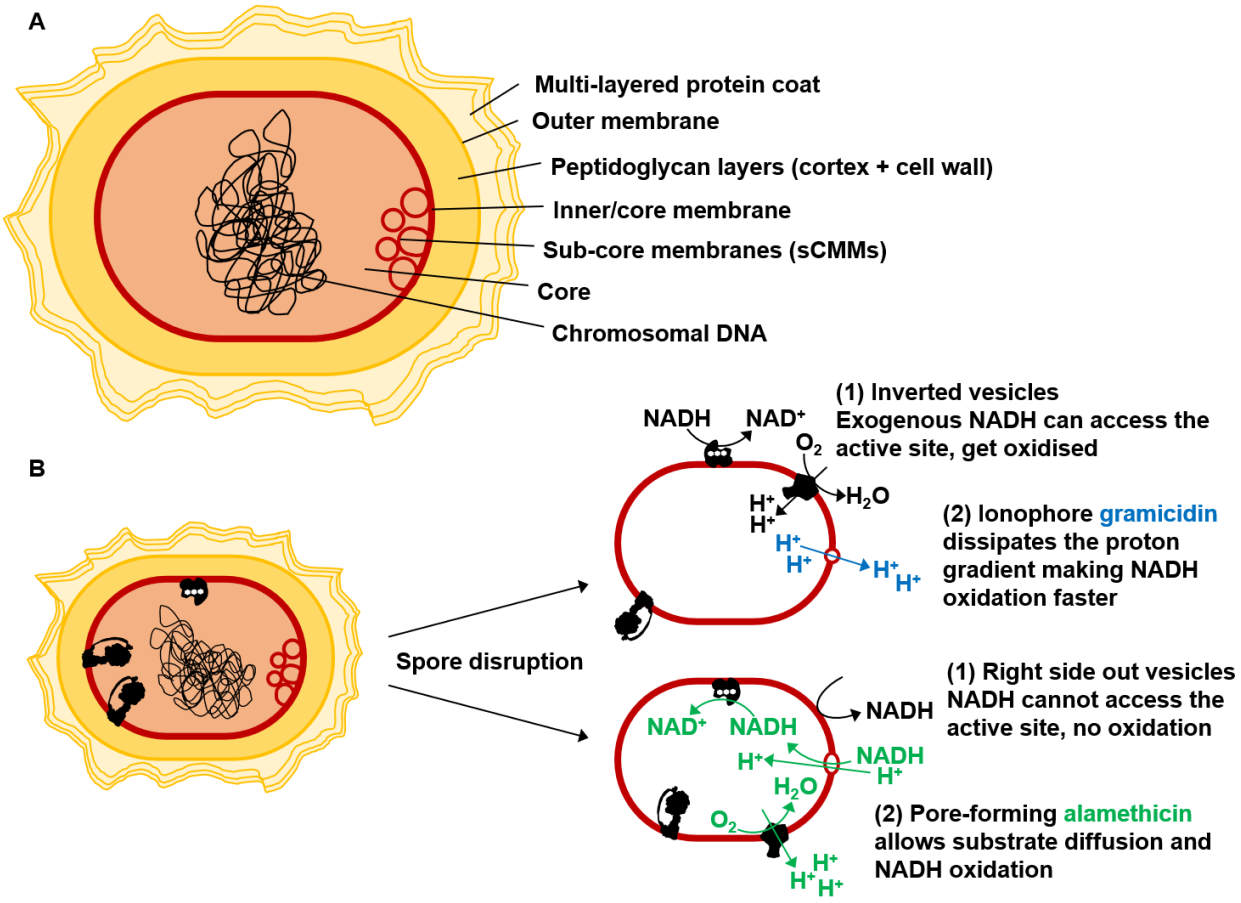

Fig 1: Situation of the inner/core membrane within the *Bacillus* spore structure and its topologies post-disruption. (A) The multilayered architecture of a *Bacillus* spore showing all the intervening layers that need to be removed as part of a spore disruption protocol to access the inner/core membranes (B) The effect of spore disruption on the inner membranes where the ETC is present. Isolated membranes will contain some vesicles that are inverted with respect to the intact spore (top image in B), whereas other vesicles will be right-side-out (bottom image in B). Inverted vesicles can oxidise NADH and pass electrons through the ETC to O_2. The ionophore gramicidin will dissipate the proton gradient generated during electron transport increasing the NADH oxidation rate in these vesicles, thus providing a maximal rate. In the right-ride-out vesicles, NADH cannot access the active site until the pore-forming alamethicin forms a large enough channel to allow passage of both protons and NADH through the membrane.

Nevertheless, the Racine & Vary method has been used in the field since with some modifications, which will be detailed later in the chapter alongside the spore disruption protocol that was eventually optimised in this work. In the literature, isolated spore membranes have been subjected to SDS-PAGE and NADH oxidation assays (Swerdlow and Setlow, 1984), western blot analyses for the identification of crucial germination proteins (Paidhungat and Setlow, 2001; Vepachedu and Setlow, 2005) and proteomic studies (Zheng et al., 2016), and for these downstream applications current methods have been sufficient. However, for

structural studies of natively expressed abundant membrane protein complexes like respiratory enzymes enabled by single-particle cryo-EM and strategies such as Build and Retrieve (Su et al., 2021), further modernisation and optimisation of these methods had to be carried out.

Our initial goal was to resolve large spore membrane protein complexes extracted by the mild detergent DDM (n-dodecyl β-D-maltoside) using blue-native polyacrylamide gel electrophoresis (BN-PAGE) as has been done for mitochondrial membranes (Blaza et al., 2014). These BN-PAGE bands would then be analysed by mass spectrometry to identify abundant proteins (like respiratory enzymes) in the dormant spore membrane that at their native and physiologically relevant expression levels could be feasible targets for structure determination by cryo-EM. Here we present the circuitous route taken towards this goal.

3.2. Results and discussion

3.2.1. Spore cultivation, harvest and washing

Culturing spores for subsequent experiments was straightforward as routine microbiology methods for both *B. subtilis* and *B. megaterium* are well-established. In Fig 2, pellets of washed *B. subtilis* and *B. megaterium* spores represent relative yields from 1 L culture. As compared to *B. subtilis*, spores of *B. megaterium* were easier to prepare in large quantities from broth cultures.

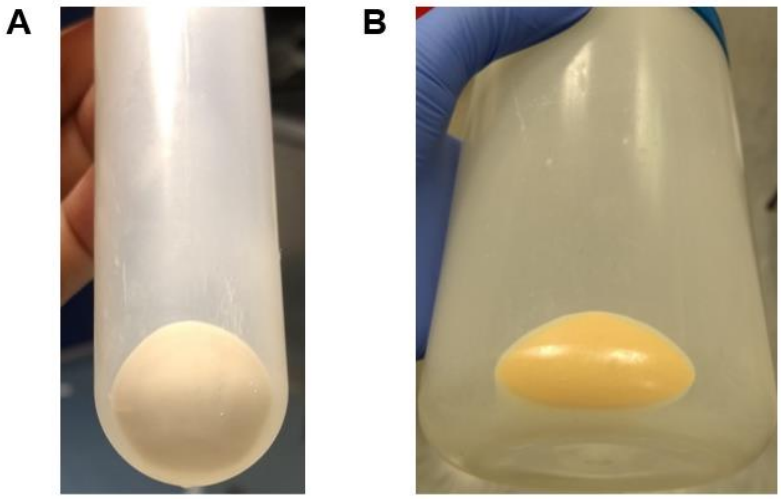

Fig 2. Spore yields from two *Bacillus* species. (A) *B. subtilis* pellet in a 40 mL round-bottom centrifuge tube, considerably smaller than the *B. megaterium* spore pellet in a 1 L centrifuge bottle (B).

3.2.2. Spore disruption and membrane isolation

Previous protocols for *Bacillus* spore inner membrane isolation (Racine and Vary, 1980; Swerdlow and Setlow, 1984; Vepachedu and Setlow, 2005; Zheng et al., 2016) served as the basis for further development in this work. The initial method used for membrane isolation from both *B. subtilis* and *B. megaterium* spores is described in chapter 2 (section 2.4). The membrane preparations following this method were not of the desired quality or quantity and did not lend themselves to analysis by BN-PAGE. This is what originally led to the introduction of size-exclusion and later anion exchange chromatography (SEC and AEX) steps – following DDM-solubilisation, we wanted to remove any small contaminants that could be interfering with BN-PAGE.

Chromatography and gel electrophoresis experiments to analyse membrane proteins from these sub-optimal preparations are detailed in sections 3.2.3 to 3.2.5 and the results are presented in Fig 3.

3.2.3. Experiments with *B. subtilis* spore membranes

Membranes isolated from *B. subtills* spores were solubilised with DDM (Fig 3A), and the DDM extracted proteins were loaded onto a pre-equilibrated SEC column. Fractions corresponding to peaks in the SEC elution profile were pooled and concentrated down to a volume of ~25 µL. These were later used for BN-PAGE and SDS-PAGE analyses. The smearing on the BN-gel was likely due to protein overloading and DNA contamination but showed bands of molecular weight >132 kDa, which was promising (Fig 3B).

However, attempts to get the same SEC elution profile as in Fig 3B with successive *B. subtilis* spore and membrane preparations failed (data not shown). For iterative optimisation, we needed spores that could be cultivated and prepared for disruption more easily. *B. subtilis* spores had to be scraped off plates and resuspended before they could be washed, only to give a fraction of the spore yield that could be obtained with *B. megaterium*. For both the ease

of handling broth cultures of spores and the higher yields, *B. megaterium* became our system of choice from this point onwards.

3.2.4. Experiments with *B. megaterium* spore membranes

DDM-solubilised *B. megaterium* membrane proteins were also subjected to SEC. Fractions corresponding to the peaks in the SEC elution profile were pooled and concentrated to a volume of ~25 µL. However, for unknown reasons, these samples could not be resolved using BN-PAGE and had to be analysed by SDS-PAGE only (Fig 3C).

As the BN-PAGE experiment was unsuccessful, we attempted running a “minimal” SDS-PAGE gel with SDS present only in the sample loading buffer – both the pre-cast gradient and running buffer used were also detergent-free. Additionally, sample loading buffer was prepared without the reducing agent 2-mercaptoethanol to make conditions even less denaturing. In contrast to soluble protein samples, detergent-solubilised membrane proteins should not be boiled during SDS-PAGE sample preparation due to their tendency to form very stable aggregates (Sagné et al., 1996). We also tested the effect boiling would have on our samples. The resulting gels are shown in Fig 3C. The bands on these gels were not sharp but samples representing the three SEC peaks showed distinct band profiles.

Peak A contained protein aggregates that were too big to enter the column matrix and were eluted in the void volume, which for this ~24 mL column is approximately 8 mL. The characteristic protein absorbance at 280 nm used in chromatographic systems to monitor protein elution is misleadingly high for protein aggregates, consistent with the prominence of peak A in the chromatogram (Fig 3C). The absence of strong protein bands in sample A was thus expected. The most obvious effect of boiling was observed in sample B – boiling destroyed bands of ≥130 kDa, giving rise to thick bands at ~40 kDa instead. The effect of the reducing agent was less apparent, indicating that there were not many disulphide linkages to be disrupted in these proteins.

Despite efforts to do everything the same way across spore/membrane preparations, the elution profiles from successive SEC runs were not perfectly consistent (Fig 3D). As BN-PAGE continued to be very difficult to optimise, we decided to focus on getting sharp SDS-PAGE bands instead for mass spectrometric analysis. This was not trivial either, given the complex nature of these samples. We therefore resorted to using different percentages of acrylamide to separate proteins on two different gels, so that the bands would be easier to cut out. This worked better on the 7.5% gel (50-200 kDa range), as compared to the 15% gel (12-45 kDa

range) which looked even busier due to the higher resolution it provided. The SEC run on 19 Nov 2020 produced samples that were eventually resolved on the SDS-PAGE gels shown in Fig 3D, and selected bands (numbered) from these gels were sent for MALDI-TOF MS analysis.

3.2.5. MALDI-TOF MS for identification of the proteins isolated/validation of inner membrane localisation

Bands from the three SDS-PAGE gels shown in Fig 3D were analysed in the Metabolomics & Proteomics Lab, Technology Facility, Department of Biology, University of York, by matrix assisted laser desorption ionization-time of flight mass spectrometry (MALDI-TOF MS). In total, 37 bands were analysed out of which 3 bands did not yield any results, most likely due to low protein abundance. Some respiratory enzymes were detected along with what could either be SpoVAF or a GerA subunit due to their high sequence identity (Table 1). This exercise allowed us to confirm that we were indeed working with the inner membranes of spores. We now needed to improve the quality of these membrane preparations.

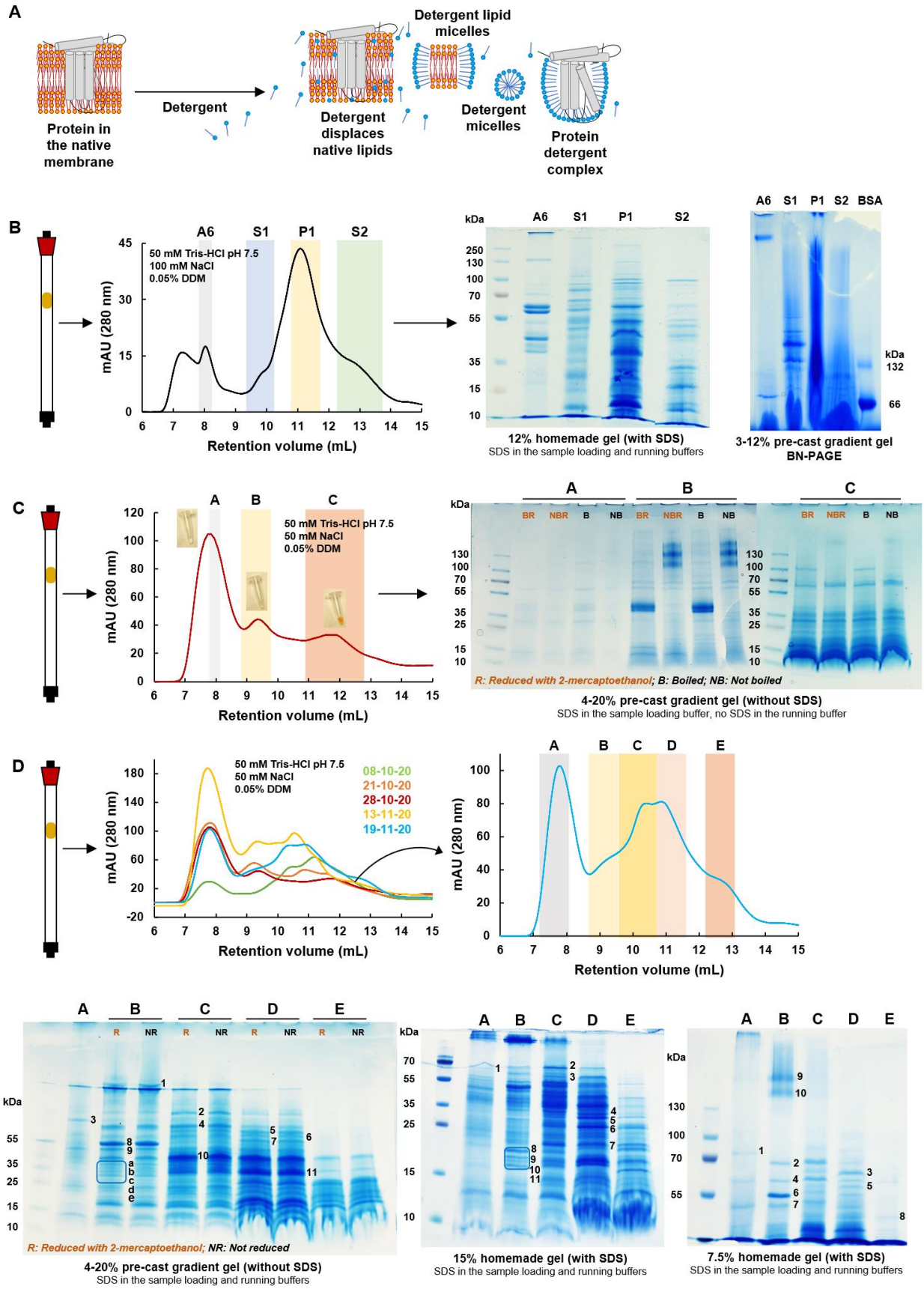

Fig 3: Chromatographic purification and gel electrophoretic analyses of *Bacillus* spore membrane proteins. (A) A cartoon of how membrane proteins are solubilised by a detergent

like DDM. Detergent molecules displace the native membrane lipids to form a micelle around the protein (protein-detergent complex), along with detergent only and detergent-lipid micelles. (B) Results of the experiment done with DDM-solubilised *B. subtilis* membranes, showing from left to right, the SEC chromatogram, SDS-PAGE and BN-PAGE gels. Fractions constituting the elution peaks designated A6, S1, P1 and S2 were pooled, concentrated, and analysed by gel electrophoresis. Bovine serum albumin (BSA) was used as the molecular weight indicator in the BN-PAGE gel. (C) For DDM-solubilised *B. megaterium* membranes, SEC was followed by a "minimal" SDS-PAGE also showing the effect of boiling and reducing agents on spore membrane protein samples labelled A, B and C. (D) A SEC chromatogram with elution profiles from 5 different experiments overlaid. Fractions corresponding to regions A-E in the 19 Nov 2020 SEC elution profile (blue) were pooled, concentrated, and resolved by SDS-PAGE employing different acrylamide percentages to get differential band separation. Bands numbered across these gels were sent for mass spectrometric identification. All the SEC runs were performed using a Superdex 200 Increase 10/300 GL column, and the elution buffers used are mentioned alongside each chromatogram.

Table 1: Protein hits from MALDI-TOF analysis of SDS-PAGE bands excised from gels shown in Fig 3D.

4-20% pre-cast gradient gel	
Band	Protein name
1	Porin
2	Clp protease ClpX Monooxygenase subunit
3	ATP-dependent zinc metalloprotease (FtsH)
4	Multifunctional fusion protein (SecDF)
5	DD-transpeptidase
6	Dihydrolipoyl dehydrogenase
7	RNA polymerase sigma factor SigA
8	ATP synthase beta subunit
9	Stage V sporulation protein AF
10	Pyruvate dehydrogenase E1 component subunit alpha
11	Flotillin-like protein FloA
a	Cyt aa_3 quinol oxidase subunit II α-ketoacid dehydrogenase subunit beta
b	No significant matches
c	ATP synthase gamma chain
d	ATP synthase gamma chain
e	AI-2E family transporter

15% homemade gel	
Band	Protein name
1	No significant matches
2	Outer membrane protein assembly factor BamA
3	DD-transpeptidase
4	Foldase protein PrsA
5	nlpA family lipoprotein
6	Amino acid ABC transporter substrate-binding protein
7	No significant matches
8	ATP synthase subunit a
9	ATP synthase subunit b
10	ATP synthase subunit b
11	Cyt *c* reductase iron-sulphur subunit
7.5% homemade gel	
Band	Protein name
1	ATP-dependent zinc metalloprotease (FtsH)
2	Protein translocase subunit SecDF
3	DD-transpeptidase
4	Dihydrolipoyl/dihydrolipoamide dehydrogenase DNA-directed RNA polymerase subunit beta
5	Nickel ABC transporter, nickel/metallophore periplasmic binding protein RNA polymerase sigma factor rpoD
6	ATP synthase alpha subunit ATP synthase beta subunit
7	GerA subunit/SpoVAF
8	NADH dehydrogenase YumB
9	Porin
10	Porin

3.2.6. Improving the quality of membrane preparations

In published spore disruption protocols, enzymatic treatment at 30/37 ºC was a point of concern. While the chemical treatment is inherently harsh, the peptidoglycan layers can

protect the core membrane and spore core from extensive damage – indeed, SDS-DTT extracted spores are still able to germinate in response to glucose (Vary, 1973). Enzymatic treatment that degrades the cortex exacerbates core rehydration, and inevitably the native state of the dormant spore is lost. However, if lysozyme degradation is performed at 4 ºC, these changes could be slowed down until mechanical disruption leads to loss of any remaining viability. To this effect, the following modifications to current protocols were implemented:

1. More spores for disruption (from 1 L to 3 L cultures, 3 times the starting material)
2. Lysozyme treatment at 4 °C
3. Ultracentrifugation instead of a high-speed spin to pull down more membrane material

3.2.7. Optimisation 1: 3x spore material, lysozyme treatment at 4 °C, ultracentrifugation for membrane spin

Using spores from 3 L of culture instead of only 1 L and an ultracentrifuge to harvest membranes gave a bigger and cleaner looking membrane pellet, which translated into more total protein content based on the absorbance at 280 nm measured by the Akta system during SEC (Fig 4B & C). However, higher protein content did not help achieve better separation of DDM-solubilised proteins, it may have even had the opposite effect. From fractions G9-H3 in Fig 4B, those highlighted in red were selected for cryo-EM grid preparation.

Another SEC run was performed with the DDM-extracted proteins but with 10% glycerol in the buffer as glycerol is routinely used to improve protein stability (Fig 4C). This gave a chromatogram that overall had the same profile as the SEC run without glycerol (Fig 4B) – most of the proteins were eluted in or very near the void volume. Fractions from regions I and II from the SEC run with glycerol were pooled separately and subjected to SEC again, this time without glycerol because glycerol reduces contrast in cryo-EM micrographs. Fractions D2 and B1 were selected from the SEC runs on regions I and II respectively, which resulted in sharper elution peaks (Fig 4D). On an SDS gel, all these fractions resolved to give nearly identical band profiles, suggesting no real separation had been achieved by SEC runs shown in Fig 4D. Nevertheless, grids were prepared with selected fractions that were successfully clipped and screened on a Glacios electron cryo-microscope, and Fig 4F shows the screening results. In the micrographs of fraction G9, large fragments of membranes could be seen. Moving away from the void volume, more distinct protein-like particles but mostly aggregates were observed.

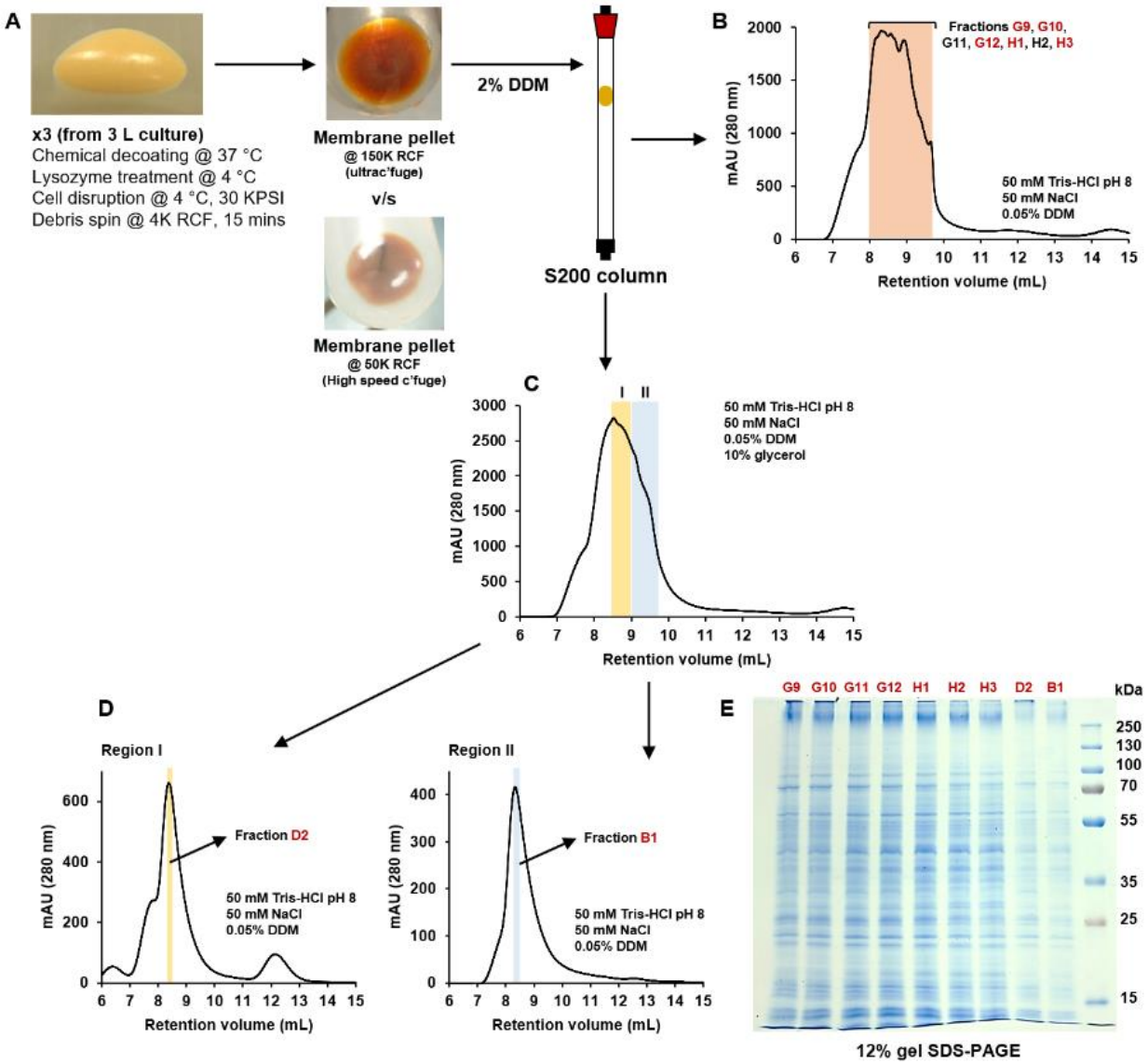
A
x3 (from 3 L culture)
Chemical decoating @ 37 °C
Lysozyme treatment @ 4 °C
Cell disruption @ 4 °C, 30 KPSI
Debris spin @ 4K RCF, 15 mins
Membrane pellet
@ 150K RCF
(ultrac'fuge)
v/s
Membrane pellet
@ 50K RCF
(High speed c'fuge)
2% DDM
S200 column
B
Fractions G9, G10, G11, G12, H1, H2, H3
50 mM Tris-HCl pH 8
50 mM NaCl
0.05% DDM
mAU (280 nm)
Retention volume (mL)
C
I
II
50 mM Tris-HCl pH 8
50 mM NaCl
0.05% DDM
10% glycerol
mAU (280 nm)
Retention volume (mL)
D
Region I
Fraction D2
50 mM Tris-HCl pH 8
50 mM NaCl
0.05% DDM
mAU (280 nm)
Retention volume (mL)
Region II
Fraction B1
50 mM Tris-HCl pH 8
50 mM NaCl
0.05% DDM
mAU (280 nm)
Retention volume (mL)
E
G9 G10 G11 G12 H1 H2 H3 D2 B1
kDa
250
130
100
70
55
35
25
15
12% gel SDS-PAGE

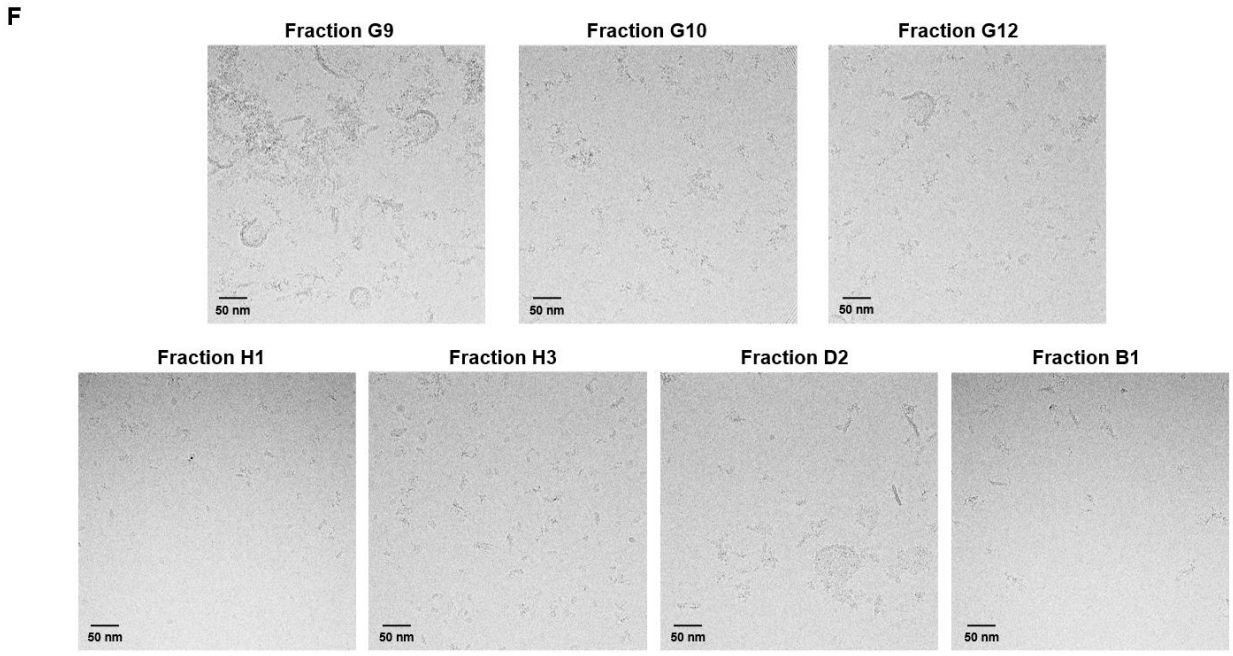
F
Fraction G9
Fraction G10
Fraction G12
Fraction H1
Fraction H3
Fraction D2
Fraction B1
50 nm

Fig 4. Results of optimisation 1. (A) Three times more spores were disrupted for membrane isolation with lysozyme treatment carried out at 4 °C. Images of the membrane pellet harvested by ultracentrifugation, and a membrane pellet obtained previously by high-speed centrifugation are shown for comparison. 2% DDM was used for membrane solubilisation, and the following clarification the DDM-extracted proteins were subjected to two SEC runs. Chromatograms of the SEC run without glycerol (B), and with 10% glycerol in the elution buffer (C). The elution profiles looked similar with most of the proteins eluting in and around the void volume. (D) Chromatograms of SEC runs performed (without 10% glycerol) on fractions corresponding to regions I and II in (C). Elution fractions highlighted in red from all SEC runs were subjected to SDS-PAGE analysis (E) and used for cryo-EM grid preparation. (F) Representative cryo-EM micrographs for each fraction, scale bar is 50 nm.

3.2.8. Optimisation 2: S6 column for SEC

Next, all other steps of spore disruption, membrane isolation and solubilisation were performed in the same way as before, but a Superose 6 Increase 10/300 GL column was used instead for SEC (Fig 5A). S6 columns have a wider fractionation range (5-5000 kDa) as compared to S200 columns (10-600 kDa), which we thought could help in separating the undesired membrane fragments from the large protein complexes that were also excluded by an S200 column. This intervention was not entirely successful either, though the SEC elution profile did suggest better separation of proteins away from the void volume (Fig 5B). Fractions from regions denoted I and II were pooled and subjected to a second SEC run – the resulting chromatograms are labelled accordingly in Fig 5C. Fractions marked in pale blue across the chromatograms were resolved using SDS-PAGE, along with all DDM-solubilised proteins ‘DDM’ and ‘SN’ which refers to the supernatant from the membrane spin. The SDS-PAGE gel in Fig 5D shows fractions from seemingly better separated regions I and II of the SEC chromatogram (Fig 5B) had nearly identical band profiles. Fractions highlighted in red were used for cryo-EM grid preparation, where fraction IIB was also gently concentrated to half the volume of the original elution fraction to give IIBx2. Grids were prepared and screened in the same way as before. Fig. 5E shows the results from this screening session. As already suggested by the SDS-PAGE band profiles, using an S6 column for SEC did not make a meaningful difference – we still observed large membrane fragments in the fractions closer to the void volume, and more dispersed aggregates in the fractions with a retention of 11-12 mL.

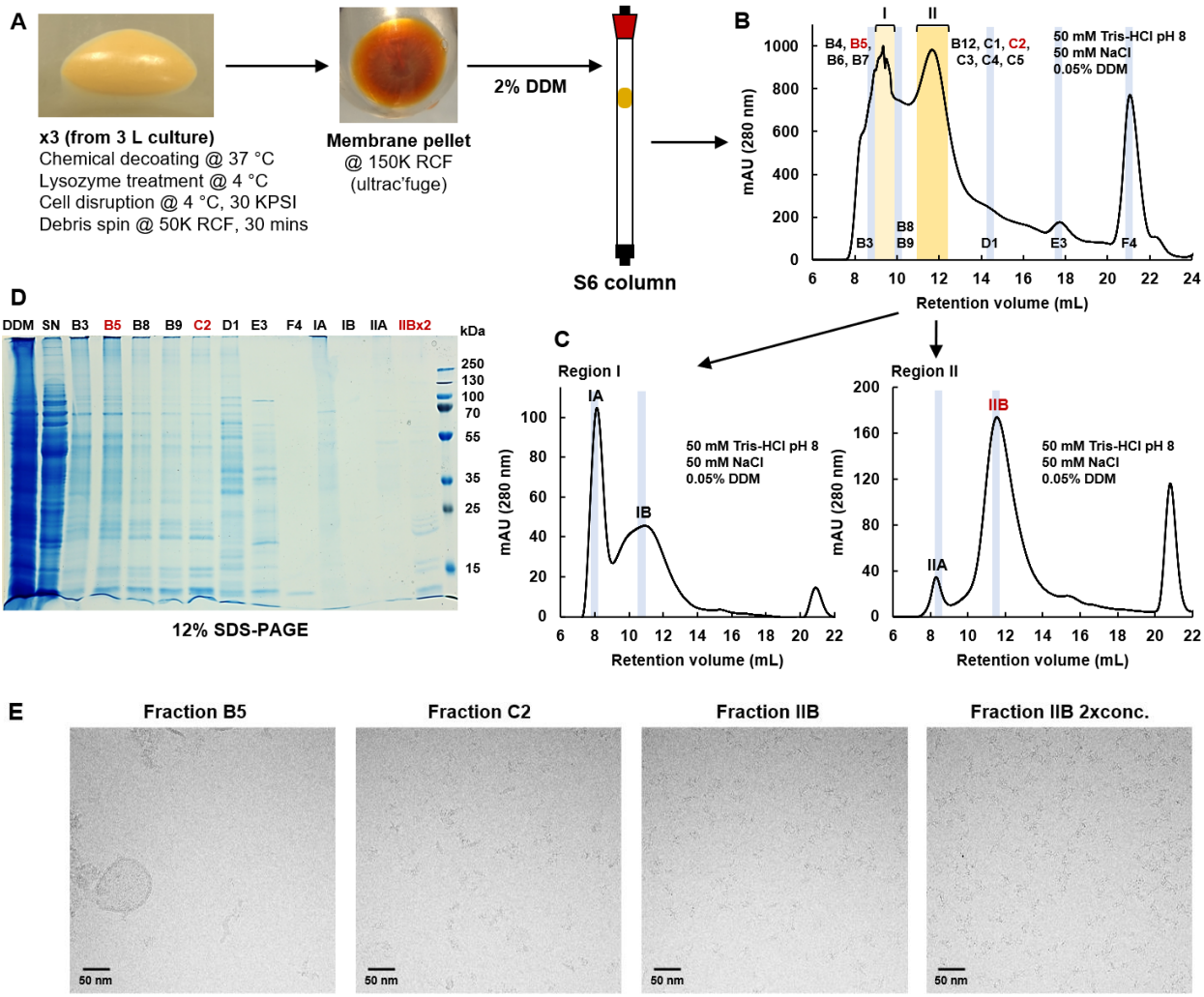

Fig 5. Results of optimisation 2. (A) Spores were disrupted for membrane isolation as described before. Membrane proteins solubilised with 2% DDM were separated by SEC using an S6 column, and the chromatogram is shown in (B). Fractions from region I (pale yellow) and II (dark yellow) were pooled, concentrated, and purified with another SEC run (C). Fractions shaded in pale blue and those highlighted in red were analysed by SDS-PAGE (D). Fractions highlighted in red were also used to prepare cryo-EM grids as before. (E) Representative cryo-EM micrographs for each fraction, scale bar is 50 nm.

3.2.9. BCA assay for protein quantification in the homogenised inner membranes

The presence of membrane fragments/vesicles in SEC fractions implied that membranes were not properly solubilised – this was probably because the detergent:protein ratio during solubilisation was not optimal. Moreover, membrane resuspension (performed by repeated pipetting) did not resuspend all the membrane fragment uniformly, which could also be a

contributing factor to the poor solubilisation by DDM. To solve this problem, the membrane pellet was processed in a dounce homogeniser until a uniform suspension was obtained. Then, a bicinchoninic acid (BCA) assay was performed for quantification of total protein concentration in the homogenised membranes, so that the detergent:protein ration could be controlled (Fig. 6B).

3.2.10. Optimisation 3: Homogenised membranes solubilised with 1% DDM, AEX (RT), S6 column for SEC using Akta Micro (RT), BN-PAGE (RT)

To achieve a more optimal detergent:protein ratio, solubilisation was carried out for 1 hour with 1% DDM in a 10 mL volume such that the total protein concentration was 10 $mg.mL^{-1}$. The DDM-solubilised membranes were clarified with centrifugation, syringe filtered, and applied to pre-equilibrated HiTrap Q FF columns to separate proteins using anion exchange chromatography (AEX). AEX utilises a positively charged resin that has an affinity for proteins with a net negative surface charge at a given pH. Bound proteins are then eluted using an increasing NaCl gradient, where the Cl^- ions displace the bound proteins – the more negatively charged a protein, the higher the salt concentration (ionic strength) needed for its elution.

The chromatogram of the AEX run is shown in Fig. 6C. Selected AEX fractions from peaks labelled A-E were resolved on a BN-PAGE gel, along with the supernatant from the membrane spin (SN). Peaks C, D and E had misleadingly high absorbance at 280 nm – the BN-PAGE gel showed that there were very few proteins in these fractions, so these were ignored. Fractions constituting peak B were concentrated and subjected to SEC using an S6 3.2/300 column (~2.4 mL column volume) on an Äkta Micro system. The small-volume tubing makes it ideal for working with sample and fractionation volumes in the microlitre range, thereby keeping proteins concentrated. Based on the BN-PAGE gel, it was difficult to say if any meaningful separation had been achieved with SEC (Fig 6D). It was also not clear how the apparent molecular weights of the most prominent and distinct bands correlated with the retention volumes of these complexes – S4 has the highest molecular weight band and lower molecular weight bands as well, yet it eluted after S2 and C which have a single prominent band of an intermediate molecular weight. This was perhaps an indication that the protein complexes were disintegrating during experiments. Nevertheless, this was the first successful BN-PAGE experiment with membrane proteins from *B. megaterium* spores.

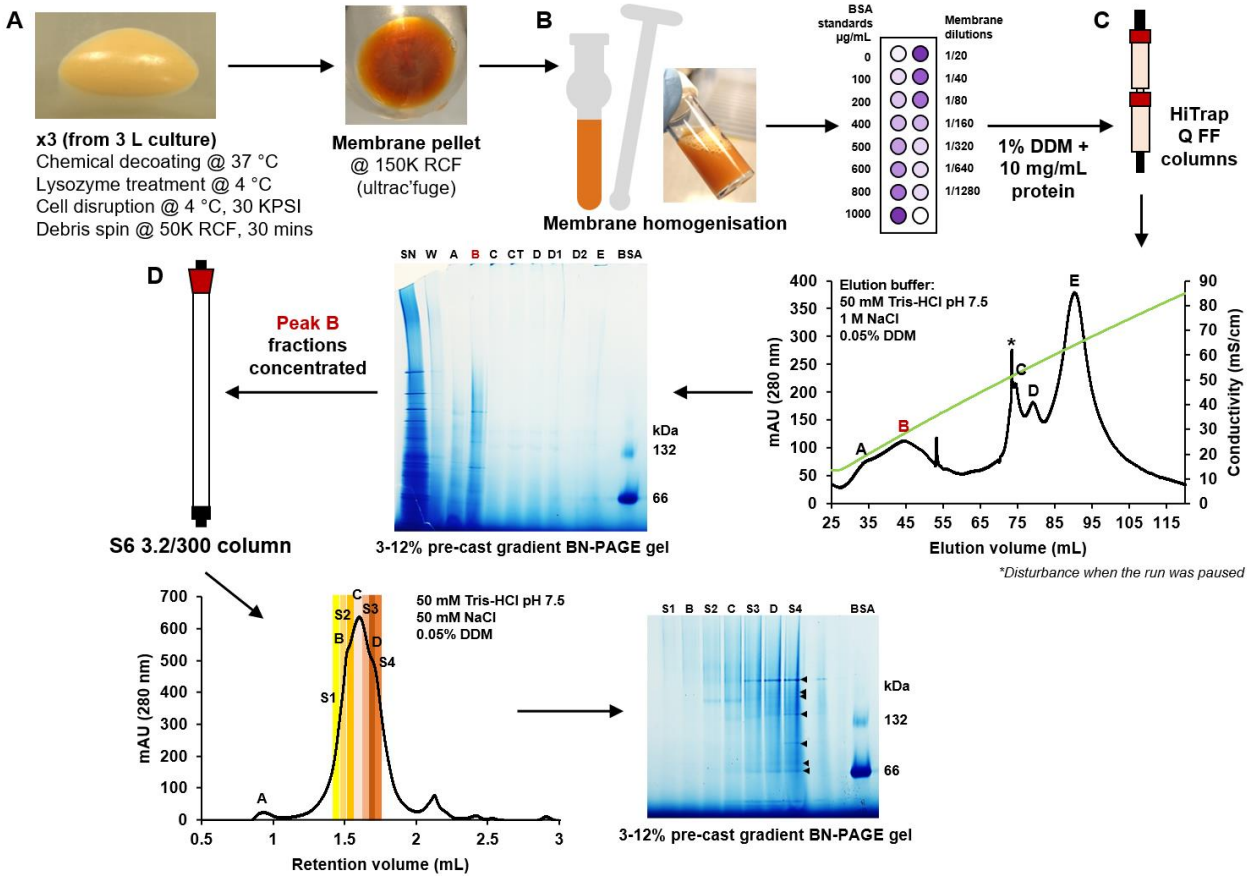

Fig 6. Results of optimisation 3. (A) Spores were disrupted for membrane isolation as described before. (B) The membrane pellet was homogenised using a dounce homogeniser, and an image of the brightly coloured suspension is shown along with a cartoon of the BCA assay performed with dilutions thereof to measure the total protein concentration. Membranes at a protein concentration of ~10 mg.mL^{-1} were solubilised with 1% DDM. (C) AEX chromatogram and BN-PAGE analysis of AEX elution fractions that constituted peaks A-E, along with membrane spin supernatant 'SN' and wash 'W'. The wash step after sample application during AEX removes any unbound proteins, and the gel showed that at pH 7.5 most proteins in the sample were bound to the column resin. Fractions of the broad AEX peak B were pooled and concentrated, and subjected to a SEC run using a ~2.4 mL S6 column and an Äkta Micro system. (D) shows the SEC chromatogram and BN-PAGE analysis of the labelled elution fractions. Arrowheads indicate the numerous protein bands resolved in fraction S4.

3.2.11. Optimisation 4: AEX (RT) with asolectin+CHAPS in the buffers, S6 column for SEC (peptidisc reconstitution) using Akta Micro (RT), BN-PAGE (RT)

Next, all other steps of spore disruption, membrane isolation and solubilisation were performed in the same way as before. However, in the buffers used for the AEX run, 0.1% (instead of 0.05%) DDM was added, along with 0.02% asolectin and 0.02% CHAPS (Blaza, Vinothkumar

and Hirst, 2018). CHAPS, a zwitterionic detergent, was used to dissolve asolectin, which is a granular powder of soyabean phospholipids. After extraction with DDM from their native lipid environment (Fig 3A), membrane proteins can be stabilised better with these soyabean phospholipids during the subsequent purification steps. The addition of asolectin+CHAPS evidently improved the stability of protein complexes during the AEX run (Fig 7B), which resolved better (more distinct bands) on the BN-PAGE gel as compared to the AEX BN-PAGE gel in Fig. 6C. Based on the differences in band profiles on this gel, fractions from regions denoted as I, II, III and IV in the AEX chromatogram were pooled and concentrated using a 30 kDa molecular weight cut-off (MWCO) centricon (Vivaspin 500). During this process, the volume was made up 2-3 times with 200 µL of a 0.5 mg.mL^{-1} peptidisc peptide solution – these short amphipathic bi-helical peptides form a disc around the membrane protein and no additional lipids are required for this reconstitution than the ones already present in the preparation (Carlson et al., 2018). The subsequent SEC runs were performed with a detergent-free buffer (Fig 7C), and selected fractions were resolved using BN-PAGE. These bands represented membrane proteins potentially reconstituted in peptidiscs.

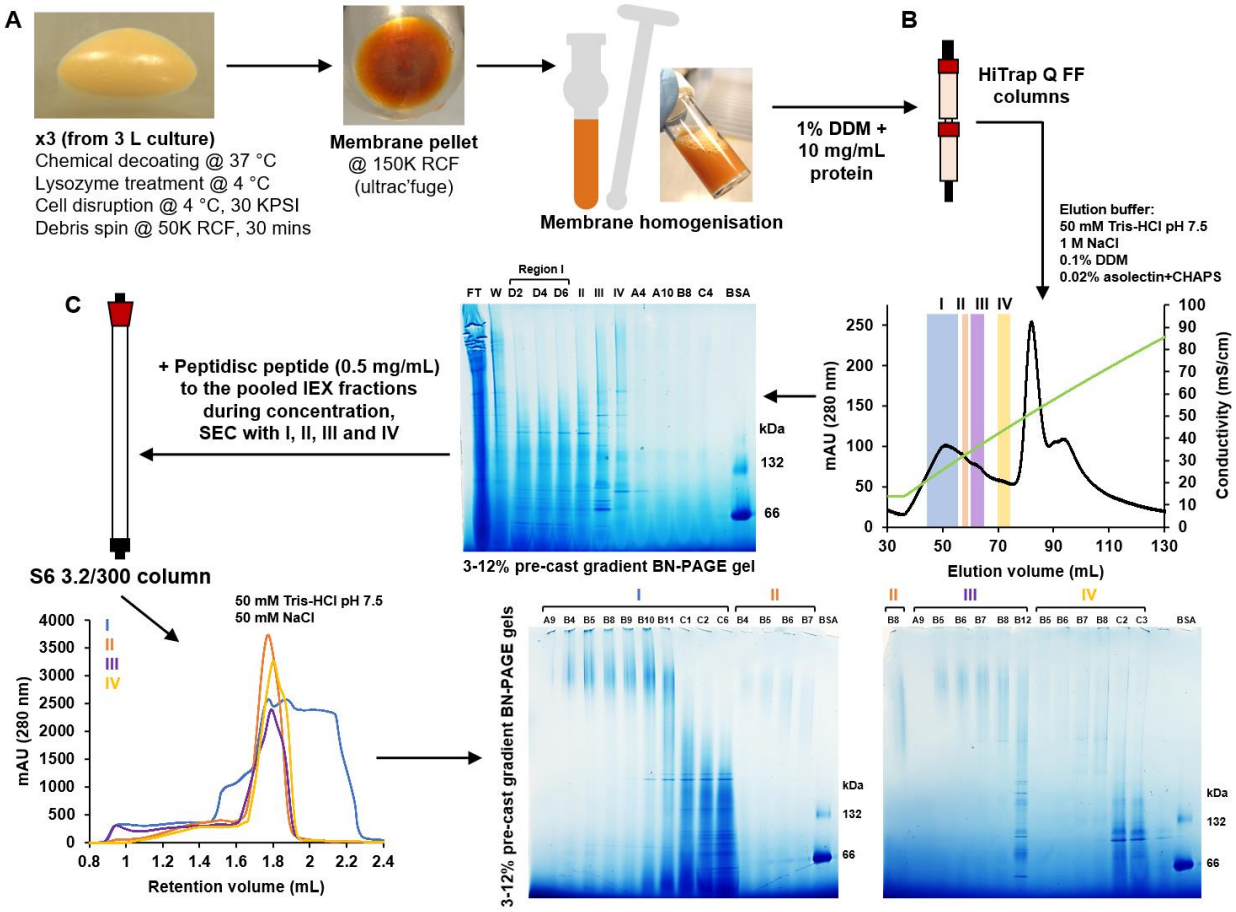

Fig 7. Results of optimisation 4. (A) Spores were disrupted for membrane isolation and the membrane pellet was homogenised as described before. Membranes at a protein concentration of ~10 mg.mL^{-1} were solubilised with 1% DDM. (B) The DDM-solubilised and

clarified membrane sample was applied to 2 connected 1 mL HiTrap Q FF columns for AEX chromatography. AEX buffers contained asolectin+CHAPS to further stabilise the detergent-solubilised membrane proteins. The BN-PAGE analysis of the AEX elution fractions is shown. Fractions corresponding to regions I-IV were separately pooled, and concentrated with the addition of peptidisc peptides. (C) Chromatogram showing the overlaid SEC runs performed with detergent-free buffer for 'on-column' peptidisc reconstitution. The accompanying BN-PAGE gels show potentially reconstituted protein complexes present in these SEC elution fractions.

3.2.12. Optimisation 5: Peptidisc reconstitution and BN-PAGE analysis at 4 °C

In this iteration, we wanted to test if we could further stabilise the DDM-solubilised membrane proteins by performing more steps of the protocol at 4 °C. AEX was still carried out at room temperature, and a longer 0-50% gradient instead of the 0-100% gradient was used for elution because previous results had shown that most of the proteins in these samples eluted with ~500 mM NaCl. By prolonging the 0-50% gradient, we therefore thought we could get better-resolved peaks, but this did not transpire. Nonetheless, fractions in the regions labelled S1, Peak, S2 and Tail (Fig 8B) were pooled and concentrated with peptidisc addition as before. Each sample was then subjected to SEC in detergent-free buffer but at 4 °C, and the subsequent BN-PAGE runs were also performed at 4 °C (Fig 8C). The peptidisc-reconstituted protein complexes were resolved as sharp distinct BN-PAGE bands especially in the S2 and Tail fractions. Compared to BN-PAGE gels in Fig 7C, these 4 °C gels had more distinct bands and less smearing in the lanes.

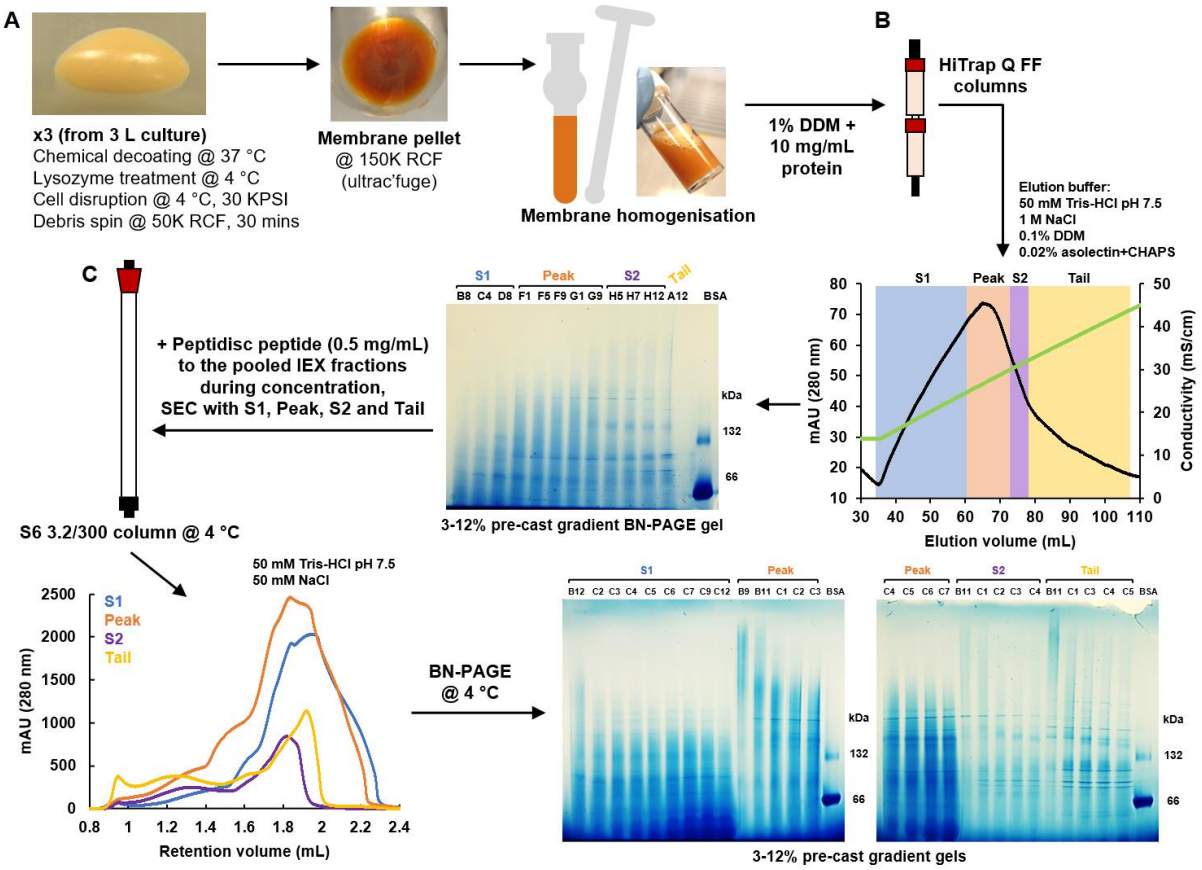

Fig 8. Results of optimisation 5. (A) Spores were disrupted for membrane isolation and the membrane pellet was homogenised as described before. Membranes at a protein concentration of ~10 mg.mL^{-1} were solubilised with 1% DDM. (B) The DDM-solubilised and clarified membrane sample was applied to 2 connected 1 mL HiTrap Q FF columns for AEX chromatography. AEX buffers contained asolectin+CHAPS to further stabilise the detergent-solubilised membrane proteins. The BN-PAGE analysis of the AEX elution fractions is shown. Fractions corresponding to regions S1, Peak, S2 and Tail were separately pooled, and concentrated with the addition of peptidisc peptides. (C) Chromatogram showing the overlaid SEC runs performed with detergent-free buffer for 'on-column' peptidisc reconstitution at 4 °C. The accompanying BN-PAGE analysis also performed at 4 °C shows potentially reconstituted protein complexes resolved as many sharp bands in a wide molecular weight range.

Thus, over the course of these 5 iterations, a protocol was optimised involving:

1. Cultivation of spores in 3 L SNB medium and disruption by chemical decoating (37 °C), lysozyme treatment (4 °C), and 4-5 passages through a cell disruptor at 30 KPSI (4 °C)
2. Removal of undegraded integument fragments and unbroken spores with a hard debris spin at 50K RCF for 30 mins (4 °C), followed by membrane isolation with ultracentrifugation at 150K RCF for 1-2 hours (4 °C)

3. Resuspension of the membrane pellet using a dounce homogeniser while keeping everything cold (4 °C)
4. DDM solubilisation at a detergent:protein ratio of 1% DDM:10 mg.mL^{-1} protein (4 °C)
5. AEX chromatography using buffers containing 0.1% DDM and 0.02% azolectin+CHAPS (room temperature)
6. Peptidisc peptide addition (0.5 mg.mL^{-1} stock) followed by SEC for 'on-column' reconstitution using detergent-free buffer (4 °C)
7. Analysis of peptidisc-reconstituted protein complexes using BN-PAGE (4 °C) – bands can be subjected to mass spectrometry for protein identification and in-gel redox activity assays to detect specific respiratory enzymes

In this protocol, AEX chromatography could be substituted relatively easily with another affinity-based technique. If the target protein in the spore membrane is Strep-tagged, for example, a Strep-Tactin column can be used for its purification.

From this point onwards, Ms. Bethany Hardman joined this project and it was decided that further optimisation of the chromatography purification protocol will be done with membranes from vegetative cells rather than spores as they are easier to produce in large quantities. As mentioned in the chapter 2, work with Ms. Hardman that showed that there was significant ribosomal contamination in the pellet obtained from the membrane spin which was removed to a satisfactory degree after 2 washes with fresh buffer (Fig 9A). Ms. Hardman was also able to separate the 2 largest species from the smaller membrane protein complexes while working with *B. megaterium* vegetative cell membranes (Fig. 9B). This formed the basis of the work with Dr. Sebastian Pintscher in Chapter 6.

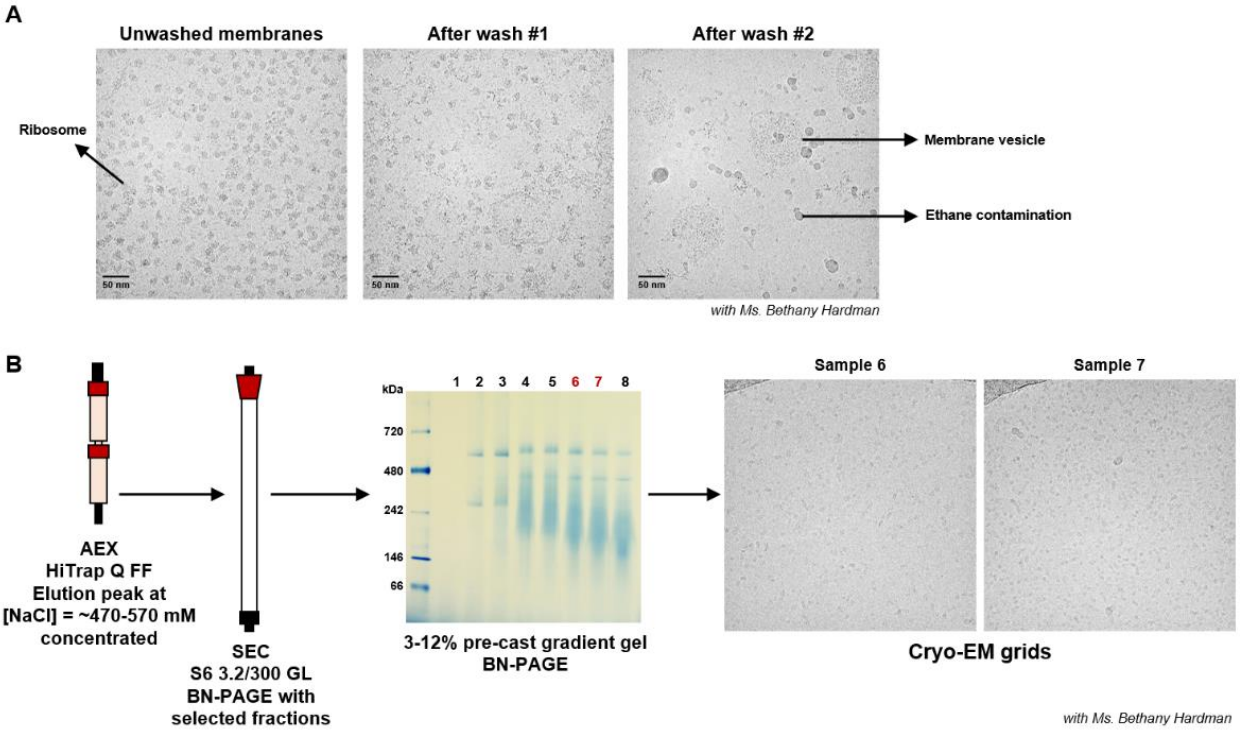

Fig 9. Shift to *B. megaterium* vegetative cell membranes and important results obtained with Ms. Hardman. (A) Progressive reduction in ribosomal contamination of cell membranes after washing steps were carried out with fresh buffer at 100-150K RCF by ultracentrifugation. Membrane vesicles decorated with proteins become visible after the second wash. (B) Overview of the protocol implemented to get separation of high molecular weight two species, one ~480 kDa and the other ~600 kDa in size in samples 4-8. AEX and SEC chromatography were performed along with BN-PAGE analysis. Grids were prepared with samples 6 and 7, highlighted in red. Screening of the cryo-EM grids (150KX magnification) showed protein-like particles.

3.2.13. Optimised spore membrane isolation protocol

Table 2: The spore membrane isolation protocol developed in this work and how it compares with other protocols used for *B. megaterium* and *B. subtilis*

Disruption step	***B. megaterium*** **(Racine & Vary 1980, Swerdlow & Setlow 1984)**	***B. subtilis*** **(Vepachedu & Setlow 2005, Zheng et. al. 2016)**	***B. megaterium*** **Method optimised in this work**
Removal of protein coat and outer membrane	0.1 M NaCl, 0.1 M DTT, 0.5% SDS, pH adjusted to 10 with NaOH, 37 ℃ for 2 hrs	0.1 M NaCl, 0.1 M NaOH, 1% SDS, 0.1 M DTT @ 70 ℃ for 30 mins/1 hr	0.1 M NaCl, 0.1 M NaOH, 0.1 M DTT, 0.5% SDS, 37 ℃ for 1 hr
Degradation of peptidoglycan cell wall and cortex with modified peptidoglycan (muramic acid-δ-lactam instead of N-acetylmuramic acid)	Enzymatic treatment with lysozyme, DNase I, RNase at 30 ℃ for 12 mins, then cooled on ice	Enzymatic treatment with lysozyme, DNase, $MgCl_2$*, RNase, protease inhibitor (PMSF) and EDTA* at 37 ℃ for 5 mins, then cooled on ice for 20 mins	1 $mg.mL^{-1}$ lysozyme, 0.01 $mg.mL^{-1}$ DNase I, 5 mM $MgCl_2$, 50 mM Tris-SO_4 pH 7.5, 50 mM NaCl, 1 cOmplete™, Mini protease inhibitor cocktail tablet, at 4 °C for 45 minutes
Fragmentation of the degraded cortex to release core contents	Mechanical disruption by sonication with glass beads or passage through a French pressure cell	Mechanical disruption with bead beating	Mechanical disruption at 30 KPSI in a cell disruptor, 4-5 passages
Removal of unbroken spores, integument fragments	Differential centrifugation at 10K RCF, 10 mins, pellet discarded	Differential centrifugation at 13K RCF, 5 mins, 4 ℃, pellet discarded	High-speed centrifugation at 50K RCF for 15-20 mins
Membrane isolation	Sucrose density gradient ultracentrifugation at 304K RCF, 1.75 hrs	Ultracentrifugation only, or precipitation with 1 M NaCl followed by ultracentrifugation at 100K RCF, 1 hr	Ultracentrifugation at 150K RCF for 2 hrs/15-16 hrs depending on whether the soluble fraction is required

Membrane washing	Purified with a sucrose gradient and washed once, or washed once then purified with a sucrose gradient and washed again by ultracentrifugation	Not washed or washed once on a shaker for 1 hr and ultracentrifuged to get final pellet	Ultracentrifugation at 150K RCF, 4 ºC, 1 hour twice with fresh buffer

DTT: dithiothreitol, * use of EDTA along with $MgCl_2$ is counterproductive as the former will chelate the Mg^{2+} ions leaving none for DNase I activation.

3.2.14. NADH:O_2 reaction assays on isolated spore and cell membranes

With the spore membrane isolation protocol optimised (Table 2) and progress made on resolving peptidisc-reconstituted membrane proteins on BN-PAGE (Fig 8C), the quality of the membrane preparations was further assessed by assaying them for NADH oxidation activity. This gives a measure of the functional state of the respiratory enzymes (and by proxy other enzymes) present in the membrane preparation – given the delicate nature of respiratory enzymes, if a method does not destroy them then we can be confident that most other proteins in the preparation have survived as well. Additionally, we wanted to compare the NADH oxidation rates of spore membranes with vegetative cell membranes and with rates reported for spore membranes isolated from *B. megaterium* in the literature (Table 4).

Membranes from *B. megaterium* late-exponential phase cells (16 hours of growth in LB broth, 30 °C, 225 rpm shaking incubation) were isolated using a method like that optimised for spores: cell lysis in the presence of lysozyme (1 small heap) and 0.01 $mg.mL^{-1}$ DNase I, 5 mM $MgCl_2$ and 1 protease inhibitor tablet by passage through a cell disruptor twice at 30 KPSI. The lysate was centrifuged (10 min, 10K RCF, 4 °C) four times to pellet any debris and the membranes isolated from the supernatant by ultracentrifugation (1 hr, 150K RCF, 4 °C). The isolated membranes were washed twice (1 hr, 150K RCF, 4 °C), aliquoted and stored at -70 °C.

With the washed spore membranes, NADH oxidation assays were performed alongside glucose dehydrogenase (GDH) assays. GDH activity would not be observed in membranes free of soluble contamination. Indeed, washed spore membranes did not have any GDH activity but oxidised NADH at a rate of 0.26 ± 0.04 µmol/min/mg. This was higher than cell membranes that oxidised NADH at a rate of 0.13 ± 0.02 µmol/min/mg. Cell membranes were

also more sensitive to 1 mM KCN: NADH oxidation was inhibited by 35.2 ± 7.8% compared to 14.6 ± 1.8% in spore membranes. Ms. Elodie Wells, who joined the project at this juncture, demonstrated that if we used a buffer containing 10 mM Tris-SO_4 pH 7.3, 250 mM sucrose instead of the 50 mM Tris-SO_4 pH 7.5, 50 mM NaCl buffer we had been using, we could get more reproducible and higher NADH oxidation rates across biological replicates. Ms. Wells confirmed that spore membranes oxidised NADH twice as fast and were ~2.5 times less sensitive to 1 mM KCN. Using NADH oxidation rates in the presence of the uncoupler gramicidin and pore-forming alamethicin, she calculated that our spore and cell membrane preparations had a high and comparable degree of vesicle inversion (>80%, Table 3).

Table 3: Consistent NADH oxidation rates and comparable % vesicle inversion obtained across biological replicates for spore membranes isolated using the optimised protocol

Membranes	**NADH oxidation rate (µmol/min/mg)**	**% inhibition by 1 mM KCN**	**% vesicle inversion**
Cell	0.16 ± 0.01	49.2	81.1
Spore preparation 1	0.3 ± 0.01	14.8	82
Spore preparation 2	0.3 ± 0.01	20	91.6
Spore preparation 3	0.3 ± 0.01	21	96.8

Data generated by Ms. Elodie Wells

Table 4: NADH oxidation rates reported in the literature for preparations of isolated spore membranes from *B. megaterium*

Study	**Strain**	**Buffer system and method**	**Rate and units as reported**	**Rate in µmol NADH.min^{-1}.mg^{-1}**	**inhibition by 1 mM KCN**
Wilkinson & Ellar 1975	KM	Phosphate, O_2 electrode	65-85 nmol O_2.min^{-1}.mg^{-1}	0.13-0.17	35%
Wilkinson et al. 1977	KM	Phosphate, O_2 electrode	44-99 nmol O_2.min^{-1}.mg^{-1}	0.08-0.19	-
Racine & Vary 1980	QM B1551	Phosphate, O_2 electrode	0.68 µmol O_2.min^{-1}.mg^{-1}	1.36	-
Swerdlow & Setlow 1984	QM B1551	Tris-hydrochloride, A_{340}	0.13 U.mg^{-1}	0.13	-
Wells & Gupta 2023	QM B1551	Tris-sulphate, sucrose, $A_{340-380}$	0.3 µmol NADH.min^{-1}.mg^{-1}	0.3	18.6%

Clarke-type O_2 electrodes were used in the earlier studies, later studies used a spectrophotometric method to measure NADH absorbance at 340 nm (A_{340}) or at 340-380 nm ($A_{340-380}$).

*U=amount of protein that oxidises 1 µmol of NADH/min; Rate of NADH oxidation is twice the O_2 consumption rate as NADH donates 2 electrons but O_2 needs 4 for reduction to $2H_2O$. This relationship was used to convert the rates reported in terms of O_2 consumption to the same units as us (µmol NADH.min^{-1}.mg^{-1}).

3.2.15. Enrichment of GDH and flavin-dependent NOX activities from the spore soluble fraction

The supernatant obtained after overnight ultracentrifugation of the spore lysate contained soluble proteins present in the core spore. This was syringe-filtered through a 0.22 µm membrane and concentrated down from ~50 mL to 5 mL using a 30 kDa MWCO centricon, then aliquoted and stored at -70 °C. Within the context of studying glucose-powered oxidative metabolism in germinating spores (chapter 5), we wanted to enrich and identify the enzymes responsible for glucose dehydrogenase and flavin-dependent NADH oxidase activities which in theory could constitute an ETC-independent pathway for NAD^+ regeneration and O_2 turnover. GDH is expressed and localised in the forespore during sporulation (Fujita, Ramaley and Freese, 1977; Rather and Moran, 1988), and oxidises more than half of the glucose that is taken up in the first 5 mins to gluconate generating NADH – NADH generation has been measured within 2-3 mins of glucose addition both enzymatically (Setlow and Setlow, 1977) and with fluorescence (Sano et al., 1988). Germinating spores consume O_2 in a KCN-insensitive manner and a soluble, FAD-dependent NADH oxidase has been being invoked as a plausible explanation in *B. cereus* and *B. megaterium* spores (Doi & Halvorsan, 1961; Racine & Vary, 1980; Spencer & Powell, 1952; Wilkinson & Ellar, 1975). However, the genes encoding neither enzyme in the spores of *B. megaterium* had been identified.

Fig 10A shows a flowchart depicting the experimental strategy followed for enrichment and separation of GDH and NOX activities. The first SEC step led to some degree of separation but as indicated by the low specific rates for the enzymatic activities, not enrichment (Fig 10B). Next, all the fractions with activity were pooled and subjected to AEX, which removed more extraneous proteins and increased specific activities (Fig 10C). AEX fractions 1-4 had distinct NOX activity whereas fractions 10-13 had high GDH activity contaminated with ~7 times less NOX activity. These were designated ‘NOX-enriched’ and ‘GDH-enriched’ fractions

respectively. The second SEC with the pooled NOX-enriched and GDH-enriched fractions resulted in nearly twice the specific activities for both, and fractions NOX-10 and GDH-6 were saved for LC/MS analysis. The overlapping fractions (5-9) from the AEX run were also subjected to a SEC step, and were used to demonstrate the FAD-dependence of the enriched NOX activity (Fig 7D).

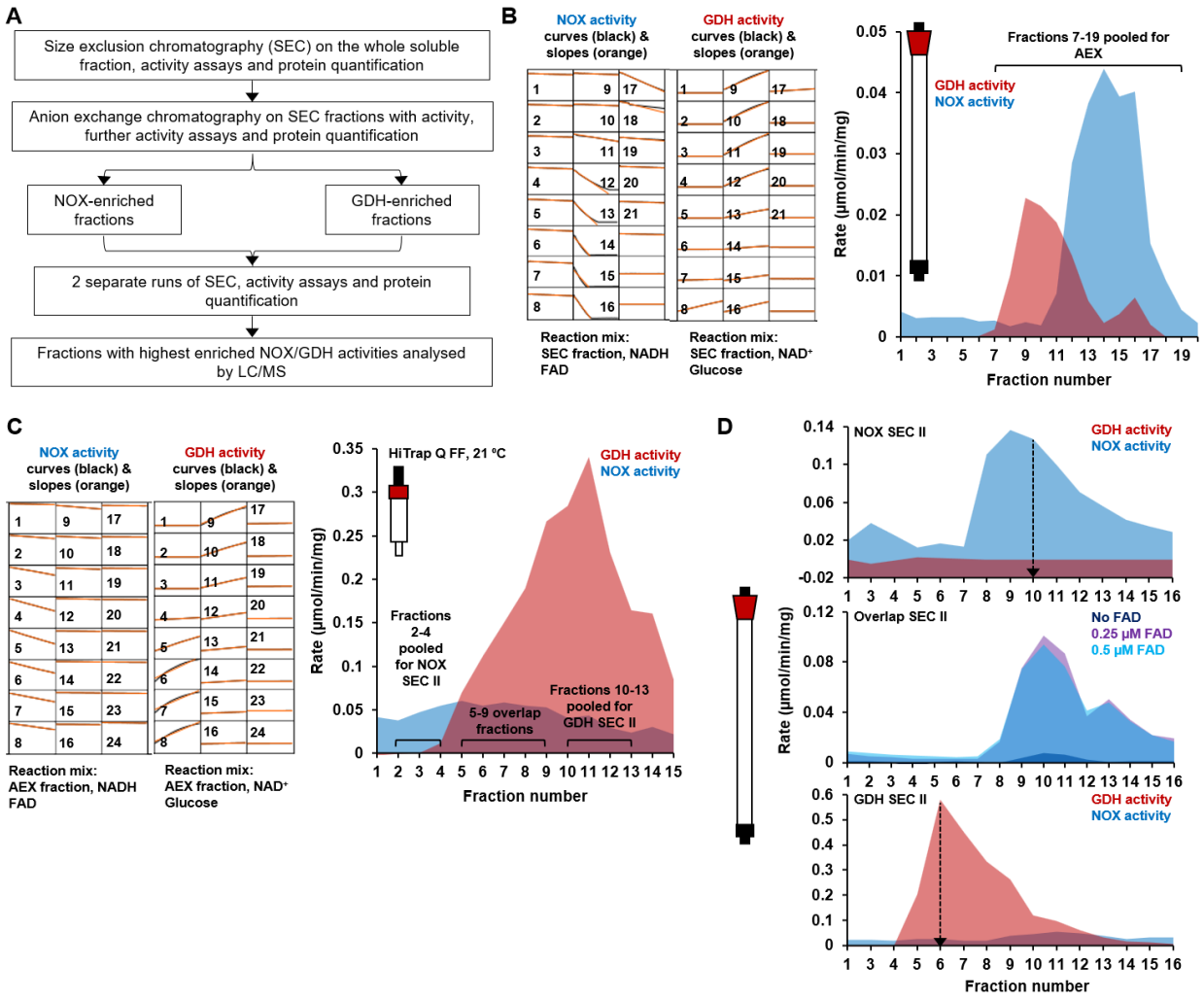

Fig 10. Enrichment of NOX and GDH activities from the whole spore soluble fraction. (A) A flowchart summarising the experimental strategy to enrich and simultaneously separate NOX and GDH activities. (B) Left panel shows curves (black) from the spectrophotometric NOX and GDH activity assays carried out for each of the SEC elution fractions, the slopes (orange) calculated by the plate reader software, and the components of the reaction. NOX activity would decrease the $A_{340-380}$ as NADH is oxidised. GDH activity would reduce NAD^+ to NADH, increasing the $A_{340-380}$. The graph on the right shows the rates of NOX (blue) and GDH (red) activities measured for each fraction numbered 1-21. Based on this, SEC elution fractions 7-19 were pooled and subjected to AEX. (C) Same as (B) but with AEX elution fractions. AEX elution fractions 2-4 were pooled and called 'NOX-enriched', pooled fractions 10-13 were 'GDH-enriched', and fractions 5-9 were the 'Overlap'. 'NOX-enriched' and 'GDH-enriched' samples were subjected to another SEC run. (D) After the second SEC, specific NOX and GDH activities were enriched and separated from each other (top and bottom graphs

respectively). In the middle panel, graph shows results of 'Overlap' fractions when assayed for NOX activity in the absence of FAD (dark blue), with 0.25 µM FAD (purple) or 0.5 µM FAD (light blue).

3.2.16. BN-PAGE with DDM-solubilised spore membranes

With optimised spore membrane preparations, we sought to repeat what had been attempted unsuccessfully at the beginning of the project. Membranes at different concentrations (2,4 and 8 mg.mL^{-1}) were solubilised with 0.5, 1 and 2% DDM and BN-PAGE was performed with the DDM-solubilised membranes clarified twice with centrifugation (16K RCF, 15 mins, 4 °C). Fig 11A shows that 4 mg.mL^{-1} protein solubilised with 1% DDM gave the most prominent bands of high molecular weight without the smearing obtained with 8 mg.mL^{-1} protein, which was likely a result of overloading and incomplete solubilisation.

4 mg.mL^{-1} protein concentration was judged ideal, and another BN-PAGE experiment was performed testing 0.5 and 1% of DDM and an even milder detergent, glyco-diosgenin (GDN). As compared to DDM, GDN has a lower critical micelle concentration or CMC, i.e. the minimum concentration above which micelles are spontaneously formed. A lower CMC of 18 µM means that GDN micelles are more stable and its molecules will not readily displace the native membrane lipids – on the other hand, DDM has a CMC of 170 µM (Lee et al., 2022). Fig 11B shows the resulting gel, where the GDN lanes had only 2-3 faint bands indicating that as expected, a 1-hour incubation period sufficient for DDM solubilisation, was insufficient for GDN to effectively extract proteins from spore membranes. In the DDM lanes, 6 prominent bands between 720 and ~242 kDa can be seen – these were labelled 1-6 and analysed by LC/MS. There were 2-3 fainter bands <242 kDa but these we ignored as we were interested in identifying the high molecular weight respiratory complexes and other co-resolving proteins.

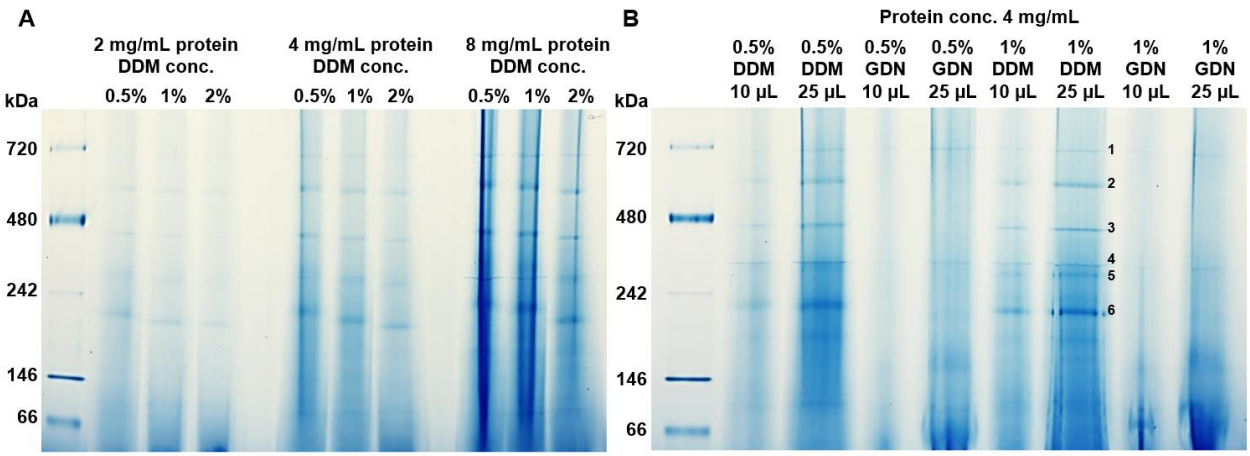

Fig 11. BN-PAGE analysis of detergent-solubilised spore membrane proteins. (A) Different membrane protein concentrations (2, 4, 8 mg.mL^{-1}) and DDM concentrations (0.5, 1, 2%) were tested to identify the ideal detergent: protein ratio that would give clearly resolved bands. Lanes with 4 mg.mL^{-1} protein had strong bands and an intermediate degree of smearing. Further optimisations were carried out with this protein concentration. (B) Two different detergents (DDM and GDN) were used at 0.5 and 1% to solubilise spore membranes containing 4 mg.mL^{-1} protein. Two loading volumes (10 µL and 25 µL) were tested as well. The clearest bands were judged to be in the lane where 1% DDM was used for solubilisation and 25 µL of the sample was loaded. Bands labelled 1-6 were excised from the gel and analysed by LC/MS.

3.2.17. LC/MS analysis of GDH/NOX enriched fractions and BN-PAGE bands of spore membranes

Fractions NOX-10 and GDH-6 (Fig 10D) and bands 1-6 from the BN-PAGE gel (Fig 11B) were analysed by the Metabolomics & Proteomics Lab, Technology Facility, Department of Biology, University of York using Liquid Chromatography tandem Mass Spectrometry (LC/MS). Dr. Chris Taylor used a Waters mClass UPLC connected to an Orbitrap Fusion Tribrid mass spectrometer for data acquisition, and Dr. Adam Dowle used Progenesis QI for chromatographic alignment and peak picking. Dr. Dowle shared a spreadsheet with us containing details of all the proteins identified in each sample, and their relative abundance across samples. The protein hits in each sample were then sorted (largest to smallest) based on their peak areas.

In these results, we found the characteristic small, acid-soluble spore protein Tlp (BMQ_2552) and spore photoproduct lyase SplB (BMQ_2226) which would be expected in the spore soluble fraction. For the GDH-enriched fraction, of the most abundant proteins only the top hits related to “glucose” are mentioned in Table 5. Similarly, for the NOX-enriched fraction, only the top hits related to “NADH” are mentioned in Table 6.

Glucose 1-dehydrogenase capable of using either $NADP^+$ or NAD^+ as a cofactor (BMQ_0838) was identified as the spore isoform – the genome contains two more glucose dehydrogenases, BMQ_1051 and BMQ_3371, as annotated in the KEGG/GenBank database (Kanehisa and Goto, 2000; Kanehisa et al., 2023). As the LC/MS peak list was originally searched against the *B. megaterium* QM B1551 subset of UniProt (The Uniprot Consortium 2023), we have the UniProt names of the protein hits in our result file from the facility. When cross-checked against the KEGG database, some discrepancies were revealed (column 1 versus 6 of Table 5). Only

the most abundant “glucose 1-dehydrogenase” was annotated as such in both the UniProt and KEGG/GeneBank databases.

Table 5: Top hits from the “glucose” search against all LC/MS results. Rel% is the percentage abundance across samples analysed by LC/MS (6 BN-PAGE bands + 2 NOX/GDH-enriched fractions). Highlighted values indicate in which of the two soluble samples (GDH-6 or NOX-10) the protein was enriched.

Name of protein from UniProt	BMQ code	Unique peptides	GDH-6 Rel%	NOX-10 Rel%	KEGG/GenBank annotation
Glucose-6 phosphate isomerase	BMQ_4937	23	86	5	
Glucose 1-dehydrogenase (NAD(P)(+))	BMQ_0838	8	72	15	Glucose 1-dehydrogenase (gdh)
Glucose-6-phosphate 1-dehydrogenase	BMQ_5210	20	84	13	-
Glucose 1-dehydrogenase (NAD(P)(+))	BMQ_2939	5	93	6	short-chain dehydrogenase/ reductase
PTS system, glucose-specific IIBC component	BMQ_1302	24	1	3	-
Glucose 1-dehydrogenase (NAD(P)(+))	BMQ_2333	2	6	86	-
Glucose-6-phosphate 1-dehydrogenase	BMQ_1958	7	4	71	-
Sugar phosphotransferase system, glucose subfamily, IIA component	BMQ_4019	3	3	97	-
Glucose 1-dehydrogenase (NAD(P)(+))	BMQ_2208	3	4	8	3-hydroxybutyrate dehydrogenase

UTP--glucose-1-phosphate uridylyltransferase	BMQ_5130	7	2	7	-
Glucose 1-dehydrogenase (NAD(P)(+))	BMQ_1269	4	0	58	oxidoreductase, short chain dehydrogenase/ reductase family protein

The top hit from the "NADH" search was FMN-dependent NADH:quinone oxidoreductase (BMQ_2186), an uncharacterised enzyme which has low sequence similarity to type II NADH dehydrogenase (Ndh) and the well-studied NADH oxidase from *Lactobacillus brevis* (LbNOX) (Hummel and Riebel, 2003; Titov et al., 2016). Instead, this is 83.17% identical to an azoreductase (AzoR2) from *B. subtilis* which has been implicated in the detoxification of thiol-reactive electrophile compounds (Töwe et al., 2007). Protein sequences of Ndh, YumB (the spore Ndh paralogue), and AzoR2 from both *B. subtilis* and *B. megaterium* were compared with LbNOX using the online Clustal Omega multiple sequence alignment tool (Madeira et al., 2022). The resulting percent identity matrix is presented in Table 7 along with the phylogenetic tree created for these sequences.

Table 6: Top hits from the "NADH" search against all LC/MS results. Rel% is the percentage abundance across samples analysed by LC/MS. Highlighted values indicate in which of the two soluble samples (GDH-6 or NOX-10) the protein was enriched.

Name of protein from UniProt	**BMQ code**	**Unique peptides**	**GDH-6 Rel%**	**NOX-10 Rel%**	**KEGG/ GenBank annotation**
FMN dependent NADH:quinone oxidoreductase	BMQ_2186	7	0	100	FMN-dependent NADH-azoreductase
NADH-dependent flavin oxidoreductase	BMQ_3949	11	0	99	No assignment
NADH-dependent butanol dehydrogenase A	BMQ_4945	8	9	89	-

NADH dehydrogenase YumB	BMQ_4965	20	1	5	-
NADH-dependent dehydrogenase	BMQ_2148	2	0	100	-
Enoyl-[acyl-carrier-protein] reductase [NADH]	BMQ_3348	4	0	5	-

Table 7: The sequence identity matrix generated using Clustal Omega (EMBL-EBI) for AzoR2, LbNOX, YumB and Ndh proteins from both *B. subtilis* and *B. megaterium*.

	AzoR2	**AzoR2**	**LbNOX**	**YumB**	**YumB**	**Ndh**	**Ndh**
AzoR2	100	83.17	19.79	20.9	21.39	16.16	16.67
AzoR2	83.17	100	20.63	20.71	22.22	15.9	17.44
LbNOX	19.79	20.63	100	20.16	19.09	21.61	24.38
YumB	20.9	20.71	20.16	100	68.24	37.02	40.36
YumB	21.39	22.22	19.09	68.24	100	34.96	38.56
Ndh	16.16	15.9	21.61	37.02	34.96	100	66.07
Ndh	16.67	17.44	24.38	40.36	38.56	66.07	100

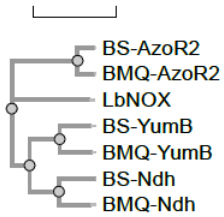

Phylogenetic tree

Blue: *B. subtilis* (BS); **Red**: *B. megaterium* (BMQ); **LbNOX** is the water-forming NADH oxidase from *L. brevis*; the phylogenetic tree was created using Clustal Omega; Highlighted values indicate the highest percentage identity that protein has with another protein.

Based on these findings, we propose that the soluble flavin-dependent NADH oxidase activities measured in disrupted spores previously can be attributed to AzoR2 (BMQ_2186) or similar enzyme(s). This class of enzymes is highly unlikely to be coupled to glucose catabolism known to occur in germinating spores and be the reason for KCN-insensitive O_2 consumption. The reducing power generated by glucose oxidation must feed into the ETC, as suggested previously (Sano et al., 1988). The more likely explanation for this KCN-insensitivity is the presence of a cytochrome *bd* oxidase (Hogarth, Wilkinson and Ellar, 1977). These ideas will be explored through subsequent chapters.

Amongst the proteins hits for the BN-PAGE bands 1-6, we first looked for “germination”, “spore” and “sporulation” related proteins. We found GerD, shown to be essential for germinosome assembly and consequently for germinant receptor-mediated germination

(Mongkolthanaruk, Robinson and Moir, 2009; Griffiths et al., 2011). The germinant receptors themselves were not detected but given their low abundance this was not surprising. We also found 4 out of the 7 proteins encoded by the spoVA locus involved in CaDPA import during sporulation and its release during germination (Gao et al., 2022). 3 out of the 5 predicted integral membrane proteins were found: spoVAA (BMQ_4390), spoVAC (BMQ_1933, BMQ_4388), spoVAF (BMQ_4384). We also found spoVAD (BMQ_4387, BMQ_1934) in the soluble fractions GDH-6 and NOX-10, which has been proposed to function as a cytoplasmic plug for a minimal channel formed by SpoVAC and SpoVEb (Gao et al. 2022). Recently, spoVAF was predicted to form an oligopentameric ion channel with YqhR in *B. subtilis*, and implicated in amplifying the germination response when germinant concentrations are low (Gao et al., 2024). In *B. megaterium*, BMQ_4475 encodes YqhR with a sequence identity of 45.8% with the *B. subtilis* protein. While we found abundant SpoVAF in all BN-PAGE bands, YqhR (which should have 1:1 stoichiometry with SpoVAF based on the structural prediction) could not be detected in our experiments.

Next, we searched for “cytochrome”, “NADH” and “ATP” related proteins with the aim of identifying all the respiratory enzymes that could constitute a functional ETC in dormant spores. This is the respiratory apparatus available to spores immediately following the initiation of germination. We found that dormant spores have the necessary respiratory enzymes to constitute a complete ETC which at least when removed from the spore context is functional (NADH:O_2 reaction assays in this chapter, section 3.2.14 and NADH-reduced haem spectra in Chapter 5).

When we inspected the individual respiratory enzymes and their genes closely, we noticed two atypical isoforms: a *yumB*-encoded type II NADH dehydrogenase and *ythAB*-encoded cyt *bd* oxidase instead of their canonical forms Ndh (BMQ_2631) and CydAB (BMQ_5231, BMQ_5230). The A and B subunits of CydAB and YthAB share a low sequence identity of 28.8% (query cover 96%) and 29.4% (query cover 19%) respectively.

In *B. subtilis*, transcriptomic profiling showed that during sporulation *ndh* and *cydAB* expression levels decline whereas *yumB* and *ythAB* levels increase (Nicolas et al., 2012). YthAB was also identified in the spore inner membrane proteome of *B. subtilis* but not in the vegetative cell membrane proteome (Zheng et al., 2016). During aerobic exponential growth of *B. subtilis*, YthAB was found to be of no importance, and a physiological role for it is yet to be identified (Winstedt and Von Wachenfeldt, 2000; Hederstedt, 2021). The significance of this will be discussed in chapter 5 where we measure electron transfer through the ETC of germinating spores in real time.

Table 8: The relative abundance of respiratory enzymes found across BN-PAGE bands 1-6 analysed by LC/MS.

		Relative abundance (%) across bands 1-6					
Respiratory enzyme	Gene name and BMQ code	Band 1	Band 2	Band 3	Band 4	Band 5	Band 6
NADH dehydrogenase	*yumB* (BMQ_4965)	8	13	15	11	25	28
Succinate dehydrogenase	*sdhA* (BMQ_4724)	0	0	99	0	0	0
	sdhB (BMQ_4723)	0	0	99	0	0	0
	sdhC (BMQ_4725)	1	0	96	1	1	1
Cyt aa_3-600 menaquinol oxidase	*qoxA* (BMQ_3130)	0	0	1	5	7	86
	qoxB (BMQ_3129)	0	0	1	5	9	85
	qoxC (BMQ_3128)	0	0	1	6	8	85
Cyt *bd* ubiquinol oxidase	*ythA* (BMQ_4878)	1	3	8	8	23	57
	ythB (BMQ_4879)	0	2	6	18	39	35
Menaquinol-cyt *c* reductase	*qcrA* (BMQ_4310)	8	42	50	0	0	0
	qcrB (BMQ_4309)	8	41	50	0	0	0
	qcrC (BMQ_4308)	7	41	50	0	0	1
Cyt *c*-551	*cccB* (BMQ_5092)	0	2	5	17	33	42
Cyt caa_3 oxidase	*ctaC* (BMQ_1372)	1	3	3	7	18	68
	ctaD (BMQ_1373)	0	4	2	7	21	66
	ctaE (BMQ_1374)	1	3	2	9	21	64
ATP synthase	*atpA* (BMQ_5150)	2	91	2	1	2	2
	atpB (BMQ_5154)	0	40	6	5	48	1
	atpC (BMQ_5147)	0	98	1	0	0	1
	atpD (BMQ_5148)	1	92	1	1	2	3
	atpF (BMQ_5152)	0	26	3	6	64	1
	atpG (BMQ_5149)	1	92	2	1	2	2
	atpH (BMQ_5151)	2	93	2	1	1	1

3.3. Conclusions and future work

3.3.1. Translation of these methods to other *Bacillus* species

In this chapter, we have demonstrated that 3 L cultures of *B. megaterium* spores can provide sufficient starting material for high-quality membrane preparations that retain respiratory activity (as assessed by NADH:O_2 reaction assays). We have optimised a protocol for chromatographic extraction of large membrane protein complexes (250-700 kDa) from these membranes, which were resolved as such by BN-PAGE. To the best of our knowledge, preparative biochemistry of this nature has not been attempted with spore membranes before. We were also able to solubilise the entire spore membrane fraction with 1% DDM and resolve proteins therein into 6 major bands using BN-PAGE. LC/MS analysis of these bands allowed us to reconstruct the membrane-bound respiratory chain present in dormant spores, and this is essential to studying how it is activated during germination (chapter 5).

After initial experiments with *B. subtilis*, we switched to using *B. megaterium* because it sporulates efficiently in broth culture and this makes the cultivation, harvest and washing of medium-scale spore cultures relatively less labour-intensive. Successful translation of these methods to other *Bacillus* species relies on how feasible it is to grow large quantities of their spores for iterative biochemical optimisation that underpinned the outcomes of this work. In this regard, there is an alignment of fundamental and applied research interests in spore biology. To use spores as industrial bioindicators of proper sterilisation in food packaging etc., it is important to produce them in a standardised manner and this can be achieved in “submerged” bioreactors (Stier and Kulozik, 2022). A study comparing sporulation efficiency of different *Bacillus* species in conventionally used media found that broth media generally supported better sporulation than solid media (Li et al., 2022).

An example is *B. cereus* that also sporulates efficiently in broth culture. In fact, BN-PAGE and LC/MS analyses of the isolated membrane fraction have been carried out previously for this species in Dr. Graham Christie’s lab (Mustafa, 2021). This could serve as a starting point for the extension of methods described in this work to *B. cereus*.

3.3.2. Purification of the affinity-tagged proteins of interest from spore membranes

Our work has shown that spore membrane protein biochemistry is not entirely intractable. Once a similar membrane isolation protocol is optimised for any other species, the resulting membrane preparations can be used to address fundamental questions about the initiation of germination. The introduction of short affinity tags into the genome for proteins like the germinant receptor GerU, and the spore-specific respiratory enzymes YumB and YthAB in *B. megaterium*, could enable their purification directly from spore membranes. In this way, these proteins would be expressed and assembled under the most physiologically relevant conditions, and isolated from their atypical environment for structural/functional characterisation. We now have a construct with Strep-tagged GerU from Dr. Christie's lab for this purpose.

Chapter 4: Loss of absorbance and enzymatic assays with germinating *Bacillus* spores

4.1. Introduction

4.1.1. The principle of loss of absorbance assays

Owing to their dense, dehydrated state, dormant spores are refractile or phase bright as observed by phase contrast microscopy. Given that there is >800 mM CaDPA in the core of the spore which is in a solid state (Kong, Setlow and Li, 2012), one would expect water movement inwards is required initially for solubilisation and bulk CaDPA release occurs later. Experiments on single spores trapped using optical tweezers have shown that there is a period of CaDPA leakage after germinant addition, which is later followed by the bulk CaDPA release that can be visualised as phase transition and measured turbidometrically as the loss of absorbance at 600 nm (A_{600}). With this set up, it was further calculated by simultaneous phase contrast microscopy and Raman spectroscopy that for individual spores of *B. subtilis* and *B. megaterium*, phase transition takes between 2-3 minutes (Wang, Setlow and Li, 2015). Naturally, all the spores in a population can cumulatively take more time to complete this process and this is what is measured in a traditional loss of A_{600} assay.

Hydration occurs with bulk release of CaDPA and ingress of water into the spore core as the cortex is progressively degraded by the cortex lytic enzymes. This results in loss of refractility and phase transition – germinating spores are phase bright. The process of germination can be divided into two phases. The first is rehydration/initiation of germination where spores can rapidly lose their initial A_{600} in response to a germinant even in a minimal buffer medium. The second is outgrowth/completion of germination which, requiring a nutrient medium, entails spore swelling, emergence, elongation and the first cell division. Outgrowth presents as increase in A_{600} (Hyatt & Levinson, 1959).

Depending on the species and germinants, the rate and degree of absorbance loss can vary considerably. Rehydration curves generated when A_{600} is plotted against time for a germinant/species tell us a) how potent the germinant is – potency of a germinant is positively correlated with the extent of A_{600} loss, and b) how synchronised the spores are in their germination response which is related to the how the germinant is processed and is an intrinsic property of the spores. A germinant could be potent and lead to high A_{600} loss, but if the spores'

response to this is unsynchronised then for a population, getting to that point of maximum A_{600} loss will take a long time. Workers very early in the development of the field realised that heating a spore suspension for a specific duration and at an optimal temperature for the species “activates” the spores and makes their germination response more synchronised (Powell & Hunter, 1955; Wen et al., 2022). This leads to bigger changes in absorbance that can be measured more reliably in the laboratory. It is not clear what heat activation does; release of DPA (Alimova et al., 2006; Scott and Ellar, 1978b) and a degree of reversible protein denaturation is associated with this treatment (Zhang, Setlow and Li, 2009). Interestingly, it does not nullify the intrinsic germination propensity of a given species; despite optimal heat activation and when germinated with their most potent germinants glucose and alanine respectively, *P. megaterium* spores still display more synchronous germination than *B. subtilis* spores (Zhang et al., 2010).

4.1.2. Glucose consumption and hydrogen peroxide detection in germinating spores

The current model for how germinant receptors initiate germination posits that these receptors are penta-/hexameric ligand-gated ion channels that, upon binding to the cognate nutrient germinants, release ions. This coordinates the opening of the SpoVA channels that release bulk CaDPA which allows progressive hydration of the spore core (Gao et al., 2023). Recent research efforts have largely focussed on understanding the how the germinant signal is received and transduced. But we are also interested in the metabolic fate of the nutrient germinants. One would expect that they are consumed by the germinating spore, and this leads us to further questions: a) when does this consumption start, b) is it essential for initiation of germination and c) how does germinant-powered metabolism fit in with sequence of events in the germination cascade? The last question will be dealt with in chapter 5.

For *B. megaterium* QM B1551, the first two questions were last addressed in a series of papers in the 1970s and 80s. Glucose uptake in a tris buffer system was measured radiometrically to start 2-3 minutes after rehydration was underway, and it was shown that even transient exposure (<1 min) to glucose could trigger germination. Non-metabolisable glucose analogues were found to initiate germination but were not taken up by the germinating spores. Therefore, it was concluded that glucose uptake was not essential for initiation of germination (Shay and Vary, 1978; Racine, Dills and Vary, 1979). These results are consistent with glucose serving as a signalling molecule; the transient exposure was probably sufficient to allow surface

adsorption of glucose (Black and Gerhardt, 1961), and the glucose analogues tested were still somehow recognisable by GerU, but not compatible with the unidentified glucose transporter in spores. In this limited capacity, glucose behaved like the non-nutrient germinant KBr that is known to initiate germination but forces spores to rely on endogenous reserves to generate ATP and NADH (Setlow & Kornberg 1970, Setlow & Setlow 1977). However, in a phosphate buffer system using a radiorespirometric method, it was shown that catabolism of glucose started at the same time as loss of A_{600} (Maruyama et al. 1980). This suggests that when available, glucose is utilised by germinating spores to generate even more ATP and NADH (Setlow and Setlow, 1977; Setlow and Kornberg, 1970). We wanted to confirm that glucose consumption started concurrently with spore rehydration and develop a model in which glucose serves the dual role of signalling molecule and source of reducing power in *B. megaterium*.

From the largely forgotten work of Otani et al., Sano et al., (Otani et al., 1986; Sano et al., 1988) and results from chapter 3 (identification of the spore isoform of glucose dehydrogenase and a functional ETC in spore membranes), we have evidence that oxidative phosphorylation (OxPhos) is the dominant energetic pathway in germinating spores. If glucose is the primary source of electrons and O_2 the terminal acceptor in the ETC, then glucose consumption will mirror oxygen consumption. The oxygen consumption rates measured for spores germinated with different glucose concentrations supporting this idea will be presented in the next chapter. Here, we measured hydrogen peroxide production in spores as another indicator of oxidative metabolism. To the best of our knowledge, there is only one other report of H_2O_2 generation in germinating spores of aerobic *B. megaterium* and to a much lesser extent in anaerobic *Clostridium perfringens* (Ando & Tsuzuki, 1987). There is also an isolated report of 10 mM H_2O_2 initiating germination in *B. subtilis* spores by an unknown mechanism (Falcone, Salvatore and Covelli, 1959). More commonly, H_2O_2 is explored for its sporicidal potential (Korza et al., 2023a). In this context, it is worth mentioning that the role of H_2O_2 has long been recognised in the breaking of plant seed dormancy – H_2O_2 imbibition pre-sowing leads to faster germination. In germinating plant seeds, H_2O_2 production has been attributed to mitochondrial OxPhos, NADPH oxidases, extracellular peroxidases etc., but a delicate balance must be struck as too much H_2O_2 can prove detrimental (Wojtyla et al., 2016).

Type-II NADH dehydrogenases (NDH-2) are known to generate ROS as a side reaction of their physiological activity (Blaza et al., 2017). If the spore isoform of NDH-2 (identified as YumB in chapter 3) is highly active as OxPhos is restarted, then this could be a source of H_2O_2 in germinating spores. The measurable H_2O_2 in germinating spores will be an underestimate of the total H_2O_2 production as the majority would be immediately neutralised by catalase and not be detectable by our assay.

4.2. Results

4.2.1. Effect of Histodenz purification, heat activation and buffer systems on spore germination

As shown in Fig 1, even extensively washed *P. megaterium* spores carry vegetative contamination/lower density spore material that can be removed using a Histodenz gradient as these float in the supernatant. The pure spore pellet must then be washed to remove the viscous Histodenz medium before the spores can be used for experimentation.

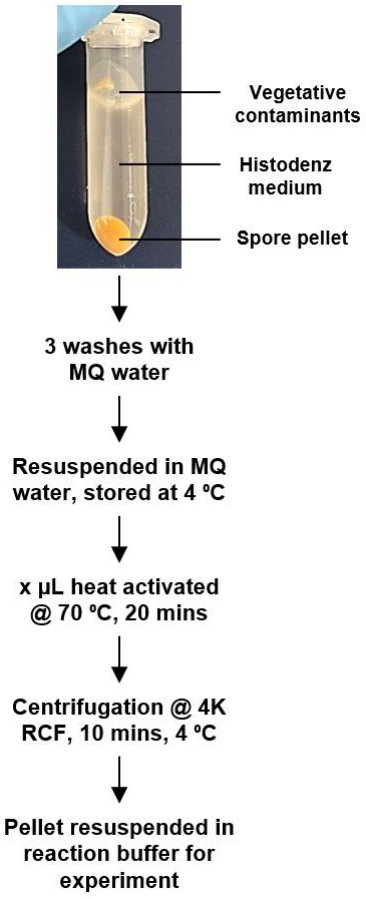

Fig 1. The Histodenz purification method followed to obtain spores free of vegetative contamination for subsequent experiments. The volume of spore suspension heat activated depended on the optical density of the final Histodenz purified spore suspension and the desired optical density for an experiment, and is therefore denoted as ‘x µL’.

We found that Histodenz purification did not make a major difference to the outcome in basic rehydration assays, but as expected, without heat activation spores could not germinate within

the timescale of these experiments (Fig 2A, 2B-i). We also tested two different buffer systems: 5 mM Tris-HCl pH 7.5 and 50 mM Potassium phosphate pH 7.5. While the extent of A_{600} loss is comparable (>60%), the rate of A_{600} loss is faster in the tris buffer system (Fig 2B-ii). Outgrowth is comparable in both buffer systems but in the tris buffer control, there is a larger drift in A_{600} baseline which is not desirable (Fig 2C). Phosphate buffer suppressed this basal loss of A_{600} and was selected as the buffer system for all subsquent germination assays.

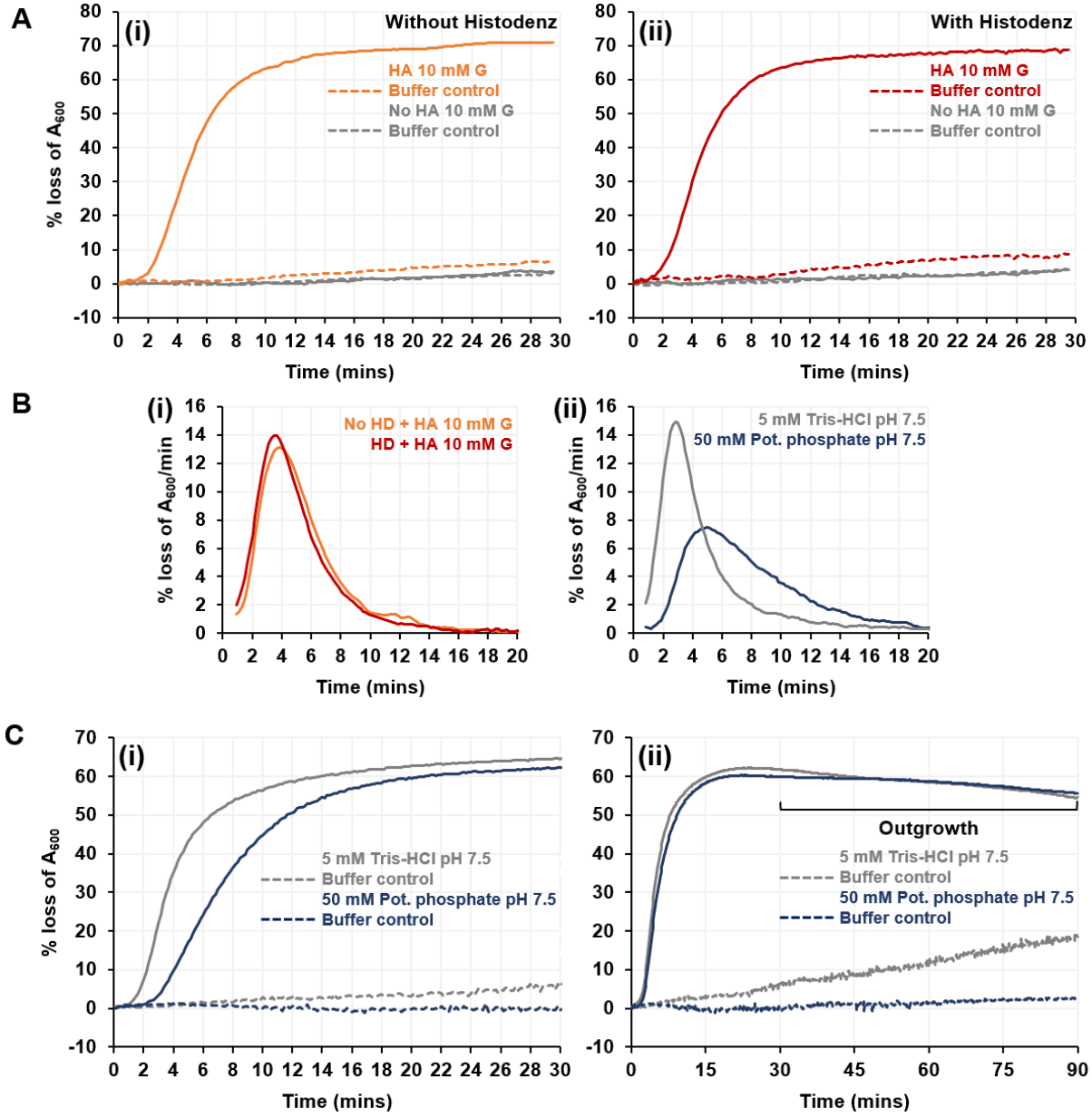

Fig 2. Spore preparation and buffer conditions for germination assays. (A) (i) Rehydration curves for spores that were washed but not Histodenz purified. Spores were either heat activated at 70 °C for 20 mins (HA) or not (No HA), and germinated with 10 mM glucose in 50 mM potassium phosphate buffer pH 7.5 at 30 °C. Glucose was not added to the buffer controls (dashed lines). (ii) Same as (i), except that these spores were Histodenz purified. (B) (i) Rate of rehydration (% loss of A600/min) achieved by spores with (red) or without (orange)

Histodenz purification. (ii) Rate of rehydration achieved by spores in the tris buffer system (grey) or the phosphate buffer system (blue) when germinated with 10 mM glucose. (C) (i) Rehydration curves for Histodenz-purified, heat-activated spores germinated with 10 mM glucose in tris (grey) or phosphate (blue) buffer system, and corresponding buffer only controls (dashed lines). (ii) Outgrowth curves for Histodenz-purified, heat-activated spores germinated with 1x nutrient broth (NB) in tris (grey) or phosphate (blue) buffer system, and corresponding buffer only controls (dashed lines).

4.2.2. Confirmation of species-specific germinant requirements

For *B. subtilis*, the amino acid L-alanine is a single potent germinant. The germination rate increases in a concentration-dependent manner when alanine concentration is in the range of 10 - 100 µM, but any higher concentrations of alanine do not lead to faster germination (Yasuda and Tochikubo, 1985). Consistent with this, we were unable to get a further dose response with 1 to 10 mM alanine (Fig 3A). In the QM B1551 strain of *B. megaterium*, as expected, we did not see a response to alanine at any concentration (Fig 3B). Conversely, *B. subtilis* does not germinate in response to glucose which is a potent single germinant for *B. megaterium*.

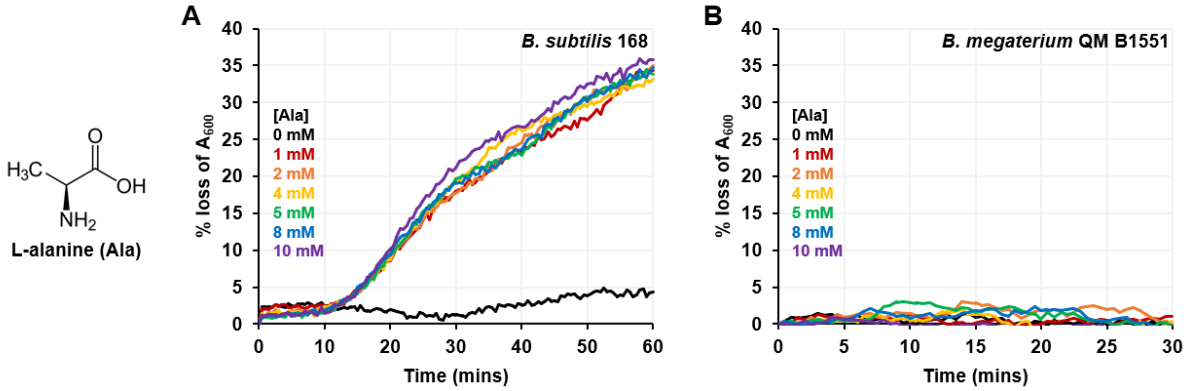

Fig 3. Distinct germinant preferences of *Bacillus* species. (A) Rehydration curves for Histodenz-purified, heat-activated *B. subtilis* spores germinated with 1-10 mM L-alanine in 50 mM potassium phosphate buffer pH 7.5 at 37 °C. (B) Same as (A) but with *B. megaterium* spores at 30 °C.

In *B. megaterium*, glucose and analogues like 1-/2-/3-deoxyglucose can lead to rapid germination [(Shay and Vary, 1978), personal communication with Dr. Graham Christie], but galactose, a C4 epimer of glucose, does not (Fig 4A). Modifications at positions 4 and 6 appear to not be tolerated and so it has been speculated that these positions could be critical for

glucose recognition. Consistent with previous studies (Hyatt & Levinson, 1961), the response to glucose is concentration-dependent even in the 1-10 mM range (Fig 4A & B). *B. megaterium* spores lost ≥60% of their initial absorbance in under 30 mins at with 4-10 mM glucose, whereas it took *B. subtilis* spores an hour to achieve roughly half of that. This makes the former ideal for biophysical studies using techniques like re-emission haem spectroscopy (chapter 5) where a coordinated signal arising from this synchronicity is highly desirable.

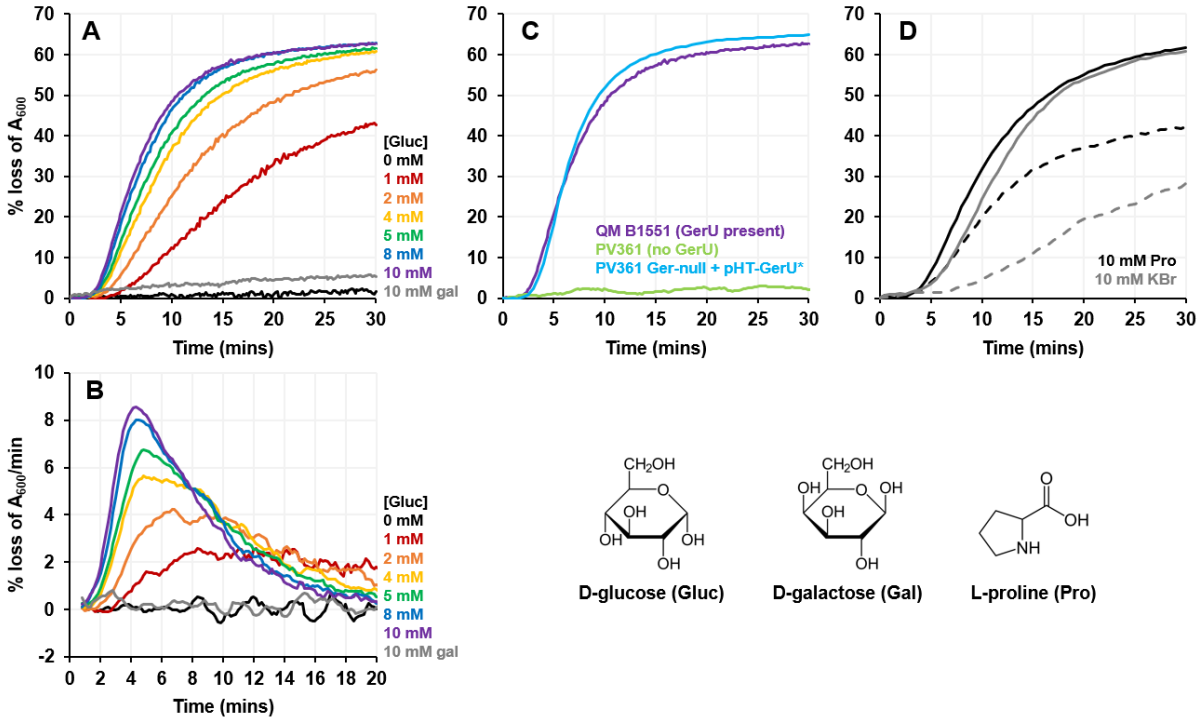

Fig 4. Initiation of germination by nutrient and non-nutrient germinants in *B. megaterium* spores. (A) Rehydration curves for Histodenz-purified, heat-activated *B. megaterium* spores germinated with 1-10 mM D-glucose and 10 mM galactose in 50 mM potassium phosphate buffer pH 7.5 at 30 °C. (B) Rate of rehydration with each glucose concentration shown in (A). (C) Rehydration curves for spores germinated with 10 mM glucose in the same way as in (A). Spores either have the receptor GerU (strain QM B1551, purple), do not have the plasmid carrying GerU (strain PV361, green), or are PV361 Ger-null spores with a plasmid carrying the chimeric GerU* (PV361 Ger-null + pHT-GerU*). (D) Rehydration curves for QM B1551 (dashed lines) and PV361 Ger-null + pHT-GerU* (solid lines) spores when germinated with 10 mM proline (black) and 10 mM KBr (grey).

Glucose response requires the plasmid-borne receptor gerU composed of GerUA, -UB and -UC (Fig 4C, QM B1551 versus the plasmidless variant PV361). In QM B1551, there is another B subunit (GerVB) that presumably in a different receptor assembly mediates the response to proline and KBr (Christie and Lowe, 2007). Consistent with the original study, the chimeric GerU* (receptor composed of GerUA, -VB and -UC) confers the ability to recognise glucose in PV361 along with an enhanced response to proline and KBr (Fig 4D). How this enigmatic

receptor can simultaneously recognise glucose with high specificity and amino acids like proline and leucine remains unclear in the absence of biochemical/structural characterisation of GerU.

4.2.3. Glucose consumption during hydration

Having confirmed that our spore preparations displayed robust germination in response to glucose, we wanted to measure when glucose consumption started with respect to loss of absorbance, and whether it was strictly linked to glucose-initiated germination. Fig 5A shows how these experiments were performed. In Fig 5B, we plotted the glucose consumption data from 3 replicates per strain that despite the high variability illustrate a clear trend, especially when plotted alongside the corresponding rehydration curves. While GerU is not present in PV361 spores, they still have other germinant receptors that mediate the response to various amino acids in nutrient broth. We therefore germinated PV361 spores with nutrient broth in the presence of 1 mM glucose. Loss of A_{600} started at the same time as glucose consumption in both QM B1551 and PV361. This demonstrates that spores germinating in response to amino acid signals will still consume glucose if it is present, even when they do not recognise glucose as a germinant. This has been shown in an alanine-responsive strain of *B. subtilis* as well (Otani et al., 1986; Tochikubo and Yasuda, 1985). Fig 5C shows data generated in an attempt to reduce variability between replicates and noise in the first 10 minutes of germination, allowing us to be confident that rehydration and glucose consumption were indeed starting concomitantly in these spores 2 minutes after glucose addition.

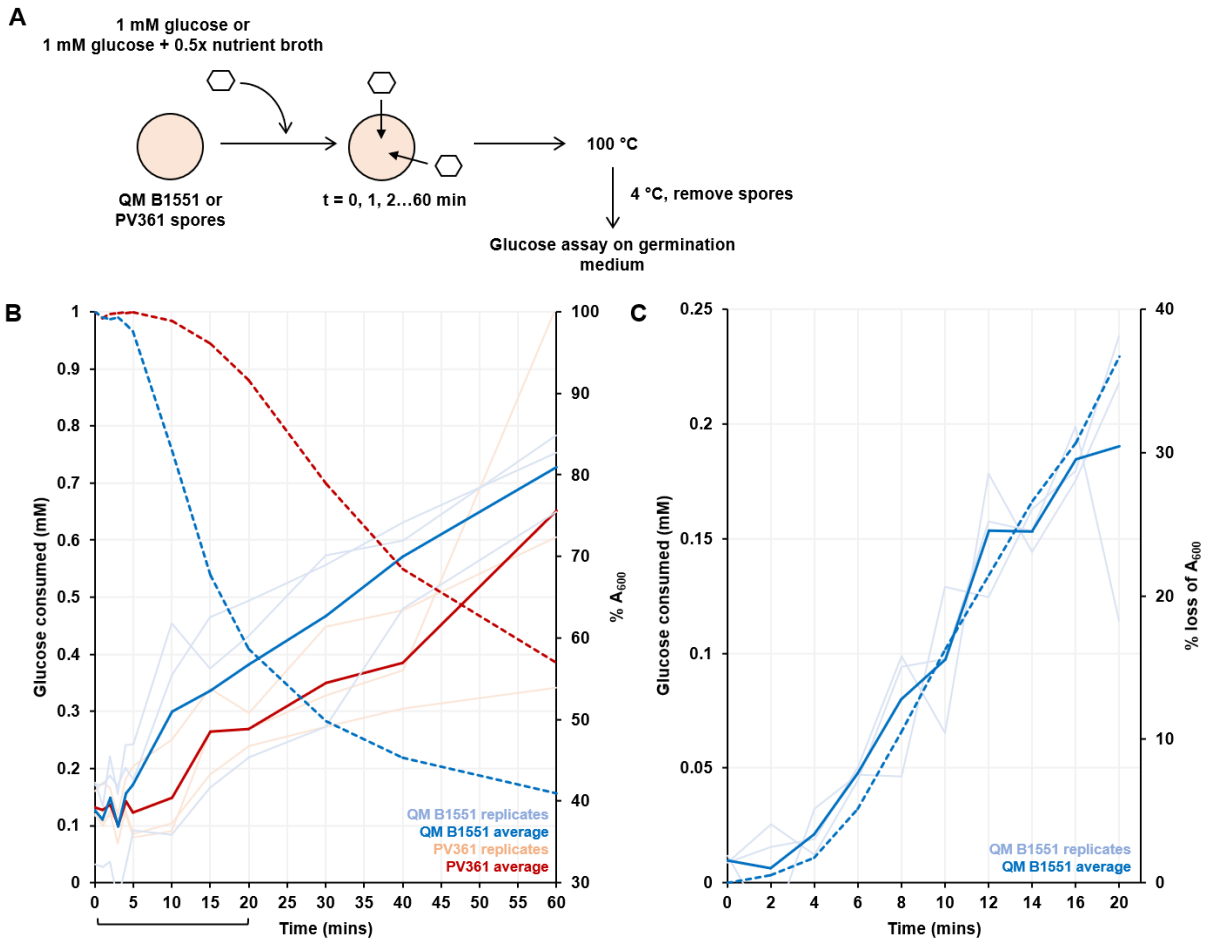

Fig 5. Glucose consumption during germination initiated by glucose/other germinants. (A) Schematic of the experiment for quantification of the remaining glucose in the germination medium following initiation with either 1 mM glucose or 1 mM glucose supplemented with 0.5x nutrient broth in QM B1551 and PV361 spores respectively, in 50 mM potassium phosphate buffer pH 7.5 at 30 °C. This was used to calculate how much glucose had been consumed by a given time point. (B) The average glucose consumption trends for QM B1551 (solid blue) and PV361 (solid red) spores along with the corresponding three biological replicates in light blue and red. Spores from the same culture were used and one biological replicate is one germination time series (0, 1, 2, 3, 4, 5, 10, 15, 20, 30, 40 and 60 mins) experiment. For each time point, the values of technical triplicates from the glucose quantification assay were averaged. The dashed lines are the % of initial A_{600} remaining for both strains, also averaged values of technical triplicates. (C) The average glucose consumption (solid blue) along with the biological replicates (light blue) in the first 20 minutes by QM B1551 spores from another culture. The % loss of A_{600} curve (dashed blue) is also shown.

4.2.4. Hydrogen peroxide production during hydration

H_2O_2 generated during spore rehydration was measured using the fluorometric Amplex red assay outlined in Fig 6A. When spores were germinated with either 1 mM or 4 mM glucose,

an exponential increase in resorufin fluorescence was observed which was proportional to the glucose concentration (Fig 6B-ii). 4 mM glucose led to a higher rate of fluorescence increase than 1 mM glucose irrespective of the HRP concentration, and the rate of fluorescence started increasing concomitantly with the loss of absorbance for both glucose concentrations tested (Fig 6C). Using the standard curve shown in Fig 6B-i, we calculated that over the course of 30 minutes, ~0.2 µM and ~0.7 µM H_2O_2 was detected with 1 mM and 4 mM glucose respectively. This proportional increase in H_2O_2 supports the idea that in germinating spores, more glucose leads to more NADH generation which in turn leads to higher NDH-2 activity and consequently more H_2O_2 production.

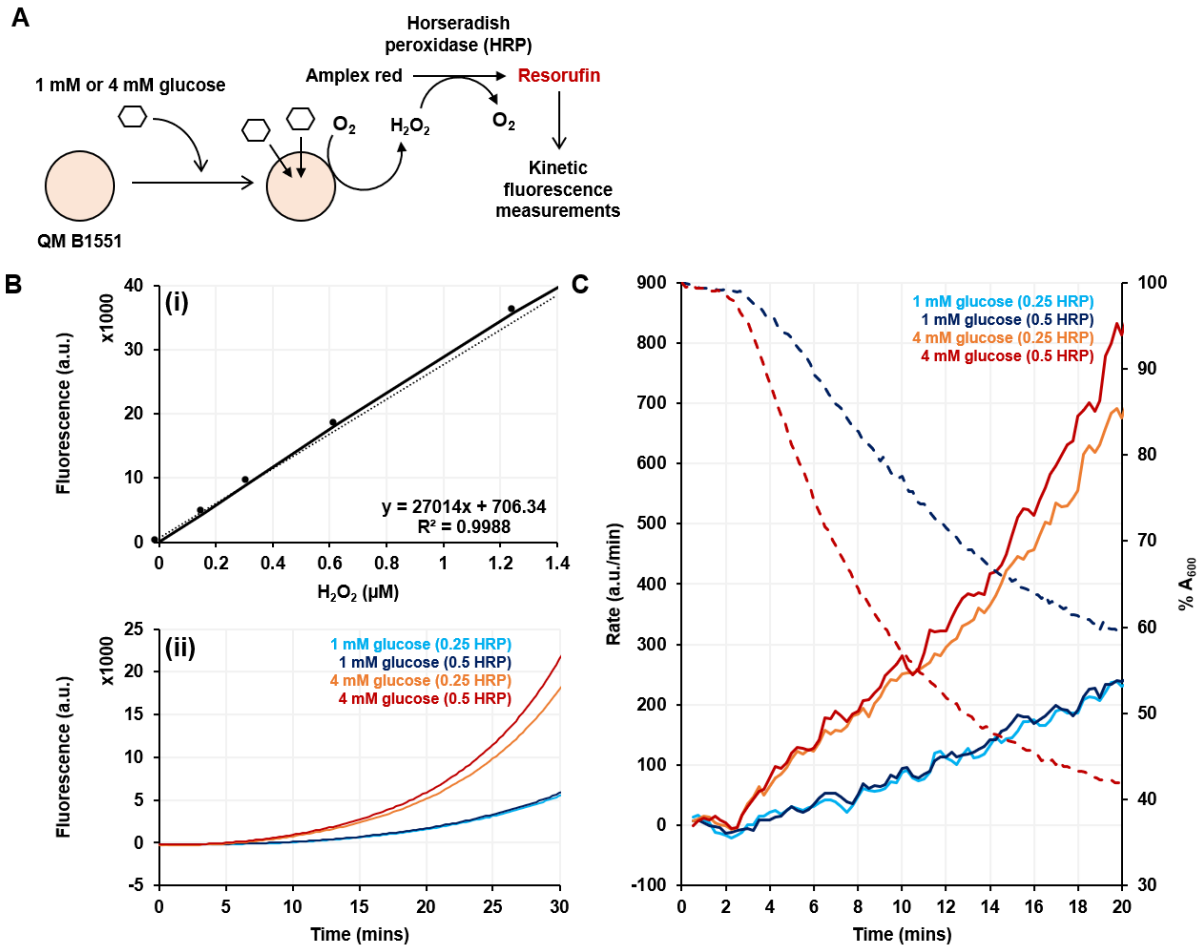

Fig 6. (A) H_2O_2 production during glucose-initiated germination. (A) Schematic of the experimental design for detection of H_2O_2 generated during spore germination initiated with either 1 or 4 mM glucose. (B) (i) The standard curve for known concentrations of H_2O_2 (0, 0.16, 0.31, 0.66, 1.25 µM) and the corresponding fluorescence signal measured at the same optic settings as the germination experiment. The linear regression, equation and R^2 value calculated for the standard curve are also displayed. (ii) Blank-subtracted fluorescence signal (a.u., arbitrary units) measured for spores germinated with 1 mM (light and dark blue) or 4 mM (red and orange) glucose in 50 mM potassium phosphate buffer pH 7.5 at 30 °C. Two concentrations of HRP were used, either 0.25 (light blue, orange) or 0.5 U/mL (dark blue, red). Each reaction was performed in duplicate and values were averaged for analysis. (C) The rate

of fluorescence gain (a.u./min) alongside % of initial A_{600} remaining when spores were germinated with 1 mM or 4 mM glucose, colour scheme indentical to B-ii.

4.2.5. Effect of metabolic inhibitors on hydration

Based on the results from our LC/MS study, we were able to reconstruct the ETC present in dormant spores (Fig 7A). From the quinol pool (Q), electrons can flow down 3 possible branches of the respiratory chain: via cyt *c*, or either of the two quinol oxidases. Cyt *caa*$_3$ oxidase and cyt *aa*$_3$-600 menaquinol oxidase are haem-copper oxidases for which CN^- is a canonical inhibitor. YthAB is a cyt *bd*-II type enzyme which is highly cyanide-insensitive (Borisov et al., 2011b).

While for mitochondrial respiratory complexes specific inhibitors have been discovered or developed that allow a great degree of experimental control over electron flow through the ETC, similarly potent inhibitors for the relatively understudied and divergent bacterial respiratory complexes are not available. Permeability of drugs through bacterial cell envelopes is a challenge as it is, but because of the multilayered architecture of spores this problem is exacerbated. To combat this, we are compelled to use excessively high concentrations of already imperfect inhibitors, which inevitably leads to off-target interactions and phenotypes that cannot be attributed to the intended mechanism of action. Nevertheless, we decided to test the effect of the following compounds on spore rehydration: thioridazine (TRZ), myxothiazol (MYX), potassium cyanide (KCN) and carbonyl cyanide p-trifluoro-methoxyphenylhydrazone (FCCP). TRZ, MYX and KCN have been shown to inhibit the activities of NDH-2 (Schurig-Briccio et al., 2014; Beites et al., 2019), menaquinol cyt *c* reductase (Thierbach and Reichenbach, 1981), and haem-copper oxidases (Wilson et al., 1994) respectively, whereas FCCP is an uncoupler of OxPhos (Burstein et al., 1979). These inhibitors and their targets are depicted in Fig 7A.

Heavily caveated, the data from these experiments show that TRZ and MYX are more effective at inhibiting rehydration than FCCP, while even 10 mM KCN is completely ineffective. Where there was inhibition, germination was still initiated and only the kinetics of absorbance loss (longer lag phase) or the extent of rehydration were affected (Fig 7B i-iv).

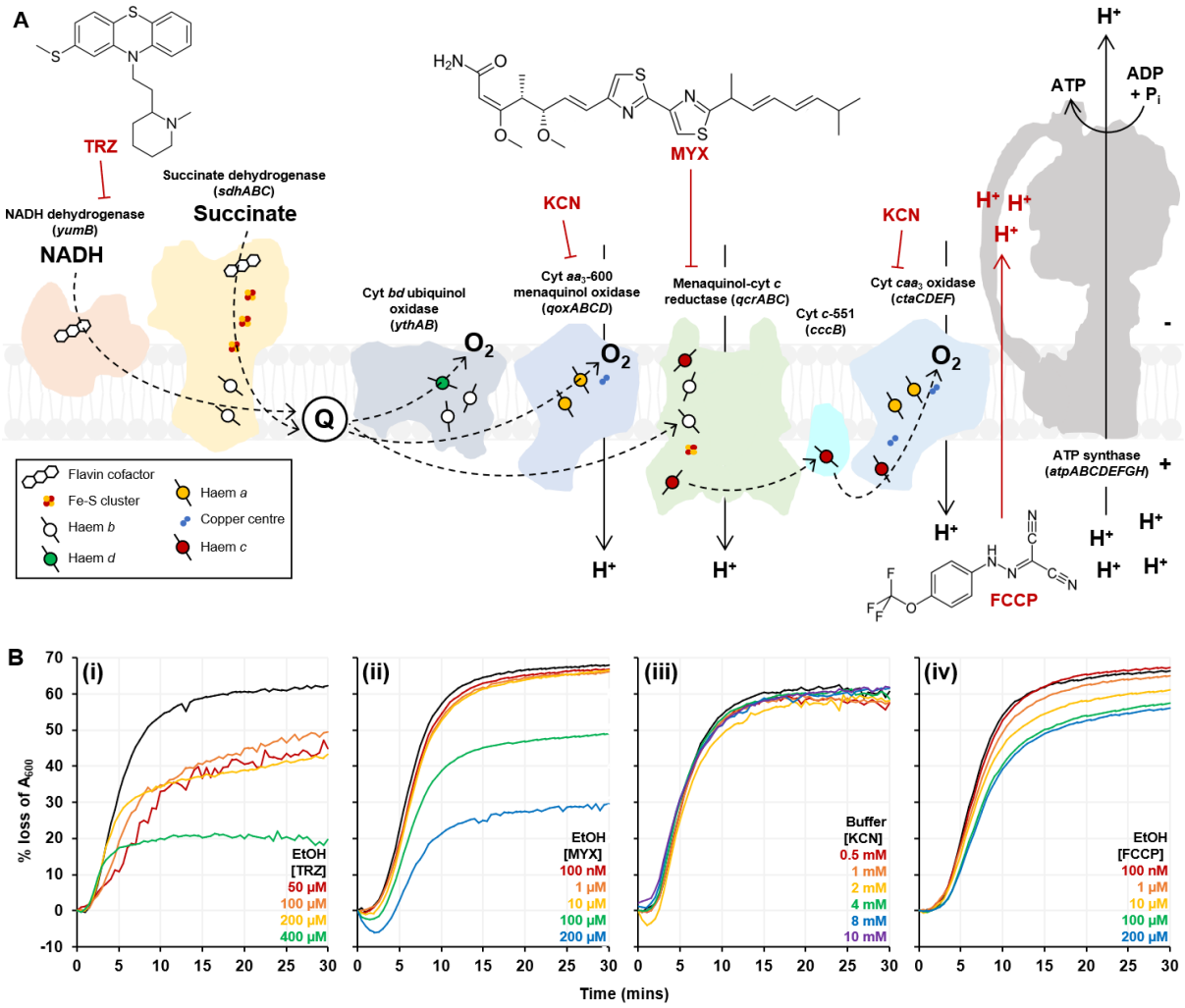

Fig 7. Effect of metabolic inhibitors on glucose-initiated spore rehydration. (A) A cartoon depiction of the ETC present in dormant spores of *B. megaterium*, inferred from LC/MS data. The gene names of the respiratory complexes are shown in parentheses. The intended targets of the inhibitors TRZ, KCN, MYX and FCCP are indicated. (B) Rehydration curves for spores germinated with 4 mM glucose in 50 mM potassium phosphate buffer pH 7.5 at 30 °C, in the presence of (i) TRZ, (ii) MYX, (iii) KCN and (iv) FCCP. Inhibitor concentrations used are indicated in each graph.

4.2.6. Effect of anoxia on hydration and outgrowth

B. megaterium is an aerobic organism, so we reasoned that a cleaner approach to exploring the nature and role of oxidative metabolism in its spores was to compare germination outcomes under normoxic and anoxic conditions. Considering rehydration as preparation for outgrowth, we wanted to re-establish the O_2-dependence of these two phases of germination using a hermetically sealed anaerobic glove box.

We knew from previous experiments that the extent and rate of hydration was glucose concentration-dependent (Fig 4A). Intriguingly, we found that loss of A_{600} started earlier under anoxia and progressed faster: with 1 mM glucose the rate of hydration was noticeably enhanced but closer to saturating concentrations (4 and 10 mM), this enhancement was diminished. Rehydration with KBr remained unaffected (Fig 8A & B).

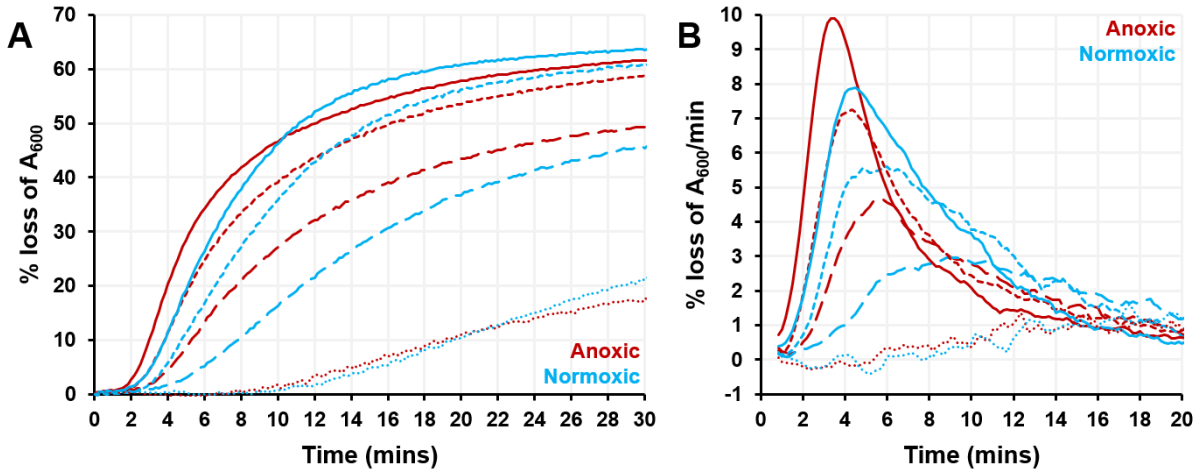

Fig 8. Effect of anoxia on rehydration in glucose/KBr-initiated germination. (A) Rehydration curves for spores when germination is initiated with 50 mM KBr (small dots), 1 mM glucose (long dashes), 4 mM glucose (short dashes) and 10 mM glucose (solid line) under normoxic (blue) or anoxic (red) conditions in 50 mM potassium phosphate buffer pH 7.5 at 30 °C. (B) Rate of rehydration with 50 mM KBr, 1 mM glucose, 4 mM glucose and 10 mM glucose under normoxic and anoxic conditions, same colour scheme as in (A).

As expected, outgrowth required the presence of both nutrient broth and O_2. 1 mM KCN had no inhibitory effect but outgrowth was inhibited by ~60% with excess KCN (Fig 9A-D). Spores germinated with glucose gained nearly twice the absorbance achieved by spores germinated with KBr (Fig 9E). Thus, despite maximum A_{600} loss, both excess KCN and KBr (instead of glucose) in the medium support similar levels of minimal outgrowth.

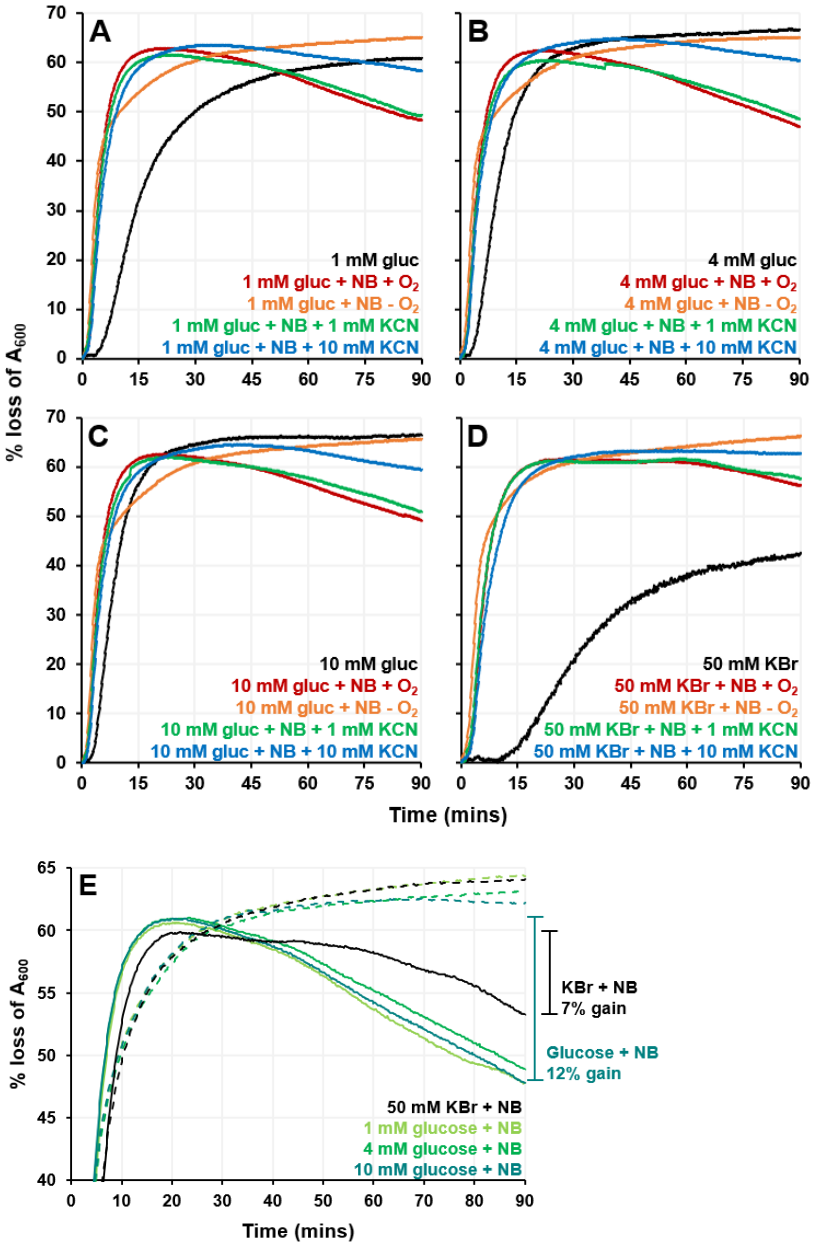

Fig 9. Effect of anoxia on outgrowth in glucose/KBr-initiated germination. Outgrowth curves for spores germinated with germinant alone (black), germinant and 1x nutrient broth with O_2 (red), germinant and 1x nutrient broth without O_2 (orange), germinant, 1x nutrient broth and either 1 mM KCN (green) or 10 mM KCN (blue). Germinants are (A) 1 mM glucose, (B) 4 mM glucose, (C) 10 mM glucose and (D) 50 mM KBr. (E) Outgrowth curves for the germinant and nutrient broth combinations with O_2 (solid line) or without O_2 (dashed line). Germinants are 50 mM KBr (black), 1 mM glucose (light green), 4 mM glucose (intermediate green) and 10 mM glucose (dark teal). % gain in A_{600} is indicated for glucose and KBr experiments.

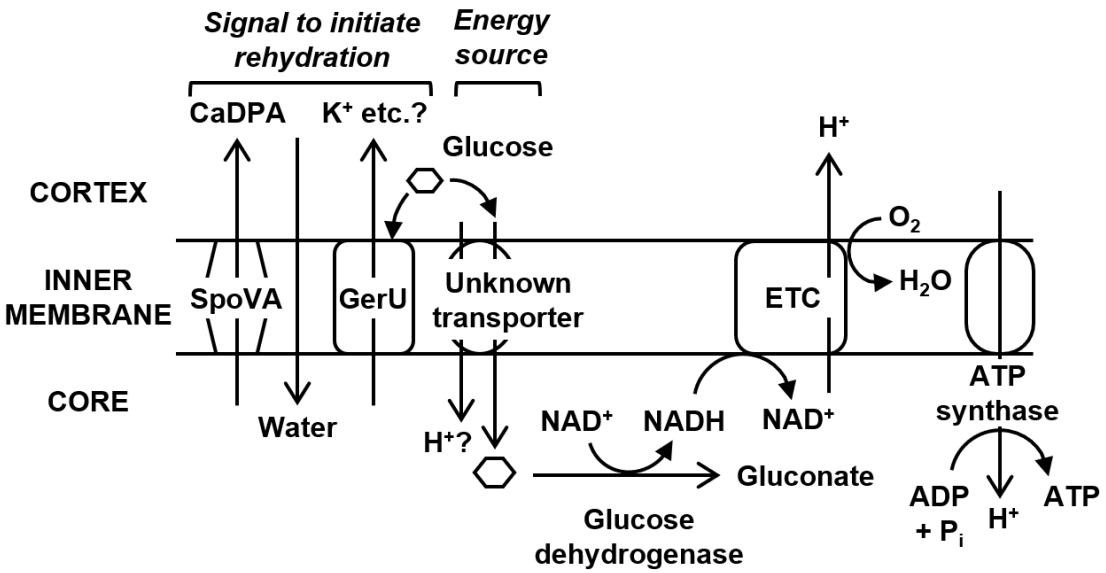

Fig 10. Proposed model for how glucose links the initiation of germination with resumption of bioenergetics and OxPhos in *B. megaterium* spores. The transmembrane movement of various ions and water is shown, that leads to core rehydration and can conceivably reestablish a membrane potential at this stage. The unknown glucose transporter could be GlcU, a glucose:H^+ symporter that will be discussed later (section 4.3.1).

In our model where glucose serves both as a signalling molecule and a source of energy in this species, we started with the assumption that some of the glucose added at the beginning of the experiment is engaged in the signalling pathway while the remaining glucose is oxidised to gluconate to generate NADH. But in the absence of the terminal electron acceptor O_2, NADH would accumulate and this in turn would slow down glucose consumption. This could lead to a situation where more glucose is now available for signalling and so A_{600} loss occurs faster. However, ETC function cannot be resumed without O_2 and so these spores are unable to conserve energy – indeed, it has been shown that both anoxia and excess KCN inhibit ATP synthesis during glucose-initiated germination (Setlow and Kornberg, 1970). We conclude that glucose-powered oxidative metabolism is restarted concurrently with rehydration to meet the energetic demands of outgrowth according to the proposed scheme in Fig 10. ETC function is central to OxPhos, and in the next chapter we will use a novel haem remission spectroscopy device to measure this in real time in germinating spores.

4.3. Discussion and future directions

In *B. subtilis*, a strong germination response can obtained with the mixture AGFK (asparagine, glucose, fructose and K^+ ions) instead of alanine alone. Based on this, it was postulated that initiation of germination requires a source of reducing power, fructose-6-phosphate (or a derivative thereof), and an amino group donor (Prasad, Diesterhaft and Freese, 1972). Assuming these metabolic requirements are largely conserved, what makes single nutrients like glucose (*B. megaterium*), alanine (*B. subtilis*) and inosine (*B. cereus*) potent germinants could be their ability to meet these needs by themselves and/or after being suitably transformed by existing pathways in spores. Yet *Bacillus* species have evolved germinant receptors that specifically recognise a range of nutrients. These perhaps reflect what the most reliable signals of nutritional availability are in their respective ecological niches, and some nutrients can be both a reliable signal and highly compatible with early metabolic requirements.

The ineffectiveness of metabolic inhibitors applied to germinating spores at very high concentrations has led to the dominant idea in the field that resumption of energetics is not essential for initiation of germination (Dills and Vary, 1978). However, we argue that if the inhibitors used are simply ineffective against spores, then any commentary on the essentiality of the enzymes supposedly being targeted is erroneous. For example, one of the inhibitors tested was rotenone which targets type I NADH dehydrogenases, but we know that spores have an NDH-2 instead (YumB) which is better targeted by phenothiazines like TRZ (Schurig-Briccio et al., 2014). In the absence of effective inhibitors, energy metabolism may have appeared to not be critical for rehydration, but all evidence strongly suggests that these processes start at the same time. Thus, we propose a rephrasing of the foundational question from ‘is energy metabolism essential for initiation of germination’ to ‘how do germinating spores restart respiration from such an energetically-depleted state’. The answers to the latter should then be the basis for more thorough and informed investigations into the link between the resumption of energy metabolism and initiation of germination.

4.3.1. Glucose transport during initiation of germination

One crucial missing piece of this puzzle is what transports the glucose into spores in the 2 minutes after glucose addition, which is when we start measuring both glucose consumption and rehydration (Fig 5C). There are two canonical pathways described in bacteria: a

phosphotransferase system (PTS) or a non-PTS glucose:H^+ symporter. The former requires phosphoenolpyruvate (PEP), a glycolytic intermediate for the immediate phosphorylation of the incoming glucose. The latter does not involve phosphorylation of incoming glucose, and is instead driven by PMF (Castro et al., 2009).

For glucose to be taken up the first way, spores would need PEP which they could potentially generate from the large 3-phosphoglycerate (3-PGA) depot as 3-PGA → 2-PGA via phosphoglycerate mutase, and 2-PGA → PEP via enolase. To use the PMF-driven symporter, spores would first need to re-establish ΔpH and/or ΔΨ (membrane potential) that constitute PMF across biological membranes. Interestingly, spores release monovalent cations (H^+, K^+ and Na^+) and leak small amounts of CaDPA almost immediately after germinant addition, with the internal spore pH rising from ~6.4 to 7.5 even before bulk CaDPA release (and phase transition) occurs (Swerdlow, Setlow and Setlow, 1981; Kong, Setlow and Li, 2012). This could conceivably generate a PMF across the atypical spore membrane and be used for glucose transport in our timeline of events (Fig 10). As such, measuring ΔΨ in spores is technically challenging and potentiometric dye-based methods can be misleading (Kikuchi et al., 2022; Li et al., 2023). Nevertheless, recent work has strongly linked the early cation release with the activation of the alanine germinant receptor GerA in *B. subtilis*, proposing that Ger receptors could function as ligand-gated ion channels (Gao et al., 2023). This cation release will be highly relevant to results presented in chapter 5.

Here we must also consider the pathways present in germinating spores for the catabolism of incoming glucose. In *B. megaterium*, glucose can be catabolised by the Embden–Meyerhof–Parnas (glycolysis), pentose-phosphate (PP) and the gluconate pathways. The gluconate pathway, in which non-phosphorylated glucose is oxidised to gluconate by glucose dehydrogenase (GDH), joins the PP pathway (Wushensky et al., 2018). All three pathways become operational in germinating spores, but the gluconate pathway is responsible for more than half of the glucose catabolism in the first 15 minutes (Otani et al., 1986). This implies that majority of the glucose consumed is non-phosphorylated and its uptake is mediated by a non-PTS permease like GlcU.

In our LC/MS study (chapter 3), PtsI (phosphoenolpyruvate-protein phosphotransferase), HprK (HPr kinase/phosphorylase), PtbA (glucose subfamily IIA component) and PtsG (glucose-specific IIBC component), all components of the PTS system, were identified in the soluble and membrane spore fractions analysed. Enolase was one of the most abundant proteins identified. We also found pyruvate kinase, and all the components of the pyruvate dehydrogenase complex (pdhA, B, C, D, bkdB), that generate ATP and NADH respectively. The non-PTS glucose:H^+ symporter, glcU, is in the same operon as glucose dehydrogenase

(gdh) in *B. subtilis* and *B. megaterium*. Both gdh and glcU are known to be expressed during sporulation in *B. subtilis* (Nicolas et al., 2012). While we identified the spore isoform of gdh, we were unable to find glcU but it has been identified in a *B. subtilis* spore membrane proteome before (Zheng et al., 2016). Further work is needed to clarify the relative contributions of PTS and non-PTS transport to glucose uptake during spore germination.

4.3.2. Methodologies of measuring ATP generation in glucose-initiated germination

ATP generation is another aspect of spore germination that should be revisited with new techniques and a modern understanding of bioenergetics.

Hyatt and Levinson (1959) showed that although spores will germinate in its absence, phosphate is required for postgerminative development/outgrowth. Later, Setlow and Kornberg (1970) observed that in glucose-germinated spores, ATP generation was inhibited without phosphate (alternative buffer not specified). Confusingly, they asserted in the main text citing KBr as an example (but not showing the data) that endogenous phosphorous reserves were sufficient for ATP generation in the first 15 minutes. Indeed, ATP production was later measured for spores germinated with glucose in 5 mM Tris pH 8 buffer without exogenous phosphate (Dills and Vary, 1978). Irrespective of the phosphate requirement, Setlow, Kornberg, Dills and Vary all interpreted their data as showing loss of A_{600} preceding increase in ATP levels. Inspecting their data closely, we think the difference in the sequence of these events is marginal. For Dills and Vary, the earlier loss of A_{600} compared to ATP generation could be attributed to the Tris buffer which in our experience also accelerates A_{600} loss (Fig 2B-ii, 2C-i). However, Dills and Vary used purer luciferin-luciferase and a luminescence biometer for their study, which was shown to be 50 times more sensitive (Chapman, Fall and Atkinson, 1971) than the method used by Setlow & Kornberg (firefly tail extracts and a scintillation counter). Before the enzymatic assay, both teams first had to subject their germinating spores to sample extraction by boiling propanol, a harsh chemical treatment.

We must be cognisant that with these methods, the steady state levels of ATP at a given time point are measured which could be low if ATP consumption is high but production is not evenly matched. In other words, ATP not being measurable at a given time point is not equivalent to the absence of ATP turnover which actually reflects the dynamic metabolic status of a cell. The relative abundance of phosphorylated metabolites (e.g. ATP:ADP ratio) is most accurately

measured by non-invasive methods like ^{31}P-NMR which has been applied to live bacterial cells before (Lohmeier-Vogel, Ung and Turner, 2004), but not to germinating bacterial spores.

As a starting point though, qualitative measurements (like those for glucose consumption and H_2O_2 production presented here) can be attempted for ATP levels as well. Such experiments could easily be performed using commerically available, highly sensitive assay kits employing recombinantly produced luciferase. What would need more deliberation is sample extraction, and whether the loss of physicochemical resistance as spores germinate leads to higher recovery at later stages of the experiment thereby exaggerating the measured ATP levels.

An altogether alternative approach to studying the energetic status of germinating spores could be to measure ETC function concomitantly with O_2 consumption as this is how ATP is normally generated by OxPhos. As will be discussed extensively in the next chapter, this would first require a reappraisal of OxPhos in spore germination.

Chapter 5: Haem remission spectroscopy on germinating spores of *B. megaterium*

5.1. Introduction

5.1.1. Bioenergetics of *Bacillus* spore germination

We remarked in the thesis introduction (section 1.6.2) that bioenergetic processes not being measureable during initiation of spore germination has over the years perhaps been misconstrued as evidence for their irrelevance. Consequently, few in the field concern themselves with how germinating spores conserve the energy they need to complete germination and outgrow. To address this state of affairs, we suggested in the previous chapter a rephrasing of the foundational question in spore germination from "is energy metabolism essential for initiation of germination' to 'how do germinating spores restart respiration from such an energetically-depleted state' (section 4.3). New answers obtained to the latter question are presented in this chapter. We will begin with a brief recapitulation of how the field has arrived at its current position on the matter.

Found in all Firmicutes spore-formers, depots of the glycolytic intermediate 3-PGA (3-phosphoglyceric acid) are thought to be chief amongst the endogenous reserves spores rely on during germination; substrate-level phosphorylation of 3-PGA derived PEP to pyruvate by pyruvate kinase can generate ATP. This is especially relevant when spores are germinated in nutrient-poor media with KBr (Setlow and Kornberg, 1970) or CaDPA (Korza et al., 2023b). In this approach to studying spore metabolism, a nutrient germinant is extraneous because the aim is to define the minimal metabolic capacity of the germinating spore and identify a vulnerability to exploit. For instance, Korza et al. proposed that phosphoglycerate mutase, the enzyme that converts 3-PGA to 2-PGA, could be a promising target in germinating spores to stop ATP generation, as spores that are unable to generate enough ATP lose viability.

But the fact of the matter is that compounds that initiate germination are invariably nutrients like sugars and amino acids, so a physiologically relevant description of spore metabolism cannot just ignore a germinant's contribution. The risk with extrapolation from this approach is illustrated when we consider that in glucose-germinated spores, 3-PGA was still utilised, and ATP production was not inhibited (as it was in KBr-germinated spores) by an enolase inhibitor (Setlow and Kornberg, 1970). The seemingly causal link between 3-PGA utilisation and ATP

production did not hold when a nutrient germinant was introduced in later studies as well (Scott and Ellar, 1978a; Sano et al., 1988). At the time of the original study, it was believed that spores did not have ETC cytochromes, instead a flavin-dependent NADH oxidase (explored in chapter 3) was present. Understandably then, it was difficult for Setlow & Kornberg to reconcile this with their observation that ATP production was inhibited by excess KCN or under anaerobiosis during glucose-initiated germination.

However, from 1975 onwards there was increasing recognition of respiratory cytochromes in developing forespores of alanine-responsive *B. megaterium* KM (Wilkinson & Ellar, 1975), cytochrome *d* was discovered spectroscopically in these forespores (Hogarth, Wilkinson and Ellar, 1977), and an increase in KCN-insensitive O_2 consumption was correlated with increasing NADH oxidase activity in membranes isolated from germinating spores (Wilkinson et al., 1977). In the strain QM B1551, NAD(P)H generation was measured to start concurrently with A_{600} loss (but interpreted as a later event) in both KBr and glucose-containing complete media, and NADH oxidation was inhibited by excess KCN/anaerobiosis. The authors wrote, "*It appears like that much of the NADH is used to generate ATP via some type of oxidative phosphorylation*" (Setlow and Setlow, 1977).

When the QM B1551 strain of *B. megaterium* was first isolated in the early 1950s, O_2 consumption of its germinated spores was measured using Warburg manometers and found to be cyanide-insensitive (Powell, 1951; Spencer & Powell, 1952). Later, using Clark-type electrodes, O_2 consumption was measured to start 5 mins after glucose addition, contributing to the prevailing idea that resumption of oxidative metabolism is not essential for initiation of germination (Dills and Vary, 1978). O_2 consumption in spores of alanine-responsive KM strain was detectable 2 mins after alanine addition, reached maximal rate after 7 mins, and was approximately halved but not entirely abolished by 10 mM KCN (Wilkinson et al., 1977).

At this juncture, there was a pivot to establishing whether this resumption of respiration was required/responsible for initiation of germination itself. Studies in both QM B1551 and KM strains concluded that this was not the case, based on measurements of ATP levels, O_2 consumption, glucose/alanine uptake and catabolism, the ineffectiveness of metabolic inhibitors/anaerobiosis in preventing A_{600} loss (discussed in chapter 4), and other experiments (Scott and Ellar, 1978a; Dills and Vary, 1978; Shay and Vary, 1978). Two influential ideas emerged: 1) metabolism is only resumed after loss of A_{600} starts, therefore resumption of metabolism cannot trigger exit from dormancy and, 2) exit from dormancy can occur even when the resumption of metabolism is prevented, so bioenergetic processes are not critical for rehydration. We reiterate here that in our opinion even marginal precedence of A_{600} loss as compared to NADH/ATP generation, O_2 consumption etc. in these studies was sometimes

interpreted as significant. Another subtler problem is this inherent contradiction: how can metabolism be measured to start alongside germination using multiple techniques, yet not be critical for a process that is triggered by nutrient availabilty and by which energetically-depleted spores get transformed back to functional cells?

In the 1980s, moving away from the concern of essentiality, a series of papers attempted to detail how metabolism was resumed in germinating QM B1551 spores. They found that concurrently with hydration, spores oxidised ~60% of the incoming glucose to gluconate in the first 5 mins and this gluconate pathway remained dominant for the first 30 minutes after glucose addition, generating NADH (Maruyama et al., 1980; Otani et al., 1986). [^{32}P] orthophosphate (P_i) incorporation into acid-soluble compounds like ATP began within 2 minutes of glucose-initiated germination (Otani, Umezawa and Sano, 1987). The authors remarked that, "*In germinating spores, ATP is probably generated by oxidation of NADH through respiratory chains, which does not depend on 3-PGA breakdown and subsequent glucose metabolism via the EM pathway…NADH required for the aerobic ATP formation is efficiently generated coupling with glucose oxidation to gluconate (catalysed by glucose dehydrogenase)...*" In their last paper on the subject, they measured concomitant glucose and O_2 consumption along with NADH generation using fluorescence (albeit with limited success), and placed their findings in the context of the field (Sano et al., 1988). As alluded to in the previous chapter, these papers have since been forgotten and are not included in the prevailing models of spore germination.

It was recently reasserted that OxPhos does not become operational until full hydration is achieved following complete CaDPA release and cortex degradation (Korza et al., 2023b). For a synchronously germinating population of *B. megaterium* spores, this corresponds to the asymptotic region of the rehydration curve, which with 10 mM glucose is reached 15 minutes after glucose addition (chapter 4, Fig 4A). As shown in Fig 1, this notion is inconsistent with the timeline for other OxPhos-related events like glucose, O_2 consumption, NADH and ATP generation that have been measured in this strain. Despite many discrepancies across studies, all of these events have been measured to start no later than 5 minutes after glucose addition. This state of confusion highlights the need for a new model of bioenergetics in germinating spores.

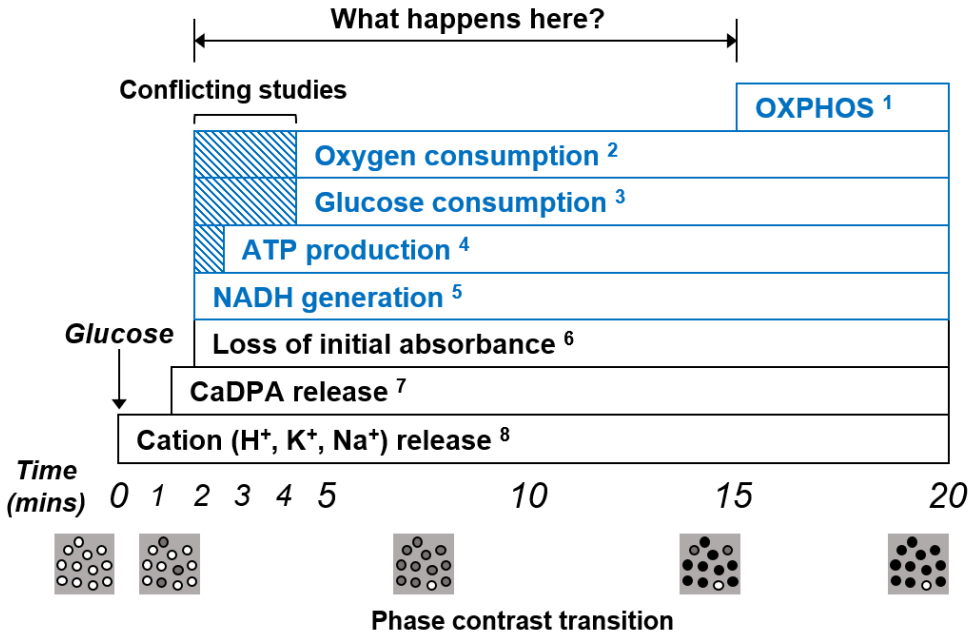

Fig 1. The timeline of events during germination in *B. megaterium* QM B1551 showing when various processes have been measured/inferred to start in the spores of this species. Findings from the following studies were used to compile this timeline: [1](Korza et al., 2023b), [2](Dills and Vary, 1978; Sano et al., 1988); [3](Racine, Dills and Vary, 1979; Maruyama et al., 1980); [4](Setlow and Kornberg, 1970; Dills and Vary, 1978; Otani, Umezawa and Sano, 1987); [5](Setlow and Setlow, 1977); [6](Setlow and Kornberg, 1970; Dills and Vary, 1978); [7](Racine, Dills and Vary, 1979); [8](Swerdlow, Setlow and Setlow, 1981). Processes shown in blue are related to energy metabolism, and the striped regions indicate the uncertainty stemming from conflicting experimental data. Small illustrations at the bottom show how spores transition from being phase bright to phase dark as observed by phase contrast microscopy during hydration (personal communication with Dr. Graham Christie).

Building on the work from Sano et al. 1988, in chapter 3, we confirmed the identity of the spore isoform of glucose dehydrogenase, and showed that the soluble flavin-dependent NADH oxidase isolated from QM B1551 spores is highy unlikely to be the terminal oxidase during rehydration when there exists a functional and branched ETC containing two uncharacterised spore-specific cytochromes. In chapter 4, we measured glucose concentration-dependent rehydration, glucose consumption and H_2O_2 production all starting ~2 minutes after germinant addition, consistent with electron transport from glucose to O_2 via the ETC. Recognising rehydration as preparation for outgrowth, we demonstrated that spores unable to conserve energy by glucose-powered OxPhos in the absence of O_2 rehydrate even faster but cannot outgrow/complete germination. In this chapter, we sought to understand the functional state of the ETC during spore rehydration using a novel haem remission spectroscopy device designed by Dr. Roger Springett (CellSpex, UK & University of York, UK) called the 'bioenergetic chamber', that also enables simultaneous O_2 consumption measurements.

Using this technique, we are in a unique position to directly address the question of when OxPhos is restarted with respect to A_{600} loss in a synchronously germinating population of *B. megaterium* spores.

5.1.2. Principles of haem spectroscopy and its use in *Bacillus* spores

Respiratory cytochromes that constitute ETCs contain prosthetic cofactors like iron-sulphur clusters and haem groups. These serve as redox centres for the sequential transfer of electrons from reductants (e.g. NADH) to terminal electron acceptors (e.g. O_2) which is coupled to PMF generation across the membrane. A haem group consists of an iron atom coordinated to a highly conjugated porphyrin ring system, and different side chain substitutions give rise to distinct types of haems. In the spore ETC, the cytochromes identified contain haems of the type *a*, *b*, *c*, and *d*. Each haem type has a characteristic and strong visible-wavelength absorbance band owing to the functionalised porphyrin ring system, but within a cytochrome this is further influenced by how the haem is ligated and the protein environment. When haems undergo reduction, these characteristic absorbance bands change so using absorbance spectroscopy, identification of which haem groups are present in a sample is straightforward. We can also quantify the haem content if we know the extinction coefficients of the haems present and absolute haem spectra (reduced - oxidised difference spectra) can be obtained.

The first low temperature haem absorption spectra of dormant *B. subtilis* spores cooled with liquid air revealed that they had only ~6% of the cytochrome content found in vegetative cells (Keilin & Hartree, 1949). No cytochromes could be detected either at room temperature or at low temperature in *B. cereus* spores, lending credence to the idea that spores used a soluble flavoprotein oxidase instead (Doi & Halvorson, 1961a). The presence of cytochromes was later confirmed in *B. subtilis* spores at room temperature (Tochikubo, 1971). Subsequently, it was suggested that these conflicting findings could be a result of optical problems arising from the high refractility of spores. When the surrounding medium is of a similar refractive index and allows more incident light to enter spores, it can be absorbed by the cytochromes instead of being scattered. Accordingly, cytochromes in *B. cereus* spores became detectable when they were suspended in glycerol (Bahnweg and Douthit, 1975). The biochemical/spectroscopic studies that followed used isolated spore membranes instead of whole spores because the latter are not permeable to common oxidising/reducing agents or

reductants like NADH which greatly restricted experimentation. Any insights into ETC function could not be gleaned from intact spores with the techniques available at the time.

Using remission haem spectroscopy, we can now attempt to see redox changes in ETC cytochromes immediately after germination is initiated with high spectral and temporal resolution. In the bioenergetic chamber, a powerful LED light source illuminates a dense spore suspension (optical density between 2-3). The back-scattered light is then collected in remission geometry (pathlength of ~39 mm where the light source and output are 10 mm apart), passed through a spectrograph and complete spectra in the desired wavelength range are collected on a sensitive CCD camera. Importantly, by only collecting the back scattered light, the remission spectroscopy apparatus employs very different optics to the more familiar transmission spectroscopy used previously. Therefore, remission spectroscopy may inherently be more suitable for room temperature studies of highly refractile spores.

The device also incorporates an O_2 optode (instead of a traditional Clarke-type electrode) which relies on the phosphorescence half-life of a platinum-porphyrin compound to measure O_2 concentration (Lee and Okura, 1997). A blend of N_2/O_2 is delivered through silicone tubing submerged in the spore suspension to maintain a constant O_2 concentration during the experiment (Hollis et al., 2003; Kim, Ripple and Springett, 2011).

5.1.3. Terminal oxidases and their catalytic cycles

As listed in chapter 3 and shown in Fig 3C later, we have identified 3 different terminal oxidases in spores: two are haem-copper oxidases (HCOs) and the third is a cyt *bd*-II type oxidase. Of the two HCOs, one is a quinol oxidase and the other a cyt *c* oxidase that oxidise quinol and reduced cyt *c* respectively to reduce O_2. The *bd* oxidase is a copper-free enzyme that oxidises quinol to reduce O_2.

Here, the catalytic cycles of these terminal oxidases are discussed along with what certain visible range spectral signatures can tell us about their functional state. This is by no means a comprehensive review of the vast literature on this subject – only knowledge essential for interpreting our spectral results is presented.

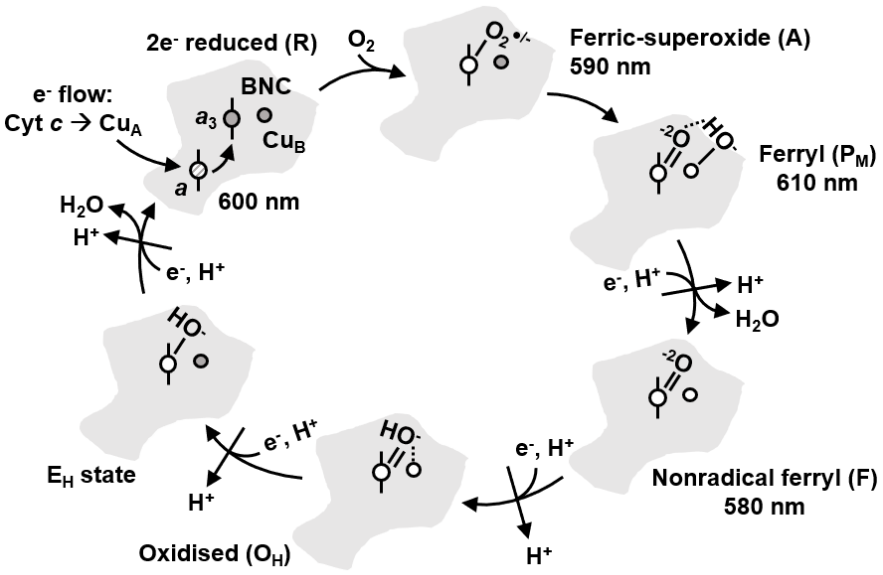

Fig 2. The canonical catalytic cycle of haem-copper oxidases (HCOs, cyt *caa*$_3$ oxidase and cyt *aa*$_3$-600 menaquinol oxidase) showing the catalytic intermediates formed at the binuclear centre (BNC, composed of Cu_B and haem a_3) and the characteristic absorbances of their α-peaks. Grey colour of the haem/copper group indicates reduced Fe^{2+}/Cu^{+}, white colour indicates oxidised Fe^{3+}/Cu^{2+} state. Haem *a* can be oxidised/reduced, shown as a striped haem centre in the R intermediate.

HCOs like cyt *caa*$_3$ and cyt *aa*$_3$-600 catalyse the following reactions to reduce O_2 to H_2O, using cyt *c* and quinol as electron donors respectively:

$$4 \text{ cyt } c_{red} + 8H^{+}_{in} + O_2 \rightarrow 4 \text{ cyt } c_{ox} + 2H_2O + 4\ H^{+}_{out}$$

$$2QH_2 + 8H^{+}_{in} + O_2 \text{ —> } 2Q + 2H_2O + 8H^{+}_{out}$$

In the catalytic cycle of HCOs (Fig 2), electrons are transferred from reduced cyt *c*/quinol to Cu_A to haem *a* (characteristic absorbance at 600 nm) and then to the binuclear centre (BNC), composed of haem a_3 and Cu_B. Once both haem a_3 and Cu_B are reduced, O_2 binds to haem a_3. Thereafter each electron and proton transfer step to the BNC is coupled with the pumping of an additional proton through the membrane which contributes to the PMF. As proton pumping is slow, numerous intermediates of haem a_3 bound to partially reduced O_2 are formed and some are stable enough to be resolved and studied by biophysical/spectroscopic methods (Wikström, Gennis and Rich, 2023). The P_M intermediate is formed by the irreversible cleavage of the O-O bond and this is not an electrogenic step, but the subsequent steps are electrogenic and are also reversible by high PMF as shown in isolated mitochondria (Wikstrom, 1981). In sub-mitochondrial particles, it was shown that ΔΨ slows down cyt *c* oxidase turnover leading to the accumulation of the F intermediate because proton uptake and

pumping required for the F→O transition are suppressed by the thermodynamic backpressure (Shimada, Tsukihara and Yoshikawa, 2023; Björck and Brzezinski, 2018).

When measured in isolated enzyme preparations, P and F are found to be minor intermediates under turnover conditions while haem *a* is considerably reduced (Mason, Nicholls and Cooper, 2009, 2014; Rocha and Springett, 2019). Challenging this, in isolated heart mitochondria, P and F were recently shown to be the dominant catalytic intermediates whereas reduced haem *a* and R state of the BNC accumulated only under hypoxia (Covian et al., 2023). However, when mitochondria are under physiological conditions within mammalian cells, the ferryl intermediates P and F are not detectable, with reduced haem *a* being the dominant spectral signature of cyt c oxidase activity (Kim, Ripple and Springett, 2011). As the ferryl intermediates P and F have never been detected *in vivo*, reduced haem *a* (peak at 600 nm) is the expected spectroscopic signature during catalytic turnover.

Cyt *bd* are tri-haem copper-free terminal oxidases unique to prokaryotes that are increasingly being recognised for their versatile roles in bacterial physiology (Friedrich, Wohlwend and Borisov, 2022). Several bacteria use *bd* oxidases under low O_2 tension conditions, allowing them to survive in hypoxic environments like those encountered during pathogenesis (Jones-Carson et al., 2016; Shepherd et al., 2016; Corbett et al., 2017). As O_2-scavenging enzymes, cyt *bd* oxidases are thought to be involved in respiratory protection of O_2-labile nitrogenase in aerotolerant N_2-fixing bacteria, and in defence against antibacterials [e.g. bedaquiline in *Mycobacterium tuberculosis*, (Mascolo and Bald, 2020)] as well as oxidative/nitrosative stress (Borisov et al., 2021a).

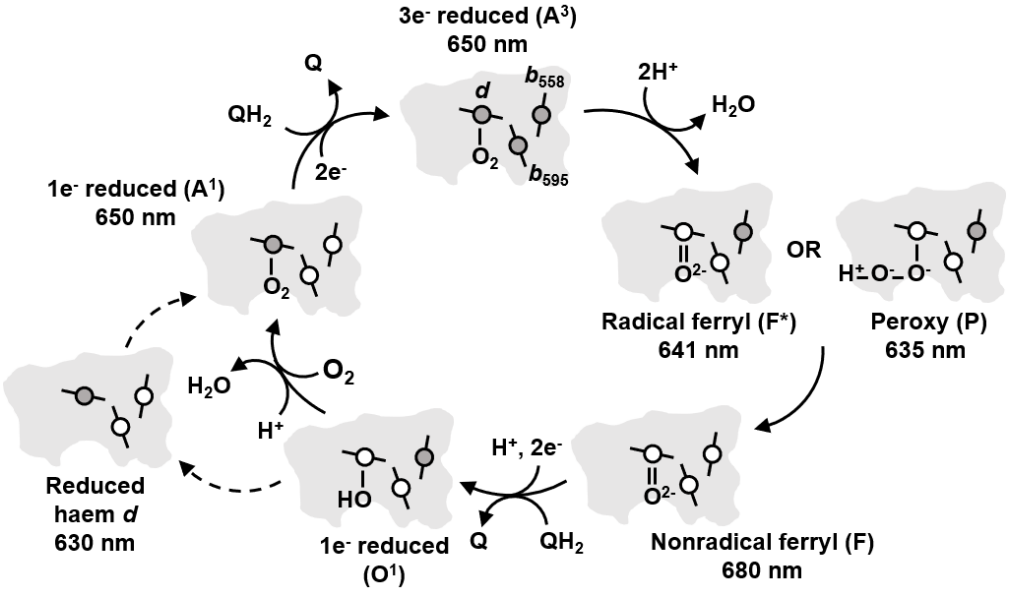

Fig 3. The canonical catalytic cycle of cyt *bd* oxidase showing the reaction intermediates formed at the di-haem site (composed of haem b_{595} and haem *d*) and the characteristic

absorbances of their α-peaks. Superscripts in A^1, O^1, A^3 indicate the number of electrons present across the redox centres in the enzyme. Grey colour of the haem group indicates reduced Fe^{2+} state, white colour indicates oxidised Fe^{3+} state.

Fig 3 shows the catalytic cycle by which cyt *bd* performs the following reaction to reduce O_2 to H_2O:

$$2QH_2 + 4H^+_{in} + O_2 \rightarrow 2Q + 2H_2O + 4H^+_{out}$$

Cyt *bd* function contributes to the PMF, but unlike HCOs, cyt *bd* does not pump protons across the membrane. Instead, protons are translocated during quinol oxidation and ejection of protons into the periplasm, and when cytoplasmic protons are taken up during O_2 reduction at the catalytic site. Cyt *bd* has a high affinity for O_2 and is unique among terminal oxidases for its ability to bind O_2 in a single-electron reduced state. Possibly as it does not pump protons, it can reduce O_2 at a much faster rate compared to HCOs (Borisov et al., 2021b). A peak at 650 nm is characteristic of haem *d* that is reduced and bound to O_2, an early catalytic intermediate called the A state (Poole et al., 1983). The 630 nm peak appears when haem *d* is reduced but not bound to O_2. It has been shown with anaerobic 1 electron-reduced cyt *bd* that increasing O_2 concentration shifts the absorbance peak from 630 nm to 650 nm whereas removing the O_2 does the reverse (Belevich et al., 2005), and that the A state of cyt *bd* is one of the dominant intermediates along with the F state (broad peak at 680 nm) under turnover conditions when measured in a purified enzyme preparation (Borisov et al., 2011a).

5.2. Results and Discussion

5.2.1. Haem spectra of isolated spore and cell membranes

In chapter 3, we showed that membranes isolated from dormant spores oxidised NADH twice as fast and were nearly 2.5 times less sensitive to KCN inhibition as compared to membranes isolated from late exponential-phase vegetative cells. We also identified a spore-specific *ythAB*-encoded cyt *bd* oxidase and suggested that its activity could explain the KCN-insensitive O_2 consumption reported in germinating spores. These results motivated us to measure haem spectra of spore and cell membranes reduced with the physiological reductant NADH and the strong chemical agent sodium dithionite ($Na_2S_2O_4$) in the bioenergetic chamber (schematic shown in Fig 4A). The $Na_2S_2O_4$-reduced minus air-oxidised difference spectra revealed qualitative differences in their ETC composition – spore membranes had a small peak at 630 nm (diagnostic of haem *d*) which was absent in cell membranes (Fig 4B & C).

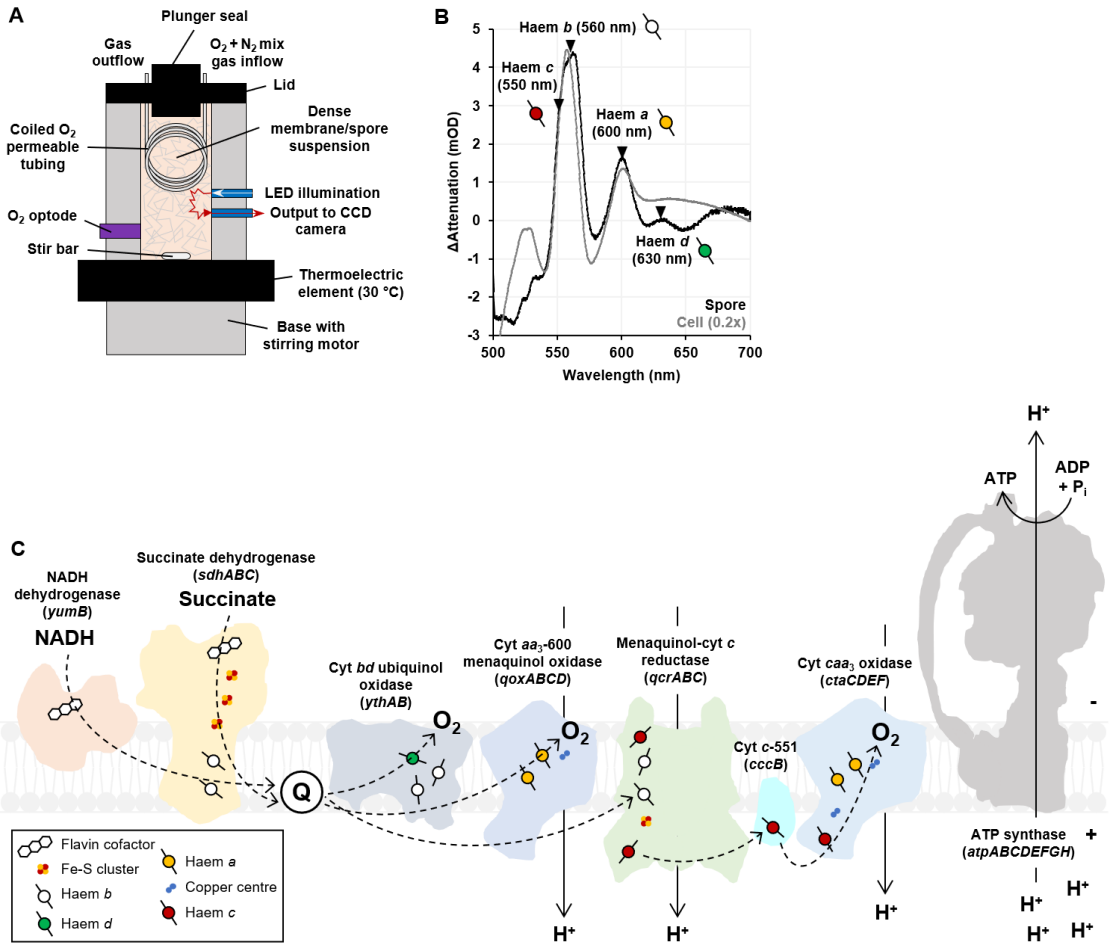

Fig 4. Remission haem spectroscopy on isolated cell and spore membranes using the bioenergetic chamber. (A) Schematic of the bioenergetic chamber highlighting the important design features. The 5 mL sample volume is constantly agitated by a stir bar, oxygenated by silicone tubing that supplies a O_2+N_2 blend to match the set O_2 concentration (100/120 µM), and maintained at the desired temperature (30 °C) by the thermoelectric element. The sample is illuminated by a white LED, and the re-emitted light is directed towards the CCD-spectrograph system. With further data processing, spectra are recorded at a temporal resolution of 500 ms, i.e. 120 spectra/min. (B) The $Na_2S_2O_4$-reduced minus air-oxidised spectra of isolated cell (grey) and spore (black) membranes fitted to linear regressions. The cell membrane spectrum was scaled down 0.2 times to be comparable. The characteristic wavelengths of reduced haems *c*, *b*, *a*, and *d* are labelled. (C) Scheme of the ETC present in dormant spores based on the mass spectrometric analysis of BN-PAGE bands obtained with DDM-solubilised isolated spore membranes (chapter 3). Haem groups and other redox centres are denoted by symbols shown in the legend on the bottom left.

Upon reduction with NADH, spore membranes were measured to consume O_2 at approximately twice the rate of cell membranes (Fig 5A), comparable with the rates obtained from the spectrophotometric NADH:O_2 reaction assays. We then compared the haem spectra 2 mins and 4 mins after NADH reduction (Fig 5B & C). For both membranes, spectral features at 550 nm, 560 nm and 600 nm indicate reduction of haems *c*, *b* and *a* respectively and the activation of the corresponding respiratory enzymes (Fig 4C). In spore membranes, there is additionally a minor shoulder at ~565 nm associated with cyt *bd* oxidase haem b_{558} reduction (Grauel et al. 2021) and a broad peak extending from 625 nm to 700 nm, centred roughly at 660 nm. It is not possible to solely assign this either to the cyt *bd* oxidase A state (650 nm) or to the charge-transfer complex formed by YumB, the spore-specific type-II NADH dehydrogenase (Blaza et al., 2017).

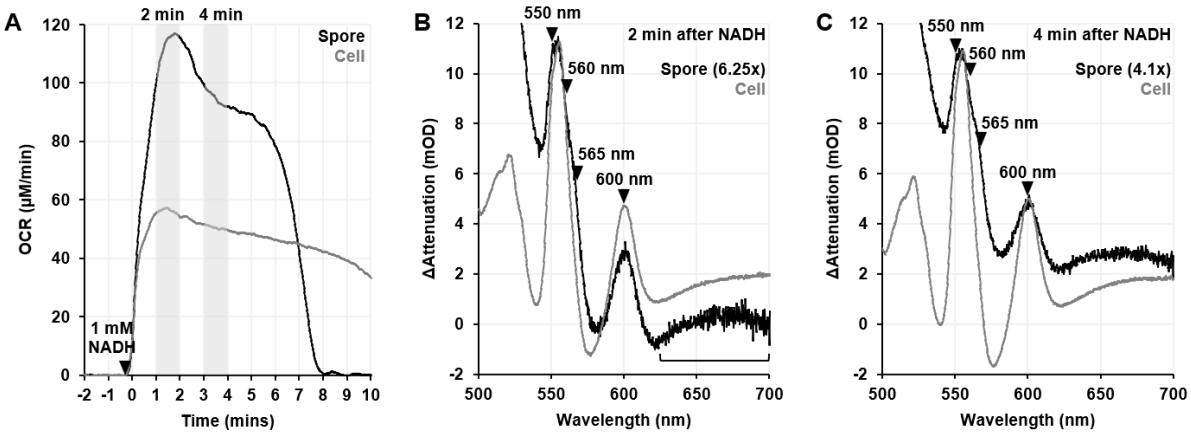

Fig 5. Studying NADH oxidation by spore and cell membranes in the bioenergetic chamber. (A) O_2 consumption rates (OCR, in µM/min) measured for spore (black) and cell (dark grey) membranes at a protein concentration of 0.25 mg.mL^{-1}, oxidising 1 mM NADH added at t=0 min. The O_2 concentration was maintained at 120 µM during the experiments. The shaded

areas (light grey) show the preceding 1-min intervals over which the recorded spectra were averaged to obtain the corresponding 2 min and 4 min spectra used in (B) and (C). (B) Comparison of difference spectra (2 min spectrum minus pre-NADH baseline) after 2 mins of NADH addition. Spore membrane spectrum (black) was scaled up 6.25 times to be comparable to the cell membrane spectrum (dark grey). (C) Same as (B) but 4 mins after NADH addition. Indicated wavelengths 550 nm, 560 nm and 565 nm, and 600 nm correspond to reduced haems of type *c*, *b*, and *a* respectively. The square bracket in (B) indicates the 625-700 nm region that is mentioned in the main text.

Throughout these experiments, haem attenuation measured for spore membranes was smaller than that measured for cell membranes, even though both were used at the same protein concentration and reduced with the same NADH concentration. Thus, spore membranes oxidise NADH considerably faster despite a lower overall haem content as compared to late-exponential phase cell membranes. Contrary to what has been reported previously in membranes from *B. cereus* (Escamilla et al., 1988), menaquinone levels in dormant spore membranes do not appear to be a limiting factor for electron transport in our hands.

5.2.2. The effect of Histodenz purification and heat activation on attenuation spectra and oxygen consumption of germinating spores

The purity of spore preparations is always important for robust experimentation (Setlow, 2019), but for a technique as sensitive as remission haem spectroscopy this becomes especially necessary because any vegetative contamination, like broken mother cell debris or defective/partially germinated spores, will have haem groups that will contaminate the measured signal. Depending on the extent of vegetative contamination, this may even overwhelm the signal from germinating spores themselves. We realised that this had been the case in our earliest experiments where insufficiently washed spores were heat activated but not Histodenz-purified. Spores were used at an optical density as high as 20 to maximise haem signal, but this led to O_2 consumption rates that exceeded the O_2 delivery capacity of the bioenergetic chamber leading to anoxia within ~2 minutes of glucose addition. Results from an early experiment in which we compared the effect of KBr and glucose is shown (Fig 6A & B).

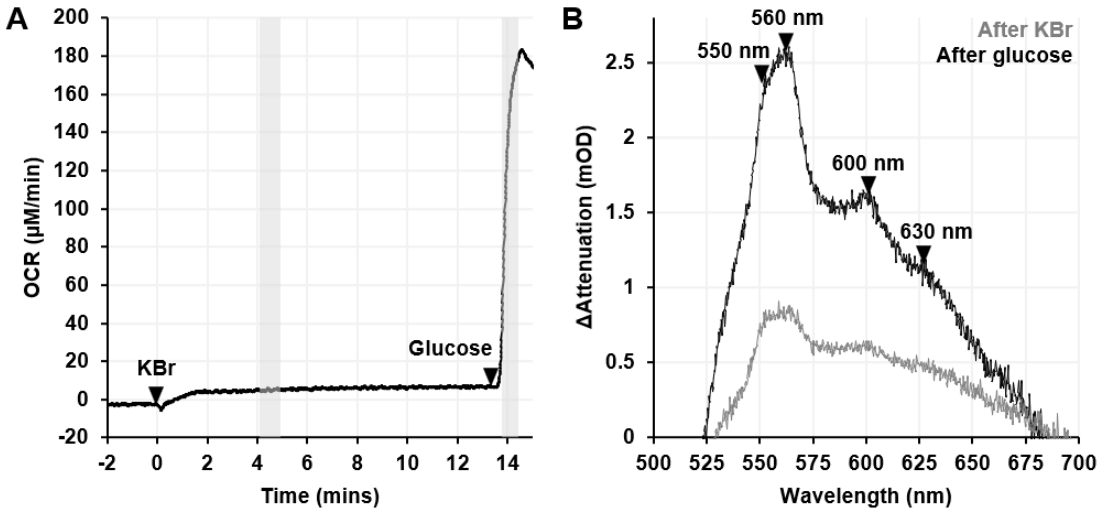

Fig 6. Misleading initial results from heat-activated but not Histodenz-purified germinating spores in the bioenergetic chamber. (A) The OCR trace with arrowheads indicating KBr and glucose additions. The O_2 concentration was maintained at 100 µM. Glucose addition led to a dramatic increase in O_2 consumption which can be explained by the high optical density (~20) used in this experiment. The shaded areas (light grey) show the ~1-min interval over which the recorded spectra were averaged to obtain the spectra used in (B). (B) Difference spectra (post KBr/glucose minus initial baseline) showing the response to KBr (dark grey) and glucose (black), fitted to linear regressions. Indicated wavelengths 550 nm, 560 nm, 600 nm correspond to reduced haems of type *c*, *b*, and *a* respectively. 630 nm (haem *d*) is labelled but is not a convincing feature.

As we gained more experience of handling spores, we started washing them thoroughly to begin with, and then used a Histodenz gradient to separate the dense, dormant spores from vegetative contamination. With these spore preparations, we began testing the effect of Histodenz purification and heat activation on the haem attenuation spectra/OCR using spores at an optical density of ~2; the results are shown in Fig 7.

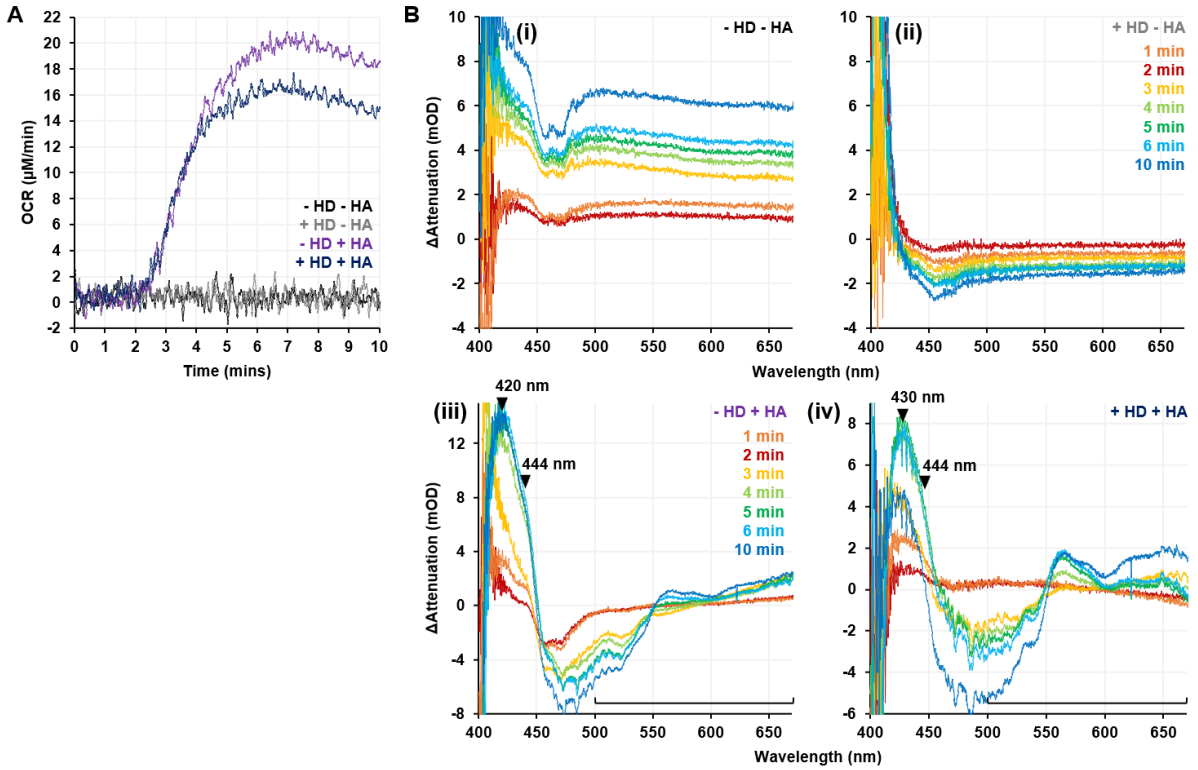

Fig 7. Effect of Histodenz purification and heat-activation during glucose-initiated germination in the bioenergetic chamber. (A) OCR traces for the 4 treatment combinations: -HD-HA (black), +HD-HA (grey), -HD+HA (purple), +HD+HA (blue) where the abbreviations HD and HA refer to Histodenz treatment and heat activation respectively. The O_2 delivery system was not used in these experiments. (B) Difference spectra (time point (T_p) minus pre-glucose baseline) for (i) -HD-HA, (ii) +HD-HA, (iii) -HD+HA, and (iv) +HD+HA spores germinated with 4 mM glucose. Spectra recorded over a 1-min interval preceding the T_p were averaged to generate the spectrum at that T_p. From these spectra, the similarly averaged baseline spectrum before glucose addition was subtracted, and these were fitted to a linear regression to generate the difference spectra shown. Peaks in the Soret region (420 nm, 430 nm, 444 nm) are indicated. The square brackets in (iii) and (iv) highlight the wavelength range examined more closely in Fig 8.

In spores that were not heat activated, glucose addition did not lead to an increase in OCR (Fig 7A). However, Histodenz purification minimised spectral changes in the 450-500 nm region that were observed without it (Fig 7B ii versus i) – these features could be linked to very slow flavin reduction (Blaza et al., 2017). When spores were heat activated, Histodenz purification did influence the spectral profiles obtained. The differences in the Soret region are indicated in Fig 7B panels iii and iv, and are difficult to confidently assign here, although in purified bovine cyt *c* oxidase and isolated mitochondria, absorbance peaks at ~430 nm and ~444 nm have been attributed to oxidised haem a_3, and to reduced haems *a* and a_3 respectively (Covian et al., 2023; Diuba et al., 2023).

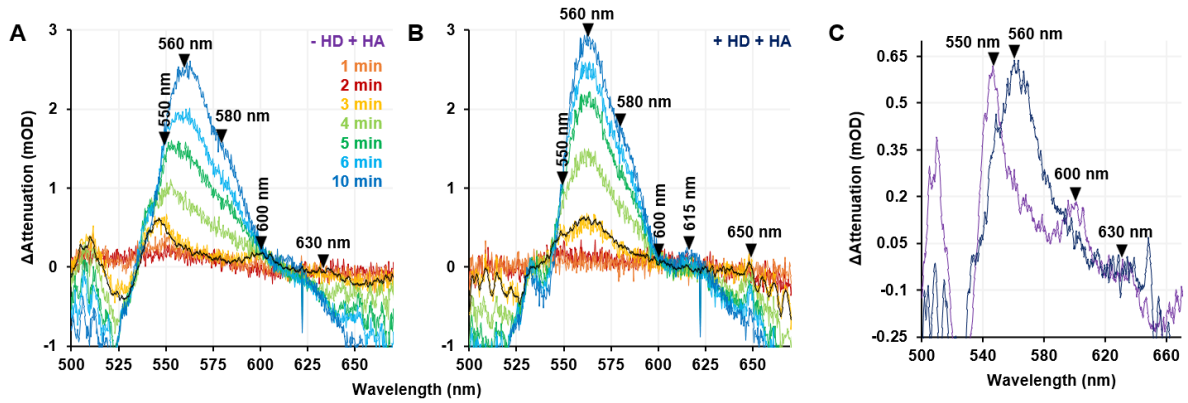

Fig 8. Effect of Histodenz purification on the haem α-peaks of glucose-germinated spores. (A) -HD+HA spores germinated with 4 mM glucose, difference spectra (T_p minus pre-glucose baseline) first truncated (480-670 nm range) and then fitted to a linear regression. (B) Same as (A) but with +HD+HA spores. (C) The 3 min spectra (Savitzsky-Golay smoothed, black) from (A) and (B) directly compared. Indicated wavelengths 550 nm, 560 nm, 600 nm correspond to reduced haems of type *c*, *b*, and *a* respectively. Shoulder at 580 nm and peak at 615 nm could be the HCO ferryl intermediates P and F. Weak features at 630 nm and 650 nm could be related to cyt *bd* oxidase.

In the 500-670 nm region, without Histodenz purification the spore spectra show more cyt *c* and *a* reduction which was eliminated in Histodenz purified spores (Fig 8A-C). Regardless of Histodenz treatment, unfamiliar features appeared at 580 nm and in the 600-700 nm region as experiments progressed which we had not observed in isolated spore membranes. These findings demonstrated that if spores are not purified carefully then erroneous conclusions about ETC function can be drawn from contaminated haem spectra. Indeed, our hypothesis based on preliminary experiments in the bioenergetic chamber (Fig 6) was that ETC function in germinating spores was like vegetative cells so we would see similar haem spectra, but results with Histodenz-purified spores proved this hypothesis incorrect.

5.2.3. The effect of galactose and other germinants on attenuation spectra and oxygen consumption of germinating spores

We then proceeded to testing galactose and the other germinants of *B. megaterium* QM B1551, proline and KBr, in the bioenergetic chamber. As expected, galactose did not cause an increase in OCR or spectral changes that looked like haem absorbance peaks (Fig 9A i & ii). In panels i-iii of Fig 9B, we can see that with KBr and proline, haem attenuation at the indicated wavelengths is noticeably smaller than changes achieved with glucose at the same

time points. The smaller haem attenuation with KBr and proline, especially at the 5 min and 10 min time points, can be explained by the slower loss of absorbance with these germinants as compared to glucose: even with 10 mM KBr/proline, ≤20% initial absorbance is lost after 10 mins as compared to ~40% lost with 4 mM glucose (Fig 2, chapter 4). Qualitatively, the spectral profiles obtained with the three germinants are similar, except the peak at 478 nm associated with flavin reduction (Blaza et al., 2017; Raibekas, Fukui and Massey, 2000) that only appears when glucose is added to spores germinating with KBr/proline, or when hydration is nearly complete with glucose alone. These spectra were less noisy than those in Fig 5, and again we could see features at ~580 nm and 625 nm with no haem *a* peak at 600 nm, a profile distinct to NADH/$Na_2S_2O_4$-reduced isolated spore membranes (Fig 4 & 5). These could correspond to the ferryl F intermediate of HCOs and reduced state of cyt *bd* oxidases respectively. To confidently assign these features to the corresponding catalytic intermediates of terminal oxidases, we decided to collect spectra in the 500-700 nm range and capture as much detail in this region as possible.

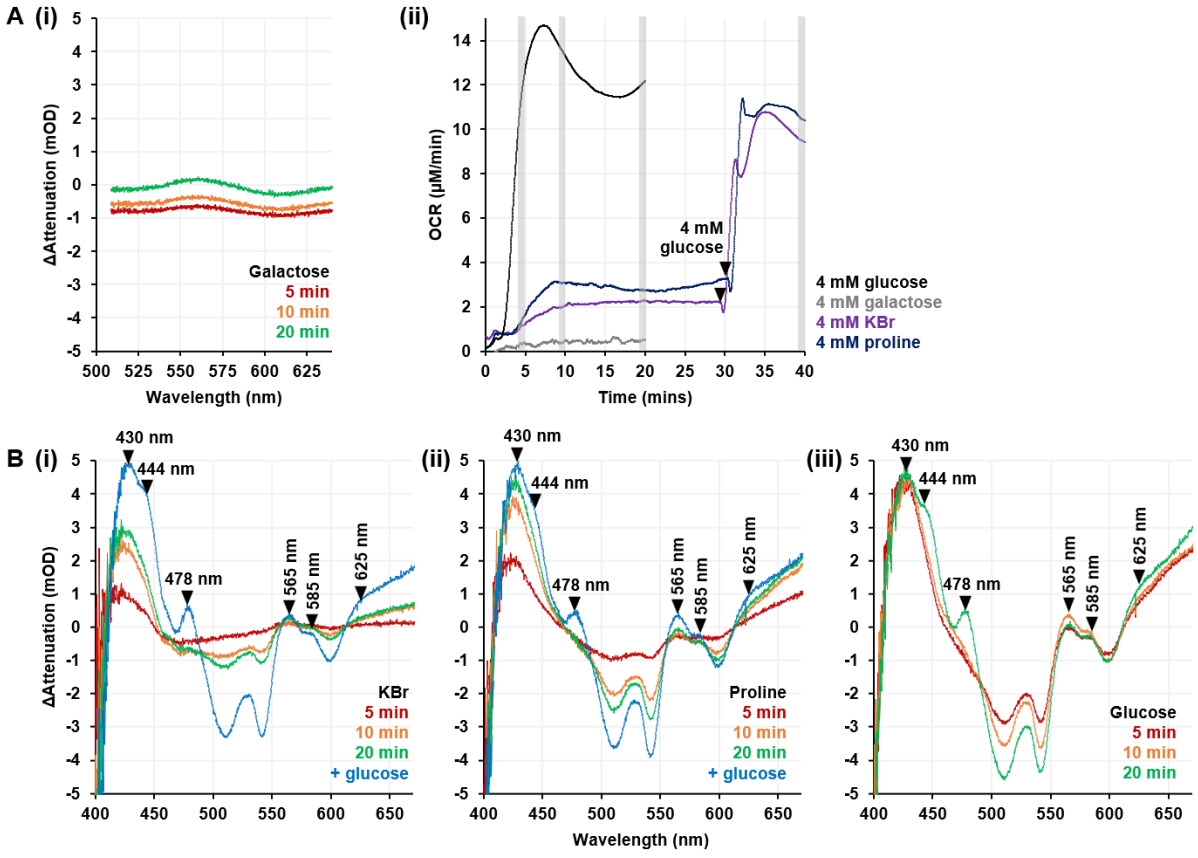

Fig 9. Studying the germination response with galactose, proline and KBr in the bioenergetic chamber. (A) Difference spectra (T_p minus pre-galactose baseline) when spores were germinated with 4 mM galactose, these were not fitted linear regressions. (B) OCRs measured in germination experiments with 4 mM galactose (grey), 4 mM glucose only (black), 4 mM KBr (purple) and 4 mM proline (blue). The O_2 delivery system was not used in these experiments. At time points indicated with arrowheads, 4 mM glucose was added in the KBr and proline

runs. Data were only recorded for 20 mins in the glucose and galactose runs. The shaded areas (light grey) show the preceding 1-min intervals over which the recorded spectra were averaged to obtain the corresponding T_p spectra used in (B). (B) Difference spectra (T_p minus pre-germinant baseline) fitted to linear regressions for spores germinated with (i) 4 mM KBr, (ii) 4 mM proline, and (iii) 4 mM glucose. Arrowheads indicate probable Soret haem a_3/*a* peaks (430 nm and 444 nm), reduced flavin (478 nm), reduced haem *b* (565 nm), probable HCO F intermediate (585 nm) and probable reduced haem *d* (625 nm).

5.2.4. The nature of O_2 consumption during glucose-initiated germination

Having observed these distinct spectral features in spores that may correspond to unusual catalytic intermediates of terminal oxidases, we wanted to reevaluate the nature of O_2 consumption in germinating spores.

First, to establish whether increase in O_2 consumption was concurrent with rehydration in our spore preparations, we used a sensitive optode to measure the OCR of germinating spores. We observed a rapid and glucose-concentration dependent increase in O_2 consumption start 2 mins after germinant addition that mirrored hydration, glucose consumption and H_2O_2 production. With 4 mM and 10 mM glucose, an initial burst in the OCR was observed, but after 20 mins the OCR for all 3 glucose concentrations tested was ~12 µM/min (Fig 10A). These data support our model where electron transport from the incoming glucose to the terminal acceptor O_2 powers germination to completion (outgrowth).

Interestingly, although the OCR measured for KBr-germinated spores is a third of that achieved with glucose, it in fact preceded the loss of absorbance by approximately 8 mins. We know that KBr liberates endogenous reserves like 3-PGA leading to some ATP and NADH generation (Setlow and Kornberg, 1970; Setlow and Setlow, 1977). Based on our spectral and O_2 consumption data, this NADH appears to be oxidised by the ETC in germinating spores. This suggests that electron transport can occur before detectable hydration, which is a provocative idea that we will revisit later.

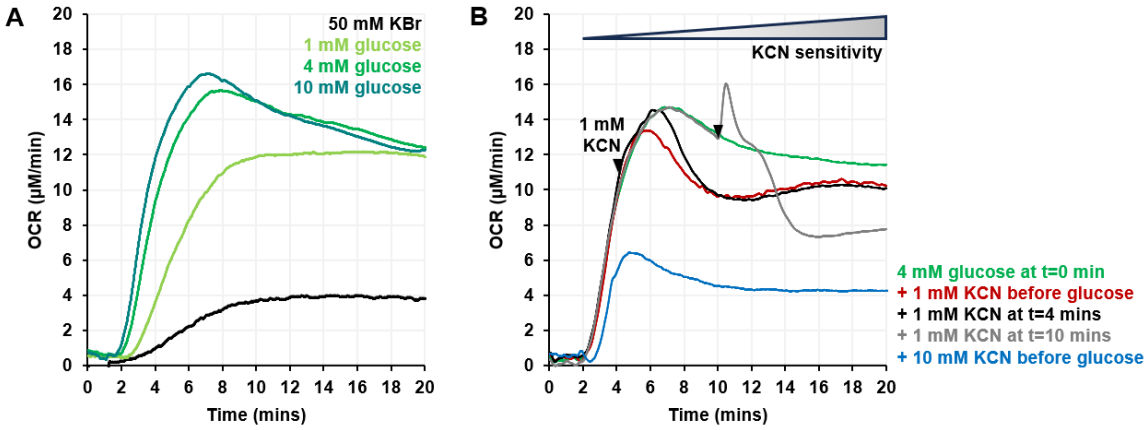

Fig 10. The glucose-concentration dependence and KCN-insensitivity of O_2 consumption during spore germination. (A) Savitzky-Golay smoothed OCR traces recorded for spores germinated with 50 mM KBr (black), 1 mM glucose (light green), 4 mM glucose (dark green) and 10 mM glucose (teal). The O_2 delivery system was not used in these experiments. (B) Savitzky-Golay smoothed, averaged OCR traces recorded for spores germinated with 4 mM glucose (green), and where indicated, poisoned with 1 mM/10 mM KCN. In separate runs, 1 mM (red) or 10 mM KCN (blue) was added before glucose addition at t=0 min. In other runs, 1 mM KCN was added either at t=4 mins (black) or at t=10 mins (grey). KCN sensitivity was found to increase with time.

Next, we wanted to look at the KCN-insensitivity of this O_2 consumption. When KCN was added before initiation of germination with glucose, its mild inhibitory effect was observed after t=5.5 mins. When KCN is added after rehydration is underway, i.e. at t=4 mins, a similarly mild inhibitory effect is observed at t=6.6 mins, which could reflect how long it takes for the KCN to get intermixed in the suspension and permeate the spores. Curiously, when KCN was added at t=10 mins at which point the rate of absorbance loss starts slowing down, there was a sharp spike in OCR which then proceeded to gradually decline over the next 5 mins, until it stabilised to roughly half of that in the control run (Fig 10B). These data show that in germinating spores, KCN sensitivity is restored with time, either because spores become more permeable to KCN and/or the O_2 consumption is mostly reliant on the cyanide-insensitive terminal oxidase like cyt *bd* oxidase. The involvement of cyt *bd* oxidase in spore ETC function is supported by data from exponential phase vegetative cells, which do not have detectable cyt *bd* oxidase and so even 1 mM KCN abolishes O_2 consumption and expectedly causes the reduction of haems *c*, *b* and *a* (Fig 11A & B).

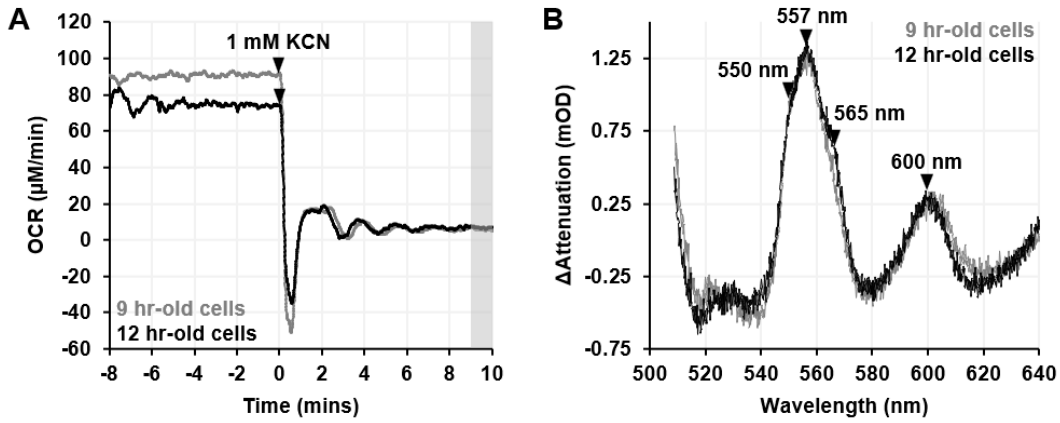

Fig 11. KCN inhibition of exponential phase vegetative cells of *B. megaterium* QM B1551. (A) OCRs measured for 9 hr-old (grey) and 12 hr-old cells (black) cultured in LB broth at 30 °C with 225 rpm shaking. OCRs shown are after the addition of 10 µM BAM15 (an uncoupler) until 1 mM KCN was added at t=0 mins. Cells were maintained at 100 µM O_2 throughout. The shaded area (light grey) shows the 1-min interval over which the recorded spectra were averaged to obtain the spectra used in (B). (B) Difference spectra (post-KCN minus initial baseline) fitted to linear regressions after KCN treatment obtained for 9 hr-old (grey) and 12 hr-old cells (black). Indicated wavelengths 550 nm, 557 nm and 565 nm, and 600 nm correspond to reduced haems of type *c*, *b*, and *a* respectively.

5.2.5. Interpreting the haem spectra during glucose-initiated germination

At this stage, we wanted to understand the hierarchy of terminal oxidase function in germinating spores. As mentioned earlier, we decided to focus on the 500-700 nm region where the spectroscopic signatures of certain catalytic intermediates are. These experiments were performed at a constant O_2 concentration unlike previous experiments because we wanted to be very careful in avoiding any spectral contamination from the O_2 optode. The optode measures the phosphorescence half-life of the platinum-porphyrin compound on its surface. This phosphorescence at 650 nm is inversely proportional to the O_2 concentration (Lee and Okura, 1997) – as the bioenergetic chamber was originally designed to study mammalian systems, this was not a concern. But it means that if O_2 concentration declines steadily during an experiment as it is consumed, the increasing signal from the optode will contaminate the measured attenuation at 650 nm where we expect to see the cyt *bd* A intermediate. As a further precaution, data were recorded in two phases: one with the LED on and the next with the LED off. The latter was subtracted from the former to remove any optode-related signal from the final attenuation spectra that were used for the analyses presented here.

In these runs, germination was initiated with three glucose concentrations: 1 mM, 4 mM, and 10 mM glucose. For each, difference spectra were generated for the indicated time points with respect to the pre-glucose baseline, shown in Fig 12A. In these difference spectra, the effect of glucose concentration manifests as bigger changes in attenuation achieved with 10 mM glucose at the earliest time points (≤6 mins), and the prominence of features related to the cyt *bd* oxidase (peaks at 630 nm and 650 nm). Both these effects can be explained by the more synchronised germination response elicited by 10 mM glucose, so we decided to inspect these spectra more closely to draw any conclusions about terminal oxidase function in germinating spores. The OCRs measured in these experiments (Fig 12B) do not reflect glucose-concentration dependence to the same extent as in Fig 10A, where OCR was measured without a constant O_2 supply to the spore suspension. Rates measured at a constant O_2 concentration thus represent the maximal rates that can be achieved by germinating spores when O_2 is not limited.

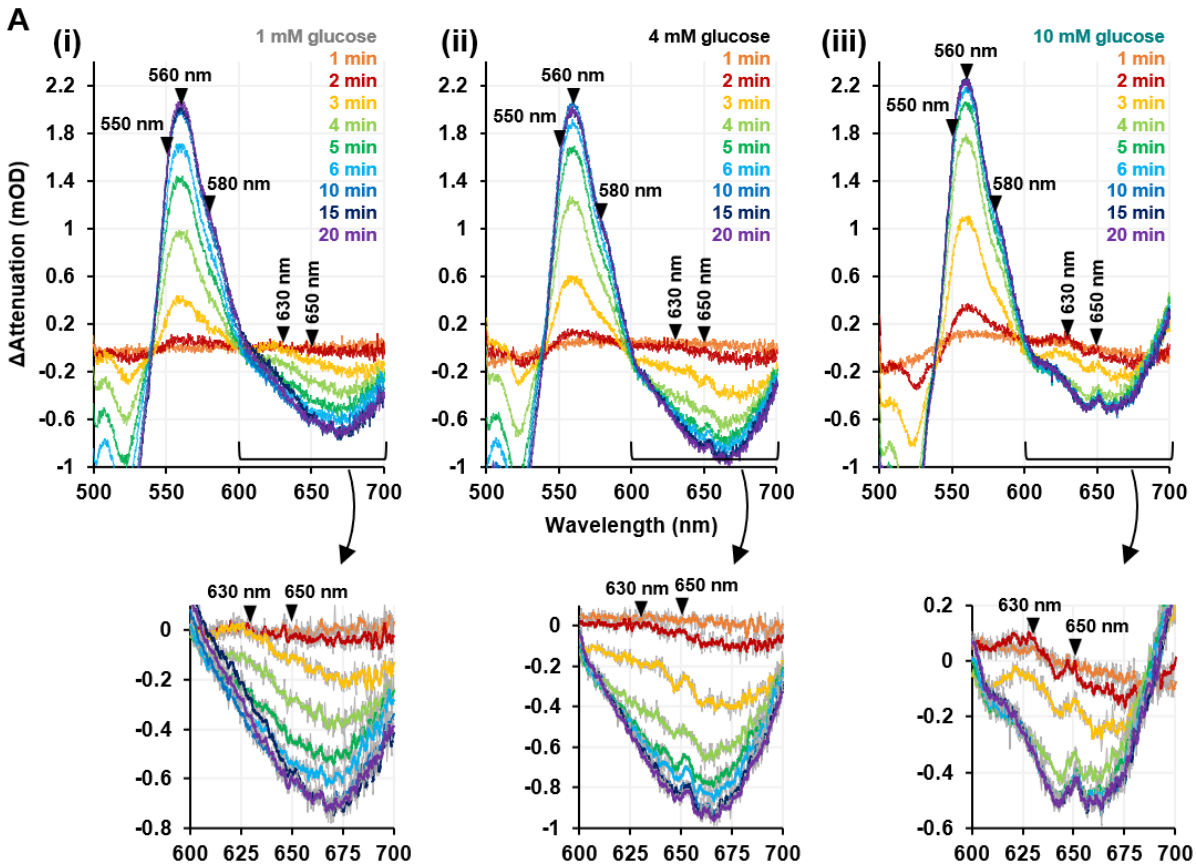

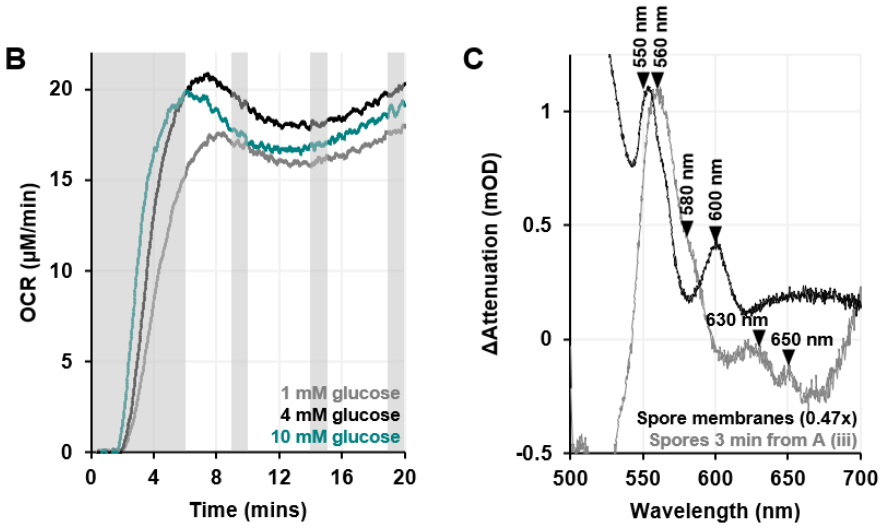

Fig 12. Studying terminal oxidase function in germination spores using remission haem spectroscopy. (A) Difference spectra (T_p minus pre-glucose baseline) for spores germinated with (i) 1 mM glucose, (ii) 4 mM glucose, and (iii) 10 mM glucose, fitted to linear regressions as described previously. The spectra in the 600-700 nm region, shown separately for clarity, are Savitzky-Golay smoothed (coloured) and the grey traces underneath are unsmoothed data. Arrowheads indicate reduced haems *c* and *b* (550 nm and 560 nm), HCO F intermediate (580 nm) and two cyt *bd* oxidase-related features: reduced haem *d* (630 nm) and O_2-bound reduced haem *d* (650 nm). (B) OCR traces recorded for spores germinated with 1 mM glucose (grey), 4 mM glucose (black) and 10 mM glucose (teal). Cells were maintained at 120 µM O_2 throughout. The shaded areas (light grey) show the 1-min intervals over which the recorded spectra were averaged to obtain the spectra used in (A). (C) The 3 min spectrum of germinating spores from A (iii) in grey compared with the scaled spectrum of isolated spore membranes after 3 mins of reduction with NADH (black).

In the 10 mM glucose spectra (Fig 12A-iii), we find a combined reduced haem c and b peak (550 nm and 560 nm), a shoulder at ~580 nm (the F intermediate of HCOs), and no peak at 600 nm (haem *a* in HCOs not reduced). These features indicate electron flow from the Q pool via menaquinol-cyt *c* reductase or directly to the HCOs, but the absence of the 600 nm haem *a* peak along with the shoulder at ~580 nm implies that the F intermediate of HCOs is the dominant catalytic intermediate in germinating spores. Intriguingly, spore membranes oxidising NADH outside the spore environment do not accumulate the F intermediate, whereas the reduced haem *a* peak is clearly visible (Fig 12C). As mentioned in the introduction to the HCO catalytic cycle, the F intermediate is associated with slowed down HCO turnover when a ΔΨ impairs proton uptake and pumping – in other words, the F intermediate accumulates when the ΔΨ pushes against the catalytic cycle of HCOs. To the best of our knowledge, this is the first observation of the F intermediate *in vivo*, under unique physiological conditions where a respiratory chain is reenergised as an organism exits dormancy. In principle, the

characteristic release of cations (K^+, H^+, Na^+) and CaDPA, the earliest recorded events in the germination cascade, could establish a substantial ΔΨ across the spore membrane which in turn suppresses HCO function. This could further explain why the spore ETC contains a cyt *bd*, which does not pump protons as part its catalytic mechanism and would therefore be less sensitive to this thermodynamic backpressure.

As cyt *bd* is a high affinity terminal oxidase typically used under low O_2 tension/stress conditions, we were initially surprised to find a spore-specific cyt *bd* isoform in the spores of an aerobic species cultured with vigorous shaking. Even more surprisingly, the small peaks at 630 nm and 650 nm in these spectra indicate that in spores germinating under O_2-replete conditions, cyt *bd* oxidase function starts within 2 mins of glucose addition. Taken together, these data show that as electron transport is restarted in germinating spores, HCO function is suppressed (conceivably due to a high ΔΨ) and cyt *bd* serves as the primary terminal oxidase.

5.2.6. Spectral decomposition for kinetic analyses

To extract more information from these complex spectra we decided to perform decomposition on them. This involves decomposing composite spectra containing multiple overlapping peaks into the individual components. Model spectra of the individual components are required to generate a template which can then be used to fit/decompose the experimental spectra, where model spectra should ideally be measured for each of the individual components. In the case of the respiratory chain, that entails purifying each enzyme and performing redox titrations and UV-visible spectroscopy, which is an elaborate undertaking. However, in the absence of such spectra, we can still use model haem spectra measured by others in different experimental systems to create a template for fitting our spectra. The components included in the template were based on the composition of the spore respiratory chain and the adequacy of the template was judged based on the residuals obtained after the fitting.

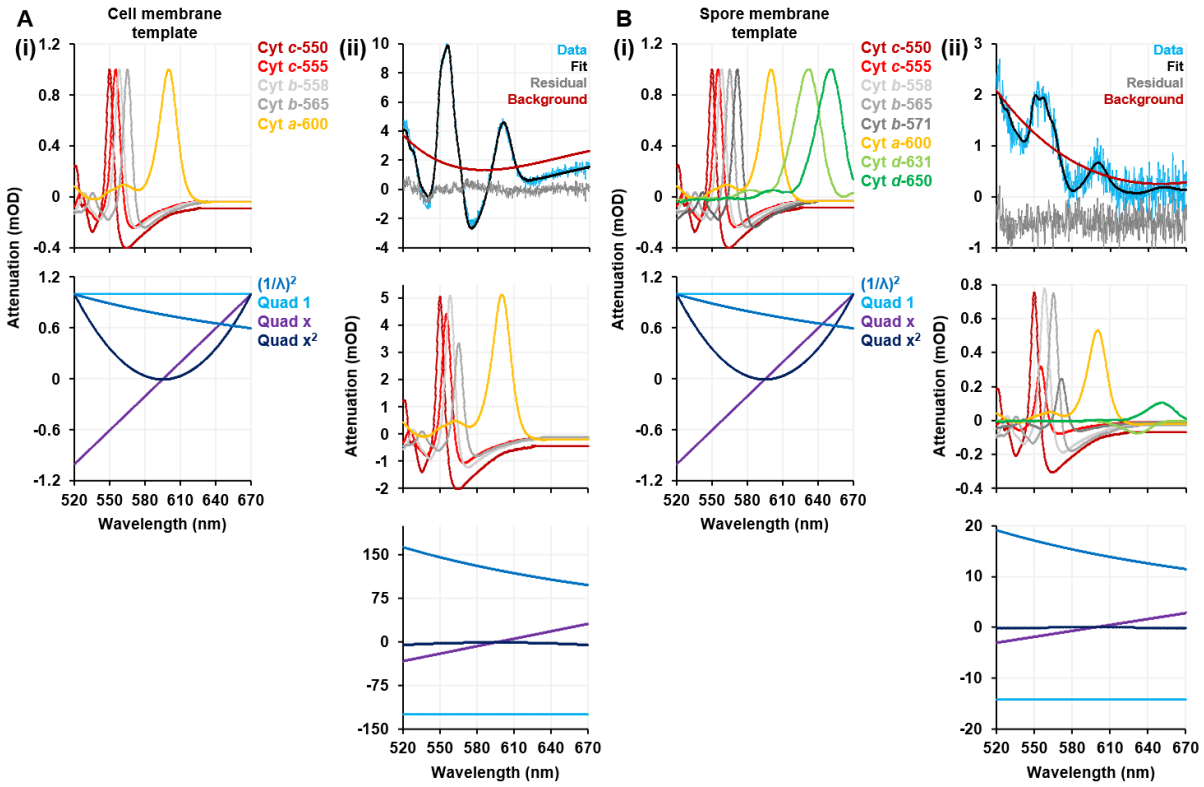

Fig 13. Development of the fitting template for decomposition analysis of complex germinating spore spectra. (A) The 'cell membrane' template consisting of (i) five haem components: cyt *c*-550, cyt *c*-555, cyt *b*-558, cyt *b*-565, and cyt *a*-600, along with four background components: $1/\lambda^2$, Quad 1, Quad x, Quad x^2, all normalised to 1. The spectrum at t=4 mins after cell membranes were reduced with 1 mM NADH was decomposed using this template. Top panel of (ii) shows the raw data (blue), the fit imposed (black), the residuals (grey), and the sum of the background components (red). Middle panel shows the fitting of the haem components, and the bottom panel shows the fitting of the background components at t=4 mins. (B) The 'spore membrane' template consisting of (i) eight haem components: cyt *c*-550, cyt *c*-555, cyt *b*-558, cyt *b*-565, cyt *b*-565, cyt *a*-600, cyt *d*-630, and cyt *d*-650 along with the four background components: $1/\lambda^2$, Quad 1, Quad x, Quad x^2, all normalised to 1. The spectrum at t=4 mins after spore membranes were reduced with 1 mM NADH was decomposed using this template. Top panel of (ii) shows the raw data (blue), the fit imposed (black), the residuals (grey, y-axis offset by -0.5 mOD for clarity), and the sum of the background components (red). Middle panel shows the fitting of the haem components, and the bottom panel shows the fitting of the background components at t=4 mins.

We started developing the template by modelling it on the simpler cell membrane spectra. To fit the cell membrane attenuation spectra in the 520-670 nm wavelength range, we included 2 components each for haems *b* and *c*, one component for haem *a*, a scatter component $(1/\lambda)^2$ where λ is the wavelength, and a quadratic background to account for baseline changes during experiments. The quadratic background comprises 3 functions of the form $y=x^2$, $y=x$, and $y=1$, where $x=(x-595)$ nm and 595 nm is the midpoint of the fitting wavelength range (Fig 13A-i).

The haem components should account for menaquinol cyt *c* reductase (haems *b* and *c*), cyt *c*-551 (haem *c*), cyt *caa*$_3$ oxidase (haems *a* and *c*), cyt *aa*$_3$-600 menaquinol oxidase (haem *a*) following reduction by NADH. Shown in Fig 13A-ii is an example of how this template fit the raw attenuation spectrum at t=4 mins after NADH addition – the residuals obtained after the fitting are negligible.

The $Na_2S_2O_4$-reduced minus oxidised difference spectra generated for both the cell and spore membranes showed that haem *d* (and cyt *bd* oxidase) is present in the latter but not the former. Therefore, to the cell membrane template we added two more components to model haem *d* and another haem *b* component (Fig 13B-i). As discussed, an absorbance peak at 630 nm indicates haem *d* reduction whereas a peak at 650 nm indicates reduced and O_2-bound haem *d*. Again, fitting the raw spore membrane spectrum at t=4 min after NADH addition using this 'spore membrane' template yielded negligible residuals (Fig 13B-ii).

Rehydrating spore spectra are more complex and as discussed already, look markedly different to NADH-reduced spore membrane spectra. We added another component, a broad feature centred at 580 nm, to the 'spore membrane' template to account for the HCO F state. This 'spore' template (Fig 14A) was used to fit the spectra that were recorded every 500 ms during spore germination. Fig 10B shows how the spectra at the indicated time points were decomposed using this template with the residuals being negligible. The attenuation fitting of each spectral component was then plotted against time to give kinetic traces that showed how that component had changed during the experiment.

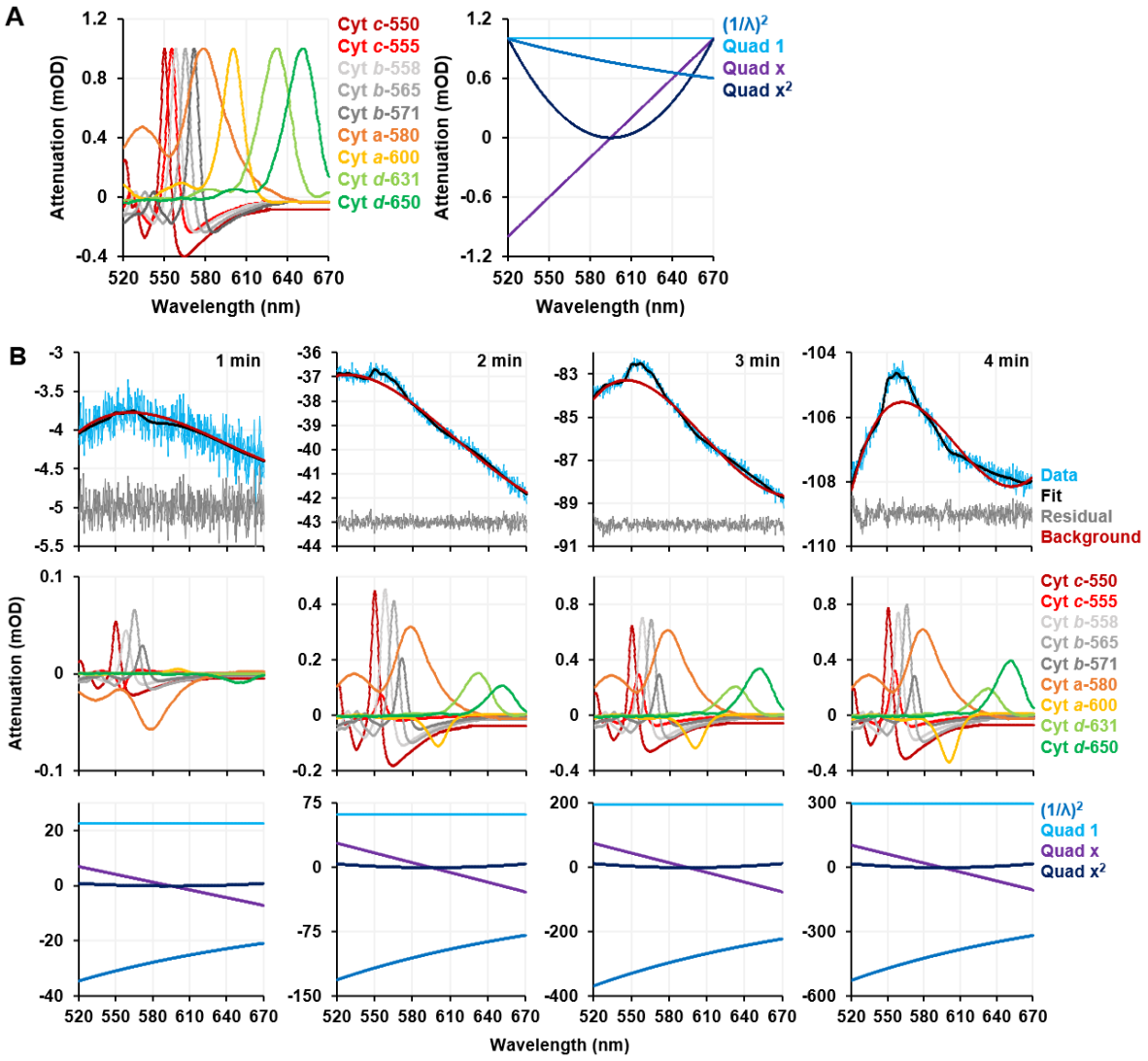

Figure 14. Spectral decomposition analysis of germinating spore spectra (10 mM glucose). (A) The haem (left) and background (right) components of the 'spore' fitting template which is the 'spore membrane' template with an additional component cyt *a*-580 (orange). (B) Top panels show the raw data (blue), the fit imposed (black), the residuals (y-axes suitably offset from 0 to be comparable, grey), and the sum of the background components (red) being fitted at the indicated time points. Middle panel shows the fitting of the nine haem components, and the bottom panel shows the four background components.

The traces for selected haem components (*c*-550, *b*-565, *a*-580, *d*-630, *d*-650) and all the background components ($1/\lambda^2$, Quad 1, Quad x, Quad x^2), scaled and offset such that they could be directly compared, are shown in Fig 15A. These traces could be divided into 2 groups based on whether they started changing ~1 min (group 1) or ~2 mins (group 2) after glucose addition at t=0 min. Unexpectedly, reduction of haems *b* and *c* along with the increase in *a*-580 were found to start at t=~1 min (group 1 events). This early electron transfer through menaquinol cyt *c* reductase to HCOs did not immediately lead to O_2 consumption. OCR started

increasing only with the appearance of the cyt *bd* intermediates (*d*-630 and *d*-650) a minute later, along with changes in the background components (group 2 events). In the bioenergetic chamber, rehydration presents as a dramatic change in the baseline absorbance, so it was expected that background components would also change at t=2 mins when loss of absorbance has been measured to start using A_{600} assays.

The major implications of these findings are that a) increase in OCR is temporally linked to cyt *bd* activity supporting the idea that it is the primary oxidase, and b) electron flow through the ETC precedes detectable rehydration. In glucose-initiated germination where glucose serves as both a signalling molecule and an exogenous energy source, we propose that OxPhos and rehydration start concurrently, with electron transport preceding detectable rehydration (Fig 15B).

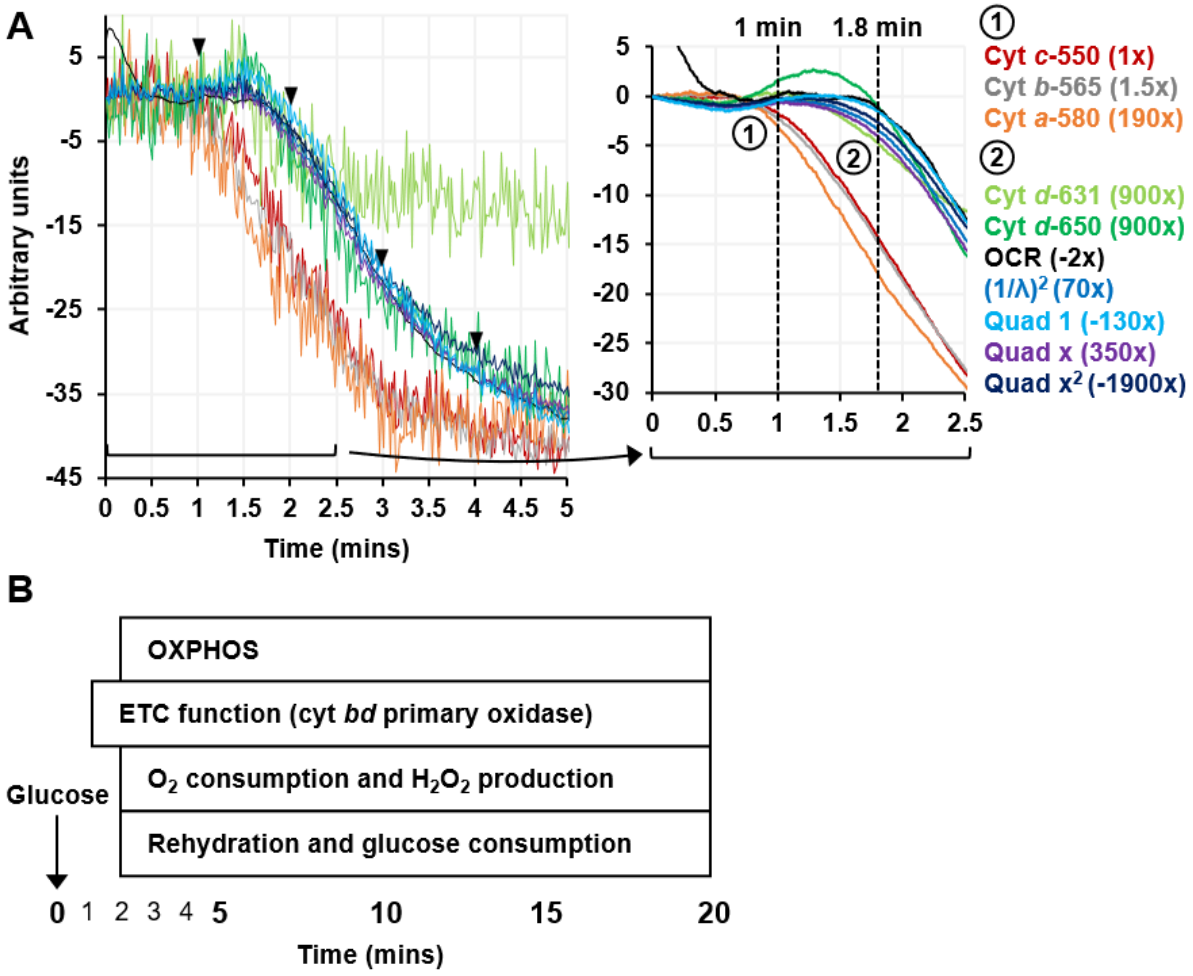

Fig 15. The kinetic analysis of spectral changes during glucose-initiated germination. (A) For spores germinated with 10 mM glucose, raw traces of selected spectral components (cyt *c*-550, cyt *b*-565, cyt *a*-580, cyt *d*-631, cyt *d*-650, $1/\lambda^2$, Quad 1, Quad x, Quad x^2) and OCR were scaled, and the y-axes were offset such that y=0 arbitrary units (a.u.) at x=0 min. The colour key and scale factors are shown on the right. Arrowheads indicate the time points 1, 2, 3, and 4 mins for which the decomposition analysis has been demonstrated in Fig 14. The side panel

shows Savitzky-Golay smoothed traces (also with y-axis offset such that y=0 a.u. at x=0 min) in the 0-2.5 min period. Events in group 1 and 2 start at ~1 min and ~1.8 mins after glucose addition respectively. They are grouped as such in the colour scheme shown on the right. (B) A simplified and updated timeline of the spore germination cascade in *B. megaterium* QM B1551, showing rehydration, glucose and O_2 consumption, and H_2O_2 production starting concurrently 2 mins after glucose addition. ETC function has now been shown to precede rehydration by ~1 min. OxPhos, that relies on ETC function to generate ATP, is therefore proposed to start with rehydration.

5.2.7. Inhibition/deletion of cyt *bd* in germinating *B. megaterium* spores

If ETC function in germinating spores relies on the *ythAB*-encoded cyt *bd*, then inhibiting the *bd* oxidase could stop electron transport and O_2 consumption and allow us to study its impact on the initiation of germination. There are potent inhibitors of cyt *bd* available, e.g. aurachin D (Lawer et al., 2022; Meunier et al., 1995), but using chemical inhibitors against spores comes with its own challenges as discussed in chapter 4. Instead, our biophysical evidence for the importance of cyt *bd* inspired our collaborators Ms. Rebecca Caldbeck and Dr. Graham Christie (University of Cambridge, UK) to make a single crossover mutant (SCO) of *ythA* such that this gene is separated from its promoter in *B. megaterium* QM B1551. Surprisingly, their preliminary data showed that disruption of the *ythAB* operon in this manner leads to a severe germination defect – these SCO mutants remain phase bright and lose minimal absorbance, being unable to initiate germination. These data are reproduced here with permission:

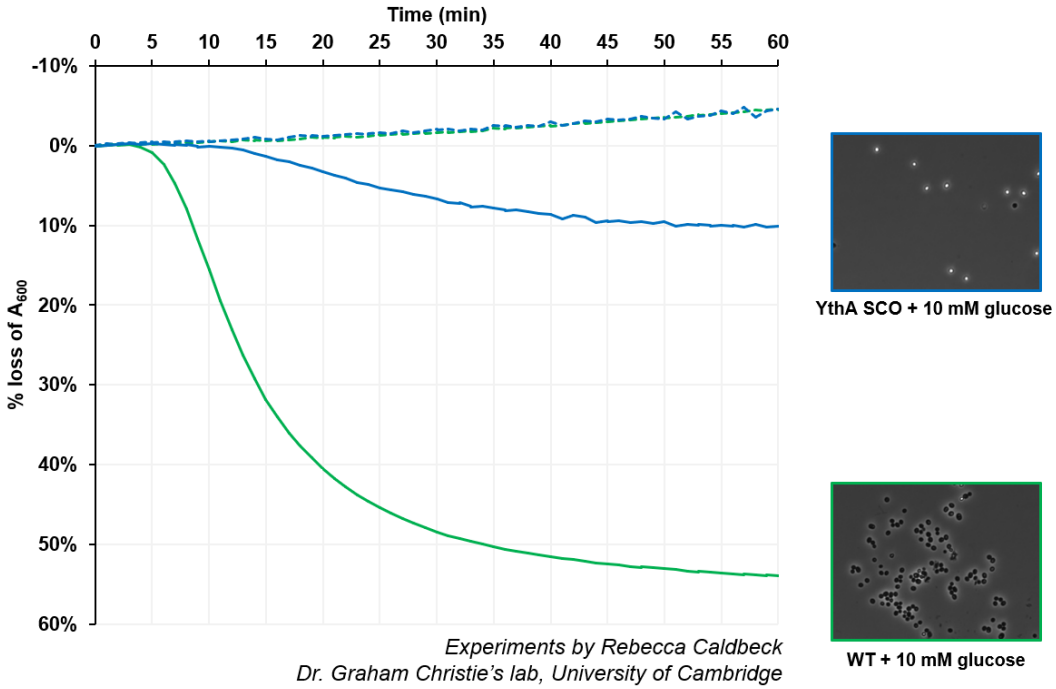

Fig 16. Rehydration curves and phase contrast micrographs for wild-type (WT) B. megaterium (green) and the YthA SCO mutant spores (blue) germinated with 10 mM glucose. Dashed lines represent the buffer only controls.

We expected the SCO spores to emulate our anoxia experiments: perhaps rehydrate faster but be unable to complete germination and outgrow, so these data are difficult to explain. Ms. Caldbeck and Dr. Christie are actively pursuing a double crossover (DCO) mutant that will have *ythA* cleanly deleted. If this phenotype is reproducible in the DCO strain, our case that bioenergetic processes are highly relevant to the study of spore germination will be strengthened further.

5.2.8. Concluding remarks

We started this chapter warning against extrapolation from experiments with the non-nutrient germinant KBr. For our argument here, we consider KBr-induced germination as an artificial experimental system to explore what spores utilising only their endogenous reserves can achieve in terms of ETC function. Do our findings support the current model that 3-PGA utilisation by substrate-level phosphorylation is how ATP is generated, or can spores even in this contrived situation restart OxPhos? As alluded to earlier, we have evidence that supports the latter idea. Based on these data, we propose that OxPhos is not a luxury process that only spores with access to an exogenous energy source can afford to restart, rather its resumption is a key process in the germination cascade. Regardless of whether electrons are exogenous or endogenous, we have shown that resumption of ETC function precedes rehydration. With this updated timeline of germination, we are now in a stronger position to address complex questions about the role of bioenergetics in the initiation of germination itself.

5.3. Future Work

B. megaterium QM B1551 was an excellent organism for this biophysical study because it has a rapid and synchronised germination response to a single nutrient germinant, and it has historically been a model for biochemical investigations – this meant there was a substantial body of prior work we could build on. However, the next logical step is to validate the interesting findings from this experimentally tractable organism in other spore-formers. We

started by searching for similar *ythAB*-encoded cyt *bd* oxidases present in other model spore-formers. Results from Protein-protein BLAST searches are shown in the following table. The query sequence was YthA from *B. megaterium* QM B1551, and the searches were performed against the non-redundant protein sequences for the individual organisms listed.

Organism	**Query cover (%)**	**Percent identity (%)**
B. cereus	98	67.2
B. anthracis	98	51.2
B. subtilis	99	68
B. thuringiensis	97	65.3
Clostridium difficile	31	42
C. perfringens	69	26

All four *Bacillus* species searched returned hits that had ≥50% sequence identity with the query sequence with almost complete coverage, suggesting that a similar enzyme is present in these spore-formers, including the pathogens *B. cereus* and *B. anthracis*; in *B. anthracis*, it has also been identified in the membrane proteome (Chen et al., 2019). Based on the preliminary genetic evidence from *B. megaterium*, similar studies could be carried out in these organisms. For *B. subtilis*, deletion strains (Δ*ythA* and Δ*ythB*) are available from the Bacillus Genetic Stock Center (Koo et al., 2017) and have been kindly provided by our collaborator Dr. Henrik Strahl (Newcastle University, UK) for experimentation.

Chapter 6: A serendipitous cryo-EM structure of succinate dehydrogenase from *B. subtilis*

6.1. Introduction

6.1.1. The original motivation for the project

In chapter 3, we described the development of a chromatographic protocol (employing soyabean phospholipids to improve membrane protein stability etc.) that could be used to purify a genomically-tagged protein complex from its native, atypical spore membrane environment and reconstituted in peptide nanodiscs for functional/structural studies. However, the work presented in chapters 4 and 5 eventually took precedence and we were unable to subject optimised spore membrane preparations to further cryo-EM analyses. However, a collaborative project with Dr. Sebastian Pintscher (Jagiellonian University, Poland) utilising *B. subtilis* cell membranes instead has served as a pilot study to assess the suitability of such membrane preparations for cryo-EM, and is the subject of this chapter.

Given our interest in *Bacillus* membrane protein biochemistry and bioenergetics, Dr. Pintscher suggested studying the structure of menaquinol-cyt *c* reductase in *Bacillus* species which is a unique cyt b_6c-type enzyme (Hederstedt, 2021), distinct to the well-characterised, ubiquitous cyt bc_1-type (Sarewicz et al., 2021) and increasingly better studied cyt b_6f-type found in cyanobacteria and photosynthetic eukaryotes (Malone et al., 2021).

Respiratory cytochromes are amongst the most abundant proteins in membranes of living organisms. As structure determination by cryo-EM is not sample intensive, respiratory cytochromes enriched/purified from a medium scale bacterial membrane preparation (e.g. from 3-6 litres of culture) can yield sufficient material for such studies. Where possible, isolating large respiratory complexes from the native source is ideal as this ensures the necessary supernumerary subunits required for successful assembly/function are available (Stroud et al., 2016). Typically, affinity tags to aid chromatographic purification are introduced either into the chromosomal DNA [e.g. (Jarman et al., 2021)], or as part of an expression plasmid that complements a strain lacking the respiratory complex of interest [e.g. (Grauel et al., 2021)]. Strep-tags, for example, can enable one-step purification for delicate membrane protein assemblies [e.g. (Czapla et al., 2012)] followed by swift cryo-EM grid preparation.

A sample must be purified to homogeneity to obtain well-diffracting protein crystals required for structure determination by X-ray crystallography (McPherson, 1999). In cryo-EM, sample

homogeneity is desirable as it makes data processing more reliable, and in some cases even automatable (Stabrin et al., 2020), but it is not a technical bottleneck in the same way. Indeed, methods such as 'Build and Retrieve' (Su et al., 2021) and structural proteomic approaches [e.g. (Ho et al., 2019)] have demonstrated that structures of abundant proteins at resolutions between 2-4 Å can be solved even from crudely enriched cellular fractions. Intrigued by these studies, we decided to pursue the structure of *B. subtilis* cyt b_6c using a similar strategy: isolation of membranes from wild-type *B. subtilis* cells, DDM-solubilisation, size-exclusion chromatography (SEC) for some degree of purification/enrichment, grid preparation with selected elution fractions, data collection using our in-house Glacios cryo-electron microscope and data processing in CryoSPARC (Punjani et al., 2017).

While we were unable to obtain a high-resolution map for cyt b_6c, we managed to refine a map of succinate dehydrogenase (SDH) to a resolution of ~3.1 Å. Our preliminary analyses have revealed that the *B. subtilis* SDH (Bsu-SDH) is a trimeric enzyme belonging to class B of the complex II superfamily. Previous attempts to crystallise Bsu-SDH had not been successful (Wöhri et al., 2008) and an experimentally determined structure of this enzyme was not available until this work.

6.2.2. Enzyme properties and classification of succinate dehydrogenases

As a component of both the citric acid cycle and the electron transport chain, SDHs (also called complex II enzymes) catalyse the following bidirectional reaction:

$$\text{Succinate} \leftrightarrow \text{Fumarate} + 2H^+ + 2e^-$$

Under aerobic conditions, complex II enzymes couple the oxidation of succinate to fumarate and reduction of quinone to quinol. Voltammetry experiments on mitochondrial complex II and *E. coli* SQR (succinate-ubiquinone oxidoreductase) showed that they display 'tunnel-diode' behaviour, i.e. they allow unidirectional electron flow from succinate to quinone despite their ability to also catalyse the reverse reaction efficiently (Sucheta et al., 1992; Pershad et al., 1999). The tunnel-diode effect has been theorised to arise from a less catalytically active conformation adopted when the flavin cofactor is reduced, but not been confirmed experimentally yet (Pershad et al., 1999; Maklashina, Cecchini and Dikanov, 2013). However, when the quinone pool is highly reduced and there is sufficient fumarate, complex II enzymes have been reported to catalyse the reverse reaction (fumarate reduction) which becomes thermodynamically favourable under hypoxic/anaerobic conditions (Maklashina, Berthold and Cecchini, 1998; Spinelli et al., 2021). Where their physiological function was first recognised

in anaerobic respiration, complex II enzymes are called quinol:fumarate reductases (QFR) (Iverson, Singh and Cecchini, 2023).

The redox chemistry in complex II enzymes is enabled by multiple cofactors: a covalently attached flavin adenine dinucleotide (FAD) where succinate oxidation/fumarate reduction occurs, iron-sulphur clusters of the type 2Fe-2S, 4Fe-4S and 3Fe-4S that mediate electron transfer, and haem *b* centre/Reiske Fe-S cluster where quinone reduction/quinol oxidation occurs. In the structurally diverse superfamily of complex II enzymes, the membrane-bound homologs are composed of 3/4 subunits that are identified by the cofactors they contain. The soluble cytoplasmic domain consists of the SdhA and SdhB subunits. SdhA (flavoprotein subunit) contains the covalently bound FAD, and SdhB (iron-sulphur subunit) hosts the Fe-S clusters. The membrane domain can consist either of one or more subunits (designated as SdhC, SdhD, SdhF), with different cofactors (haem *b* or Rieske Fe-S cluster) and quinone substrate preferences (Iverson, Singh and Cecchini, 2023).

While the soluble domain displays a high degree of conservation across species, the membrane domain is known to be evolutionarily divergent and is the criterion for classification of enzymes in the complex II superfamily; six classes (denoted A-F) are currently recognised (Fig 1). Members of class A, represented by the trimeric Sdh2 from *Mycobacterium smegmatis* (Gong et al., 2020), have a di-haem membrane domain composed of two subunits SdhC and SdhD (3 transmembrane helices each), along with an accessory subunit SdhF (a single TM helix). Members of Class B, represented by the dimeric QFR from *Wolinella succinogens* (Madej et al., 2006), have a di-haem membrane domain as well but with only one subunit (5 TM helices). Class C enzymes typified by monomeric mitochondrial homologs and the trimeric *E. coli* SQR (Yankovskaya et al., 2003), have a membrane domain composed of 2 subunits (3 TM helices each) but only 1 haem *b*. The monomeric QFR from *E. coli* represents class D, with a membrane domain like that found in class C members but lacking a haem *b*. The cofactor present instead has not yet been identified (Iverson et al., 2002). Class E, which does not have a structurally characterised member, is proposed to have monotopic enzymes with a Zn^{2+} atom and a 4Fe-4S cluster coordinated by the membrane-associated helices (Juhnke et al., 2009). Finally, members of class F represented by monomeric Sdh1 from *M. smegmatis*, have a membrane domain composed of a single subunit (4 TM helices) with a Rieske Fe-S cluster instead of a haem centre (Zhou et al., 2021).

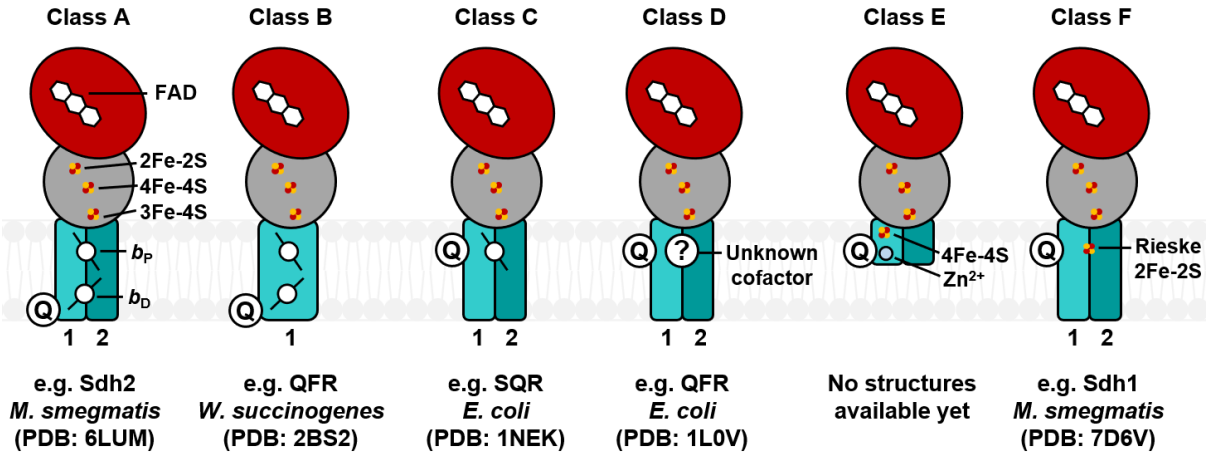

Fig 1. Classification of enzymes in the complex II superfamily. Cartoon depictions of the six recognised classes (denoted A-F) are shown, adapted from (Iverson, Singh and Cecchini, 2023) and (Maklashina, 2022). The flavin subunit (red) and the Fe-S subunit (grey) constitute the soluble domain which is largely conserved. In the membrane domain (teal), the different cofactors, quinone binding sites, and the number of subunits present are indicated. Abbreviations b_P and b_D refer to proximal and distal haem b groups respectively.

Bsu-SDH, encoded by the genes sdhA (BSU28440), sdhB (BSU28430) and sdhC (BSU28450), is known to consist of a flavoprotein subunit (SdhA, 586 residues, 65.1 kDa), an Fe-S subunit (SdhB, 253 residues, 28.4 kDa), and an integral membrane cytochrome subunit (SdhC, 202 residues, 22.9 kDa) with 5 TM helices and 2 haem *b* groups, consistent with class B of the complex II superfamily [(Hederstedt, 2021), Fig 1). The redox potentials of haem groups b_P and b_D have been measured to be +65 mV and -95 mV respectively, and menaquinone-7 (-74 mV) is the quinone substrate which binds close to haem b_D (Lemma, Unden and Kröger, 1990; Matsson et al., 2000; Schnorpfeil et al., 2001).

6.2. Results and Discussion

6.2.1. Experimental strategy and overview of cryo-EM results

The experimental strategy employed in this work is illustrated in Fig 2. Haem spectra of *B. subtilis* cells measured during vegetative growth suggested that there was a pronounced increase in total cytochrome content between 9-24 hours of growth (done with Ms. Hardman as part of her MChem project). Thus, late-exponential phase cells harvested conveniently after 16 hours of overnight incubation were used to obtain high quantities of cytochromes.

In the BN-PAGE gel, the presence of numerous membrane protein complexes in the ~200-600 kDa molecular weight range shows that large complexes were enriched to some degree by SEC. Unsurprisingly, the micrographs obtained with these samples were crowded and the particles very heterogeneous. In the 'Build and Retrieve' method, the blob picker feature of CryoSPARC was used quite effectively to identify and pick particles in the first instance (Su et al., 2021). We decided to do the same with Dr. Pintscher's support who has substantial experience of cryo-EM data processing using CryoSPARC. After particles were picked, they were grouped in 200-300 2D classes and this was performed iteratively to remove junk particles. We also realised that the machine-learning based particle-picking tool TOPAZ (Bepler et al., 2019) performed better on our datasets once it was trained on selected, mostly clean 2D classes. With the successive removal of the poorest particles, 2D classes like the ones shown in Fig 2 were obtained for ATP synthase, a probable cyt b_6c and SDH.

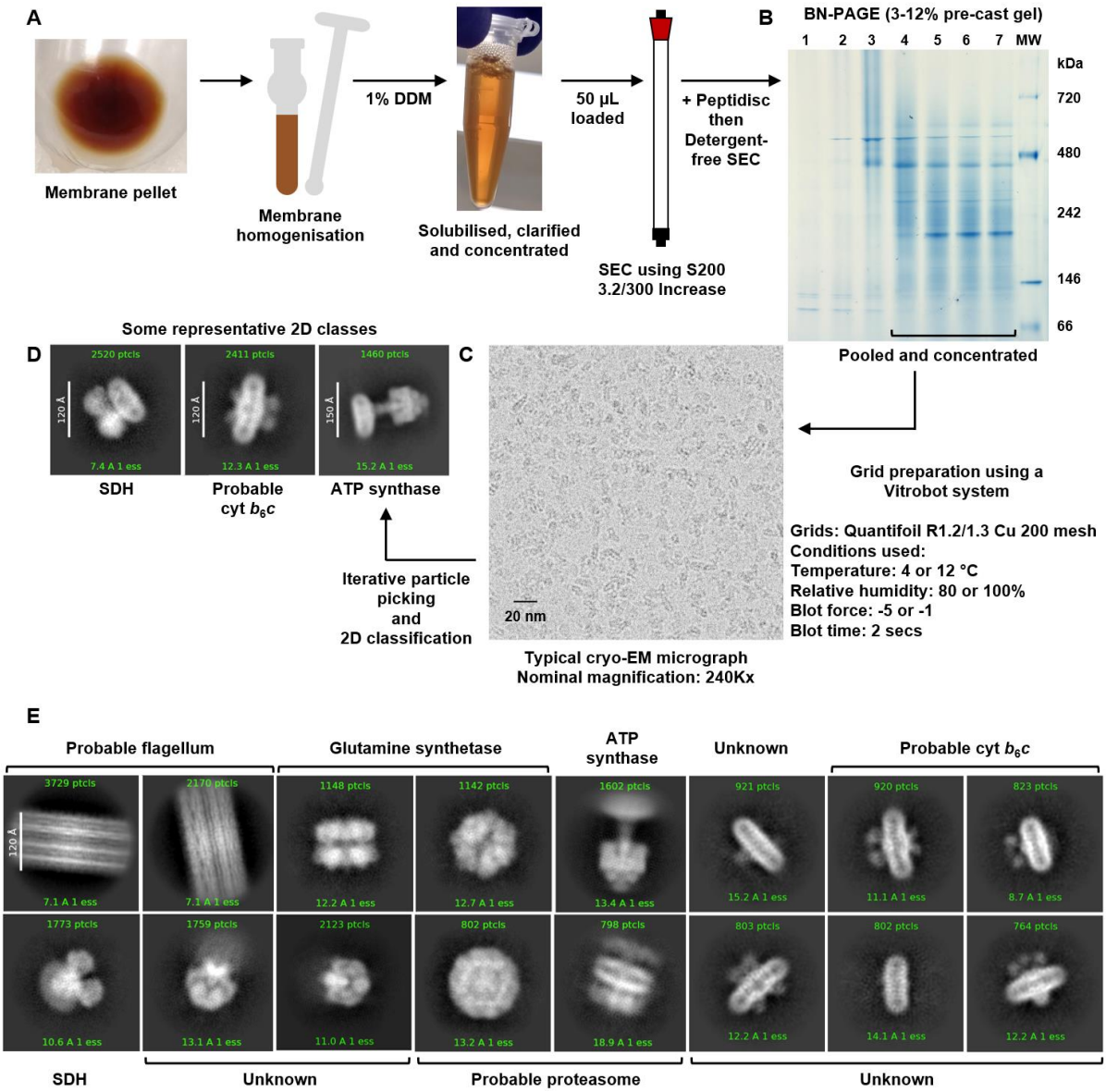

Fig 2. Cryo-EM study of large membrane protein complexes from late-exponential phase *B. subtilis* cells. Membranes were isolated from 16 hour-old cells grown in LB, washed and homogenised (protein concentration 17.84 mg.mL^{-1}), DDM-solubilised and clarified (A) as described in chapter 3. In two separate experiments, Peptidisc peptides were either added or not after the first SEC run which also reduced DDM concentration to 0.01% from 1% used for solubilisation. When Peptidisc peptides were added, another SEC run was performed with detergent-free buffer. The SEC elution fractions were resolved using BN-PAGE (B), and fractions were pooled based on similar band profiles. Pooled samples were used unconcentrated, 2x, 4x, 8x concentrated to prepare cryo-EM grids as described. In the micrographs collected from these grids, the crowded particles represented multiple orientations of numerous proteins (C). Successive rounds of iterative particle picking and 2D classification had to be performed to get recognisable 2D classes shown in (D): ATP synthase (scale bar is 150 Å), a probable cyt b_6c and SDH (scale bar is 120 Å). (E) Some more distinctive 2D classes obtained during the successive rounds of iterative particle picking and 2D classification, labelled as the proteins they possibly represent. The scale bar is 120 Å.

With satisfactory particle classes, 3D ab-initio reconstructions were carried out for each protein. Then, heterogeneous refinement (simultaneous particle classification and map refinement) followed by non-uniform refinement (Punjani, Zhang and Fleet, 2020) gave us the maps shown in Fig 3. Models of cyt b_6c and SDH generated by Dr. Pintscher using AlphaFold (Jumper et al., 2021), and an experimental cryo-EM structure of *Bacillus* ATP synthase (PDB entry: 6N2Z) were fitted into the corresponding maps using UCSF ChimeraX (Meng et al., 2023).

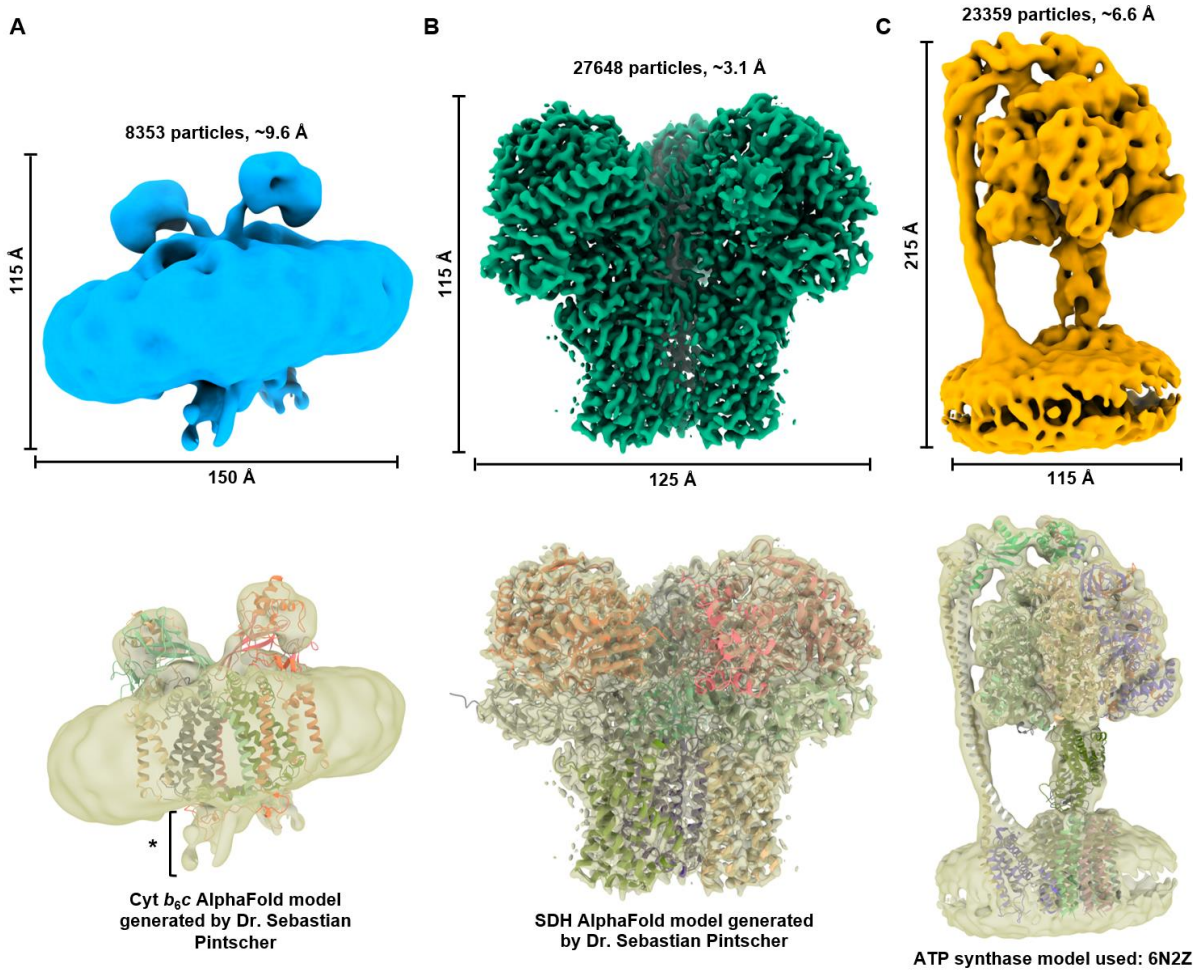

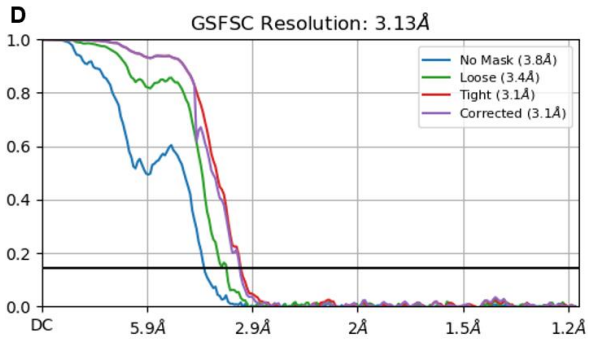

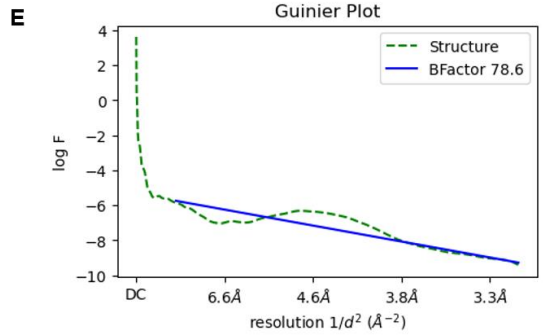

F

Magnification	240,000x
Voltage	200 kV
Electron exposure (e⁻/Å²)	50
Defocus range (μm)	-2 to -0.6
Pixel size (Å)	0.574
Number of frames/movie	40
Data processing software	CryoSPARC v4.4.0
Symmetry imposed	C3
Micrographs processed	41,649
Total number of particles used	27,648
Map resolution (FSC=0.143/Å)	3.13 Å

Fig 3. Overview of results from the cryo-EM study of crudely enriched *B. subtilis* membrane proteins. (A) A 9.6 Å map of the probable cyt b_6c, reconstructed using 8353 particles. The

dimensions are shown in angstroms, estimated using the tape measure feature in ChimeraX. An AlphaFold (AF) model of *B. subtilis* cyt b_6c was unable to account for the density indicated with an asterisk. The detergent belt around the protein can be seen at this volume threshold. (B) A 3.1 Å map of SDH reconstructed using 27648 particles, fitted with the AF model. (C) A 6.6 Å map of ATP synthase reconstructed using 23359 particles, fitted with an experimental structure from *Bacillus* PS3 (PDB: 6N2Z). (D) The gold-standard Fourier shell correlation (GSFSC) graph for the SDH map shown in (B) at the default FSC threshold set at 0.143. (E) B-factor of -78.6 derived from the Guinier plot used for B-factor sharpening/correction of the final SDH map. (F) Table with key data processing statistics for the SDH map.

Despite the poor resolution of the cyt b_6c map (9.6 Å), the AlphaFold model appeared to not account for all the density (the indicated region in Fig 3A) and is perhaps missing a supernumerary subunit. A considerably improved resolution is required to confirm this. The ATP synthase map at an overall resolution of 6.6 Å was fitted adequately with the *Bacillus* PS3 ATP synthase model of rotational state 2 [Fig 3C, (Guo and Rubinstein, 2022)]. The best map was obtained for SDH at a global resolution of 3.1 Å. The AlphaFold model fitted the map density remarkably well (Fig 3B). The analysis presented next is based on this initial fitting as the model is yet to be thoroughly checked and refined.

6.2.2. Salient features in the cryo-EM structure of Bsu-SDH

Like Sdh2 from *M. smegmatis* (class A) and SQR from *E. coli* (class C), we found Bsu-SDH to be a trimer with a molecular weight of ~350 kDa (Fig 4A & B). This makes Bsu-SDH the first trimeric member to be characterised structurally in class B of the complex II superfamily, which is currently exemplified by the dimeric QFR from *W. succinogenes*. As expected, the Bsu-SDH monomer (~116.4 kDa) is composed of the flavin subunit (SdhA), the Fe-S subunit (SdhB) and a single membrane cytochrome subunit (SdhC) with the associated cofactors present in the predicted arrangement (Fig 4C).

A BLAST search with Bsu-SdhA against sequences in the Protein Data Bank (PDB) yielded *M. smegmatis* Sdh2 (6LUM) and *E. coli* QFR (1L0V) as the best hits (sequence identities of 34.7% and 33.5% respectively, query coverage >93%). With Bsu-SdhB as the query sequence, the highest sequence identities of 29.5% and 25.3% were found with *W. succinogenes* QFR (1E7P, 2BS2) and *E. coli* (1L0V) respectively. Bsu-SdhC returned no hits, but this was not surprising as the membrane subunits are known to be highly divergent.

Next, structural alignments were carried out for Bsu-SdhA and Bsu-SdhC separately. Bsu-SdhA was compared to the corresponding subunit from *M. smegmatis* Sdh2, *E. coli* SQR, *W.*

succinogenes QFR, and *Sus scrofa* (porcine) mitochondrial complex II (Sun et al., 2005). As expected, the flavin subunit architecture is largely conserved across these species (Fig 5).

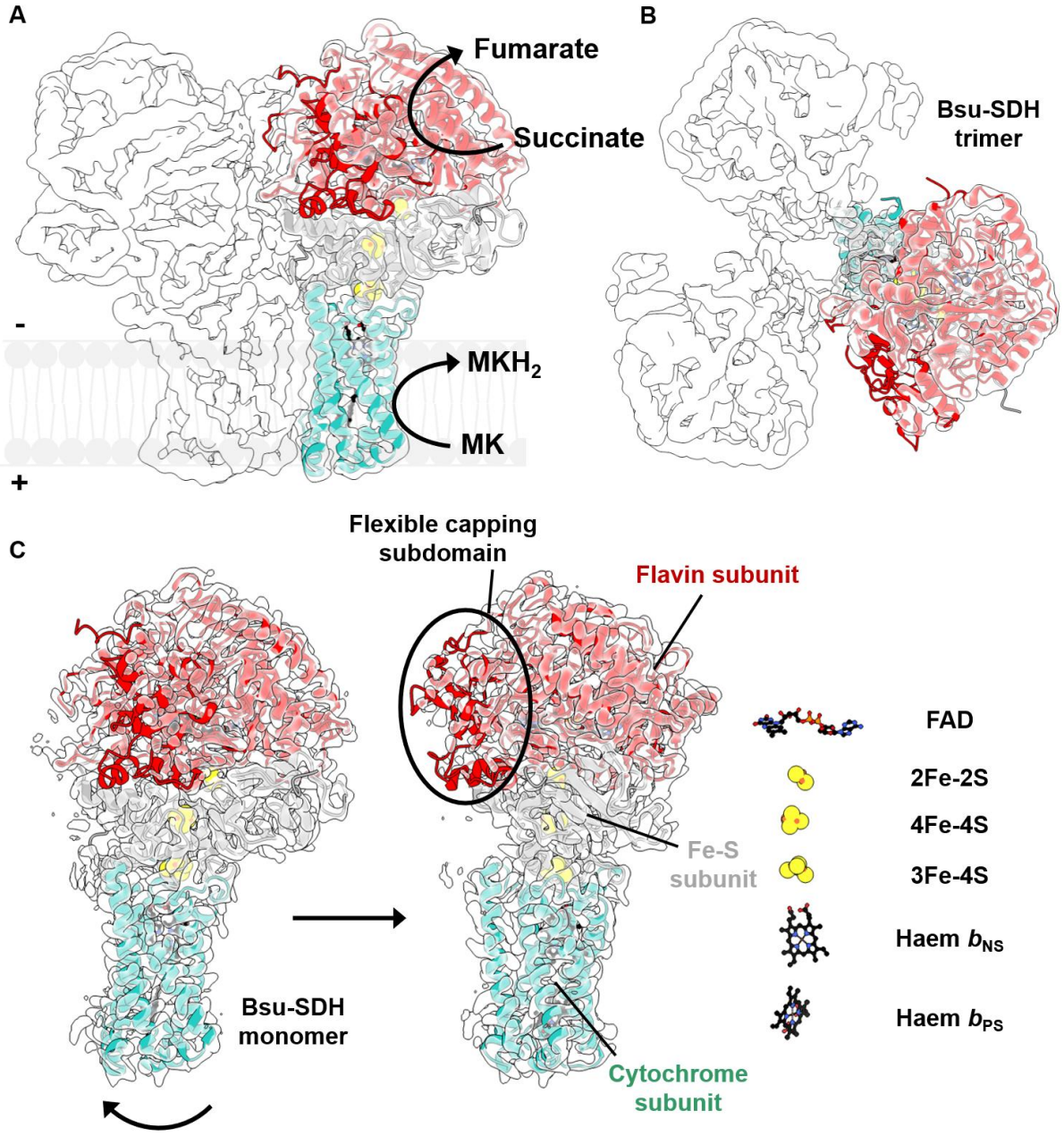

Fig 4. Important structural features of Bsu-SDH. (A) Side profile of the Gaussian-smoothed transparent map of the Bsu-SDH trimer with the AlphaFold model of a monomer fitted. (B) Top view of (A) showing the trimeric state. (C) The sharpened map of Bsu-SDH extracted around the monomeric model, which rotated slightly clockwise allows a better view of the flexible capping subdomain in the flavin subunit (red). This capping domain will become relevant later. Also shown are the Fe-S subunit (grey) and the integral membrane cytochrome subunit (teal). The cofactors are visualised without the protein backbone. Abbreviations used are FAD: flavin adenine dinucleotide; Fe-S: iron-sulphur cluster; b_{NS}: negative-side haem *b*; b_{PS}: positive-side

haem *b*, in reference to the cell membrane surface charge, as indicated in (A). b_{NS} and b_{PS} are equivalent to the conventional b_P and b_D respectively.

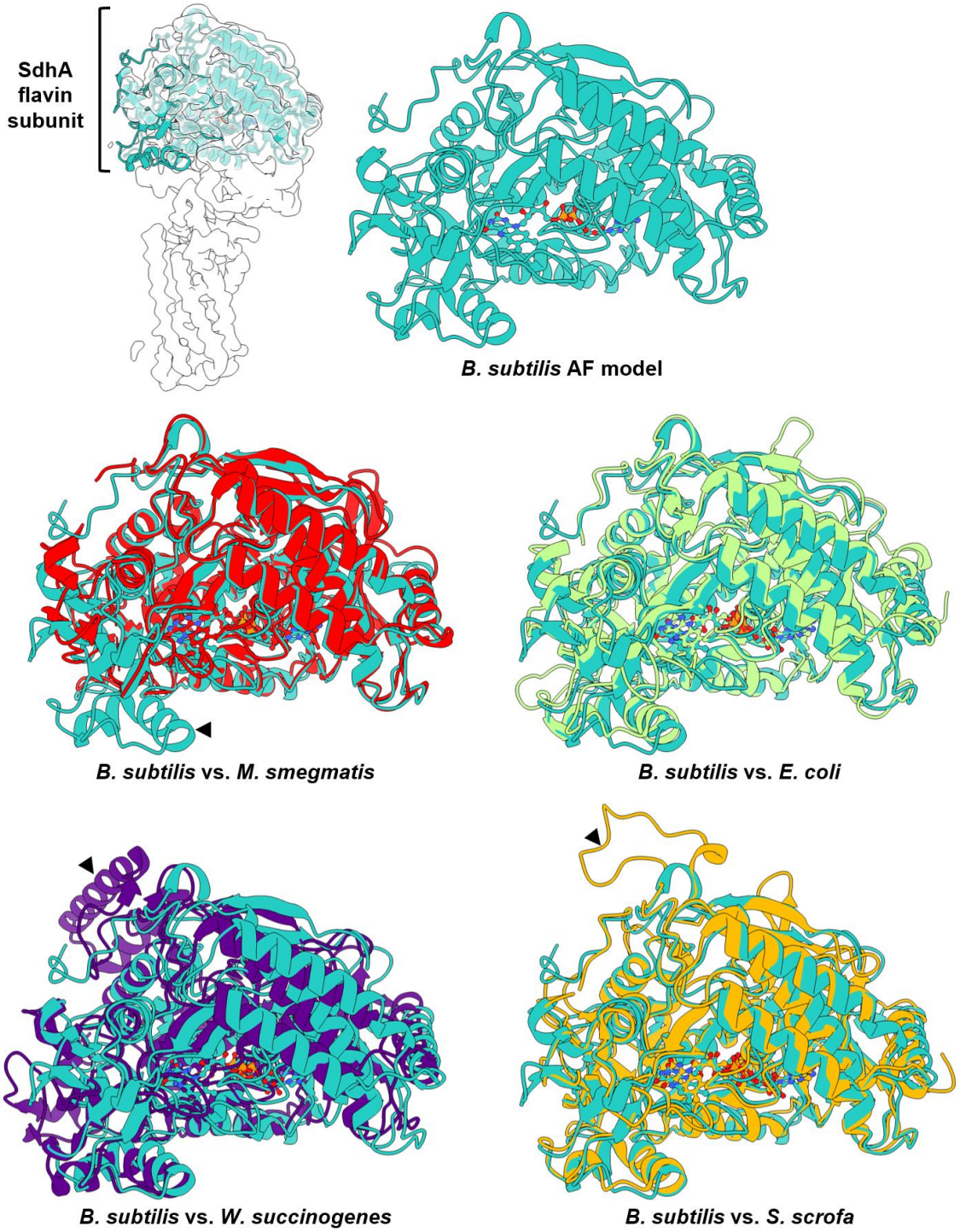

Fig 5. The conserved architecture of SdhA (flavin subunit) across species. Structural alignments of Bsu-SdhA AF model with SdhA from *M. smegmatis* Sdh2 (red, PDB: 6LUM), *E. coli* SQR (light green, PDB: 1NEK), *W. succinogenes* QFR (purple, PDB: 2BS2), and *S. scrofa* SDH (yellow, 1ZOY), performed using the Matchmaker tool (Meng et al., 2006) in ChimeraX. Some obvious differences are indicated with arrowheads.

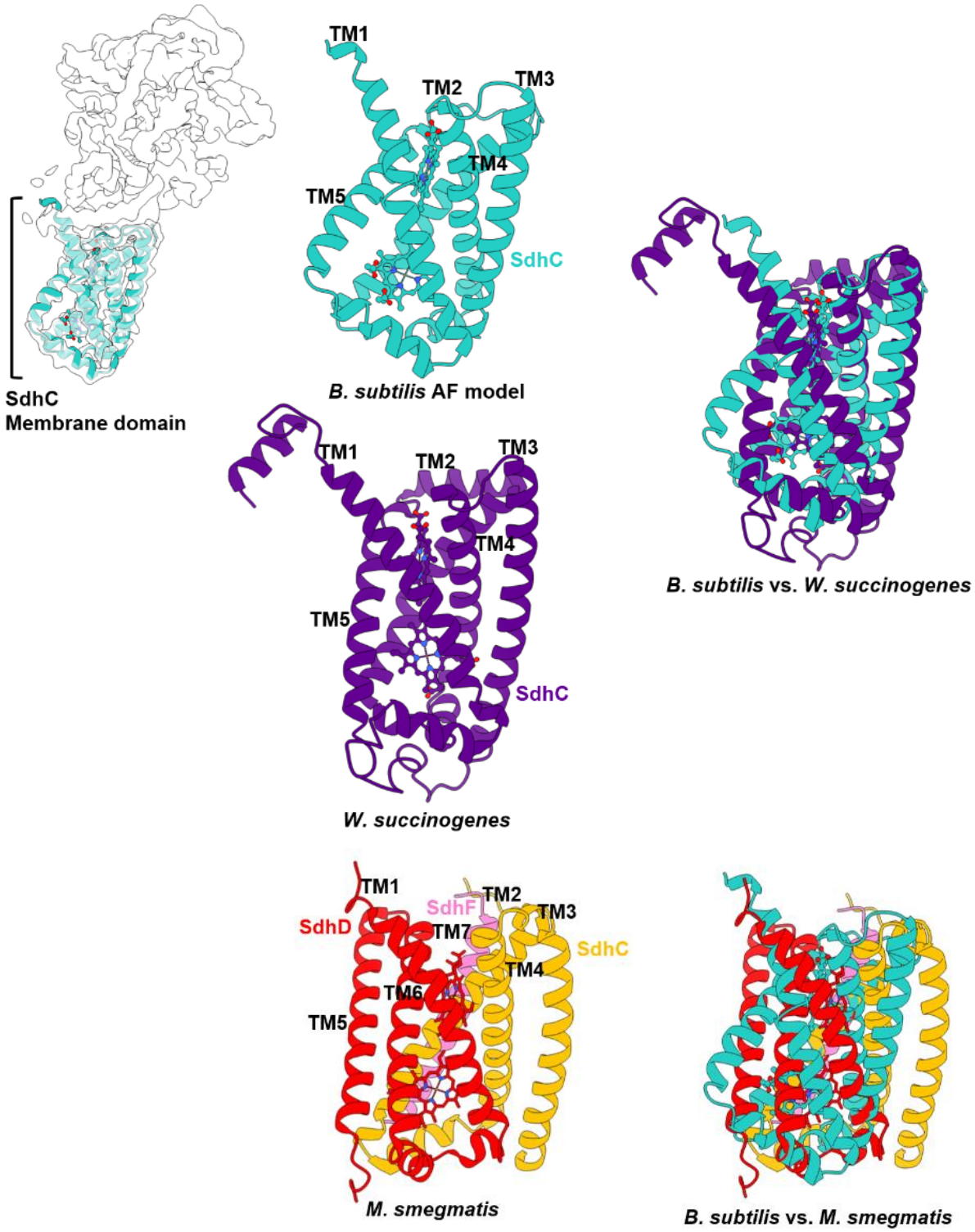

Fig 6. Conserved membrane domain architecture of class B complex II enzymes. Structural alignments of Bsu-SdhC with SdhC of *W. succinogenes* QFR (purple, PDB: 2BS2) and the membrane domain of *M. smegmatis* Sdh2 (PDB: 6LUM), composed of subunits SdhC (yellow), SdhD (red) and SdhF (pink). These were also performed using the Matchmaker tool in ChimeraX. Transmembrane (TM) helices are labelled to make comparing their positions and relative orientations across structures easier.

The membrane domain Bsu-SdhC was aligned with the corresponding subunits from *W. succinogenes* QFR and *M. smegmatis* Sdh2. We reasoned that these would be the most comparable as they are also di-haem-containing enzymes of classes B and A respectively in the complex II superfamily. SdhC subunits from *B. subtilis* and *W. succinogenes* showed a high degree of structural homology, consistent with these enzymes belonging to the same class. Aside from the di-haem groups, the membrane domain of *M. smegmatis* Sdh2 differs from Bsu-SdhC in the number of constituent subunits (Sdh2 has two subunits SdhC and SdhD coordinating the haem groups), in possessing an accessory subunit (SdhF) and in the number of TM helices (Sdh2 has seven). The membrane domain of *M. smegmatis* Sdh2 thus has a distinct architecture and does not align as well with Bsu-SdhC as the *W. succinogenes* SdhC subunit (Fig 6).

In both representations of the Bsu-SDH map (Fig 4A & C, Gaussian-smoothed vs. sharp), there is a region of SdhA for which the map density is clearly weak. This is the capping subdomain of the flavin subunit (Fig 4C) that in *the M. smegmatis* Sdh1 cryo-EM structure was also observed to be disordered (Zhou et al., 2021). In crystal structures of SdhA in complex with the assembly factor SdhE (Maher et al., 2018), and in co-crystals of *W. succinogenes* QFR without/with fumarate (Lancaster et al., 1999; Lancaster, Groß and Simon, 2001), rotational movement of the capping subdomain has been described before. The capping subdomain is connected to the flavin subdomain by a small hinge consisting of two β strands, and it has been suggested that this hinge-mediated flexibility controls substrate access to the flavin active site: when the capping subdomain is rotated away from the flavin subdomain, the ‘open’ conformation allows the substrate to enter the active site. Substrate binding then induces the rotation of the capping subdomain towards the flavin subdomain, and in this ‘closed’ conformation the active site is no longer accessible (Cecchini et al., 2002; Lancaster, 2011).

The *W. succinogenes* QFR structures, ‘open’ (PDB: 1QLB, wild-type enzyme co-crystallised with fumarate) and ‘closed’ (PDB: 1E7P, point mutation in the membrane domain, co-crystallised with malonate, a competitive inhibitor of fumarate reduction) were closely inspected to visualise the extent of capping subdomain movement previously seen in a complex II enzyme. In the surface representations shown, this conformational change is appreciable (Fig 7). It was estimated that the capping subdomain in the ‘closed’ state was rotated towards the flavin subdomain by 14° (Lancaster, Groß and Simon, 2001), but in crystal structures of other flavoproteins where this subdomain is a general feature, rotation of >30° has been observed (Iverson et al., 2000).

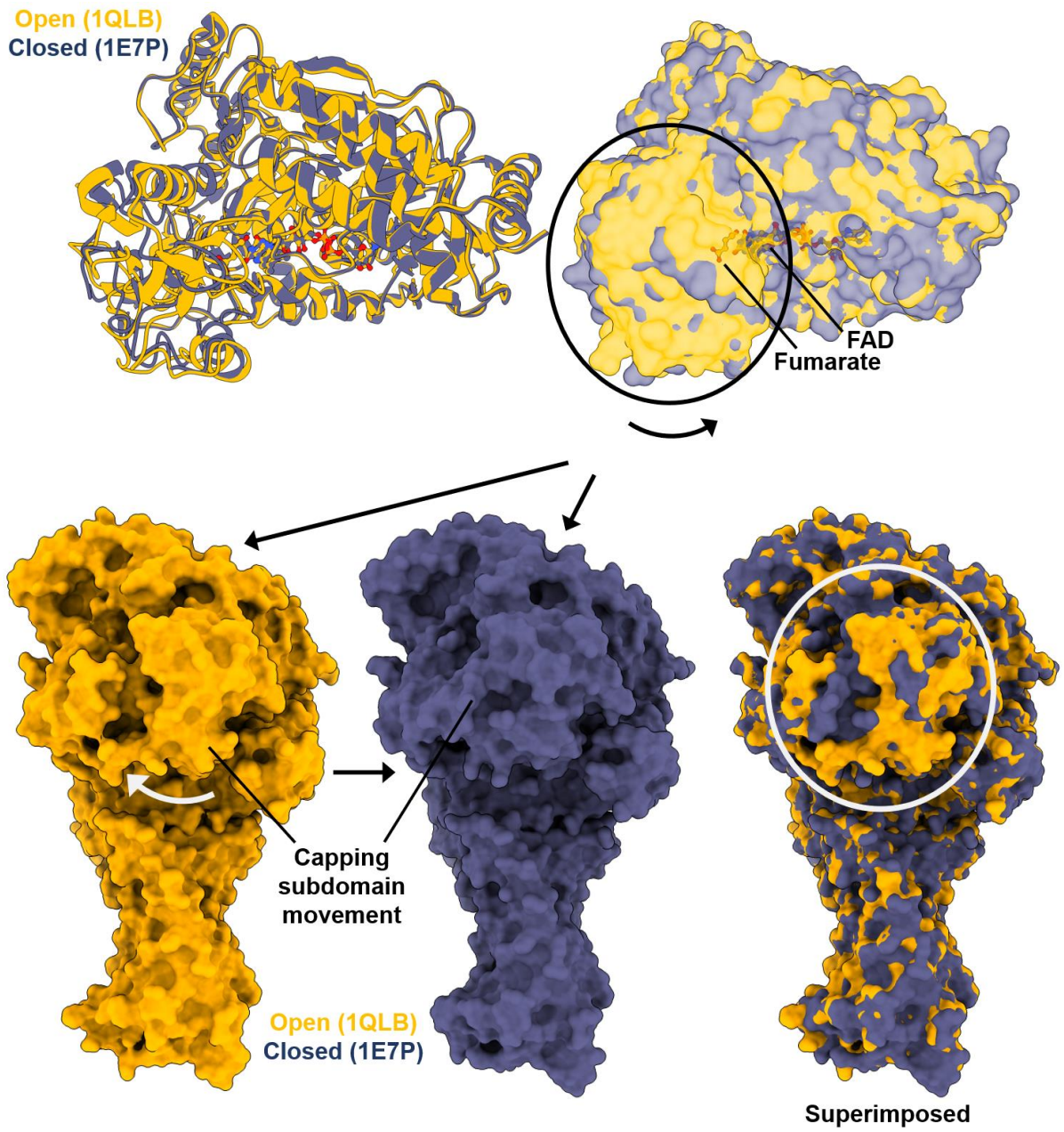

Fig 7. Movement of capping subdomain captured in crystal structures of *W. succinogenes* QFR. The 'open' conformation (yellow) is represented by the structure 1QLB, whereas the 'closed' conformation is represented by 1E7P. In both the cartoon and surface depictions of the flavin subunits, differences in the loops comprising the encircled capping subdomain can be seen. Fumarate (where malonate binds as well) along with the FAD cofactor are labelled to show their position relative to the capping subdomain. Rotating the structures anticlockwise slightly allows a better view of the subdomain movement with respect to the rest of the monomer. The white arrow in the 'open' conformer indicates the direction of rotation giving the 'closed' conformer. The two conformers superimposed are also shown.

The weak density in the Bsu-SDH map obtained for the capping subdomain hinted at the presence of these ‘open’ and ‘closed’ conformers in our dataset. A mask for the capping subdomain (Fig 8) was generated in ChimeraX using the Segger package implemented as the Segment Map tool (Pintilie et al., 2010). In CryoSPARC, this mask was used for focussed 3D classification of C3 symmetry-expanded particles.

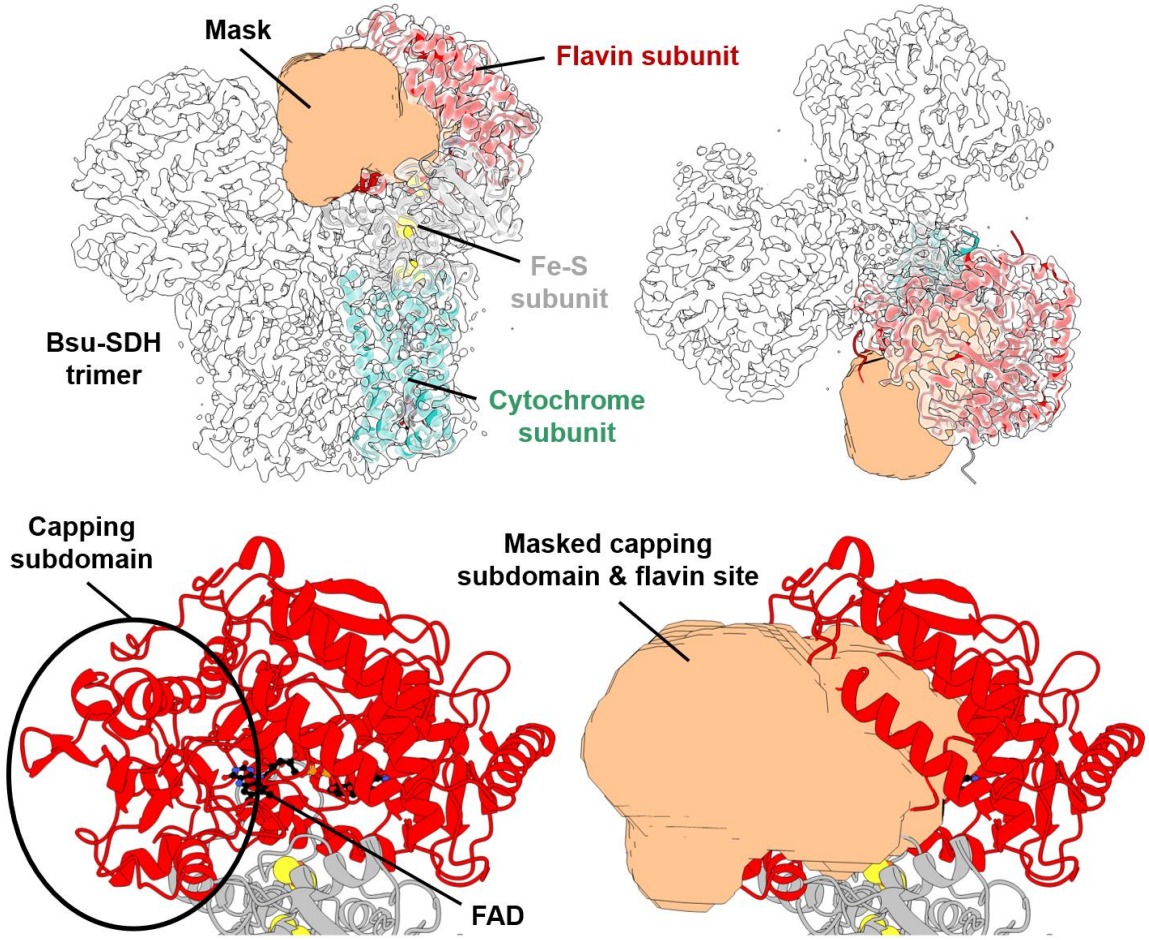

Fig 8. Mask generation for focussed 3D classification. The Bsu-SDH map was Gaussian-smoothed and segmented in ChimeraX, with appropriate region(s) selected to create a mask that would encompass the capping subdomain and the flavin site. This map was then binarised, rescaled to the same box size as the original map, and used as the focus mask during 3D classification.

Symmetry expansion around the C3 point-group meant that each monomer was considered as an individual particle, thereby boosting the number of particles from 27648 (trimeric) to 82944 monomeric particles and allowing the classification of each protomer independently. After focussed 3D classification of 82944 particles, we obtained 3 classes reflecting three different conformations, each at an overall lower resolution of ~5.8 Å. Nevertheless, surface representations of the three conformers showed unmistakable rotational movement of the

capping subdomain. Following the nomenclature from the *W. succinogenes* crystal structures (Fig 7), these are referred to as ‘open’ (state 1), ‘intermediate’ (state 2) and ‘closed’ (state 3) in Fig 9.

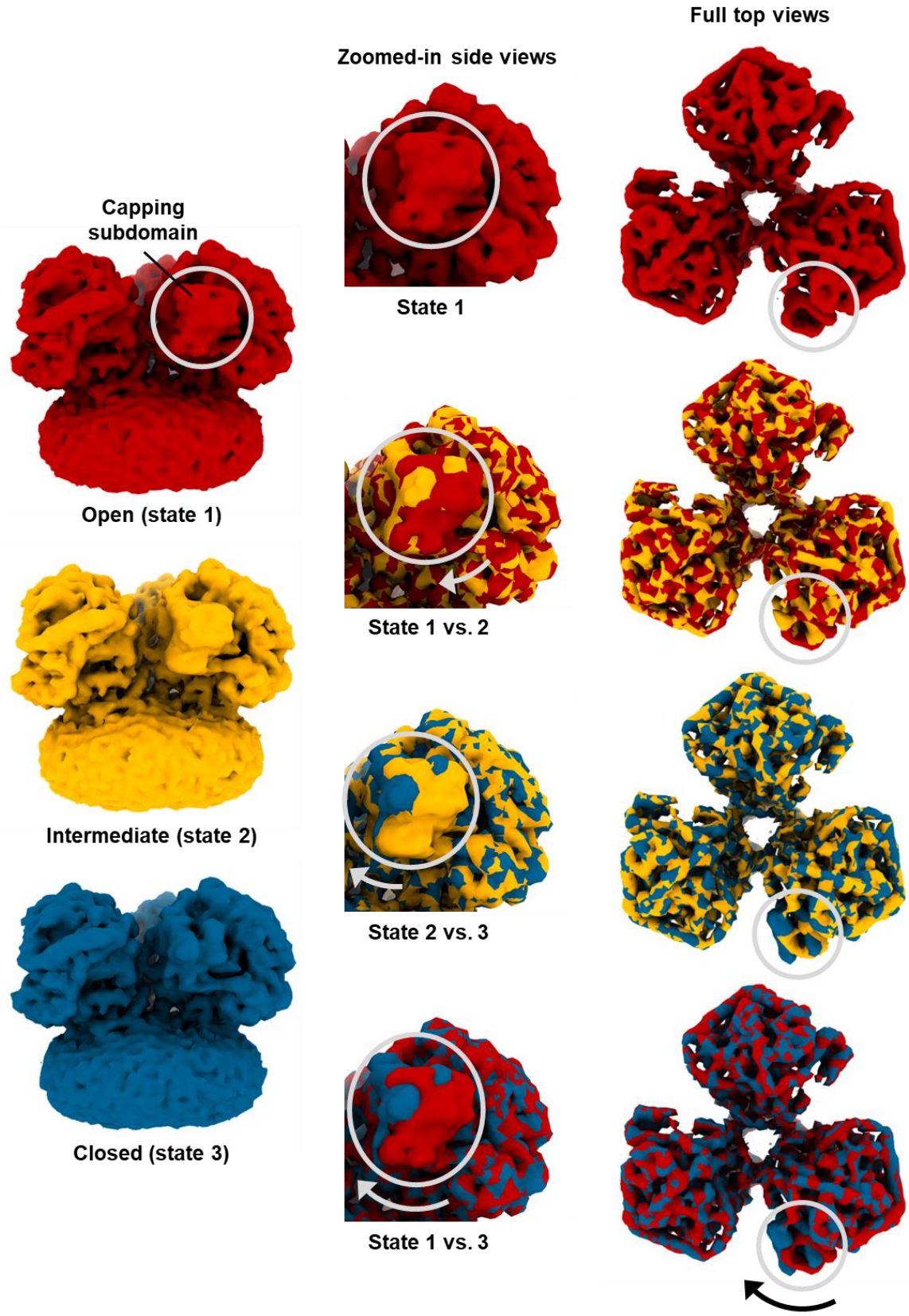

Fig 9. Rotational movement of the capping subdomain in Bsu-SDH. The three conformers obtained from focussed 3D classification are shown with the capping subdomain of SdhA encircled. Analogous to the *W. succinogenes* QFR conformers, the Bsu-SDH conformers are named 'open' (red, state 1), 'intermediate' (yellow, state 2), and 'closed' (blue, state 3). Anticlockwise rotation indicated by arrows leads to the transition from 'open' state 1 to 'closed' state 3 via the 'intermediate' state 2. Zoomed-in side views of the subdomain and top views of the superimposed maps are shown for comparison.

6.3. Conclusions and future work

We have serendipitously obtained a high-resolution cryo-EM reconstruction of SDH, an abundant respiratory enzyme, without affinity purification from crudely enriched membranes of wild-type *B. subtilis*. With the focussed 3D classification approach, we have shown that it is possible to further extract information of potential mechanistic relevance from such datasets, like the capping subdomain movement which has not been observed in native preparations of complex II enzymes before by cryo-EM. We speculate that the capping subdomain restricting substrate access to an already reduced flavin site could explain the tunnel diode effect described in mammalian and *E. coli* complex II enzymes. The disadvantage of our experimental strategy is that without purifying Bsu-SDH using affinity chromatography, we cannot easily refine its different conformers to a higher resolution, or attempt to correlate structural conformations with functional states.

The next steps in this project are to finish model-building and refinement for the 3.1 Å Bsu-SDH map and its 5.8 Å maps of conformers. Our collaborator Dr. Pintscher has recently obtained a cryo-EM dataset with purified *E. coli* SQR prepared using expression constructs provided by Dr. Gary Cecchini (University of California, San Francisco, USA). Grids were made with and without excess succinate, and the ambition is to get the enzyme in its different conformations, and sufficient particles for each conformation to achieve a high resolution of 2-3 Å. This will enable us to compare the low-resolution Bsu-SDH conformers to a well-studied system and investigate the mechanistic relevance of the capping subdomain movement.

Chapter 7: Conclusions and future directions

"*Each piece, or part, of the whole of nature is always merely an approximation to the complete truth, or the complete truth so far as we know it. In fact, everything we know is only some kind of approximation, because we know that we do not know all the laws as yet. Therefore, things must be learned only to be unlearned again or, more likely, to be corrected.*"

—Richard Feynman, The Feynman Lectures on Physics (1961-63)

With the work presented in this thesis, we have attempted to address the following practical and conceptual gaps in the field:

1. The long-standing interest in spore membrane proteins like the Ger receptors and SpoVA channels required for initiation of germination, but the lack of suitable membrane protein biochemistry methods to isolate them from spores and study their structure/function
2. The renewed interest in transmembrane movement of cations as the earliest event in spore germination, but the lack of new studies investigating the resumption of bioenergetics in germinating spores

In chapter 3, the tractability of spore membrane protein biochemistry was demonstrated using the model organism *B. megaterium* QM B1551. A membrane isolation protocol was optimised, along with a chromatographic method to extract large complexes from the resulting membrane preparations. NADH:O_2 reaction assays on these preparations confirmed retention of respiratory function. In fact, spore membranes were found to oxidise NADH twice as fast and in a more cyanide-insensitive manner than membranes isolated from late-exponential phase cells. Spore membranes were solubilised with the mild detergent DDM, and resolved as 6 high molecular weight bands using BN-PAGE. LC/MS analysis of these bands revealed the composition of the membrane-bound respiratory chain present in dormant spores. Intriguingly, two uncharacterised enzymes, YumB and YthAB were found that had replaced their canonical counterparts Ndh and CydAB respectively in spores. We identified the spore isoform of glucose dehydrogenase implicated in early glucose catabolism by germinating spores, and showed that the soluble NADH oxidase that has been invoked in the old literature to explain cyanide-insensitive O_2 consumption by germinating spores was highly unlikely to constitute a soluble, ETC-independent respiratory system.

In chapter 4, the relationship between glucose-initiated germination and glucose-powered oxidative metabolism in germinating spores was consolidated. We measured rehydration starting concurrently with glucose consumption and H_2O_2 production, supporting a model where electrons are transported from glucose to O_2 and H_2O_2 is a by-product of NDH-2 activity, i.e. YumB in the spore ETC. Glucose simultaneously acts as a signalling molecule to activate GerU and as a source of electrons. Glucose dehydrogenase oxidises glucose to gluconate generating NADH, which feeds electrons into the respiratory chain. During germination, rehydration can be viewed as a preparative phase for outgrowth – spores that cannot conserve sufficient energy in the absence of O_2 during this period my lose their absorbance even faster but they cannot outgrow. Oxidative metabolism thus powers germination to completion.

In chapter 5, the role of the respiratory chain in the oxidative metabolism that had been inferred from biochemical and microbiological data in chapter 4 was delineated using a novel biophysical technique. Remission haem spectroscopy allowed us to measure electron transport through the ETC non-invasively in real-time in germination spores. It was shown that 2 minutes after germination was initiated with glucose, spores used an uncharacterised cyt *bd* oxidase (YthAB) to restart oxidative metabolism. The other two haem-copper oxidases (HCOs), were found in their F state – this intermediate is known to accumulate when a $\Delta\Psi$ pushes against the catalytic cycle of proton-pumping HCOs. To the best of our knowledge, this is the first observation of the F intermediate *in vivo*, and could further explain the need for a non-proton pumping terminal oxidase like cyt *bd* that is less sensitive to such thermodynamic backpressure in germinating spores.

While the current consensus in the field is that resumption of bioenergetics is not essential for initiation of germination and starts only after core rehydration is completed, we have shown that electron transfer in the spore ETC precedes detectable hydration by a minute. Counterintuitively, this effect is even more pronounced with the non-nutrient germinant KBr, where electron transport and O_2 consumption preceded loss of absorbance by 8 mins. These findings lead us to a model in which some molecules of a germinant bind to the Ger receptor initiating cation release, while other molecules are co-transported into the spore core utilising this cation gradient. The incoming germinants serve as an electron source for the ETC, or endogenous reserves are liberated to generate reducing power. In the ETC, electrons are transferred to the HCOs (thereby regenerating NAD^+) but their catalytic cycle is suppressed by a $\Delta\Psi$, so O_2 is not reduced immediately. Meanwhile, CaDPA leakage by the SpoVA channel also starts, followed by bulk CaDPA release which allows progressive core rehydration and loss of absorbance. When glucose is the germinant, cyt *bd* activity and O_2 reduction start simultaneously with rehydration, whereas when KBr is used bulk CaDPA release starts much later. It is possible that the potency of the glucose germination signal masks this underlying

sequence of events where YthAB-dependent oxidative metabolism starts first, and there is perhaps an energetic threshold that must be reached before core rehydration can start; it is not known how activities of either the SpoVA channel or cyt *bd* are regulated. Supporting this hypothesis is preliminary genetic evidence from Dr. Christie's lab which shows that disrupting the *ythAB* operon led to a severe germination defect – these spores remained phase bright and could not initiate germination. However, this is not easily reconciled with data from our germination experiments where an even faster loss of absorbance was measured during anaerobiosis, but outgrowth was entirely inhibited by the absence of O_2. This phenotype is currently being verified using a Δ*ythA* mutant in Dr. Christie's lab. Our work paves the way for many follow-up studies, including but not restricted to: purification and functional/structural characterisation of YthAB (and any unidentified accessory subunits), similar characterisation of spore HCOs and their F state, the role of YthAB during late-stage sporulation, the energetics of CaDPA/water transport during sporulation/germination, etc.

In chapter 6, the suitability of membrane preparations such as those optimised in chapter 3 was assessed for cryo-EM strategies that involve only crude enrichment of very heterogeneous samples. Membranes from *B. subtilis* cells were used for this and a map of the *B. subtilis* succinate dehydrogenase (SDH) was refined serendipitously to a resolution of 3.1 Å. Like Sdh2 from *M. smegmatis* (class A) and SQR from *E. coli* (class C), we found Bsu-SDH to be a trimer. This makes Bsu-SDH the first trimeric member to be characterised structurally in class B of the complex II superfamily, which is currently exemplified by the dimeric fumarate reductase from *W. succinogenes*. With a focussed 3D classification approach, we have shown that it is possible to extract information of potential mechanistic relevance from such heterogeneous datasets, like the capping subdomain movement which had not been observed in native preparations of complex II enzymes before by cryo-EM. It was clear, however, that this strategy has many limitations and thus the best use of the optimised spore membrane preparations would be in purifying affinity-tagged proteins of interest from them, like the Strep-tagged GerU receptor complex (strain now available for experimentation).

References

Alberts, B. et al. (2002). *Molecular Biology of the Cell 4th Edition: International Student Edition*. Routledge. [Online]. Available at: https://books.google.co.uk/books?id=ozigkQEACAAJ.

Al-Hinai, M. A., Jones, S. W. and Papoutsakis, E. T. (2015). The *Clostridium* Sporulation Programs: Diversity and Preservation of Endospore Differentiation. *Microbiology and Molecular Biology Reviews*, 79 (1), pp.19–37. [Online]. Available at: doi:10.1128/MMBR.00025-14/ASSET/90440E15-B659-4F44-B3EC-1144A8E44019/ASSETS/GRAPHIC/ZMR0011523800007.JPEG [Accessed 23 March 2024].

Alimova, A. et al. (2006). Proteins and dipicolinic acid released during heat shock activation of *Bacillus subtilis* spores probed by optical spectroscopy. *Applied Optics, Vol. 45, Issue 3, pp. 445-450*, 45 (3), pp.445–450. [Online]. Available at: doi:10.1364/AO.45.000445 [Accessed 29 March 2024].

Allen, B. et al. (2023). Diversity and metabolic energy in bacteria. *FEMS Microbiology Letters*, 370. [Online]. Available at: doi:10.1093/FEMSLE/FNAD043 [Accessed 25 March 2024].

Ando, Y. and Tsuzuki, T. (1987). Hydrogen peroxide release from bacterial spores during germination. *Letters in Applied Microbiology*, 4 (4), pp.65–69. [Online]. Available at: doi:10.1111/J.1472-765X.1987.TB01585.X [Accessed 21 February 2023].

de Andrade Cavalcante, D. et al. (2019). Ultrastructural analysis of spores from diverse Bacillales species isolated from Brazilian soil. *Environmental Microbiology Reports*, 11 (2), pp.155–164. [Online]. Available at: doi:10.1111/1758-2229.12713 [Accessed 22 March 2024].

André, S., Vallaeys, T. and Planchon, S. (2017). Spore-forming bacteria responsible for food spoilage. *Research in Microbiology*, 168 (4), pp.379–387. [Online]. Available at: doi:10.1016/J.RESMIC.2016.10.003 [Accessed 22 March 2024].

Artzi, L. et al. (2021). Dormant spores sense amino acids through the B subunits of their germination receptors. *Nature Communications 2021 12:1*, 12 (1), pp.1–8. [Online]. Available at: doi:10.1038/s41467-021-27235-2 [Accessed 9 August 2022].

Bahnweg, G. and Douthit, H. A. (1975). Cytochrome Pigments in Spores of *Bacillus cereus* T. *Journal of Bacteriology*, 121 (2), p.737. [Online]. Available at: doi:10.1128/jb.121.2.737-739.1975 [Accessed 31 January 2022].

Barák, I. (2021). Special Issue "*Bacillus subtilis* as a Model Organism to Study Basic Cell Processes". *Microorganisms 2021, Vol. 9, Page 2459*, 9 (12), p.2459. [Online]. Available at: doi:10.3390/MICROORGANISMS9122459 [Accessed 22 March 2024].

Bary, A. (1884). *Vergleichende morphologie und biologie der pilze, mycetozoen und bacterien*. Engelmann.

Bath, J. et al. (2000). Role of *Bacillus subtilis* SpoIIIE in DNA transport across the mother cell-prespore division septum. *Science*, 290 (5493), pp.995–997. [Online]. Available at: doi:10.1126/SCIENCE.290.5493.995/SUPPL_FILE/1054624S1_THUMB.GIF [Accessed 22 March 2024].

Bauda, E. et al. (2024). Ultrastructure of macromolecular assemblies contributing to bacterial spore resistance revealed by in situ cryo-electron tomography. *Nature Communications 2024 15:1*, 15 (1), pp.1–12. [Online]. Available at: doi:10.1038/s41467-024-45770-6 [Accessed 26 March 2024].

Beaman, T. C. and Gerhardt, P. (1986). Heat resistance of bacterial spores correlated with protoplast dehydration, mineralization, and thermal adaptation. *Applied and Environmental Microbiology*, 52 (6), pp.1242–1246. [Online]. Available at: doi:10.1128/AEM.52.6.1242-1246.1986 [Accessed 23 March 2024].

Beites, T. et al. (2019). Plasticity of the *Mycobacterium tuberculosis* respiratory chain and its impact on tuberculosis drug development. *Nature Communications 2019 10:1*, 10 (1), pp.1–12. [Online]. Available at: doi:10.1038/s41467-019-12956-2 [Accessed 29 March 2024].

Belevich, I. et al. (2005). Oxygenated complex of cytochrome *bd* from *Escherichia coli*: Stability and photolability. *FEBS Letters*, 579 (21), pp.4567–4570. [Online]. Available at: doi:10.1016/J.FEBSLET.2005.07.011 [Accessed 29 March 2024].

Benarroch, J. M. and Asally, M. (2020). The Microbiologist's Guide to Membrane Potential Dynamics. *Trends in Microbiology*, 28 (4), pp.304–314. [Online]. Available at: doi:10.1016/J.TIM.2019.12.008 [Accessed 2 November 2023].

Bepler, T. et al. (2019). Positive-unlabeled convolutional neural networks for particle picking in cryo-electron micrographs. *Nature Methods 2019 16:11*, 16 (11), pp.1153–1160. [Online]. Available at: doi:10.1038/s41592-019-0575-8 [Accessed 19 March 2024].

Beskrovnaya, P. et al. (2021). Structural, Metabolic and Evolutionary Comparison of Bacterial Endospore and Exospore Formation. *Frontiers in Microbiology*, 12, p.630573. [Online]. Available at: doi:10.3389/FMICB.2021.630573/BIBTEX [Accessed 22 March 2024].

Biedendieck, R. et al. (2021). The “beauty in the beast”—the multiple uses of *Priestia megaterium* in biotechnology. *Applied Microbiology and Biotechnology 2021 105:14*, 105 (14), pp.5719–5737. [Online]. Available at: doi:10.1007/S00253-021-11424-6 [Accessed 25 March 2024].

Biquet-Bisquert, A. et al. (2023). Spatio-temporal dynamics of the proton motive force on single bacterial cells. *bioRxiv*, p.2023.04.03.535353. [Online]. Available at: doi:10.1101/2023.04.03.535353 [Accessed 26 March 2024].

Björck, M. L. and Brzezinski, P. (2018). Control of transmembrane charge transfer in cytochrome *c* oxidase by the membrane potential. *Nature Communications 2018 9:1*, 9 (1), pp.1–8. [Online]. Available at: doi:10.1038/s41467-018-05615-5 [Accessed 31 March 2024].

Black, S. H. and Gerhardt, P. (1961). Permeability of bacterial spores I. *Journal of Bacteriology*, 82 (5), pp.743–749. [Online]. Available at: doi:10.1128/JB.82.5.743-749.1961 [Accessed 31 March 2024].

Blaza, J. N. et al. (2014). Kinetic evidence against partitioning of the ubiquinone pool and the catalytic relevance of respiratory-chain supercomplexes. *Proceedings of the National Academy of Sciences of the United States of America*, 111 (44), pp.15735–15740. [Online]. Available at: doi:10.1073/PNAS.1413855111/SUPPL_FILE/PNAS.201413855SI.PDF [Accessed 28 March 2024].

Blaza, J. N. et al. (2017). The mechanism of catalysis by type-II NADH:quinone oxidoreductases. *Scientific Reports 2017 7:1*, 7 (1), pp.1–11. [Online]. Available at: doi:10.1038/srep40165 [Accessed 28 March 2024].

Blaza, J. N., Vinothkumar, K. R. and Hirst, J. (2018). Structure of the Deactive State of Mammalian Respiratory Complex I. *Structure*, 26 (2), pp.312-319.e3. [Online]. Available at: doi:10.1016/j.str.2017.12.014 [Accessed 28 March 2024].

Borisov, V. B. et al. (2011a). Catalytic intermediates of cytochrome *bd* terminal oxidase at steady-state: Ferryl and oxy-ferrous species dominate. *Biochimica et Biophysica Acta (BBA) - Bioenergetics*, 1807 (5), pp.503–509. [Online]. Available at: doi:10.1016/J.BBABIO.2011.02.007 [Accessed 29 March 2024].

Borisov, V. B. et al. (2011b). The cytochrome *bd* respiratory oxygen reductases. *Biochimica et Biophysica Acta (BBA) - Bioenergetics*, 1807 (11), pp.1398–1413. [Online]. Available at: doi:10.1016/J.BBABIO.2011.06.016 [Accessed 29 March 2024].

Borisov, V. B. et al. (2021a). Bacterial Oxidases of the Cytochrome *bd* Family: Redox Enzymes of Unique Structure, Function, and Utility as Drug Targets. *Antioxidants and Redox Signaling*, 34 (16), pp.1280–1318. [Online]. Available at: doi:10.1089/ARS.2020.8039/ASSET/IMAGES/LARGE/ARS.2020.8039_FIGURE21.JPEG [Accessed 6 March 2024].

Borisov, V. B. et al. (2021b). ROS Defense Systems and Terminal Oxidases in Bacteria. *Antioxidants*, 10 (6). [Online]. Available at: doi:10.3390/ANTIOX10060839 [Accessed 6 March 2024].

Borisov, V. B. and Forte, E. (2022). Bioenergetics and Reactive Nitrogen Species in Bacteria. *International Journal of Molecular Sciences 2022, Vol. 23, Page 7321*, 23 (13), p.7321. [Online]. Available at: doi:10.3390/IJMS23137321 [Accessed 25 March 2024].

Breedijk, R. M. P. et al. (2020). A live-cell super-resolution technique demonstrated by imaging germinosomes in wild-type bacterial spores. *Scientific Reports 2020 10:1*, 10 (1), pp.1–12. [Online]. Available at: doi:10.1038/s41598-020-62377-1 [Accessed 25 March 2024].

Bressuire-Isoard, C., Broussolle, V. and Carlin, F. (2018). Sporulation environment influences spore properties in *Bacillus*: evidence and insights on underlying molecular and physiological mechanisms. *FEMS Microbiology Reviews*, 42 (5), pp.614–626. [Online]. Available at: doi:10.1093/FEMSRE/FUY021 [Accessed 8 March 2024].

Britton, R. A. et al. (2002). Genome-wide analysis of the stationary-phase sigma factor (Sigma-H) regulon of *Bacillus subtilis*. *Journal of Bacteriology*, 184 (17), pp.4881–4890. [Online]. Available at: doi:10.1128/JB.184.17.4881-4890.2002/ASSET/D44371E0-7101-407B-8E77-3B753B480911/ASSETS/GRAPHIC/JB1720401002.JPEG [Accessed 23 March 2024].

Burstein, C., Tiankova, L. and Kepes, A. (1979). Respiratory Control in *Escherichia coli* K12. *European Journal of Biochemistry*, 94 (2), pp.387–392. [Online]. Available at: doi:10.1111/J.1432-1033.1979.TB12905.X [Accessed 29 March 2024].

Carlson, M. L. et al. (2018). The peptidisc, a simple method for stabilizing membrane proteins in detergent-free solution. *eLife*, 7. [Online]. Available at: doi:10.7554/ELIFE.34085 [Accessed 3 September 2021].

Castro, R. et al. (2009). Characterization of the individual glucose uptake systems of *Lactococcus lactis*: mannose-PTS, cellobiose-PTS and the novel GlcU permease. *Molecular Microbiology*, 71 (3), pp.795–806. [Online]. Available at: doi:10.1111/J.1365-2958.2008.06564.X [Accessed 15 February 2024].

Cecchini, G. et al. (2002). Succinate dehydrogenase and fumarate reductase from *Escherichia coli*. *Biochimica et Biophysica Acta (BBA) - Bioenergetics*, 1553 (1–2), pp.140–157. [Online]. Available at: doi:10.1016/S0005-2728(01)00238-9 [Accessed 19 March 2024].

Chan, H. et al. (2022). Genetic Screens Identify Additional Genes Implicated in Envelope Remodeling during the Engulfment Stage of *Bacillus subtilis* Sporulation. *mBio*, 13 (5). [Online]. Available at: doi:10.1128/MBIO.01732-22/SUPPL_FILE/MBIO.01732-22-S0008.TIF [Accessed 22 March 2024].

Chapman, A. G., Fall, L. and Atkinson, D. E. (1971). Adenylate Energy Charge in *Escherichia coli* During Growth and Starvation. *Journal of Bacteriology*, 108 (3), pp.1072–1086. [Online]. Available at: doi:10.1128/JB.108.3.1072-1086.1971 [Accessed 8 March 2024].

Chapman, G. B. (1956). Electron microscopy of ultra-thin sections of bacteria. *Journal of Bacteriology*, 71 (3), pp.348–355. [Online]. Available at: doi:10.1128/JB.71.3.348-355.1956 [Accessed 26 March 2024].

Chen, Y. et al. (2019). Membrane proteomes and ion transporters in *Bacillus anthracis* and *Bacillus subtilis* dormant and germinating spores. *Journal of Bacteriology*, 201 (6), pp.662–680. [Online]. Available at: doi:10.1128/JB.00662-18/SUPPL_FILE/JB.00662-18-S0001.PDF [Accessed 22 August 2022].

Christie, G. and Lowe, C. R. (2007). Role of Chromosomal and Plasmid-Borne Receptor Homologues in the Response of *Bacillus megaterium* QM B1551 Spores to Germinants. *Journal of Bacteriology*, 189 (12), p.4375. [Online]. Available at: doi:10.1128/JB.00110-07 [Accessed 9 August 2022].

Christie, G. and Setlow, P. (2020). Bacillus spore germination: Knowns, unknowns and what we need to learn. *Cellular Signalling*, 74, Elsevier Inc., p.109729. [Online]. Available at: doi:10.1016/j.cellsig.2020.109729 [Accessed 14 December 2020].

Corbett, D. et al. (2017). Listeria monocytogenes Has Both Cytochrome *bd*-type and Cytochrome aa_3-type Terminal Oxidases, Which Allow Growth at Different Oxygen Levels, and Both Are Important in Infection. *Infection and Immunity*, 85 (11). [Online]. Available at: doi:10.1128/IAI.00354-17 [Accessed 31 March 2024].

Covian, R. et al. (2023). Spectroscopic identification of the catalytic intermediates of cytochrome *c* oxidase in respiring heart mitochondria. *Biochimica et Biophysica Acta (BBA) - Bioenergetics*, 1864 (2), p.148934. [Online]. Available at: doi:10.1016/J.BBABIO.2022.148934 [Accessed 8 March 2024].

Cowan, A. E. et al. (2004). Lipids in the inner membrane of dormant spores of *Bacillus species* are largely immobile. *Proceedings of the National Academy of Sciences of the United States of America*, 101 (20), pp.7733–7738. [Online]. Available at: doi:10.1073/pnas.0306859101 [Accessed 15 December 2020].

Czapla, M. et al. (2012). Fusing two cytochromes *b* of *Rhodobacter capsulatus* cytochrome bc_1 using various linkers defines a set of protein templates for asymmetric mutagenesis. *Protein Engineering, Design and Selection*, 25 (1), pp.15–25. [Online]. Available at: doi:10.1093/PROTEIN/GZR055 [Accessed 27 March 2024].

Deshevaya, E. A. et al. (2024). Survival of microorganisms during two-year exposure in outer space near the ISS. *Scientific Reports 2024 14:1*, 14 (1), pp.1–11. [Online]. Available at: doi:10.1038/s41598-023-49525-z [Accessed 23 March 2024].

Dills, S. S. and Vary, J. C. (1978). An evaluation of respiration chain-associated functions during initiation of germination of *Bacillus megaterium* spores. *Biochimica et Biophysica Acta (BBA) - General Subjects*, 541 (3), pp.301–311. [Online]. Available at: doi:10.1016/0304-4165(78)90190-3 [Accessed 27 July 2021].

Diuba, A. V. et al. (2023). Individual heme *a* and heme a_3 contributions to the Soret absorption spectrum of the reduced bovine cytochrome *c* oxidase. *Biochimica et Biophysica Acta (BBA) - Bioenergetics*, 1864 (2), p.148937. [Online]. Available at: doi:10.1016/J.BBABIO.2022.148937 [Accessed 8 March 2024].

Doi, R. H. and Halvorson, H. (1961a). Comparison of Electron Transport Systems in Vegetative Cells and Spores of *Bacillus Cereus*. *Journal of Bacteriology*, 81 (1), p.51. [Online]. Available at: doi:10.1128/jb.81.1.51-58.1961 [Accessed 31 January 2022].

Doi, R. H. and Halvorson, H. (1961b). Mechanism of dipicolinic acid stimulation of the soluble reduced diphosphopyridine nucleotide oxidase of spores. *Journal of bacteriology*, 81, pp.642–648. [Online]. Available at: doi:10.1128/JB.81.4.642-648.1961/ASSET/5BB8C091-ACBC-4D74-B5B5-AD8CFAF134D1/ASSETS/JB.81.4.642-648.1961.FP.PNG [Accessed 1 July 2022].

Eichenberger, P. (2012). Genomics and cellular biology of endospore formation. *Bacillus: cellular and molecular biology*, 2, pp.319–350.

English, J. D. and Vary, P. S. (1986). Isolation of recombination-defective and UV-sensitive mutants of *Bacillus megaterium*. *Journal of Bacteriology*, 165 (1), pp.155–160. [Online]. Available at: doi:10.1128/JB.165.1.155-160.1986 [Accessed 31 March 2024].

Eppinger, M. et al. (2011). Genome sequences of the biotechnologically important *Bacillus megaterium* strains QM B1551 and DSM319. *Journal of Bacteriology*, 193 (16), pp.4199–4213. [Online]. Available at: doi:10.1128/JB.00449-11 [Accessed 18 May 2021].

Errington, J. and van der Aart, L. T. (2020). Microbe profile: *Bacillus subtilis*: Model organism for cellular development, and industrial workhorse. *Microbiology (United Kingdom)*, 166 (5), pp.425–427. [Online]. Available at: doi:10.1099/MIC.0.000922/CITE/REFWORKS [Accessed 22 March 2024].

Escamilla, J. E. et al. (1986). Respiratory systems of the *Bacillus cereus* mother cell and forespore. *Journal of Bacteriology*, 167 (2), p.544. [Online]. Available at: doi:10.1128/JB.167.2.544-550.1986 [Accessed 2 August 2021].

Escamilla, J. E. et al. (1988). Role of menaquinone in inactivation and activation of the *Bacillus cereus* forespore respiratory system. *Journal of Bacteriology*, 170 (12), pp.5908–5912. [Online]. Available at: doi:10.1128/JB.170.12.5908-5912.1988 [Accessed 21 February 2023].

Escamilla, J. E. and Benito, M. C. (1984). Respiratory system of vegetative and sporulating *Bacillus cereus*. *Journal of Bacteriology*, 160 (1), p.473. [Online]. Available at: doi:10.1128/JB.160.1.473-477.1984 [Accessed 9 August 2022].

Evans, R. et al. (2022). Protein complex prediction with AlphaFold-Multimer. *bioRxiv*, p.2021.10.04.463034. [Online]. Available at: doi:10.1101/2021.10.04.463034 [Accessed 25 March 2024].

Falcone, G., Salvatore, G. and Covelli, I. (1959). Mechanism of induction of spore germination in *Bacillus subtilis* by L-alanine and hydrogen peroxide. *Biochimica et Biophysica Acta*, 36 (2), pp.390–397. [Online]. Available at: doi:10.1016/0006-3002(59)90181-7 [Accessed 26 April 2023].

Feniouk, B. A., Suzuki, T. and Yoshida, M. (2007). Regulatory interplay between proton motive force, ADP, phosphate, and subunit ε in bacterial ATP synthase. *Journal of Biological Chemistry*, 282 (1), pp.764–772. [Online]. Available at: doi:10.1074/jbc.M606321200 [Accessed 26 March 2024].

Foerster, H. F. and Foster, J. W. (1966). Response of *Bacillus* Spores to Combinations of Germinative Compounds. *Journal of Bacteriology*, 91 (3), p.1168. [Online]. Available at: doi:10.1128/JB.91.3.1168-1177.1966 [Accessed 9 August 2022].

Frentz, Z. and Dworkin, J. (2020). Bioluminescence dynamics in single germinating bacterial spores reveal metabolic heterogeneity. *Journal of the Royal Society Interface*, 17 (170). [Online]. Available at: doi:10.1098/RSIF.2020.0350 [Accessed 24 March 2024].

Friedrich, T., Wohlwend, D. and Borisov, V. B. (2022). Recent Advances in Structural Studies of Cytochrome *bd* and Its Potential Application as a Drug Target. *International Journal of Molecular Sciences*, 23 (6). [Online]. Available at: doi:10.3390/IJMS23063166 [Accessed 6 March 2024].

Fujita, Y., Ramaley, R. and Freese, E. (1977). Location and properties of glucose dehydrogenase in sporulating cells and spores of *Bacillus subtilis*. *Journal of bacteriology*, 132 (1), pp.282–293. [Online]. Available at: doi:10.1128/JB.132.1.282-293.1977 [Accessed 10 August 2022].

Galperin, M. Y. et al. (2022). Conservation and Evolution of the Sporulation Gene Set in Diverse Members of the Firmicutes. *Journal of Bacteriology*, 204 (6). [Online]. Available at: doi:10.1128/JB.00079-22 [Accessed 10 August 2022].

Gao, Y. et al. (2022). The SpoVA membrane complex is required for dipicolinic acid import during sporulation and export during germination. *Genes & Development*, 36 (9–10), pp.634–646. [Online]. Available at: doi:10.1101/GAD.349488.122 [Accessed 22 August 2022].

Gao, Y. et al. (2023). Bacterial spore germination receptors are nutrient-gated ion channels. *Science*, 380 (6643), pp.387–391. [Online]. Available at: doi:10.1126/SCIENCE.ADG9829/SUPPL_FILE/SCENCE.ADG9829_MDAR_REPRODUCIBILITY_CHECKLIST.PDF [Accessed 15 February 2024].

Gao, Y. et al. (2024). SpoVAF and FigP assemble into oligomeric ion channels that enhance spore germination. *Genes & Development*, 38 (1–2), pp.31–45. [Online]. Available at: doi:10.1101/GAD.351353.123 [Accessed 24 March 2024].

Garg, R. and Maldener, I. (2021). The Formation of Spore-Like Akinetes: A Survival Strategy of Filamentous Cyanobacteria. *Microbial Physiology*, 31 (3), pp.296–305. [Online]. Available at: doi:10.1159/000517443 [Accessed 22 March 2024].

Ghosh, S. et al. (2015). Analysis of metabolism in dormant spores of *Bacillus* species by ^{31}P nuclear magnetic resonance analysis of low-molecular-weight compounds. *Journal of*

Bacteriology, 197 (5), pp.992–1001. [Online]. Available at: doi:10.1128/JB.02520-14 [Accessed 15 December 2020].

Gong, H. et al. (2020). Cryo-EM structure of trimeric *Mycobacterium smegmatis* succinate dehydrogenase with a membrane-anchor SdhF. *Nature Communications 2020 11:1*, 11 (1), pp.1–8. [Online]. Available at: doi:10.1038/s41467-020-18011-9 [Accessed 19 March 2024].

Goodgame, R. W. (1996). Understanding intestinal spore-forming protozoa: *Cryptosporidia*, *Microsporidia*, *Isospora*, and *Cyclospora*. *Annals of Internal Medicine*, 124 (4), pp.429–441. [Online]. Available at: doi:10.7326/0003-4819-124-4-199602150-00008/ASSET/IMAGES/8FF5.JPG [Accessed 22 March 2024].

Gostimskaya, I. S. et al. (2003). In situ assay of the intramitochondrial enzymes: use of alamethicin for permeabilization of mitochondria. *Analytical Biochemistry*, 313 (1), pp.46–52. [Online]. Available at: doi:10.1016/S0003-2697(02)00534-1 [Accessed 26 March 2024].

Gould, G. W. (2006). History of science – spores. *Journal of Applied Microbiology*, 101 (3), pp.507–513. [Online]. Available at: doi:10.1111/J.1365-2672.2006.02888.X [Accessed 22 March 2024].

Grauel, A. et al. (2021). Structure of *Escherichia coli* cytochrome *bd*-II type oxidase with bound aurachin D. *Nature Communications 2021 12:1*, 12 (1), pp.1–11. [Online]. Available at: doi:10.1038/s41467-021-26835-2 [Accessed 6 March 2024].

Greene, R. A. and Slepecky, R. A. (1972). Minimal Requirements for Commitment to Sporulation in *Bacillus megaterium*. *Journal of Bacteriology*, 111 (2), pp.557–565. [Online]. Available at: doi:10.1128/JB.111.2.557-565.1972 [Accessed 8 March 2024].

Griffiths, K. K. et al. (2011). Germination proteins in the inner membrane of dormant *Bacillus subtilis* spores colocalize in a discrete cluster. *Molecular Microbiology*, 81 (4), pp.1061–1077. [Online]. Available at: doi:10.1111/J.1365-2958.2011.07753.X [Accessed 25 March 2024].

Guo, H. and Rubinstein, J. L. (2022). Structure of ATP synthase under strain during catalysis. *Nature Communications 2022 13:1*, 13 (1), pp.1–9. [Online]. Available at: doi:10.1038/s41467-022-29893-2 [Accessed 31 March 2024].

Gupta, R. S. et al. (2020). Robust demarcation of 17 distinct *Bacillus* species clades, proposed as novel *Bacillaceae* genera, by phylogenomics and comparative genomic analyses: Description of *Robertmurraya kyonggiensis* sp. nov. and proposal for an emended genus *Bacillus* limiting it only to the members of the *Subtilis* and *Cereus* clades of species. *International Journal of Systematic and Evolutionary Microbiology*, 70 (11), pp.5753–5798.

[Online]. Available at: doi:10.1099/IJSEM.0.004475/CITE/REFWORKS [Accessed 22 August 2022].

Gupta, S. et al. (2013). Investigating the functional hierarchy of *Bacillus megaterium* PV361 spore germinant receptors. *Journal of Bacteriology*, 195 (13), pp.3045–3053. [Online]. Available at: doi:10.1128/JB.00325-13 [Accessed 15 December 2020].

Hardwick, W. A. and Foster, J. W. (1952). On The Nature of Sporogenesis in Some Aerobic Bacteria. *Journal of General Physiology*, 35 (6), pp.907–927. [Online]. Available at: doi:10.1085/JGP.35.6.907 [Accessed 8 March 2024].

Hederstedt, L. (2021). Molecular Biology of *Bacillus subtilis* Cytochromes anno 2020. *Biochemistry (Moscow) 2020 86:1*, 86 (1), pp.8–21. [Online]. Available at: doi:10.1134/S0006297921010028 [Accessed 20 March 2024].

Higgins, D. and Dworkin, J. (2012). Recent progress in *Bacillus subtilis* sporulation. *FEMS Microbiology Reviews*, 36 (1), pp.131–148. [Online]. Available at: doi:10.1111/J.1574-6976.2011.00310.X [Accessed 22 March 2024].

Ho, C. M. et al. (2019). Bottom-up structural proteomics: cryoEM of protein complexes enriched from the cellular milieu. *Nature Methods 2019 17:1*, 17 (1), pp.79–85. [Online]. Available at: doi:10.1038/s41592-019-0637-y [Accessed 19 March 2024].

Hogarth, C., Wilkinson, B. J. and Ellar, D. J. (1977). Cyanide-resistant electron transport in sporulating *Bacillus megaterium* KM. *Biochimica et Biophysica Acta (BBA) - Bioenergetics*, 461 (1), pp.109–123. [Online]. Available at: doi:10.1016/0005-2728(77)90073-1 [Accessed 9 August 2022].

Hollis, V. S. et al. (2003). Monitoring cytochrome redox changes in the mitochondria of intact cells using multi-wavelength visible light spectroscopy. *Biochimica et Biophysica Acta (BBA) - Bioenergetics*, 1607 (2–3), pp.191–202. [Online]. Available at: doi:10.1016/J.BBABIO.2003.09.012 [Accessed 8 March 2024].

Hummel, W. and Riebel, B. (2003). Isolation and biochemical characterization of a new NADH oxidase from *Lactobacillus brevis*. *Biotechnology Letters*, 25 (1), pp.51–54. [Online]. Available at: doi:10.1023/A:1021730131633/METRICS [Accessed 2 November 2023].

Hyatt, M. T. and Levinson, H. S. (1959). Utilization of phosphates in the postgerminative development of spores of *Bacillus megaterium*. *Journal of bacteriology*, 77 (4), pp.487–496. [Online]. Available at: doi:10.1128/JB.77.4.487-496.1959 [Accessed 26 April 2023].

Hyatt, M. T. and Levinson, H. S. (1961). Interaction of heat, glucose, L-alanine, and potassium nitrate in spore germination of *Bacillus megaterium*. *Journal of Bacteriology*, 81 (2), p.204. [Online]. Available at: doi:10.1128/JB.81.2.204-211.1961 [Accessed 2 November 2023].

Iverson, T. M. et al. (2000). Analyzing your complexes: structure of the quinol-fumarate reductase respiratory complex. *Current Opinion in Structural Biology*, 10 (4), pp.448–455. [Online]. Available at: doi:10.1016/S0959-440X(00)00113-5 [Accessed 20 March 2024].

Iverson, T. M. et al. (2002). Crystallographic studies of the *Escherichia coli* quinol-fumarate reductase with inhibitors bound to the quinol-binding site. *Journal of Biological Chemistry*, 277 (18), pp.16124–16130. [Online]. Available at: doi:10.1074/jbc.M200815200 [Accessed 19 March 2024].

Iverson, T. M., Singh, P. K. and Cecchini, G. (2023). An evolving view of complex II—noncanonical complexes, megacomplexes, respiration, signaling, and beyond. *Journal of Biological Chemistry*, 299 (6), p.104761. [Online]. Available at: doi:10.1016/J.JBC.2023.104761 [Accessed 20 March 2024].

Janganan, T. K. et al. (2020). Architecture and Self-Assembly of *Clostridium sporogenes* and *Clostridium botulinum* Spore Surfaces Illustrate a General Protective Strategy across Spore Formers. *mSphere*, 5 (4). [Online]. Available at: doi:10.1128/MSPHERE.00424-20/SUPPL_FILE/MSPHERE.00424-20-SD001.XLSX [Accessed 23 March 2024].

Jarman, O. D. et al. (2021). *Paracoccus denitrificans*: a genetically tractable model system for studying respiratory complex I. *Scientific Reports 2021 11:1*, 11 (1), pp.1–14. [Online]. Available at: doi:10.1038/s41598-021-89575-9 [Accessed 19 March 2024].

Jones-Carson, J. et al. (2016). Cytochrome *bd*-dependent bioenergetics and antinitrosative defenses in *Salmonella* pathogenesis. *mBio*, 7 (6). [Online]. Available at: doi:10.1128/MBIO.02052-16/SUPPL_FILE/MBO006163115ST2.DOCX [Accessed 6 March 2024].

Juhnke, H. D. et al. (2009). Production, characterization and determination of the real catalytic properties of the putative ‘succinate dehydrogenase’ from *Wolinella succinogenes*. *Molecular Microbiology*, 71 (5), p.1088. [Online]. Available at: doi:10.1111/J.1365-2958.2008.06581.X [Accessed 19 March 2024].

Jumper, J. et al. (2021). Highly accurate protein structure prediction with AlphaFold. *Nature 2021 596:7873*, 596 (7873), pp.583–589. [Online]. Available at: doi:10.1038/s41586-021-03819-2 [Accessed 19 March 2024].

Kaieda, S. et al. (2013). Mobility of core water in *Bacillus subtilis* Spores by 2H NMR. *Biophysical Journal*, 105 (9), pp.2016–2023. [Online]. Available at: doi:10.1016/j.bpj.2013.09.022 [Accessed 24 March 2024].

Kaila, V. R. I. and Wikström, M. (2021). Architecture of bacterial respiratory chains. *Nature Reviews Microbiology 2021 19:5*, 19 (5), pp.319–330. [Online]. Available at: doi:10.1038/s41579-020-00486-4 [Accessed 2 November 2023].

Kailas, L. et al. (2011). Surface architecture of endospores of the *Bacillus cereus*/*anthracis*/*thuringiensis* family at the subnanometer scale. *Proceedings of the National Academy of Sciences of the United States of America*, 108 (38), pp.16014–16019. [Online]. Available at: doi:10.1073/PNAS.1109419108/SUPPL_FILE/PNAS.201109419SI.PDF [Accessed 26 March 2024].

Kanehisa, M. et al. (2023). KEGG for taxonomy-based analysis of pathways and genomes. *Nucleic Acids Research*, 51 (D1), pp.D587–D592. [Online]. Available at: doi:10.1093/NAR/GKAC963 [Accessed 22 March 2024].

Kanehisa, M. and Goto, S. (2000). KEGG: Kyoto Encyclopedia of Genes and Genomes. *Nucleic Acids Research*, 28 (1), pp.27–30. [Online]. Available at: doi:10.1093/NAR/28.1.27 [Accessed 22 March 2024].

Keilin, D. (1959). The Leeuwenhoek Lecture - The problem of anabiosis or latent life: history and current concept. *Proceedings of the Royal Society of London. Series B - Biological Sciences*, 150 (939), pp.149–191. [Online]. Available at: doi:10.1098/RSPB.1959.0013 [Accessed 21 March 2024].

Keilin, D. and Hartree, E. F. (1949). Effect of Low Temperature on the Absorption Spectra of Haemoproteins; with Observations on the Absorption Spectrum of Oxygen. *Nature*, 164 (4163), pp.254–259. [Online]. Available at: doi:10.1038/164254a0.

Kennedy, M. J., Reader, S. L. and Swierczynski, L. M. (1994). Preservation records of micro-organisms: Evidence of the tenacity of life. *Microbiology*, 140 (10), pp.2513–2529. [Online]. Available at: doi:10.1099/00221287-140-10-2513/CITE/REFWORKS [Accessed 27 March 2024].

Khanna, K. et al. (2019). The molecular architecture of engulfment during *Bacillus subtilis* sporulation. *eLife*, 8. [Online]. Available at: doi:10.7554/ELIFE.45257 [Accessed 26 March 2024].

Khanna, K., Lopez-Garrido, J. and Pogliano, K. (2020). Shaping an Endospore: Architectural Transformations during *Bacillus subtilis* Sporulation. *Annual Review of Microbiology*, 74

(Volume 74, 2020), pp.361–386. [Online]. Available at: doi:10.1146/ANNUREV-MICRO-022520-074650/CITE/REFWORKS [Accessed 22 March 2024].

Kikuchi, K. et al. (2022). Electrochemical potential enables dormant spores to integrate environmental signals. *Science*, 378 (6615), pp.43–49. [Online]. Available at: doi:10.1126/SCIENCE.ABL7484/SUPPL_FILE/SCIENCE.ABL7484_MOVIES_S1_TO_S4.ZIP [Accessed 25 March 2024].

Kilian, M. and Bischofs, I. B. (2023). Co-evolution at protein–protein interfaces guides inference of stoichiometry of oligomeric protein complexes by de novo structure prediction. *Molecular Microbiology*, 120 (5), pp.763–782. [Online]. Available at: doi:10.1111/MMI.15169 [Accessed 25 March 2024].

Kim, N., Ripple, M. O. and Springett, R. (2011). Spectral components of the α-band of cytochrome oxidase. *Biochimica et Biophysica Acta (BBA) - Bioenergetics*, 1807 (7), pp.779–787. [Online]. Available at: doi:10.1016/J.BBABIO.2011.03.008 [Accessed 8 March 2024].

Klobutcher, L. A., Ragkousi, K. and Setlow, P. (2006). The *Bacillus subtilis* spore coat provides ‘eat resistance’ during phagocytic predation by the protozoan *Tetrahymena thermophila*. *Proceedings of the National Academy of Sciences of the United States of America*, 103 (1), pp.165–170. [Online]. Available at: doi:10.1073/PNAS.0507121102/SUPPL_FILE/INDEX.HTML [Accessed 23 March 2024].

Kong, L., Setlow, P. and Li, Y. Q. (2012). Analysis of the Raman spectra of Ca^{2+}-dipicolinic acid alone and in the bacterial spore core in both aqueous and dehydrated environments. *Analyst*, 137 (16), pp.3683–3689. [Online]. Available at: doi:10.1039/C2AN35468C [Accessed 2 November 2023].

Koo, B. M. et al. (2017). Construction and Analysis of Two Genome-Scale Deletion Libraries for *Bacillus subtilis*. *Cell Systems*, 4 (3), pp.291-305.e7. [Online]. Available at: doi:10.1016/J.CELS.2016.12.013 [Accessed 8 March 2024].

Korza, G. et al. (2023a). Expression of the 2Duf protein in wild-type *Bacillus subtilis* spores stabilizes inner membrane proteins and increases spore resistance to wet heat and hydrogen peroxide. *Journal of applied microbiology*, 134 (3). [Online]. Available at: doi:10.1093/JAMBIO/LXAD040 [Accessed 15 February 2024].

Korza, G. et al. (2023b). Role of *Bacillus subtilis* Spore Core Water Content and pH in the Accumulation and Utilization of Spores’ Large 3-Phosphoglyceric Acid Depot, and the Crucial Role of This Depot in Generating ATP Early during Spore Germination.

Microorganisms, 11 (1). [Online]. Available at: doi:10.3390/MICROORGANISMS11010195 [Accessed 8 March 2024].

Kristiansen, J. and Škaloud, P. (2016). Chrysophyta. *Handbook of the Protists*, pp.1–38. [Online]. Available at: doi:10.1007/978-3-319-32669-6_43-1 [Accessed 22 March 2024].

Kühlbrandt, W. (2019). Structure and Mechanisms of F-Type ATP Synthases. *Annual Review of Biochemistry*, 88 (Volume 88, 2019), pp.515–549. [Online]. Available at: doi:10.1146/ANNUREV-BIOCHEM-013118-110903/CITE/REFWORKS [Accessed 26 March 2024].

Kuliešienė, N. et al. (2021). Changes in Energy Status of *Saccharomyces cerevisiae* Cells during Dehydration and Rehydration. *Microorganisms 2021, Vol. 9, Page 444*, 9 (2), p.444. [Online]. Available at: doi:10.3390/MICROORGANISMS9020444 [Accessed 24 March 2024].

Laaberki, M. H. and Dworkin, J. (2008). Role of spore coat proteins in the resistance of *Bacillus subtilis* spores to *Caenorhabditis elegans* predation. *Journal of Bacteriology*, 190 (18), pp.6197–6203. [Online]. Available at: doi:10.1128/JB.00623-08/ASSET/8C5144EA-728B-4322-9D4F-BAEC0840E8E4/ASSETS/GRAPHIC/ZJB0170880640003.JPEG [Accessed 23 March 2024].

Lancaster, C. R. D. et al. (1999). Structure of fumarate reductase from *Wolinella succinogenes* at 2.2 Å resolution. *Nature 1999 402:6760*, 402 (6760), pp.377–385. [Online]. Available at: doi:10.1038/46483 [Accessed 19 March 2024].

Lancaster, C. R. D. (2011). The Superfamily of Succinate:Quinone Oxidoreductases and its Implications for the Cyanobacterial Enzymes. *Bioenergetic Processes of Cyanobacteria*, pp.469–511. [Online]. Available at: doi:10.1007/978-94-007-0388-9_17 [Accessed 19 March 2024].

Lancaster, C. R. D., Groß, R. and Simon, J. (2001). A third crystal form of *Wolinella succinogenes* quinol:fumarate reductase reveals domain closure at the site of fumarate reduction. *European Journal of Biochemistry*, 268 (6), pp.1820–1827. [Online]. Available at: doi:10.1046/J.1432-1327.2001.02053.X [Accessed 19 March 2024].

Laue, M. et al. (2018). Intracellular membranes of bacterial endospores are reservoirs for spore core membrane expansion during spore germination. *Scientific Reports 2018 8:1*, 8 (1), pp.1–12. [Online]. Available at: doi:10.1038/s41598-018-29879-5 [Accessed 10 August 2022].

Lauraeus, M., Morgan, J. E. and Wikström, M. (1993). Peroxy and Ferryl Intermediates of the Quinol-Oxidizing Cytochrome aa_3 from *Bacillus subtilis*. *Biochemistry*, 32 (10), pp.2664–

2670. [Online]. Available at: doi:10.1021/BI00061A026/ASSET/BI00061A026.FP.PNG_V03 [Accessed 29 March 2024].

Lawer, A. et al. (2022). Synthesis and Biological Evaluation of Aurachin D Analogues as Inhibitors of *Mycobacterium tuberculosis* Cytochrome *bd* Oxidase. *ACS Medicinal Chemistry Letters*, 13 (10), pp.1663–1669. [Online]. Available at: doi:10.1021/ACSMEDCHEMLETT.2C00401/ASSET/IMAGES/LARGE/ML2C00401_0003.JPEG [Accessed 31 March 2024].

Lee, H. J. et al. (2022). Impact of novel detergents on membrane protein studies. *Chem*, 8 (4), pp.980–1013. [Online]. Available at: doi:10.1016/J.CHEMPR.2022.02.007 [Accessed 28 March 2024].

Lee, K. S. et al. (2008). Structure of a protein–DNA complex essential for DNA protection in spores of *Bacillus* species. *Proceedings of the National Academy of Sciences*, 105 (8), pp.2806–2811. [Online]. Available at: doi:10.1073/pnas.0708244105.

Lee, S. K. and Okura, I. (1997). Photostable Optical Oxygen Sensing Material: PlatinumTetrakis(pentafluorophenyl)porphyrin Immobilized in Polystyrene. *Analytical Communications*, 34 (6), pp.185–188. [Online]. Available at: doi:10.1039/A701130J [Accessed 8 March 2024].

Leighton, T. J. and Doi, R. H. (1971). The stability of messenger ribonucleic acid during sporulation in *Bacillus subtilis*. *Journal of Biological Chemistry*, 246 (10), pp.3189–3195.

Lemma, E., Unden, G. and Kröger, A. (1990). Menaquinone is an obligatory component of the chain catalyzing succinate respiration in *Bacillus subtilis*. *Archives of Microbiology*, 155 (1), pp.62–67. [Online]. Available at: doi:10.1007/BF00291276/METRICS [Accessed 20 March 2024].

Li, L. et al. (2022). Optimization of sporulation and purification methods for sporicidal efficacy assessment on *Bacillus* spores. *Journal of Industrial Microbiology and Biotechnology*, 49 (4), p.14. [Online]. Available at: doi:10.1093/JIMB/KUAC014 [Accessed 29 March 2024].

Li, Y. et al. (2010). Crystal Structure of the GerBC Component of a *Bacillus subtilis* Spore Germinant Receptor. *Journal of Molecular Biology*, 402 (1), pp.8–16. [Online]. Available at: doi:10.1016/J.JMB.2010.07.018 [Accessed 25 March 2024].

Li, Y. et al. (2014). Structural and Functional Analysis of the GerD Spore Germination Protein of *Bacillus* Species. *Journal of Molecular Biology*, 426 (9), pp.1995–2008. [Online]. Available at: doi:10.1016/J.JMB.2014.02.004 [Accessed 25 March 2024].

Li, Y. et al. (2019). Structural and functional analyses of the N-terminal domain of the A subunit of a *Bacillus megaterium* spore germinant receptor. *Proceedings of the National Academy of Sciences of the United States of America*, 166 (23), pp.11470–11479. [Online]. Available at: doi:10.1073/PNAS.1903675116/SUPPL_FILE/PNAS.1903675116.SAPP.PDF [Accessed 25 March 2024].

Li, Y. Q. et al. (2023). Thioflavin-T does not report on electrochemical potential and memory of dormant or germinating bacterial spores. *mBio*, 14 (5). [Online]. Available at: doi:10.1128/MBIO.02220-23/SUPPL_FILE/MBIO.02220-23-S0003.AVI [Accessed 25 March 2024].

Liao, G. L. and Palmer, G. (1996). The reduced minus oxidized difference spectra of cytochromes *a* and a_3. *Biochimica et Biophysica Acta (BBA) - Bioenergetics*, 1274 (3), pp.109–111. [Online]. Available at: doi:10.1016/0005-2728(96)00014-X [Accessed 31 March 2024].

Lohmeier-Vogel, E. M., Ung, S. and Turner, R. J. (2004). In vivo ^{31}P nuclear magnetic resonance investigation of tellurite toxicity in *Escherichia coli*. *Applied and Environmental Microbiology*, 70 (12), pp.7342–7347. [Online]. Available at: doi:10.1128/AEM.70.12.7342-7347.2004/ASSET/276D5910-54D1-45CC-8D76-6D69215E2695/ASSETS/GRAPHIC/ZAM0120450530007.JPEG [Accessed 29 March 2024].

Madeira, F. et al. (2022). Search and sequence analysis tools services from EMBL-EBI in 2022. *Nucleic Acids Research*, 50 (W1), pp.W276–W279. [Online]. Available at: doi:10.1093/NAR/GKAC240 [Accessed 28 March 2024].

Madej, M. G. et al. (2006). Evidence for transmembrane proton transfer in a dihaem-containing membrane protein complex. *EMBO Journal*, 25 (20), pp.4963–4970. [Online]. Available at: doi:10.1038/SJ.EMBOJ.7601361/SUPPL_FILE/EMBJ7601361-SUP-0001.PDF [Accessed 19 March 2024].

Magge, A. et al. (2009). Analysis of dye binding by and membrane potential in spores of *Bacillus* species. *Journal of Applied Microbiology*, 106 (3), pp.814–824. [Online]. Available at: doi:10.1111/J.1365-2672.2008.04048.X [Accessed 25 March 2024].

Maher, M. J. et al. (2018). Crystal structure of bacterial succinate:quinone oxidoreductase flavoprotein SdhA in complex with its assembly factor SdhE. *Proceedings of the National Academy of Sciences of the United States of America*, 115 (12), pp.2982–2987. [Online]. Available at: doi:10.1073/PNAS.1800195115/SUPPL_FILE/PNAS.201800195SI.PDF [Accessed 19 March 2024].

Maklashina, E. (2022). Structural Insight into Evolution of the Quinone Binding Site in Complex II. *Biochemistry (Moscow)*, 87 (8), pp.752–761. [Online]. Available at: doi:10.1134/S0006297922080077/FIGURES/5 [Accessed 20 March 2024].

Maklashina, E., Berthold, D. A. and Cecchini, G. (1998). Anaerobic expression of *Escherichia coli* succinate dehydrogenase: Functional replacement of fumarate reductase in the respiratory chain during anaerobic growth. *Journal of Bacteriology*, 180 (22), pp.5989–5996. [Online]. Available at: doi:10.1128/JB.180.22.5989-5996.1998/ASSET/578C0D0C-7936-4DA6-B8FE-086241BC3C1C/ASSETS/GRAPHIC/JB2280634003.JPEG [Accessed 20 March 2024].

Maklashina, E., Cecchini, G. and Dikanov, S. A. (2013). Defining a direction: Electron transfer and catalysis in *Escherichia coli* complex II enzymes. *Biochimica et Biophysica Acta (BBA) - Bioenergetics*, 1827 (5), pp.668–678. [Online]. Available at: doi:10.1016/J.BBABIO.2013.01.010 [Accessed 20 March 2024].

Malone, L. A. et al. (2021). Cytochrome b_6f – Orchestrator of photosynthetic electron transfer. *Biochimica et Biophysica Acta (BBA) - Bioenergetics*, 1862 (5), p.148380. [Online]. Available at: doi:10.1016/J.BBABIO.2021.148380 [Accessed 20 March 2024].

Martin, N. H., Quintana-Pérez, F. M. and Evanowski, R. L. (2023). SYMPOSIUM REVIEW: Sources, transmission, and tracking of sporeforming bacterial contaminants in dairy systems. *JDS Communications*, 5 (2), pp.172–177. [Online]. Available at: doi:10.3168/jdsc.2023-0428 [Accessed 22 March 2024].

Maruyama, T. et al. (1980). Glucose catabolism during germination of *Bacillus megaterium* spores. *Journal of Bacteriology*, 141 (3), p.1443. [Online]. Available at: /pmc/articles/PMC293847/?report=abstract [Accessed 27 July 2021].

Mascolo, L. and Bald, D. (2020). Cytochrome *bd* in *Mycobacterium tuberculosis*: A respiratory chain protein involved in the defense against antibacterials. *Progress in Biophysics and Molecular Biology*, 152, pp.55–63. [Online]. Available at: doi:10.1016/J.PBIOMOLBIO.2019.11.002 [Accessed 6 March 2024].

Mason, M. G., Nicholls, P. and Cooper, C. E. (2009). The steady-state mechanism of cytochrome *c* oxidase: redox interactions between metal centres. *Biochemical Journal*, 422 (2), pp.237–246. [Online]. Available at: doi:10.1042/BJ20082220 [Accessed 31 March 2024].

Mason, M. G., Nicholls, P. and Cooper, C. E. (2014). Re-evaluation of the near infrared spectra of mitochondrial cytochrome *c* oxidase: Implications for non-invasive in vivo monitoring of tissues. *Biochimica et Biophysica Acta (BBA) - Bioenergetics*, 1837 (11),

pp.1882–1891. [Online]. Available at: doi:10.1016/J.BBABIO.2014.08.005 [Accessed 31 March 2024].

Matsson, M. et al. (2000). The Distal Heme Center in *Bacillus subtilis* Succinate:Quinone Reductase Is Crucial for Electron Transfer to Menaquinone. *Biochemistry*, 39 (29), pp.8617–8624. [Online]. Available at: doi:10.1021/BI000271M [Accessed 20 March 2024].

Mckenney, P. T., Driks, A. and Eichenberger, P. (2012). The *Bacillus subtilis* endospore: assembly and functions of the multilayered coat. *Nature Reviews Microbiology 2012 11:1*, 11 (1), pp.33–44. [Online]. Available at: doi:10.1038/nrmicro2921 [Accessed 23 March 2024].

McPherson, A. (1999). *Crystallization of biological macromolecules*.

Meng, E. C. et al. (2006). Tools for integrated sequence-structure analysis with UCSF Chimera. *BMC Bioinformatics*, 7 (1), pp.1–10. [Online]. Available at: doi:10.1186/1471-2105-7-339/TABLES/2 [Accessed 19 March 2024].

Meng, E. C. et al. (2023). UCSF ChimeraX: Tools for structure building and analysis. *Protein Science*, 32 (11), p.e4792. [Online]. Available at: doi:10.1002/PRO.4792 [Accessed 19 March 2024].

Meunier, B. et al. (1995). New Inhibitors of the Quinol Oxidation Sites of Bacterial Cytochromes *bo* and *bd*. *Biochemistry*, 34 (3), pp.1076–1083. [Online]. Available at: doi:10.1021/BI00003A044/ASSET/BI00003A044.FP.PNG_V03 [Accessed 31 March 2024].

Meyrat, A. and von Ballmoos, C. (2019). ATP synthesis at physiological nucleotide concentrations. *Scientific Reports 2019 9:1*, 9 (1), pp.1–10. [Online]. Available at: doi:10.1038/s41598-019-38564-0 [Accessed 26 March 2024].

MITCHELL, P. (1961). Coupling of Phosphorylation to Electron and Hydrogen Transfer by a Chemi-Osmotic type of Mechanism. *Nature*, 191 (4784), pp.144–148. [Online]. Available at: doi:10.1038/191144a0.

Moir, A. (2023). Spore germination receptors – a new paradigm. *Trends in Microbiology*, 31 (8), pp.767–768. [Online]. Available at: doi:10.1016/j.tim.2023.05.012 [Accessed 26 March 2024].

Molle, V. et al. (2003). The *Spo0A* regulon of *Bacillus subtilis*. *Molecular Microbiology*, 50 (5), pp.1683–1701. [Online]. Available at: doi:10.1046/J.1365-2958.2003.03818.X [Accessed 22 March 2024].

Mongkolthanaruk, W., Robinson, C. and Moir, A. (2009). Localization of the GerD spore germination protein in the *Bacillus subtilis* spore. *Microbiology*, 155 (4), pp.1146–1151.

[Online]. Available at: doi:10.1099/MIC.0.023853-0/CITE/REFWORKS [Accessed 31 March 2024].

Mustafa, A. (2021). *Molecular analyses of YhcN/YlaJ and spore-associated proteins involved in germination of Bacillus cereus spores*. [Online]. [Apollo - University of Cambridge Repository]. Available at: https://www.repository.cam.ac.uk/items/ed4edb9f-03a9-47e0-9df8-3addc5333992 [Accessed 29 March 2024].

Naranjo-Ortiz, M. A. and Gabaldón, T. (2019). Fungal evolution: diversity, taxonomy and phylogeny of the Fungi. *Biological Reviews*, 94 (6), pp.2101–2137. [Online]. Available at: doi:10.1111/BRV.12550 [Accessed 22 March 2024].

Nicolas, P. et al. (2012). Condition-dependent transcriptome reveals high-level regulatory architecture in *Bacillus subtilis*. *Science*, 335 (6072), pp.1103–1106. [Online]. Available at: doi:10.1126/SCIENCE.1206848/SUPPL_FILE/1206848.NICOLAS.SOM.PDF [Accessed 22 March 2024].

Otani, M. et al. (1986). Predominance of gluconate formation from glucose during germination of *Bacillus megaterium* QM B1551 spores. *Journal of Bacteriology*, 167 (1), p.148. [Online]. Available at: doi:10.1128/JB.167.1.148-152.1986 [Accessed 27 July 2021].

Otani, M., Umezawa, C. and Sano, K. (1987). A Highly Sensitive Method for Detection of ^{32}P Incorporation into Acid-Soluble Compounds and Its Application to Evaluate ATP-Forming Ability of *Bacillus megaterium* QM B1551 Spores at the Very Early Stage of Germination. *Microbiology and Immunology*, 31 (10), pp.967–974. [Online]. Available at: doi:10.1111/J.1348-0421.1987.TB01329.X [Accessed 6 September 2021].

Paidhungat, M. and Setlow, P. (2001). Localization of a germinant receptor protein (GerBA) to the inner membrane of *Bacillus subtilis* spores. *Journal of Bacteriology*, 183 (13), pp.3982–3990. [Online]. Available at: doi:10.1128/JB.183.13.3982-3990.2001/ASSET/03E226FB-4B3D-41B1-B5AA-A0B1A18683BF/ASSETS/GRAPHIC/JB1311696007.JPEG [Accessed 24 March 2024].

Perez-Valdespino, A. et al. (2014). Function of the SpoVAEa and SpoVAF proteins of *Bacillus subtilis* spores. *Journal of Bacteriology*, 196 (11), pp.2077–2088. [Online]. Available at: doi:10.1128/JB.01546-14 [Accessed 15 December 2020].

Pershad, H. R. et al. (1999). Voltammetric studies of bidirectional catalytic electron transport in *Escherichia coli* succinate dehydrogenase: comparison with the enzyme from beef heart mitochondria. *Biochimica et Biophysica Acta (BBA) - Bioenergetics*, 1412 (3), pp.262–272. [Online]. Available at: doi:10.1016/S0005-2728(99)00066-3 [Accessed 20 March 2024].

Phillips, R. (2021). Schrödinger's What Is Life? at 75. *Cell Systems*, 12 (6), pp.465–476. [Online]. Available at: doi:10.1016/J.CELS.2021.05.013 [Accessed 24 March 2024].

Pintilie, G. D. et al. (2010). Quantitative analysis of cryo-EM density map segmentation by watershed and scale-space filtering, and fitting of structures by alignment to regions. *Journal of Structural Biology*, 170 (3), pp.427–438. [Online]. Available at: doi:10.1016/J.JSB.2010.03.007 [Accessed 20 March 2024].

Poole, R. K. et al. (1983). The 650 and chromophore in *Escherichia coli* is an 'oxy-' or oxygenated compound, not the oxidized form of cytochrome oxidase *d*: a hypothesis. *Journal of general microbiology*, 129 (5), pp.1335–1344. [Online]. Available at: doi:10.1099/00221287-129-5-1335 [Accessed 6 March 2024].

Powell, J. F. (1951). The sporulation and germination of a strain of *Bacillus megatherium*. *Journal of general microbiology*, 5 (5 Suppl.), pp.993–1000. [Online]. Available at: doi:10.1099/00221287-5-5-993/CITE/REFWORKS [Accessed 22 August 2022].

Powell, J. F. and Hunter, J. R. (1955). Spore germination in the genus *Bacillus*: the modification of germination requirements as a result of preheating. *Journal of general microbiology*, 13 (1), pp.59–67. [Online]. Available at: doi:10.1099/00221287-13-1-59/CITE/REFWORKS [Accessed 22 August 2022].

Pradhan, B. et al. (2021). Endospore Appendages: a novel pilus superfamily from the endospores of pathogenic Bacilli. *The EMBO Journal*, 40 (17). [Online]. Available at: doi:10.15252/EMBJ.2020106887/SUPPL_FILE/EMBJ2020106887-SUP-0003-TABLEEV1.XLSX [Accessed 26 March 2024].

Prasad, C., Diesterhaft, M. and Freese, E. (1972). Initiation of Spore Germination in Glycolytic Mutants of *Bacillus subtilis*. *Journal of Bacteriology*, 110 (1), p.321. [Online]. Available at: doi:10.1128/JB.110.1.321-328.1972 [Accessed 27 November 2022].

Punjani, A. et al. (2017). cryoSPARC: algorithms for rapid unsupervised cryo-EM structure determination. *Nature Methods 2017 14:3*, 14 (3), pp.290–296. [Online]. Available at: doi:10.1038/nmeth.4169 [Accessed 19 March 2024].

Punjani, A., Zhang, H. and Fleet, D. J. (2020). Non-uniform refinement: adaptive regularization improves single-particle cryo-EM reconstruction. *Nature Methods 2020 17:12*, 17 (12), pp.1214–1221. [Online]. Available at: doi:10.1038/s41592-020-00990-8 [Accessed 19 March 2024].

Racine, F. M., Dills, S. S. and Vary, J. C. (1979). Glucose-triggered germination of *Bacillus megaterium* spores. *Journal of Bacteriology*, 138 (2), p.442. [Online]. Available at: /pmc/articles/PMC218196/?report=abstract [Accessed 27 July 2021].

Racine, F. M. and Vary, J. C. (1980). Isolation and properties of membranes from *Bacillus megaterium* spores. *Journal of Bacteriology*, 143 (3), pp.1208–1214. [Online]. Available at: doi:10.1128/JB.143.3.1208-1214.1980 [Accessed 23 August 2022].

Raibekas, A. A., Fukui, K. and Massey, V. (2000). Design and properties of human D-amino acid oxidase with covalently attached flavin. *Proceedings of the National Academy of Sciences of the United States of America*, 97 (7), pp.3089–3093. [Online]. Available at: doi:10.1073/PNAS.97.7.3089/ASSET/F54A7721-D0E7-4534-AEC1-6AB41523C101/ASSETS/GRAPHIC/PQ0405595006.JPEG [Accessed 8 March 2024].

Rather, P. N. and Moran, C. P. (1988). Compartment-specific transcription in *Bacillus subtilis*: identification of the promoter for gdh. *Journal of Bacteriology*, 170 (11), pp.5086–5092. [Online]. Available at: doi:10.1128/JB.170.11.5086-5092.1988 [Accessed 31 March 2024].

Ripple, M. O., Kim, N. and Springett, R. (2013). Mammalian Complex I Pumps 4 Protons per 2 Electrons at High and Physiological Proton Motive Force in Living Cells*. *Journal of Biological Chemistry*, 288 (8), pp.5374–5380. [Online]. Available at: doi:10.1074/JBC.M112.438945 [Accessed 8 March 2024].

Rocha, M. and Springett, R. (2019). Measuring the functionality of the mitochondrial pumping complexes with multi-wavelength spectroscopy. *Biochimica et Biophysica Acta (BBA) - Bioenergetics*, 1860 (1), pp.89–101. [Online]. Available at: doi:10.1016/J.BBABIO.2018.11.013 [Accessed 8 March 2024].

Rode, L. J. (1968). Correlation Between Spore Structure and Spore Properties in *Bacillus megaterium*. *Journal of Bacteriology*, 95 (6), pp.1979–1986. [Online]. Available at: doi:10.1128/JB.95.6.1979-1986.1968 [Accessed 26 April 2023].

Rode, L. J. and Foster, J. W. (1962). Ionic germination of spores of *Bacillus megaterium* QM B1551. *Archiv für Mikrobiologie*, 43 (2), pp.183–200. [Online]. Available at: doi:10.1007/BF00406435/METRICS [Accessed 26 April 2023].

Rode, L. J., Lewis, C. W. And Foster, J. W. (1962). Electron Microscopy of Spores of *Bacillus Megaterium* with Special Reference to the Effects of Fixation and Thin Sectioning. *Journal of Cell Biology*, 13 (3), pp.423–435. [Online]. Available at: doi:10.1083/JCB.13.3.423 [Accessed 26 March 2024].

Rodenburg, C. M. et al. (2014). Cryo-EM analysis of the organization of BclA and BxpB in the *Bacillus anthracis* exosporium. *Journal of Structural Biology*, 186 (1), pp.181–187. [Online]. Available at: doi:10.1016/J.JSB.2014.02.018 [Accessed 26 March 2024].

Rosental, L., Nonogaki, H. and Fait, A. (2014). Activation and regulation of primary metabolism during seed germination. *Seed Science Research*, 24 (1), pp.1–15. [Online]. Available at: doi:10.1017/S0960258513000391 [Accessed 24 March 2024].

Ross, C. and Abel-Santos, E. (2009). The Ger Receptor Family from Sporulating Bacteria. *Current Issues in Molecular Biology 2010, Vol. 12, Pages 147-158*, 12 (3), pp.147–158. [Online]. Available at: doi:10.21775/CIMB.012.147 [Accessed 26 March 2024].

Sagné, C. et al. (1996). SDS-resistant aggregation of membrane proteins: application to the purification of the vesicular monoamine transporter. *Biochemical Journal*, 316 (3), pp.825–831. [Online]. Available at: doi:10.1042/BJ3160825 [Accessed 27 March 2024].

Sano, K. et al. (1988). Primary Role of NADH Formed by Glucose Dehydrogenase in ATP Provision at the Early Stage of Spore Germination in *Bacillus megaterium* QM B1551. *Microbiology and Immunology*, 32 (9), pp.877–885. [Online]. Available at: doi:10.1111/J.1348-0421.1988.TB01449.X [Accessed 28 July 2021].

Santo, L. Y. and Doi, R. H. (1974). Ultrastructural Analysis During Germination and Outgrowth of *Bacillus subtilis* Spores. *Journal of Bacteriology*, 120 (1), pp.475–481. [Online]. Available at: doi:10.1128/JB.120.1.475-481.1974 [Accessed 26 March 2024].

Sarewicz, M. et al. (2021). Catalytic reactions and energy conservation in the cytochrome bc_1 and b_6f complexes of energy-transducing membranes. *Chemical Reviews*, 121 (4), pp.2020–2108. [Online]. Available at: doi:10.1021/ACS.CHEMREV.0C00712/ASSET/IMAGES/MEDIUM/CR0C00712_0029.GIF [Accessed 20 March 2024].

Savitzky, A. and Golay, M. J. E. (1964). Smoothing and Differentiation of Data by Simplified Least Squares Procedures. *Analytical Chemistry*, 36 (8), pp.1627–1639. [Online]. Available at: doi:10.1021/AC60214A047/ASSET/AC60214A047.FP.PNG_V03 [Accessed 31 March 2024].

Schaeffer, P., Millet, J. and Aubert, J. P. (1965). Catabolic repression of bacterial sporulation. *Proceedings of the National Academy of Sciences of the United States of America*, 54 (3), pp.704–711. [Online]. Available at: doi:10.1073/PNAS.54.3.704/ASSET/1CB18960-D6C1-4E86-94E2-B118E795ACAD/ASSETS/PNAS.54.3.704.FP.PNG [Accessed 8 March 2024].

Schäfer, G. (2004). *Chapter 1: Respiratory Chains in Archaea: From Minimal Systems to Supercomplexes*. pp.1–33. [Online]. Available at: doi:10.1007/978-1-4020-3163-2_1 [Accessed 25 March 2024].

Schnorpfeil, M. et al. (2001). Generation of a proton potential by succinate dehydrogenase of *Bacillus subtilis* functioning as a fumarate reductase. *European Journal of Biochemistry*, 268 (10), pp.3069–3074. [Online]. Available at: doi:10.1046/J.1432-1327.2001.02202.X [Accessed 20 March 2024].

Schrödinger, E. (1944). *What is Life?: The Physical Aspect of the Living Cell*. Cambridge U.P. [Online]. Available at: https://books.google.co.uk/books?id=OuiBzwEACAAJ.

Schurig-Briccio, L. A. et al. (2014). Characterization of the type 2 NADH:menaquinone oxidoreductases from *Staphylococcus aureus* and the bactericidal action of phenothiazines. *Biochimica et Biophysica Acta (BBA) - Bioenergetics*, 1837 (7), pp.954–963. [Online]. Available at: doi:10.1016/J.BBABIO.2014.03.017 [Accessed 29 March 2024].

Scott, I. R. and Ellar, D. J. (1978a). Metabolism and the triggering of germination of *Bacillus megaterium*. Concentrations of amino acids, organic acids, adenine nucleotides and nicotinamide nucleotides during germination. *Biochemical Journal*, 174 (2), pp.627–634. [Online]. Available at: doi:10.1042/bj1740627 [Accessed 15 December 2020].

Scott, I. R. and Ellar, D. J. (1978b). Study of calcium dipicolinate release during bacterial spore germination by using a new, sensitive assay for dipicolinate. *Journal of Bacteriology*, 135 (1), pp.133–137. [Online]. Available at: doi:10.1128/JB.135.1.133-137.1978 [Accessed 7 April 2023].

Setlow, P. (2019). Observations on research with spores of Bacillales and Clostridiales species. *Journal of Applied Microbiology*, 126 (2), pp.348–358. [Online]. Available at: doi:10.1111/JAM.14067 [Accessed 10 August 2022].

Setlow, P. and Christie, G. (2021). What's new and notable in bacterial spore killing! *World Journal of Microbiology and Biotechnology 2021 37:8*, 37 (8), pp.1–13. [Online]. Available at: doi:10.1007/S11274-021-03108-0 [Accessed 23 March 2024].

Setlow, P. and Christie, G. (2023). New Thoughts on an Old Topic: Secrets of Bacterial Spore Resistance Slowly Being Revealed. *Microbiology and Molecular Biology Reviews*, 87 (2). [Online]. Available at: doi:10.1128/MMBR.00080-22 [Accessed 23 March 2024].

Setlow, P. and Kornberg, A. (1970). Biochemical studies of bacterial sporulation and germination. XXII. Energy metabolism in early stages of germination of *Bacillus megaterium* spores. *The Journal of biological chemistry*, 245 (14), pp.3637–3644.

Setlow, R. and Setlow, P. (1977). Levels of oxidized and reduced pyridine nucleotides in dormant spores and during growth, sporulation, and spore germination of *Bacillus megaterium*. *Journal of Bacteriology*, 129 (2), pp.857–865. [Online]. Available at: doi:10.1128/JB.129.2.857-865.1977 [Accessed 16 June 2022].

Sexton, D. L. and Tocheva, E. I. (2020). Ultrastructure of Exospore Formation in *Streptomyces* Revealed by Cryo-Electron Tomography. *Frontiers in Microbiology*, 11, p.581135. [Online]. Available at: doi:10.3389/FMICB.2020.581135/BIBTEX [Accessed 22 March 2024].

Shay, L. K. and Vary, J. C. (1978). Biochemical studies on glucose-initiated germination in *Bacillus megaterium*. *Biochimica et Biophysica Acta (BBA) - General Subjects*, 538 (2), pp.284–292. [Online]. Available at: doi:10.1016/0304-4165(78)90356-2 [Accessed 27 July 2021].

Shepherd, M. et al. (2016). The cytochrome *bd*-I respiratory oxidase augments survival of multidrug-resistant *Escherichia coli* during infection. *Scientific Reports 2016 6:1*, 6 (1), pp.1–10. [Online]. Available at: doi:10.1038/srep35285 [Accessed 6 March 2024].

Shimada, A., Tsukihara, T. and Yoshikawa, S. (2023). Recent progress in experimental studies on the catalytic mechanism of cytochrome *c* oxidase. *Frontiers in Chemistry*, 11, p.1108190. [Online]. Available at: doi:10.3389/FCHEM.2023.1108190/BIBTEX [Accessed 31 March 2024].

Shinkarev, V. P., Crofts, A. R. and Wraight, C. A. (2006). Spectral and kinetic resolution of the bc_1 complex components in situ: A simple and robust alternative to the traditional difference wavelength approach. *Biochimica et Biophysica Acta (BBA) - Bioenergetics*, 1757 (4), pp.273–283. [Online]. Available at: doi:10.1016/J.BBABIO.2006.04.003 [Accessed 31 March 2024].

Shuster, B. et al. (2019). Contributions of crust proteins to spore surface properties in *Bacillus subtilis*. *Molecular Microbiology*, 111 (3), pp.825–843. [Online]. Available at: doi:10.1111/MMI.14194 [Accessed 23 March 2024].

Slater, E. C. (2003). Keilin, cytochrome, and the respiratory chain. *Journal of Biological Chemistry*, 278 (19), pp.16455–16461. [Online]. Available at: doi:10.1074/jbc.X200011200 [Accessed 23 March 2024].

Slepecky, R. and Foster, J. W. (1959). Alterations in metal content of spores of *Bacillus megaterium* and the effect on some spore properties. *Journal of bacteriology*, 78 (1), pp.117–123. [Online]. Available at: doi:10.1128/JB.78.1.117-123.1959/ASSET/8BC16300-

12DB-4F44-BFDC-BAF15E162851/ASSETS/JB.78.1.117-123.1959.FP.PNG [Accessed 8 March 2024].

Sleutel, M. et al. (2023). A novel class of ultra-stable endospore appendages decorated with collagen-like tip fibrillae. *bioRxiv*, p.2023.10.23.563578. [Online]. Available at: doi:10.1101/2023.10.23.563578.

Slieman, T. A., Rebeil, R. and Nicholson, W. L. (2000). Spore photoproduct (SP) lyase from *Bacillus subtilis* specifically binds to and cleaves SP (5-thyminyl-5,6-dihydrothymine) but not cyclobutane pyrimidine dimers in UV-irradiated DNA. *Journal of Bacteriology*, 182 (22), pp.6412–6417. [Online]. Available at: doi:10.1128/JB.182.22.6412-6417.2000/ASSET/0EDB1512-5F14-411D-8573-5C1BCEE17C3F/ASSETS/GRAPHIC/JB2200519005.JPEG [Accessed 23 March 2024].

Spencer, R. E. and Powell, J. F. (1952). Flavin-adenine dinucleotide and diaphorase in resting and germinated spores, and vegetative cells of *Bacillus subtilis* and *Bacillus megatherium*. *Biochemical Journal*, 51 (2), pp.239–245. [Online]. Available at: doi:10.1042/BJ0510239 [Accessed 9 August 2022].

Spinelli, J. B. et al. (2021). Fumarate is a terminal electron acceptor in the mammalian electron transport chain. *Science*, 374 (6572), pp.1227–1237. [Online]. Available at: doi:10.1126/SCIENCE.ABI7495/SUPPL_FILE/SCIENCE.ABI7495_MDAR_REPRODUCIBILITY_CHECKLIST.PDF [Accessed 20 March 2024].

Stabrin, M. et al. (2020). TranSPHIRE: automated and feedback-optimized on-the-fly processing for cryo-EM. *Nature Communications 2020 11:1*, 11 (1), pp.1–14. [Online]. Available at: doi:10.1038/s41467-020-19513-2 [Accessed 19 March 2024].

Stewart, K. A. V. and Setlow, P. (2013). Numbers of individual nutrient germinant receptors and other germination proteins in spores of *Bacillus subtilis*. *Journal of Bacteriology*, 195 (16), pp.3575–3582. [Online]. Available at: doi:10.1128/JB.00377-13/ASSET/0DBF086F-DBBA-4B91-99AC-DDAFF5B0A705/ASSETS/GRAPHIC/ZJB9990927160006.JPEG [Accessed 25 March 2024].

Stier, P. and Kulozik, U. (2022). Comparison of one-step with two-step production of *Bacillus atrophaeus* spores for use as bioindicators. *MicrobiologyOpen*, 11 (6), p.e1332. [Online]. Available at: doi:10.1002/MBO3.1332 [Accessed 29 March 2024].

Strahl, H. and Hamoen, L. W. (2010). Membrane potential is important for bacterial cell division. *Proceedings of the National Academy of Sciences of the United States of America*,

107 (27), pp.12281–12286. [Online]. Available at: doi:10.1073/PNAS.1005485107/SUPPL_FILE/SM01.AVI [Accessed 25 March 2024].

Stroud, D. A. et al. (2016). Accessory subunits are integral for assembly and function of human mitochondrial complex I. *Nature 2016 538:7623*, 538 (7623), pp.123–126. [Online]. Available at: doi:10.1038/nature19754 [Accessed 19 March 2024].

Su, C. C. et al. (2021). A 'Build and Retrieve' methodology to simultaneously solve cryo-EM structures of membrane proteins. *Nature Methods*, 18 (1), pp.69–75. [Online]. Available at: doi:10.1038/s41592-020-01021-2 [Accessed 18 May 2021].

Sucheta, A. et al. (1992). Diode-like behaviour of a mitochondrial electron-transport enzyme. *Nature 1992 356:6367*, 356 (6367), pp.361–362. [Online]. Available at: doi:10.1038/356361a0 [Accessed 31 March 2024].

Sun, F. et al. (2005). Crystal structure of mitochondrial respiratory membrane protein Complex II. *Cell*, 121 (7), pp.1043–1057. [Online]. Available at: doi:10.1016/j.cell.2005.05.025 [Accessed 19 March 2024].

Sunde, E. P. et al. (2009). The physical state of water in bacterial spores. *Proceedings of the National Academy of Sciences of the United States of America*, 106 (46), pp.19334–19339. [Online]. Available at: doi:10.1073/PNAS.0908712106/SUPPL_FILE/APPENDIX_PDF.PDF [Accessed 10 August 2022].

Swerdlow, B. M., Setlow, B. and Setlow, P. (1981). Levels of H^+ and other monovalent cations in dormant and germinating spores of *Bacillus megaterium*. *Journal of Bacteriology*, 148 (1), p.20. [Online]. Available at: doi:10.1128/JB.148.1.20-29.1981 [Accessed 22 August 2022].

Swerdlow, R. D. and Setlow, P. (1984). Isolation and characterization of two distinct fractions from the inner membrane of dormant *Bacillus megaterium* spores. *Journal of Bacteriology*, 158 (1), pp.9–15. [Online]. Available at: doi:10.1128/JB.158.1.9-15.1984 [Accessed 9 August 2022].

Thierbach, G. and Reichenbach, H. (1981). Myxothiazol, a new inhibitor of the cytochrome *b*-c_1 segment of the respiratory chain. *Biochimica et Biophysica Acta (BBA) - Bioenergetics*, 638 (2), pp.282–289. [Online]. Available at: doi:10.1016/0005-2728(81)90238-3 [Accessed 29 March 2024].

Titov, D. V. et al. (2016). Complementation of mitochondrial electron transport chain by manipulation of the NAD^+/NADH ratio. *Science (New York, N.Y.)*, 352 (6282), pp.231–235. [Online]. Available at: doi:10.1126/SCIENCE.AAD4017 [Accessed 2 November 2023].

Tocheva, E. I., Ortega, D. R. and Jensen, G. J. (2016). Sporulation, bacterial cell envelopes and the origin of life. *Nature Reviews Microbiology 2016 14:8*, 14 (8), pp.535–542. [Online]. Available at: doi:10.1038/nrmicro.2016.85 [Accessed 26 March 2024].

Tochikubo, K. (1971). Changes in terminal respiratory pathways of *Bacillus subtilis* during germination, outgrowth and vegetative growth. *Journal of Bacteriology*, 108 (2), pp.652–661. [Online]. Available at: doi:10.1128/JB.108.2.652-661.1971 [Accessed 31 January 2022].

Tochikubo, K. and Yasuda, Y. (1985). Possibility of Association and Activation of Glucose Dehydrogenase during Germination and Outgrowth of *Bacillus subtilis* Spores. *Microbiology and Immunology*, 29 (3), pp.213–228. [Online]. Available at: doi:10.1111/J.1348-0421.1985.TB00821.X [Accessed 29 March 2023].

Töwe, S. et al. (2007). The MarR-type repressor MhqR (YkvE) regulates multiple dioxygenases/glyoxalases and an azoreductase which confer resistance to 2-methylhydroquinone and catechol in *Bacillus subtilis*. *Molecular Microbiology*, 66 (1), pp.40–54. [Online]. Available at: doi:10.1111/J.1365-2958.2007.05891.X [Accessed 28 March 2023].

Trchounian, A. and Trchounian, K. (2019). Fermentation Revisited: How Do Microorganisms Survive Under Energy-Limited Conditions? *Trends in Biochemical Sciences*, 44 (5), pp.391–400. [Online]. Available at: doi:10.1016/J.TIBS.2018.12.009 [Accessed 26 March 2024].

Vary, J. C. (1973). Germination of *Bacillus megaterium* Spores After Various Extraction Procedures. *Journal of Bacteriology*, 116 (2), pp.797–802. [Online]. Available at: doi:10.1128/JB.116.2.797-802.1973 [Accessed 6 September 2022].

Vary, P. S. (1994). Prime time for *Bacillus megaterium*. *Microbiology*, 140 (5), pp.1001–1013. [Online]. Available at: doi:10.1099/13500872-140-5-1001/CITE/REFWORKS [Accessed 10 August 2022].

Vary, P. S. et al. (2007). *Bacillus megaterium*-from simple soil bacterium to industrial protein production host. *Applied Microbiology and Biotechnology*, 76 (5), pp.957–967. [Online]. Available at: doi:10.1007/S00253-007-1089-3/FIGURES/6 [Accessed 25 March 2024].

Velásquez, J. et al. (2014). *Bacillus subtilis* spore protein SpoVAC functions as a mechanosensitive channel. *Molecular Microbiology*, 92 (4), pp.813–823. [Online]. Available at: doi:10.1111/MMI.12591 [Accessed 25 March 2024].

Vepachedu, V. R. and Setlow, P. (2005). Localization of SpoVAD to the inner membrane of spores of *Bacillus subtilis*. *Journal of Bacteriology*, 187 (16), pp.5677–5682. [Online].

Available at: doi:10.1128/JB.187.16.5677-5682.2005/ASSET/9346EA5B-D84D-4723-98D2-DC99342749DB/ASSETS/GRAPHIC/ZJB0160549950005.JPEG [Accessed 24 March 2024].

Vieira, V. M. N. C. S. et al. (2018). Differentiation of haploid and diploid fertilities in *Gracilaria chilensis* affect ploidy ratio. *BMC Evolutionary Biology*, 18 (1), pp.1–11. [Online]. Available at: doi:10.1186/S12862-018-1287-X/FIGURES/5 [Accessed 22 March 2024].

Walker, J. E. (2013). The ATP synthase: the understood, the uncertain and the unknown. *Biochemical Society Transactions*, 41 (1), pp.1–16. [Online]. Available at: doi:10.1042/BST20110773 [Accessed 26 March 2024].

Wallace, S. et al. (2011). Evolutionary development of the plant spore and pollen wall. *AoB PLANTS*, 2011 (1), p.27. [Online]. Available at: doi:10.1093/AOBPLA/PLR027 [Accessed 22 March 2024].

Wang, S., Setlow, P. and Li, Y. Q. (2015). Slow leakage of Ca-dipicolinic acid from individual *Bacillus* spores during initiation of spore germination. *Journal of Bacteriology*, 197 (6), pp.1095–1103. [Online]. Available at: doi:10.1128/JB.02490-14/SUPPL_FILE/ZJB999093528SO1.PDF [Accessed 10 August 2022].

Wang, Y. et al. (2021). Dynamics of germinosome formation and FRET-based analysis of interactions between GerD and germinant receptor subunits in *Bacillus cereus* spores. *International Journal of Molecular Sciences*, 22 (20), p.11230. [Online]. Available at: doi:10.3390/IJMS222011230/S1 [Accessed 25 March 2024].

Wang, Y. et al. (2022). Visualization of SpoVAEa Protein Dynamics in Dormant Spores of *Bacillus cereus* and Dynamic Changes in Their Germinosomes and SpoVAEa during Germination. *Microbiology Spectrum*, 10 (3). [Online]. Available at: doi:10.1128/SPECTRUM.00666-22/SUPPL_FILE/SPECTRUM.00666-22-S001.PDF [Accessed 25 March 2024].

Weart, R. B. et al. (2007). A Metabolic Sensor Governing Cell Size in Bacteria. *Cell*, 130 (2), pp.335–347. [Online]. Available at: doi:10.1016/j.cell.2007.05.043 [Accessed 30 March 2024].

Wen, J. et al. (2022). Heat Activation and Inactivation of Bacterial Spores: Is There an Overlap? *Applied and Environmental Microbiology*, 88 (5). [Online]. Available at: doi:10.1128/AEM.02324-21/ASSET/081C73F8-5FDF-491A-AE5D-60C86F83E31B/ASSETS/IMAGES/LARGE/AEM.02324-21-F007.JPG [Accessed 29 March 2024].

Wikstrom, M. (1981). Energy-dependent reversal of the cytochrome oxidase reaction. *Proceedings of the National Academy of Sciences*, 78 (7), pp.4051–4054. [Online]. Available at: doi:10.1073/PNAS.78.7.4051 [Accessed 31 March 2024].

Wikström, M., Gennis, R. B. and Rich, P. R. (2023). Structures of the intermediates in the catalytic cycle of mitochondrial cytochrome *c* oxidase. *Biochimica et Biophysica Acta (BBA) - Bioenergetics*, 1864 (2), p.148933. [Online]. Available at: doi:10.1016/J.BBABIO.2022.148933 [Accessed 6 March 2024].

Wilkinson, B. J. et al. (1977). Rapid, chloramphenicol-resistant, activation of membrane electron transport on germination of *Bacillus* spores. *Nature 1977 266:5598*, 266 (5598), pp.174–176. [Online]. Available at: doi:10.1038/266174a0 [Accessed 27 July 2021].

Wilkinson, B. J. and Ellar, D. J. (1975). Morphogenesis of the Membrane-Bound Electron-Transport System in Sporulating *Bacillus megaterium* KM. *European Journal of Biochemistry*, 55 (1), pp.131–139. [Online]. Available at: doi:10.1111/j.1432-1033.1975.tb02145.x [Accessed 18 May 2021].

Wilson, M. T. et al. (1994). Probing the oxygen binding site of cytochrome *c* oxidase by cyanide. *Journal of Biological Chemistry*, 269 (39), pp.24114–24119. [Online]. Available at: doi:10.1016/S0021-9258(19)51055-9 [Accessed 29 March 2024].

Winstedt, L. and Von Wachenfeldt, C. (2000). Terminal oxidases of *Bacillus subtilis* strain 168: One quinol oxidase, cytochrome aa_3 or cytochrome *bd*, is required for aerobic growth. *Journal of Bacteriology*, 182 (23), pp.6557–6564. [Online]. Available at: doi:10.1128/JB.182.23.6557-6564.2000/ASSET/F137B5BD-143B-4952-809E-E58C5757A15D/ASSETS/GRAPHIC/JB2300872005.JPEG [Accessed 31 March 2024].

Wöhri, A. B. et al. (2008). A Lipidic-Sponge Phase Screen for Membrane Protein Crystallization. *Structure*, 16 (7), pp.1003–1009. [Online]. Available at: doi:10.1016/j.str.2008.06.003 [Accessed 20 March 2024].

Wojtyla, Ł. et al. (2016). Different Modes of Hydrogen Peroxide Action During Seed Germination. *Frontiers in Plant Science*, 7 (FEB2016), p.66. [Online]. Available at: doi:10.3389/FPLS.2016.00066 [Accessed 15 February 2024].

Wushensky, J. A. et al. (2018). Flux Connections Between Gluconate Pathway, Glycolysis, and Pentose-Phosphate Pathway During Carbohydrate Metabolism in *Bacillus megaterium* QM B1551. *Frontiers in microbiology*, 9, p.2789. [Online]. Available at: doi:10.3389/fmicb.2018.02789.

Yankovskaya, V. et al. (2003). Architecture of succinate dehydrogenase and reactive oxygen species generation. *Science*, 299 (5607), pp.700–704. [Online]. Available at: doi:10.1126/SCIENCE.1079605/SUPPL_FILE/YANKOVSKAYA.SOM.PDF.PDF [Accessed 19 March 2024].

Yasuda, Y. and Tochikubo, K. (1985). Germination-Initiation and Inhibitory Activities of L- and D-Alanine Analogues for *Bacillus subtilis* Spores. *Microbiology and Immunology*, 29 (3), pp.229–241. [Online]. Available at: doi:10.1111/J.1348-0421.1985.TB00822.X [Accessed 9 February 2024].

Yi, X. et al. (2011). Synergism between different germinant receptors in the germination of *Bacillus subtilis* spores. *Journal of Bacteriology*, 193 (18), pp.4664–4671. [Online]. Available at: doi:10.1128/JB.05343-11/SUPPL_FILE/FIGURES.DOCX [Accessed 25 March 2024].

Zeytuni, N. et al. (2017). Near-atomic resolution cryoelectron microscopy structure of the 30-fold homooligomeric SpoIIIAG channel essential to spore formation in *Bacillus subtilis*. *Proceedings of the National Academy of Sciences of the United States of America*, 114 (34), pp.E7073–E7081. [Online]. Available at: doi:10.1073/PNAS.1704310114/SUPPL_FILE/PNAS.201704310SI.PDF [Accessed 26 March 2024].

Zhang, P. et al. (2010). Factors affecting variability in time between addition of nutrient germinants and rapid dipicolinic acid release during germination of spores of *Bacillus species*. *Journal of Bacteriology*, 192 (14), pp.3608–3619. [Online]. Available at: doi:10.1128/JB.00345-10/SUPPL_FILE/PZETALSUP.DOC [Accessed 1 April 2024].

Zhang, P., Setlow, P. and Li, Y. (2009). Characterization of single heat-activated *Bacillus* spores using laser tweezers Raman spectroscopy. *Optics Express*, 17 (19), pp.16480–16491. [Online]. Available at: doi:10.1364/OE.17.016480.

Zheng, L. et al. (2016). *Bacillus subtilis* Spore Inner Membrane Proteome. *Journal of Proteome Research*, 15 (2), pp.585–594. [Online]. Available at: doi:10.1021/ACS.JPROTEOME.5B00976/SUPPL_FILE/PR5B00976_SI_001.XLSX [Accessed 22 August 2022].

Zhou, X. et al. (2021). Architecture of the Mycobacterial succinate dehydrogenase with a membrane-embedded rieske FeS cluster. *Proceedings of the National Academy of Sciences of the United States of America*, 118 (15). [Online]. Available at: doi:10.1073/PNAS.2022308118/-/DCSUPPLEMENTAL [Accessed 19 March 2024].